

International PrimeNet Workshop

September, 26 – 28, 2011, Jülich, Germany

Summary of Contributions

Contents

Introduction	1
η, η' and ϕ Decays from Experimental and Theoretical Perspectives	3
Introduction: Rare η Decays and Tests of Fundamental Symmetries	5
<i>A. Wirzba</i>	
Search for Exotic Effects in the $\eta \rightarrow e^+e^-$ Decay	9
<i>M. Bertowski</i>	
Analysis of the C-Violating Decay $\eta \rightarrow \pi^0 + \gamma^* \rightarrow \pi^0 + e^+ + e^-$ with WASA-at-COSY	11
<i>F. Bergmann</i>	
Theoretical Perspectives on $\eta, \eta' \rightarrow 4\pi$ Decays	13
<i>B. Kubis</i>	
Pluto: A Multi-Purpose Event Generator Framework for Rare η Decays	16
<i>I. Fröhlich</i>	
Dalitz Plot Analysis for $\eta \rightarrow \pi^+\pi^-\pi^0$ at KLOE	18
<i>L. Caldeira Balkeståhl</i>	
The $\eta \rightarrow \pi^+\pi^-\pi^0$ Decay With WASA-at-COSY	21
<i>P. Adlarson</i>	
Berne-Lund-Valencia Dispersive Treatment of $\eta \rightarrow 3\pi$	24
<i>S. Lanz</i>	
Prague-Lund-Marseille (Analytical) Dispersive Approach to $\eta \rightarrow 3\pi$	27
<i>M. Zdráhal</i>	
$\eta \rightarrow 3\pi$ in Resummed χPT: Dalitz Plot Parameters	30
<i>M. Kolesár</i>	
Model-Independent Approach to $\eta \rightarrow \pi^+\pi^-\gamma$ and $\eta' \rightarrow \pi^+\pi^-\gamma$	33
<i>F. Stollenwerk</i>	
Study of $\eta \rightarrow \pi^+\pi^-\gamma$ Decay	35
<i>C. Di Donato</i>	
In Search of the Box Anomaly by Studying $\eta \rightarrow \pi^+\pi^-\gamma$	38
<i>D. Lersch</i>	
Radiative Decays of Pseudoscalars and Vectors	40
<i>C. Terschläusen</i>	
π^0 Decays Measured with WASA-at-COSY	43
<i>C.-O. Gullström</i>	

Study of the $\eta \rightarrow e^+e^-\gamma$ Decay	45
<i>M. Hodana</i>	
Analysis of the Double Dalitz Decay $\eta \rightarrow e^+e^-e^+e^-$	48
<i>P. Wurm</i>	
Determination of the Electromagnetic η Transition Form Factor	51
<i>V. Metag</i>	
Dalitz Decay of the ω Meson	52
<i>F. A. Khan</i>	
Study of the $\phi \rightarrow \eta e^+e^-$ Decay at KLOE	54
<i>J. Zdebik</i>	
Electromagnetic Transition Form Factors of Pseudoscalar and Vector Mesons	58
<i>C. Terschläsen</i>	
Investigation of $\omega \rightarrow \pi^+\pi^-\pi^0$ with WASA-AT-COSY	61
<i>L. Heijkenkjöld and S. Sawant</i>	
Dispersive Analyses of $\omega/\phi \rightarrow 3\pi$ and $\eta' \rightarrow \eta\pi\pi$	63
<i>S. P. Schneider and F. Niecknig</i>	
Measurement of $\eta' \rightarrow \eta\pi^+\pi^-$ with KLOE and KLOE-2	68
<i>C. F. Redmer</i>	
Hard Pion Chiral Perturbation Theory: What is it and is it relevant for η' decays?	68
<i>J. Bijnens</i>	
Hunting Resonance Poles	71
<i>P. Masjuan</i>	
Exploring Low-Energy QCD Using a Generalized Linear Sigma Model	74
<i>A. H. Fariborz</i>	
The η Decay Program at WASA-at-COSY	77
<i>D. Coderre</i>	
Decays of Light Mesons in CLAS	80
<i>M. Amaryan</i>	
Meson Production in photon-induced reactions and from NN collisions	85
Study of η Meson Production with a Polarized Proton Beam	87
<i>I. Ozerianska</i>	
Determination of the η Mass with the Crystal Ball at MAMI-B	90
<i>A. Nikolaev</i>	
High Precision η Meson Mass Determination at COSY-ANKE	91
<i>P. Goslawski</i>	
Measurement of the η' Meson Total Width at the COSY-11 Facility	94
<i>E. Czerwiński</i>	
Two-Pion Production in Isoscalar NN Collisions: ABC Effect and Resonance	96
<i>M. Bashkanov</i>	

ABC Effect in Double-Pionic Fusion to ${}^3\text{He}$	100
<i>E. Perez del Rio</i>	
Two-Pion Production in Proton-Proton Collisions	103
<i>T. Skorodko</i>	
Overview on One and Double Pion Production in pp Collisions in HADES	106
<i>M. Gumberidze</i>	
Exclusive Channels in pp at 3.5 GeV	111
<i>A. Dybczak</i>	
Overview of e^+e^- Production in $p + p$ and $p + n$ Collisions	114
<i>P. Salabura</i>	
HADES Spectrometer and Future Experiments with Pion Beams	117
<i>H. Kuc</i>	
Two-Photon Physics at KLOE/KLOE-2	119
<i>I. Prado Longhi</i>	
Roy–Steiner Equations for $\gamma\gamma \rightarrow \pi\pi$	122
<i>M. Hoferichter</i>	
Measurement of the Double Polarization Observable G in π^0 and η Photoproduction	125
<i>A. Thiel</i>	
The $N^*(1535)$ Excitation – The Electromagnetic Transition Form Factors	128
<i>G. Ramalho</i>	
The Structure around $W = 1680$ MeV in η-Photoproduction off the Neutron	131
<i>D. Werthmüller</i>	
Interaction of η and η' with Nucleons and Nuclei	135
A Theoretical Approach to $\eta'N$ Scattering	137
<i>A. Ramos</i>	
Search for η-mesic ${}^4\text{He}$ with WASA-at-COSY	140
<i>W. Krzemień</i>	
List of Participants	143

Introduction

This workshop is part of the activities in the project Study of Strongly Interacting Matter (acronym HadronPhysics2), which is an integrating activity of the Seventh Framework Program of EU. This HP2 project contains several activities, one of them being the network PrimeNet having the focus on Meson Physics in Low-Energy QCD. This network is created to exchange information on experimental and theoretical ongoing activities on mainly η and η' physics at different European accelerator facilities and institutes.

The present workshop included the three general topics:

1. η, η' and ϕ decays from experimental and theoretical perspectives.
2. Meson production in photon-induced reactions and from NN collisions as well as e^+e^- production from pp collisions.
3. Interaction of η and η' with nucleons and nuclei.

The talks covered the very recent achievements in the respective fields from the experimental facilities KLOE at DAPHNE, Crystal Ball at MAMI, Crystal Ball and TAPS at ELSA, and WASA-at-COSY, as well as from different theory institutes. Electronic versions of the talks can be found on the PrimeNet homepage <http://www.fz-juelich.de/ikp/primenet>

The detailed program was arranged by a program committee led by Dieter Grzonka and Susan Schadmand.

The workshop was held Sept 26-28, 2011, at the Forschungszentrum Jülich, enjoying kind hospitality and support from the Forschungszentrum.

Financial support is gratefully acknowledged from the European Commission under the 7th Framework Programme through the 'Research Infrastructures' action of the 'Capacities' Programme; Call: FP7-INFRASTRUCTURES-2008-1, Grant Agreement N. 227431.

Dieter Grzonka, Susan Schadmand, Bo Höistad and Christoph Redmer

η, η' and ϕ Decays

from Experimental and Theoretical Perspectives

INTRODUCTION: RARE η DECAYS AND TESTS OF FUNDAMENTAL SYMMETRIES

ANDREAS WIRZBA*

1.1 Introduction

The organizers asked me to give an introductory talk for this meeting. Because of time limitations and also my ignorance about other subjects, I interpreted this task in a somewhat restricted sense by only concentrating on the physics of rare η decays. This is of course only a small subset of the various topics covered in this meeting. Many other aspects would have deserved dedicated introductions as well. Let me also remark that I heavily relied on Ref. [1] in preparing this talk, a joint paper with Andrzej Kupsc about tests of fundamental symmetries in rare η decays.

After these disclaimers, I would like to start with two questions: Why is the η meson interesting in general and why are the rare η decays especially interesting? Well, the η is special, because of essentially three reasons: it is a Pseudo-Goldstone boson of the strong interaction part of the Standard Model (SM), *i.e.* its mass and all its interactions vanish in the chiral limit, the limit of vanishing quark masses and external momenta. It is a neutral meson with respect to all its internal quantum numbers. Finally, it is the heaviest of the octet of pseudoscalar mesons and therefore many decay channels are energetically accessible. The last two arguments do hold of course for its heavier “nonet-brother”, the η' meson as well which, however, is not a Pseudo-Goldstone boson, because the $U_A(1)$ symmetry is *explicitly* broken by the non-perturbative instanton physics.

Although both mesons possess many open decay channels, all the decays — with the exception of the allowed decay $\eta' \rightarrow \eta\pi\pi$ — are suppressed in one way or the other: by the conservation of Noether currents (in the chiral limit) which in turn may be broken by (quantum) anomalies, by the conservation of parity, C -parity, CP , G -parity etc. Since the η and η' are eigenstates of G , P , C and CP , namely $I^G(J^{PC}) = 0^+(0^{-+})$, both mesons can serve as “test laboratories” for the conservation or rather the breaking of these discrete symmetries. Moreover, since there is mixing, namely the singlet-octet mixing of the η and η' mesons because of the $U_A(1)$ breaking, and — to a lesser degree — the mixing with the π^0 meson because of isospin breaking, there is also some access to these mixing and breaking phenomena as well.

In responding to the second question one should keep in mind that the pertinent SM-mechanisms of rare decays have to be small to begin with. Moreover, symmetry-violating decays are rare by nature, as otherwise we would not speak about a symmetry. Thus, by studying rare η decays, we have the chance to encounter a window of opportunity for experimental searches for physics beyond the SM. Since many different final states are energetically accessible, a variety of different symmetry tests is possible. These tests include searches for rare or forbidden decays, for asymmetries among the decay products in not-so-rare decays, and for light dark-matter particles if there is a discrepancy between SM expectations and experimental results. Since the η and η' mesons belong to the class of flavor-neutral (light) mesons, especially flavor-conserving symmetry violating mechanisms are tested – complementary to the flavor-changing CP tests with kaons or B -mesons.

1.2 CP tests

Most of the CP tests in η decays are modeled in analogy to CP -violating decays for the K_L meson. Whereas the latter are flavor-changing, the former decays test – as mentioned above – a *flavor-conserving* CP violating mechanism.

*Institut für Kernphysik, Institute for Advanced Simulation and Jülich Center for Hadron Physics, Forschungszentrum Jülich, D-52425 Jülich, Germany; a.wirzba@fz-juelich.de

1.2.1 $\eta \rightarrow \pi\pi$

As reviewed in Ref. [2], theory predicts very tiny branching ratios for the $\eta \rightarrow \pi\pi$ decays. Since the flavor is conserved, these CP -violating decays have to be second order weak decays in the SM (governed by the CKM matrix), *i.e.* they are proportional to $G_F^2 \sin^2 \theta_C$. In addition, there are dynamical suppressions such that the upper bound on the branching ratio is given by $\mathcal{B}(\text{CKM}_{\text{SM}}) \leq 2 \times 10^{-27}$. The contribution of the CP -violating QCD θ term to this decay is indirectly constrained by the empirical upper bound on the electric dipole moment d_n of the neutron which in turn limits the QCD vacuum angle, such that $\mathcal{B}(\theta_{\text{QCD}}) \leq 3 \times 10^{-17}$, whereas the ‘extra Higgs’ models allow a slightly larger upper bound, $\mathcal{B}(\text{extra Higgs}) \leq 1.2 \times 10^{-15}$. According to Gorchtein [3], the empirical bound on d_n can be used directly to determine an upper bound for the branching ratio of $\eta \rightarrow \pi\pi$, no matter what the underlying CP -violating mechanism will turn out to be: for a larger value of the branching ratio than 3.5×10^{-14} the CP -violating part of the η -loop contributions alone would already violate the bound on d_n .

The empirical numbers for the upper bounds are much larger: $\mathcal{B}(\eta \rightarrow \pi^+\pi^-) \leq 1.3 \times 10^{-5}$ from the KLOE collaboration [4] and $\mathcal{B}(\eta \rightarrow \pi^0\pi^0) \leq 3.5 \times 10^{-4}$ from GAMS-4 π [5].

1.2.2 η decay asymmetries

The decay $\eta \rightarrow \pi^+\pi^-\gamma$ is governed by the CP -allowed M_1 amplitude which can be traced back to the chiral triangle and box anomalies. Still, this decay can be used to test the CP violation in η decays, if an interference with any CP -violating (direct) E_1 term can be made visible. In principle, there might exist the interference with the Bremsradiation-modified decay $\eta \rightarrow \pi^+\pi^-$ as well, but as shown in Sect. 1.2.1 this is very unlikely because of the tiny branching ratio of the $\eta \rightarrow \pi\pi$ decay. Geng, Ng and Wu [6] suggested to measure the (linear) polarization state of the outgoing photon, since differential cross section measurements are insensitive to the interference patterns. In the same year, Gao [7] proposed to concentrate – in analogy to the CP experiment in the K_L system – on the $\eta \rightarrow \pi^+\pi^-e^+e^-$ decay and to measure rather the asymmetry between the pion and lepton decay planes which is sensitive to the interference term between the M_1 and E_1 decay amplitudes. Gao estimated the theoretical bound on the asymmetry as $A_{\text{theo}} \leq 0.02$ by invoking an unconventional flavor-conserving CP -violating electric dipole mechanism (originally suggested in Ref. [6]), which is especially sensitive to the $s\bar{s}$ quark content of the η and therefore not constrained but other CP tests. The KLOE collaboration [8] measured $A_{\text{emp}} = (-0.6 \pm 2.5 \pm 1.8) \times 10^{-2}$ as empirical value which is both compatible with the theoretical bound and with zero of course.

1.2.3 New types of CP tests without kaon-analog case

Whereas the upper cases were modeled according to K_L decays, Nefkens [9] suggested a CP test involving the η meson which has no analog in the kaon or B -meson sectors, namely the decay $\eta \rightarrow 4\pi^0$ which is characterized by a very low excess energy of 7.9 MeV. It is forbidden if all pion pairs are in relative S or P -wave states. In the SM, it can only proceed by D -wave or higher interactions which are – because of phase space limitations – extremely suppressed. For more information on this and other four-pion decays of the η and η' , please consult the talk of Bastian Kubis [11] in this conference. Since the decay is characterized by a unique 8 photon signal and as there is a very low background from direct pion production, this decay in fact is the most sensitive of any of the measured η decays: $\mathcal{B}(\eta \rightarrow 4\pi^0) < 6.9 \cdot 10^{-7}$ [10]. The experimental limit on the branching ratio of the $\eta' \rightarrow 4\pi^0$ decay, however, is larger: $5 \cdot 10^{-4}$ [12].

1.3 Tests of the C symmetry in rare η decays

Any decay of the η (or η') meson into neutrals including an *odd* number of photons in the final state would be a signal for C violation. The simplest example, $\eta \rightarrow 3\gamma$ is heavily suppressed as each 2-photon-pair has to be at least in a relative $J = 2$ state. The $J = 0$ case would correspond to a radiative $0 \rightarrow 0$ transition which is forbidden because of angular momentum conservation [13], and the $J = 1$ case would violate the Bose symmetry. The experimental upper limit for the branching ratio is $1.6 \cdot 10^{-5}$ [14]. The next simplest case, $\eta \rightarrow \pi^0\gamma$ is again an example for the forbidden radiative $0 \rightarrow 0$ transition. The empirical upper limit on its branching ratio is $9 \cdot 10^{-5}$ from the Crystal Ball experiment [15]. The Crystal Ball collaboration [16] gives also the best limits on the branching ratios $\mathcal{B}(\eta \rightarrow \pi^0\pi^0\gamma) < 5 \cdot 10^{-4}$ and $\mathcal{B}(\eta \rightarrow 3\pi^0\gamma) < 6 \cdot 10^{-5}$, respectively [16].

1.3.1 The decay $\eta \rightarrow \pi^0 e^+ e^-$ as C symmetry test

The branching ratio for the C -allowed process $\eta \rightarrow \pi^0 \gamma^* \gamma^* \rightarrow \pi^0 e^+ e^-$, which involves two virtual photons, was estimated to be of the order 10^{-8} [17]. Therefore any measurement with a branching ratio $\mathcal{B}(\eta \rightarrow \pi^0 e^+ e^-)$ larger than this value would be a clear signal for C violation. Note, however, that the decay mechanism with one off-shell photon is not only suppressed by C , but also by a vanishing transition form factor in the on-shell limit, since the ‘‘parent’’ decay $\eta \rightarrow \pi^0 \gamma$ is – as mentioned above – a radiative $0 \rightarrow 0$ transition. The current upper limit of the branching ratio $\mathcal{B}(\eta \rightarrow \pi^0 e^+ e^-)$ is equal to $4.5 \cdot 10^{-5}$ 90% CL, from an experiment performed in the 70s of the last century [18]. For further details, especially about the measurement of the WASA-at-COSY collaboration, please consult the presentation of Florian Bergmann [19].

The C invariance can also be tested in, *e.g.*, $\eta \rightarrow \pi^+ \pi^- \gamma$ and in $\eta \rightarrow \pi^+ \pi^- \pi^0$ decays by π^\pm asymmetry measurements in the η rest frame. Most of the measurements date again back to the 70s of the last century. For the asymmetries in the $\eta \rightarrow \pi^+ \pi^- \pi^0$ decay there exist recent upper bounds from the KLOE collaboration with 10^{-3} sensitivity [20].

1.4 Dark particle searches

Note that rare dilepton decays of η mesons and pseudoscalar mesons $P = \pi^0, \eta, \eta'$ in general can be used as candidates for light dark-matter particle searches. Since the tree-level decay via a virtual Z boson is minuscule, the leading order decay process is $P \rightarrow \gamma^* \gamma^* \rightarrow l^+ l^-$. The latter is suppressed not only by two powers of the fine-structure constant α , but also by the helicity mismatch of the outgoing leptons, *i.e.* $\mathcal{B}(P \rightarrow l^+ l^-) / \mathcal{B}(P \rightarrow \gamma \gamma) \sim (\frac{\alpha}{\pi} \frac{m_l}{m_P})^2$ where m_P and m_l are the masses of the decaying meson and the leptons $l^\pm = e^\pm$ (or also μ^\pm in the η, η' cases), respectively. For the $\pi^0 \rightarrow e^+ e^-$ decay, the branching ratio is of order $\mathcal{O}(10^{-7})$. In fact, the best experimental [21] and theoretical [22] values of $\mathcal{B}(\pi^0 \rightarrow e^+ e^-)$, namely $(7.48 \pm 0.29_{\text{stat}} \pm 0.25_{\text{syst}}) \cdot 10^{-8}$ and $(6.23 \pm 0.09) \cdot 10^{-8}$, respectively, differ by three standard deviations.

Kahn and collaborators [23] suggested as a possible explanation of this excess the tree-level exchange of an off-shell neutral vector boson U (pioneered by Fayet [24]) of mass $m_U \sim (10 - 100)$ MeV. According to the light dark matter models of Refs. [25, 26], this U boson mediates the annihilation reaction $\chi \chi \rightarrow e^+ e^-$ of a neutral scalar dark matter particle χ of $(1 - 10)$ MeV mass, such that the produced positrons could account for the bright 511 keV line emanating from the center of the Galaxy. Kahn et al. could resolve the mismatch between experiment and theory of the $\pi^0 \rightarrow e^+ e^-$ decay by assuming that the neutral vector meson U would couple to the u and d quark fields of the π^0 and the $e^+ e^-$ dilepton pair with a common axial-vector coupling $g_A \equiv g_A^u - g_A^d \equiv g_A^e$ of strength $g_A = (2.0 \pm 0.5) \cdot 10^{-4} \cdot m_U / (10 \text{ MeV})$. If the octet axial-vector quark-coupling is assumed to be of the same order as above, the U boson contribution to the branching ratio $\text{BR}(\eta \rightarrow e^+ e^-)$ is estimated as $\sim 10^{-9}$, which is of the same order as the predictions of Dorokhov and collaborators [22] and much smaller than the experimental bound $2.7 \cdot 10^{-5}$ of the CELSIUS/WASA collaboration [27]. However, the branching ratio $\mathcal{B}(\eta \rightarrow \mu^+ \mu^-)$ is then predicted to be nearly an order of magnitude larger than the measured value $\mathcal{B}(\eta \rightarrow \mu^+ \mu^-) \sim (5.7 \pm 0.9) \cdot 10^{-6}$ [28], unless the axial-vector coupling of the U meson to the muon is smaller than g_A^e or the octet axial-vector quark coupling is smaller than $g_A^u - g_A^d$ or both. This limits of course the predictive power of the above presented U boson exchange mechanism.

Another variant of dark matter U gauge bosons, which acquires a mass scale of 1 MeV to a few GeV via a ‘dark Higgs mechanism’ and which couples vectorially to all SM charged fields with a strength $\epsilon \sim 10^{-3}$ or less, was suggested by Reece and Wang [29] (see also [30]). This type of U -boson would also couple to SM weak neutral currents; however, the corresponding coupling constant would be suppressed by a factor of order m_V^2 / m_Z^2 . Therefore, this variant cannot explain the missing excess of the $\pi^0 \rightarrow e^+ e^-$ decay. First searches for U bosons of the Reece and Wang type are on the way, carried out by the KLOE collaboration. The relevant channels are, *e.g.*, the decays $\phi \rightarrow \eta U$, $U \rightarrow e^+ e^-$ and $\eta \rightarrow \gamma U$, $U \rightarrow e^+ e^-$. A signature for a U boson would be a peak in the pertinent Dalitz decay $\phi \rightarrow \eta e^+ e^-$ or $\eta \rightarrow \gamma e^+ e^-$, while the background for such searches is the standard Dalitz decay.

Finally note that there may be attractive alternatives for U boson searches which are not affected by resolving a narrow peak structure on a large conversion background: namely the C -forbidden η decays, *e.g.* the above mentioned decay $\eta \rightarrow \pi^0 e^+ e^-$ would be an ideal candidate from the background point of view.

Bibliography

- [1] A. Kupsc and A. Wirzba, arXiv:1103.3860 [hep-ph].
- [2] C. Jarlskog and E. Shabalin, *Phys. Rev.*, **D52**, 248, (1995); *Phys. Scripta*, **T99**, 23, (2002).
- [3] M. Gorchtein, arXiv:0803.2906 [hep-ph].
- [4] F. Ambrosino et al. [KLOE Collaboration], *Phys. Lett.*, **B606**, 276, (2005).
- [5] A. M. Blik et al., *Phys. Atom. Nucl.*, **70**, 693, (2007).
- [6] C. Q. Geng, J. N. Ng and T. H. Wu, *Mod. Phys. Lett.*, **A17**, 1489, (2002).
- [7] D.-N. Gao, *Mod. Phys. Lett.*, **A17**, 1583, (2002).
- [8] F. Ambrosino et al. [KLOE Collaboration], *Phys. Lett.*, **B675**, 283, (2009).
- [9] B. M. K. Nefkens, *Proc. of the Int. Conf. on Mesons and Nuclei at Intermediate Energies*, Dubna, Russia, 1994.
- [10] S. Prakhov et al. [Crystal Ball Collaboration], *Phys. Rev. Lett.*, **84**, 4802, (2000).
- [11] F.-K. Guo, B. Kubis and A. Wirzba, these proceedings.
- [12] D. Alde et al., *Z. Phys.*, **C36**, 603, (1987).
- [13] J. J. Sakurai, *Invariance Principles and Elementary Particles*, Princeton Univ. Press, 1964.
- [14] A. Aloisio et al. [KLOE Collaboration], *Phys. Lett.*, **B591**, 49, (2004).
- [15] B. M. K. Nefkens et al., *Phys. Rev.*, **C72**, 035212, (2005).
- [16] B. M. K. Nefkens et al. [Crystal Ball Collaboration], *Phys. Rev. Lett.*, **94**, 041601, (2005).
- [17] T. P. Cheng, *Phys. Rev.*, **162**, 1734, (1967).
- [18] M. R. Jane et al., *Phys. Lett.*, **B59**, 99, (1975).
- [19] F. Bergmann [for the WASA-at-COSY Collaboration], these proceedings.
- [20] F. Ambrosino et al. [KLOE Collaboration], *JHEP*, **05**, 006, (2008).
- [21] E. Abouzaid et al. [KTeV Collaboration], *Phys. Rev.*, **D75**, 012004, (2007).
- [22] A. E. Dorokhov and M. A. Ivanov, *Phys. Rev.*, **D75**, 11400, (2007); *JETP Lett.*, **87**, 531, (2008); A. E. Dorokhov, M. A. Ivanov and S. G. Kovalenko, *Phys. Lett.*, **B677**, 145, (2009).
- [23] Y. Kahn, M. Schmitt, T. M. P. Tait, *Phys. Rev.*, **D78**, 115002, (2008).
- [24] P. Fayet, *Nucl. Phys.*, **B187**, 184, (1981); *Phys. Lett.*, **B96**, 83, (1980).
- [25] C. Boehm and P. Fayet, *Nucl. Phys.*, **B683**, 219, (2004).
- [26] C. Boehm et al., *J. Phys.*, **G30**, 279, (2004); *Phys. Rev. Lett.*, **92**, 101301, (2004).
- [27] M. Berlowski et al. [CELSIUS/WASA Collaboration], *Phys. Rev.*, **D77**, 032004, (2008).
- [28] R. Abegg et al., *Phys. Rev.*, **D50**, 92, (1994).
- [29] M. Reece and L.-T. Wang, *JHEP*, **07**, 051 (2009).
- [30] P. Fayet, *Nucl. Phys.*, **B347**, 743, (1990); C. Bouchiat and P. Fayet, *Phys. Lett.*, **B608**, 87, (2005).

SEARCH FOR EXOTIC EFFECTS IN THE $\eta \rightarrow e^+e^-$ DECAY

MARCIN BERŁOWSKI*
for the WASA-at-COSY Collaboration

1.1 Introduction

The goal of the preliminary analysis is presented here the search for the very rare η meson decay $\eta \rightarrow e^+e^-$. From the experimental point of view this decay is very hard to observe due to the highly suppressed branching ratio (BR). In the Standard Model (SM) this fourth-order electromagnetic transition, predicted (see Ref. [1]) at the level of $\sim 10^{-9}$, is described by the leading order Feynman amplitude in Fig. 1.1. The branching ratio is thus suppressed with respect to the $\eta \rightarrow \gamma\gamma$ decay by:

$$BR_{theo}[\eta \rightarrow e^+e^-] \sim BR[\eta \rightarrow \gamma\gamma] \cdot \alpha^2 \cdot (m_e/m_\eta)^2,$$

where α is the fine structure constant and the $(m_e/m_\eta)^2$ dependance stems from helicity conservation [2]. Currently the best limit $BR_{exp} < 2.7 \cdot 10^{-5}$ at $CL = 90\%$ comes from the CELSIUS/WASA experiment [3] and it is five orders of magnitude bigger than the value expected from SM calculations.

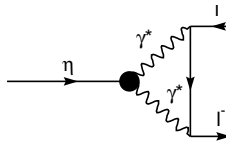


Figure 1.1: The conventional mechanism for neutral meson decay into an lepton-antilepton pair.

1.2 The $\eta \rightarrow e^+e^-$ decay as a probe of new physics

The η meson decay into an e^+e^- pair became one of the most interesting topics in low-energy hadron physics, since there is a possible admixture of non-SM processes that can enhance the BR of this decay. The most recent and very precise experimental value of $BR(\pi^0 \rightarrow e^+e^-) = (7.49 \pm 0.29 \pm 0.25) \cdot 10^{-8}$ determined by the KTeV collaboration exceeds the latest theoretical calculations from Dorokhov and collaborators [4] by 3 standard deviations. The suggestion from Kahn *et al.* [5] is that the possible explanation can be the exchange of an off-shell neutral boson U of mass $m_U \sim (10 - 100)MeV$. The U boson was previously proposed by Boehm *et al.* [6] in the light dark matter models to mediate the annihilation of a neutral scalar dark matter particle χ of (1-10) MeV mass in the reaction $\chi\chi \rightarrow e^+e^-$. This models were used as an explanation for a 511 keV line emanating from the center of the Galaxy due to excess positrons produced in this annihilation process [5]. An observation of a signal above the level predicted in the SM calculations could be evidence for an unconventional process which enhances this decay rate.

1.3 Data analysis

The experiment was performed using the WASA detector [7] at the COoler SYnchrotron COSY, located in the Forschungszentrum Jülich, Germany. The η mesons were produced in the reaction $pp \rightarrow pp\eta$ at 1.4 GeV proton beam energy. We used a special trigger in which a high energy deposit in both sides of the electromagnetic calorimeter was demanded. This type of trigger should equally favor electromagnetic decays of η mesons like $\eta \rightarrow \gamma\gamma$, $\eta \rightarrow e^+e^-\gamma$, $\eta \rightarrow e^+e^-$. Using the $\eta \rightarrow \gamma\gamma$

*National Centre for Nuclear Research, Marcin.Berlowski@fuw.edu.pl

decay channel we estimate the number of η mesons collected in the 2 week data sample to be $\sim 4.4 \cdot 10^7$. This number is approximately forty times bigger than the data sample used in the previous analysis [3]. It was found that the main sources of background are $pp \rightarrow p p \pi^+ \pi^-$ due to a 100 time larger cross section, $pp \rightarrow p(\Delta(1232) \rightarrow p[\gamma^* \rightarrow e^+ e^-])$ having the same particles in the final state as $\eta \rightarrow e^+ e^-$ and $pp \rightarrow p p(\eta \rightarrow e^+ e^- \gamma)$ due to the same final state particles if the mass of the virtual photon is large and the photon is not observed.

One of the analysis highlights, the charged particle identification by energy deposited in the electromagnetic calorimeter (SEC) is shown on the Fig. 1.2.

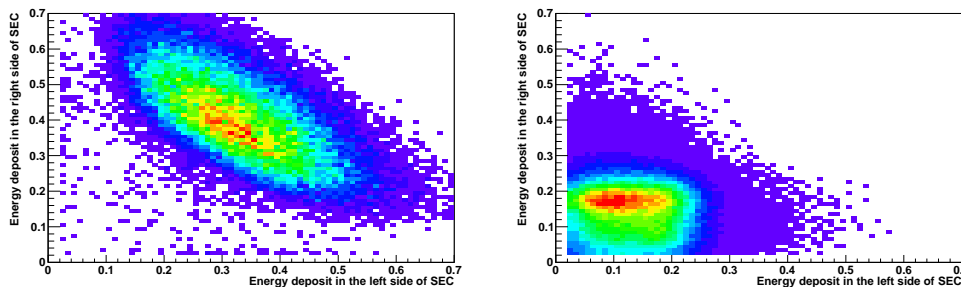


Figure 1.2: Energy deposit in each side of the electromagnetic calorimeter for: MC simulated $\eta \rightarrow e^+ e^-$ signal (left panel), MC direct production of two charged pions (right panel).

1.4 Results and conclusions

After the full data analysis we identified 182 event candidates in the entire data sample in the plot of missing mass deducted from two protons before subtracting non-eta background. At this level the Monte Carlo signal acceptance is estimated to be 4.8%. The background coming from $pp \rightarrow p p \pi^+ \pi^-$ and $pp \rightarrow p(\Delta(1232) \rightarrow p[\gamma^* \rightarrow e^+ e^-])$ is subtracted by a polynomial fit on the missing mass plot and the expected background is coming from the $\eta \rightarrow e^+ e^- \gamma$ decay channel with 5.6 ± 1.1 events. The remaining number of events after background subtraction is consistent within errors with the expected number of events coming from $\eta \rightarrow e^+ e^- \gamma$. No events of $\eta \rightarrow e^+ e^-$ corresponds to the BR upper limit better than the previously published one [3] by an order of magnitude.

Based on $\eta \rightarrow e^+ e^- \gamma$ we have proven the ability to detect and reconstruct $e^+ e^-$ pairs with different masses. At this stage of the analysis we are able to go an order of magnitude below the present limit [3] for the BR of $\eta \rightarrow e^+ e^-$ decay. Four times bigger statistics of the same reaction with the same trigger is still available for analysis. We plan an additional eight weeks of data taking using the same incident proton energy and improved experimental conditions.

This publication has been supported by the European Commission under the 7th Framework Programme through the 'Research Infrastructures' action of the 'Capacities' Programme. Call: FP7-INFRASTRUCTURES-2008-1, Grant Agreement N. 227431.

Bibliography

- [1] A.E. Dorokhov et al., *Phys. Lett.*, **B677**, 145 (2009) arXiv:hep-ph/0903.4249.
- [2] Q. Chang and Y. -D. Yang, *Phys. Lett.*, **B676**, 88, (2009) arXiv:hep-ph/0808.2933.
- [3] M. Berłowski et al., *Phys. Rev.*, **D77**, 032004, (2008) arXiv:hep-ph/0711.3531.
- [4] A.E. Dorokhov and M.A. Ivanov, *Phys. Rev.*, **D75**, 114007 (2007) arXiv:hep-ph/0704.3498.
- [5] Y. Kahn et al., *Phys. Rev.*, **D78**, 115002, (2008) arXiv:hep-ph/0712.0007.
- [6] C. Boehm and P. Fayet, *Nucl. Phys.*, **B683**, 219-263 (2004) arXiv:hep-ph/0305261.
- [7] C. Bargholtz et al., *Nucl. Instrum. Meth.*, **A594**, 339-350 2008 arXiv:nucl-ex/0803.2657.

ANALYSIS OF THE C -VIOLATING DECAY

$$\eta \rightarrow \pi^0 + \gamma^* \rightarrow \pi^0 + e^+ + e^-$$

WITH WASA-AT-COSY

FLORIAN BERGMANN*

for the WASA-at-COSY Collaboration

1.1 Introduction

The decay $\eta \rightarrow \pi^0 + \gamma^* \rightarrow \pi^0 + e^+ + e^-$ is forbidden since it violates the C -parity conservation:

$$C = C_{\pi^0} \cdot C_{\gamma^*} = (+1) \cdot (-1) = -1 \neq +1 = C_{\eta}. \quad (1.1)$$

So far this decay has not yet been observed, but an upper limit for the branching ratio has been determined in previous experiments under the assumption of a phase space distribution for the emission of the ejectiles:

$$\text{BR}(\eta \rightarrow \pi^0 + e^+ + e^-) < 4 \cdot 10^{-5}[1] \quad (1.2)$$

Recent high statistics measurements with WASA-at-COSY [2] aim at lowering the existing upper limit to test C -parity conservation with increased sensitivity. For the C -violating decay $\eta \rightarrow \pi^0 + \gamma^* \rightarrow \pi^0 + e^+ + e^-$ different decay model assumptions exist which have to be taken into account for the analysis, e.g.: decay via a virtual photon, vector meson dominance (see Fig. 1.1).

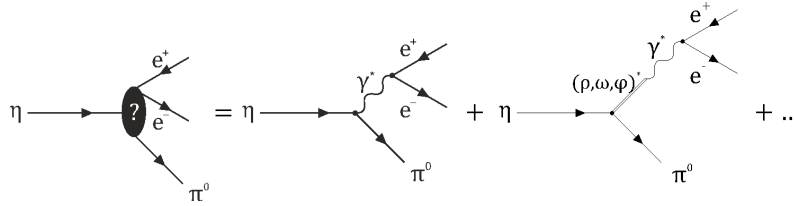


Figure 1.1: Feynman diagrams of the decay $\eta \rightarrow \pi^0 + \gamma^* \rightarrow \pi^0 + e^+ + e^-$ assuming different models.

1.2 Analysis

For the analysis two data sets are used. One with 10^7 registered $p + d \rightarrow {}^3\text{He} + \eta$ events from a beam time in 2008 and the other one with $2 \cdot 10^7$ such η -events from a beam time in 2009.

The first step in the analysis is a preselection on $p + d \rightarrow {}^3\text{He} + X$ events via ${}^3\text{He}$ identification using the ΔE - E method in the forward detector system which consists of a tracking device and an array of thin plastic scintillators. The next step is a preselection on the signature of the decay $\eta \rightarrow \pi^0 + e^+ + e^- \rightarrow \gamma + \gamma + e^+ + e^-$, requiring two neutral particles in the central detector (2γ), one positively and one negatively charged particle in the central detector (e^+ , e^-) and one charged particle in the forward detector (${}^3\text{He}$). In order to determine further selection conditions all possible background reactions like (multi-)pion production and other η -decay channels are simulated. For choosing further possible selection conditions the underlying mechanisms for the decay $\eta \rightarrow \pi^0 + e^+ + e^-$ have to be taken into account. This is illustrated in Fig. 1.2 for the invariant mass distribution of the lepton pair.

Before searching for the optimal set of cuts one has to determine the number of events from each background channel which are still left after the preselection. For this purpose the measured data (2008) has been fitted by a Monte Carlo cocktail using the same fit parameters for all differential spectra. This results in an accurate description of the data (See Fig. 1.3).

*Westfälische Wilhelms-Universität Münster, florianbergmann@uni-muenster.de

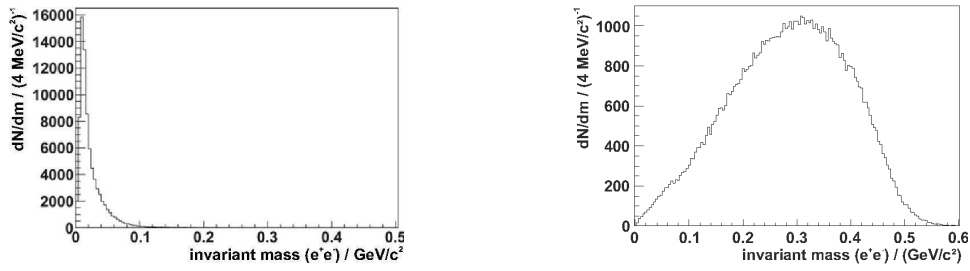


Figure 1.2: Simulated invariant mass of the lepton pair for different decay mechanisms. Left: $\eta \rightarrow \pi^0 + \gamma^* \rightarrow \pi^0 + e^+ + e^-$, right: $\eta \rightarrow \pi^0 + e^+ + e^-$; both assuming a phase space distribution. Further simulations of decay mechanisms which, e.g., consider vector meson dominance are planned.

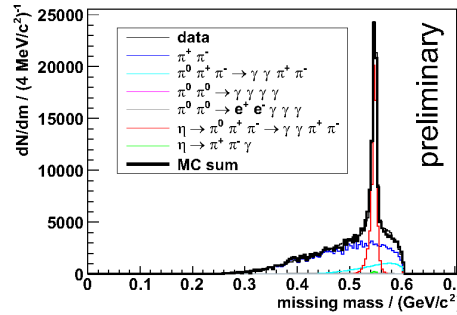


Figure 1.3: Missing mass of the measured data fitted with a Monte Carlo cocktail.

For the determination of the optimal selection conditions the evaluation function $G = S_R \cdot \frac{S_R}{B_R}$ is used for all cuts, where S_R is the relative signal and B_R the relative background after applying the cuts. Only Monte Carlo data are used to find the optimal set of cuts via varying the cuts and maximizing the evaluation function G .

1.3 Preliminary Results and Outlook

The 2008 data set has been analyzed by A. Winnemöller [3]: After applying the optimal set of cuts 9920 out of 10^6 simulated $\eta \rightarrow \pi^0 + \gamma^* \rightarrow \pi^0 + e^+ + e^-$ events remain and according to the simulations the background is reduced by a factor $1.7 \cdot 10^8$. In agreement with the simulations one event candidate remains in the measured data after applying all cuts.

Currently further $2 \cdot 10^7$ $p + d \rightarrow {}^3\text{He} + \eta$ events from 2009 are analyzed considering different model assumptions. Additionally, significantly more $p + p \rightarrow p + p + \eta$ events are available for the analysis and further $p + p \rightarrow p + p + X$ beamtimes are planned.

This publication has been supported by the European Commission under the 7th Framework Programme through the 'Research Infrastructures' action of the 'Capacities' Programme. Call: FP7-INFRASTRUCTURES-2008-1, Grant Agreement N. 227431.

Bibliography

- [1] K. Nakamura et al., *Review of Particle Physics. Journal of Physics G: Nuclear and Particle Physics*, 37(075021):186, (2010).
- [2] H.-H. Adam et al. (WASA-at-COSY Collaboration), *arXiv:nucl-ex/0411038*
- [3] A. Winnemöller, *PhD thesis, Westfälische Wilhelms-Universität Münster*, (2011).

THEORETICAL PERSPECTIVES ON $\eta, \eta' \rightarrow 4\pi$ DECAYS

FENG-KUN GUO^{*}, BASTIAN KUBIS^{*†} AND ANDREAS WIRZBA[‡]

1.1 Introduction: anomalous processes

Processes in low-energy QCD that involve an odd number of (pseudo-)Goldstone bosons (and possibly photons), which are, therefore, of odd intrinsic parity, are thought to be governed by the Wess–Zumino–Witten term [1] via chiral anomalies. While the so-called triangle- and box-anomaly terms are well-tested in processes such as e.g. $\pi^0, \eta \rightarrow \gamma\gamma$ (triangle) or $\gamma\pi \rightarrow \pi\pi, \eta \rightarrow \pi\pi\gamma$ (box), the pentagon-anomaly remains more elusive; the simplest possible process that is usually cited is $K^+K^- \rightarrow \pi^+\pi^-\pi^0$, which however has not been experimentally tested yet. A different set of processes involving five light pseudoscalars are the four-pion decays of η and η' . Experimental information about these is also scarce, only upper limits on branching ratios exist [2]; however, this may change in the near future for at least some of the possible final states.

In principle, the decays $\eta' \rightarrow 4\pi$ seem not terribly forbidden by approximate symmetries: they are neither isospin-forbidden, nor electromagnetic. $\eta \rightarrow 4\pi$, in contrast, is essentially suppressed by tiny phase space: only the decay into $4\pi^0$ is kinematically allowed ($M_\eta - 4M_{\pi^0} = 7.9$ MeV, $M_\eta - 2(M_{\pi^\pm} + M_{\pi^0}) = -1.2$ MeV). The fact that anomalous amplitudes always involve the totally antisymmetric tensor $\epsilon_{\mu\nu\alpha\beta}$ furthermore shows that no two pseudoscalars are allowed to be in a relative S-wave; the decays $\eta' \rightarrow 2(\pi^+\pi^-)$ and $\eta' \rightarrow \pi^+\pi^-2\pi^0$ are therefore P-wave-dominated. As furthermore Bose symmetry forbids $2\pi^0$ to be in an odd partial wave, $\eta' \rightarrow 4\pi^0$ and $\eta \rightarrow 4\pi^0$ even require all π^0 to be at least in relative D-waves [3]. This, combined with the tiny phase space available, leads to the notion of $\eta \rightarrow 4\pi^0$ being CP-forbidden [2], although strictly-speaking it is only S-wave CP-forbidden.

1.2 Charged final states: $\eta' \rightarrow 2(\pi^+\pi^-), \eta' \rightarrow \pi^+\pi^-2\pi^0$

In the following, we assume the standard $\eta\eta'$ mixing in terms of singlet (η_0) and octet (η_8) states, i.e. $|\eta\rangle = 1/3|\eta_0\rangle + 2\sqrt{2}/3|\eta_8\rangle$, $|\eta'\rangle = 2\sqrt{2}/3|\eta_0\rangle - 1/3|\eta_8\rangle$. The flavor structure of the chiral anomaly does not allow for direct contributions of the Wess–Zumino–Witten term to the decays $\eta, \eta' \rightarrow 4\pi$. The leading amplitude to the two channels involving charged pions in the final state occurs at one loop or $\mathcal{O}(p^6)$ in terms of chiral power counting, and is given as the sum of kaon loops and local counterterms, see Fig. 1.1. For instance, the decay amplitude for $\eta_8 \rightarrow \pi^+(p_1)\pi^-(p_2)\pi^+(p_3)\pi^-(p_4)$ is given by [4]

$$\begin{aligned} \mathcal{A}(\eta_8 \rightarrow \pi^+\pi^-\pi^+\pi^-) &= \frac{N_c \epsilon_{\mu\nu\alpha\beta}}{3\sqrt{3}F_\pi^5} p_1^\mu p_2^\nu p_3^\alpha p_4^\beta [F_8(s_{12}) + F_8(s_{34}) - F_8(s_{14}) - F_8(s_{23})] , \\ F_8(s) &= \frac{1}{8\pi^2 F_\pi^2} \left\{ (s - 4M_K^2) \bar{J}_{KK}(s) - \frac{s}{16\pi^2} \left(2 \log \frac{M_K}{\mu} + \frac{1}{3} \right) \right\} - 16C_{12}^{Wr}(\mu)s , \\ \bar{J}_{KK}(s) &= \frac{1}{8\pi^2} \{ 1 - \sigma_K \operatorname{arccot} \sigma_K \} , \quad \sigma_K = \sqrt{\frac{4M_K^2}{s} - 1} , \end{aligned} \quad (1.1)$$

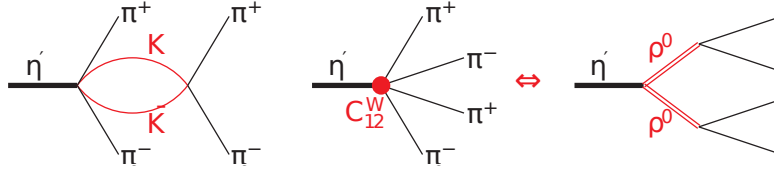
where $s_{ij} = (p_i + p_j)^2$. The corresponding η_0 amplitude consists of local contributions only. The scale dependence of the counterterm C_{12}^{Wr} is known [5] and cancels the one of the loop contribution. $\eta_8 \rightarrow \pi^+(p_1)\pi^0(p_2)\pi^-(p_3)\pi^0(p_4)$ is given by the same amplitude Eq. (1.1) up to a sign.

In order to estimate the finite part of the coupling constant C_{12}^{Wr} , we resort to resonance saturation. While this has been studied in a more general setting recently [6], we employ the hidden-local-symmetry (HLS) formalism to calculate vector-meson contributions, see Fig. 1.1. We

^{*}Helmholtz-Institut für Strahlen- und Kernphysik and Bethe Center for Theoretical Physics, Universität Bonn

[†]kubis@hiskp.uni-bonn.de

[‡]Institute for Advanced Simulation and Jülich Center for Hadron Physics, Forschungszentrum Jülich

Figure 1.1: Feynman graphs contributing to $\eta' \rightarrow 2(\pi^+\pi^-)$.

only need two (combinations of) coupling constants occurring in the anomalous sector [7], $c_1 - c_2$ and c_3 . The two chiral constants contributing to five-pseudoscalar amplitudes at $\mathcal{O}(p^6)$ (only one of them contributes to $\eta' \rightarrow 4\pi$) are given in terms of these by

$$C_1^{Wr}(M_\rho) = -2C_{12}^{Wr}(M_\rho) = \frac{3(c_1 - c_2 + c_3)}{128\pi^2 M_\rho^2}. \quad (1.2)$$

The HLS couplings are often assumed to be given roughly by $c_1 - c_2 \approx c_3 \approx 1$. A more extensive phenomenological study finds $c_1 - c_2 \approx 1.21$, $c_3 \approx 0.93$ [8]. Comparing the relative importance of counterterm (=vector-meson) contributions to kaon loops in Eq. (1.1), we find that the decay amplitude is entirely dominated by the vector-meson terms. Furthermore, as the maximum allowed kinematical range in $\eta' \rightarrow 4\pi$ is $\sqrt{s_{ij}} \leq M_{\eta'} - 2M_\pi \approx 680$ MeV, it is necessary to retain the full ρ propagators for a phenomenologically reliable description. This, at the same time, takes care of the essential P-wave $\pi\pi$ final-state interactions.

We calculate the branching ratios as functions of the HLS couplings, before inserting the two sets of numerical values quoted above. In the isospin limit, $2 \times \text{BR}(\eta' \rightarrow 2(\pi^+\pi^-)) = \text{BR}(\eta' \rightarrow \pi^+\pi^-2\pi^0)$; we adjust for the correct phase space by using the pion masses M_{π^\pm} and $(M_{\pi^\pm} + M_{\pi^0})/2$, respectively. We find

$$\begin{aligned} \text{BR}(\eta' \rightarrow 2(\pi^+\pi^-)) &= [0.15(c_1 - c_2)^2 + 0.46(c_1 - c_2)c_3 + 0.37c_3^2] \times 10^{-4} = \{0.97, 1.04\} \times 10^{-4}, \\ \text{BR}(\eta' \rightarrow \pi^+\pi^-2\pi^0) &= [0.34(c_1 - c_2)^2 + 1.07(c_1 - c_2)c_3 + 0.85c_3^2] \times 10^{-4} = \{2.26, 2.44\} \times 10^{-4}. \end{aligned} \quad (1.3)$$

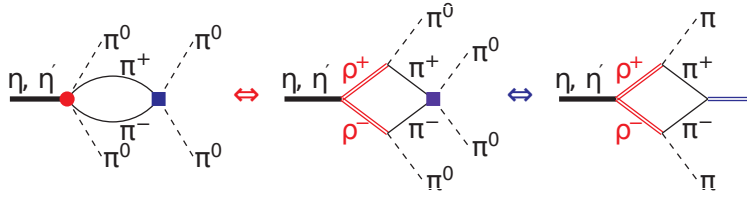
These numbers are to be compared to the available experimental upper limits, $\text{BR}(\eta' \rightarrow 2(\pi^+\pi^-)) < 2.4 \times 10^{-4}$ and $\text{BR}(\eta' \rightarrow \pi^+\pi^-2\pi^0) < 2.6 \times 10^{-3}$ [2].

1.3 Neutral final states: $\eta' \rightarrow 4\pi^0$, $\eta \rightarrow 4\pi^0$

As we have mentioned in the introduction, the P-wave mechanism described in the previous section, proceeding essentially via two ρ intermediate resonances, cannot contribute to the $4\pi^0$ final states. In fact, we can show that the D-wave characteristic of $\eta, \eta' \rightarrow 4\pi^0$ suppresses these decays to $\mathcal{O}(p^{10})$ in chiral power counting, that is to the level of three loops in the anomalous sector. This is in particular due to the flavor and isospin structure of the anomaly, which does not contain five-meson vertices including $2\pi^0$ at leading order ($\mathcal{O}(p^4)$), and to the chiral structure of meson-meson scattering amplitudes, which only allows for S- and P-waves at tree level ($\mathcal{O}(p^2)$). As a complete three-loop calculation would be a formidable task and is beyond the scope of our exploratory study, we instead construct a decay mechanism that, we believe, ought to capture at least the correct order of magnitude. This is built on the observation that we *can* calculate the leading imaginary part of the decay amplitude at $\mathcal{O}(p^{10})$, which is given by a $\pi^+\pi^-$ intermediate state, see Fig. 1.2. As indicated, we thereby insert the full vector-meson amplitude for $\eta, \eta' \rightarrow \pi^+\pi^-2\pi^0$ described in the previous section. We then reconstruct the “full” D-wave $\pi\pi$ final-state amplitude by requiring that it is proportional to the Omnès function $\Omega_2^0(s)$ (assuming dominance of isospin $I = 0$), which near threshold behaves like

$$\text{Im} \Omega_2^0(s) \approx \sqrt{1 - \frac{4M_\pi^2}{s}} \times t_2^0(s), \quad (1.4)$$

where t_2^0 is the appropriate $\pi\pi$ partial wave of isospin $I = 0$ and angular momentum $\ell = 2$. Well above threshold, however, the Omnès function can well be approximated by the $f_2(1270)$ resonance, $\Omega_2^0(s) \approx M_{f_2}^2 / (M_{f_2}^2 - s)$. The resulting decay mechanism is indicated in Fig. 1.2. Note

Figure 1.2: D-wave mechanism for $\eta, \eta' \rightarrow 4\pi^0$.

that it is far from a real f_2 dominance picture, as the ρ is not “short-ranged” on the scale of the f_2 mass. For the branching ratios, we find

$$\begin{aligned} \text{BR}(\eta' \rightarrow 4\pi^0) &= [0.4(c_1 - c_2)^2 + 1.6(c_1 - c_2)c_3 + 1.6c_3^2] \times 10^{-8} = \{3.6, 3.8\} \times 10^{-8}, \\ \text{BR}(\eta \rightarrow 4\pi^0) &= [0.3(c_1 - c_2)^2 + 1.0(c_1 - c_2)c_3 + 1.0c_3^2] \times 10^{-30} = \{2.4, 2.5\} \times 10^{-30}. \end{aligned} \quad (1.5)$$

While the D-wave mechanism therefore suppresses the decay $\eta' \rightarrow 4\pi^0$ by 3–4 orders of magnitude compared to the charged final states, the suppression of $\eta \rightarrow 4\pi^0$ due to the combination of D-wave and tiny phase space is enormous, and any experimental signal for this channel could indeed be interpreted as a sign of CP violation.

1.4 CP violation through the QCD θ -term

One possible source of strong CP violation is the so-called QCD θ -term, linked to the $U(1)_A$ anomaly, that can also be treated on an effective-Lagrangian level [9]. It induces effects such as an electric dipole moment of the neutron, and also allows for the decay $\eta \rightarrow 2\pi$. In addition, it induces a CP-violating S-wave mechanism for the decay $\eta \rightarrow 4\pi^0$ [4],

$$\mathcal{A}(\eta \xrightarrow{\text{CP}} 4\pi^0) = -\sqrt{\frac{2}{3}} \frac{M_{\eta'}^2}{3F_\pi^3} \times \bar{\theta}_0. \quad (1.6)$$

The resulting branching ratio is given by

$$\text{BR}(\eta \xrightarrow{\text{CP}} 4\pi^0) = 5.2 \times 10^{-5} \times \bar{\theta}_0^2, \quad (1.7)$$

which, were $\bar{\theta}_0$ a quantity of natural size, would demonstrate the enhancement of the CP-violating S-wave mechanism compared to the CP-conserving D-wave one, see Eq. (1.5). However, current limits from neutron electric dipole moment measurements suggest $\bar{\theta}_0 \lesssim 10^{-11}$ [10], which puts also this result beyond any experimental reach.

Bibliography

- [1] J. Wess, B. Zumino, *Phys. Lett.* **B37**, 95 (1971); E. Witten, *Nucl. Phys.* **B223**, 422 (1983).
- [2] K. Nakamura *et al.* [Particle Data Group], *J. Phys.* **G37**, 075021 (2010).
- [3] A. Kupść, A. Wirzba, arXiv:1103.3860 [hep-ph].
- [4] F.-K. Guo, B. Kubis, A. Wirzba, arXiv:1111.5949 [hep-ph].
- [5] J. Bijnens, L. Girlanda, P. Talavera, *Eur. Phys. J.* **C23**, 539 (2002) [arXiv:hep-ph/0110400].
- [6] K. Kampf, J. Novotný, *Phys. Rev.* **D84**, 014036 (2011) [arXiv:1104.3137 [hep-ph]].
- [7] T. Fujiwara, T. Kugo, H. Terao, S. Uehara, K. Yamawaki, *Prog. Theor. Phys.* **73**, 926 (1985); M. Bando, T. Kugo, K. Yamawaki, *Phys. Rept.* **164**, 217 (1988).
- [8] M. Benayoun, P. David, L. DelBuono, O. Leitner, *Eur. Phys. J.* **C65**, 211 (2010) [arXiv:0907.4047 [hep-ph]].
- [9] R. J. Crewther, P. Di Vecchia, G. Veneziano, E. Witten, *Phys. Lett.* **B88**, 123 (1979) [Erratum-ibid. **B91**, 487 (1980)]; A. Pich, E. de Rafael, *Nucl. Phys.* **B367**, 313 (1991).
- [10] K. Ottnad, B. Kubis, U.-G. Meißner, F.-K. Guo, *Phys. Lett.* **B687**, 42 (2010) [arXiv:0911.3981 [hep-ph]].

PLUTO: A MULTI-PURPOSE EVENT GENERATOR FRAMEWORK FOR RARE η DECAYS

*INGO FRÖHLICH**

1.1 Introduction

In this contribution, the new design and recent developments of the simulation package Pluto [1] have been presented. Pluto's main mission is to offer a modular framework with an object-oriented structure, thereby making additions such as new particles, decays of resonances, new models up to modules for entire changes easily applicable [2]. Overall consistency is ensured by a plugin- and distribution manager. Particular features are the support of a modular structure for physics process descriptions, and the possibility to access the particle stream for in-line modifications. Additional configurations can be attached by the user by a dedicated script language ("PlutoScript") without re-compiling the package, which makes Pluto extremely configurable.

1.2 Rare η decays

The rare η decays have been implemented into Pluto via means of a dedicated "plugin". This ensures that changes introduced by the new implementation do not affect simulations done by other users.

The models follow basically calculations done by Wirzba and Petri [3], but leaving out tiny effects like magnetic form factors.

1.2.1 $\eta \rightarrow e^+e^-e^+e^-$

This decay implementation is done via two virtual photons:

```

PReaction my_reaction("_T1=2.2","p","d",
    "He3 eta[dilepton [e+ e-] dilepton [e+ e-]]");

```

In the first step of the event generation Pluto samples the mass of the 2 dileptons. This is very similar to the implementation of the η Dalitz decay of the base package. The shape of the dilepton spectrum is based on an implementation provided by A. Kupsc [4].

In a second step, the angular distributions are sampled via the rejection method. This can be done as the correction is only about 20%, which means that only a small fraction of events have to be resampled. Moreover, the angular distributions of the "simple" generator are isotropic and therefore equally populated.

1.2.2 $\eta \rightarrow \pi^+\pi^-e^+e^-$

This decay implementation uses the a "genbod" technique: Here, the first step of the 4-body decay is done via a modified genbod algorithm, where the mass distribution $M(q^2) = F(q^2)/(8 \cdot q^2)$ is folded into the genbod model (with q as the four-momentum of the virtual photon). This is done, because a generation of events in a 4-body space is numerically difficult and would result in large computing times. On the other hand, a pure rejection method (using an unmodified genbod), as in the previous case, is not possible, because the pole of $M(q^2)$ is located in a region where no events are generated by genbod.

For the form factor by default a "simple VMD model" is used:

$$F(q^2) = m_v^2 / (m_v^2 - q^2) \tag{1.1}$$

*Goethe-Universität Frankfurt, Froehlich@physik.uni-frankfurt.de

with $m_\nu = 0.77\text{GeV}$.

In total, the following matrix element is used:

$$A^2 = M(q^2) * s_{\pi\pi} * \beta_\pi^2 \sin^2(\theta_\pi) * \lambda(m_\nu^2, s_{\pi\pi}, q^2) (1 + \beta_e^2 * \sin^2(\theta_e) * \sin^2(\phi)) \quad (1.2)$$

with $s_{\pi\pi}$ as the invariant mass of the pion pair, and the factor $\beta_x = \sqrt{1 - \frac{4m_x^2}{s_{xx}}}$. In the case of the dilepton pair, s_{ee} is the invariant mass of the virtual photon.

1.3 Scripting with Pluto

The idea behind scripting with Pluto is to combine objects like histograms and ntuples via a flexible batch language with the main event loop, model objects, and the internal data base of Pluto. The commands of the batch script are compiled by Pluto in advance and can be executed as often as required without additional delay. This execution can be done inside the event loop which allows for modifications of particles, e.g. to write acceptance filters or include smearing effects.

Furthermore, it is also possible to call many public available Pluto-methods of the utility class (for random sampling) and all methods of the Pluto particle class, which is inherited from TLorentzVector. As the script can combine ROOT-objects (histograms and ntuples) with the event loop, particle properties can be converted very quickly to histograms and ntuples. And finally, the script can be packed together with acceptance and resolution matrices to form a universal, common format for a detector description.

1.4 Examples

Finally, the application of the script method is discussed. Exchanging, e.g., the widely discussed ω form factor is a quite simple action¹:

```
PSimpleVMDFF *ff = new PSimpleVMDFF("vmd_ff_dd@w_to_dilepton_pi0/formfactor",
                                     "VMD form factor",-1);
ff->AddEquation("_ff2 = 0.17918225/( (0.4225- _q2)*(0.4225- _q2) + 0.000676)");
makeDistributionManager()->Add(ff);
```

The basic syntax is based on the ROOT TFormula class, but with a lot of extensions. For details, reference is made to the full manual which is available at the Pluto web page [1].

Considering, that the form factor model of rate eta decays is a separated model, the form factor can be read via:

```
PSimpleVMDFF *ff = (PSimpleVMDFF*)makeDistributionManager()->
  GetDistribution("eta_ee_pipi_vmd_ff");
```

and therefore exchanged via similar means

Bibliography

- [1] www-hades.gsi.de/pluto
- [2] I. Fröhlich *et al.*, PoS **ACAT2007** (2007) 076 [arXiv:0708.2382 [nucl-ex]]; I. Fröhlich, T. Galatyuk, R. Holzmann, J. Markert, B. Ramstein, P. Salabura and J. Stroth, J. Phys. Conf. Ser. **219** (2010) 032039 [arXiv:0905.2568 [nucl-ex]].
- [3] A. Wirzba and T. Petri, internal report, Jülich (2009) and priv. comm.
- [4] A. Kupsc, priv. comm.

¹This is, just to keep it to be an example, the old form factor of Landsberg.

DALITZ PLOT ANALYSIS FOR $\eta \rightarrow \pi^+\pi^-\pi^0$ AT KLOE

LI CALDEIRA BALKESTÅHL*
on behalf of the KLOE-2 Collaboration

1.1 Theoretical Motivation

The decay $\eta \rightarrow \pi^+\pi^-\pi^0$ is an isospin-violating process sensitive to the light quark mass double ratio:

$$Q^2 = \frac{m_s^2 - \hat{m}^2}{m_d^2 - m_u^2}, \text{ where } \hat{m} = \frac{1}{2}(m_d + m_u) \quad (1.1)$$

The $\eta \rightarrow \pi^+\pi^-\pi^0$ decay rate is proportional to Q^{-4} and it has been calculated at leading order (LO) and next-to-leading order (NLO) in χ PT. The values obtained, $\Gamma_{LO} \sim 70$ eV and $\Gamma_{NLO} = 160 \pm 50$ eV, are significantly lower than the experimental value $\Gamma_{exp} = 296 \pm 16$ eV, obtained from a fit to all the available data [1]. The difference between LO and NLO calculations and the discrepancy with data at NLO are evidence of the slow convergence of the χ PT series, due to strong pion rescattering effects in the final state. These effects can be treated by means of dispersion relations as recently proposed in Ref. [2]. The relations contain four parameters to be fixed either matching the LO χ PT results or by a fit to experimental data. Using the first approach G. Colangelo and coauthors [2] obtained $Q = 22.3 \pm 0.4$, in good agreement with most of the results presented in Fig. 1.1, where the gray elliptic band corresponds to the 2- σ range of the Q -value above. Other plotted constraints come from lattice calculations.

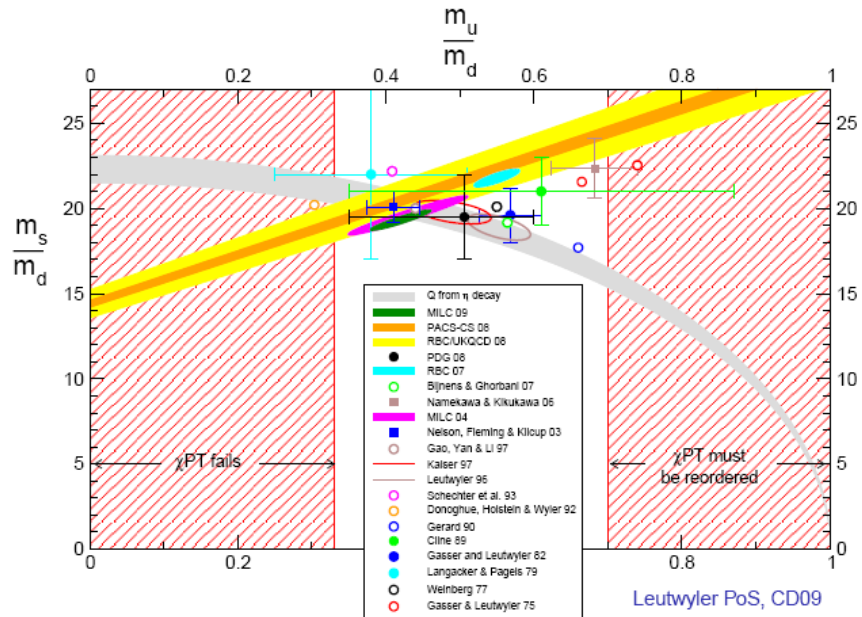


Figure 1.1: Ratio of the light quark masses. The gray band corresponds to $Q = 22.3 \pm 0.8$ [3].

*Department of Physics and Astronomy, Uppsala University, li.caldeira_balkestahl@physics.uu.se

1.2 Data analysis

The KLOE detector, at the DAΦNE collider, consists of a large volume drift chamber and a lead-scintillating fibers calorimeter. The detector usually takes data at the ϕ -meson peak ($\sqrt{s} = 1.019$ GeV). The experiment took data in years 2001-2002 and 2004-2006, integrating a total luminosity 2.5 fb^{-1} at the ϕ -peak and 240 pb^{-1} at the center-of-mass energy of 1 GeV. KLOE-2 has been approved to collect $\sim 20 \text{ fb}^{-1}$ in 3-4 years of data taking at the upgraded DAΦNE facility, which is expected to operate with a factor ~ 3 improvement in luminosity.

The KLOE collaboration published the Dalitz plot analysis of the $\eta \rightarrow \pi^+\pi^-\pi^0$ decay in year 2008 [4]. In the paper, based on $\sim 500 \text{ pb}^{-1}$ of integrated luminosity, the Dalitz plot density shown in Fig. 1.2 was fitted by:

$$|A(X, Y)|^2 \simeq 1 + aY + bY^2 + cX + dX^2 + eXY + fY^3 + gX^3 + hX^2Y + lXY^2 \quad (1.2)$$

obtaining:

$$a = -1.090 \pm 0.005(\text{stat})_{-0.019}^{+0.008}(\text{sys}) \quad b = 0.124 \pm 0.006(\text{stat}) \pm 0.010(\text{sys})$$

$$d = 0.057 \pm 0.006(\text{stat})_{-0.016}^{+0.007}(\text{sys}) \quad f = 0.14 \pm 0.01(\text{stat}) \pm 0.02(\text{sys})$$

and the other parameters consistent with zero. The c and e parameters are expected to be zero from C-invariance.

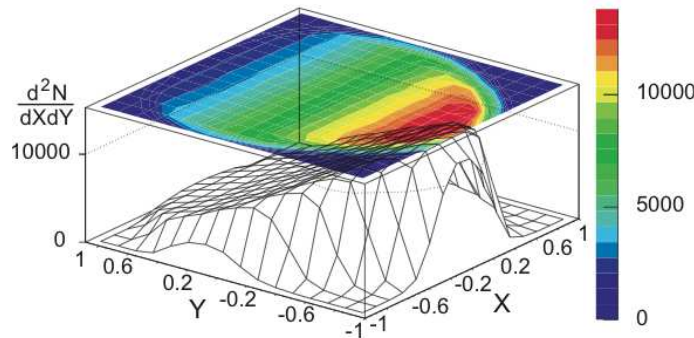


Figure 1.2: Dalitz plot density measured by KLOE[4] on the basis of $\sim 500 \text{ pb}^{-1}$ integrated luminosity.

The results have been recently used by S. Lanz and coworkers to fix the parameters of the dispersion relations in the framework of the analysis presented in Ref. [2]. The resulting Q -value is $Q = 21.31 \pm 0.60$ [5] and the Dalitz plot density obtained is in better agreement with the measurement performed on the $\eta \rightarrow \pi^0\pi^0\pi^0$ sample [6] than previous calculations based on the matching of the dispersion-relation parameters with one-loop χ PT results. The KLOE results have also been used in analytic dispersive analysis [7] for the value of R ($R = \frac{m_s - \hat{m}_i}{m_d - m_u}$), both in a direct fit to the results, and in a correction to χ PT NNLO low energy constants.

More data on $\eta \rightarrow \pi^+\pi^-\pi^0$ are needed to understand the origin of the residual tension between data and theoretical calculations, concerning both, the comparison between neutral and charged channel, and the Q -value.

On the experimental side, a new analysis of the $\eta \rightarrow \pi^+\pi^-\pi^0$ sample (Fig. 1.3) is in progress to improve on the statistical sample and to overcome some limitations of the previous analysis. For the latter, the selection efficiency is measured directly from minimum bias events, while in the old analysis it was evaluated from Monte Carlo simulation, giving a large contribution to the systematics. Further improvement on the precision of the Dalitz plot distribution is expected: *i*) replacing the kinematical fit, requiring 4-momentum conservation and the speed of light for photons, with constraints from the two-body ϕ decay kinematics; *ii*) eliminating the request of vertex reconstruction and the cut on the total number of tracks in drift chamber; *iii*) introducing the particle identification via time-of-flight measurement with the calorimeter; *iv*) performing the analysis on an independent, larger data sample.

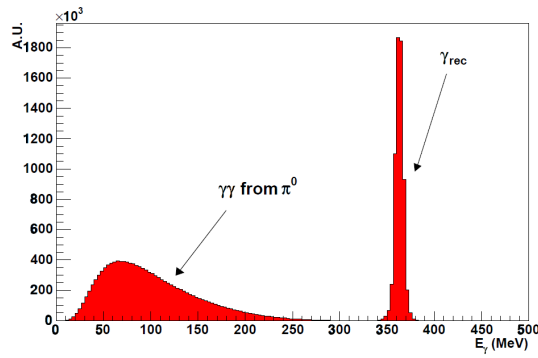


Figure 1.3: Energy distribution of the photons from $\phi \rightarrow \eta\gamma \rightarrow \pi^+\pi^-\gamma\gamma$.

Bibliography

- [1] K. Nakamura et al. (Particle Data Group), *Journal of Physics G***37**, 075021 (2010).
- [2] G. Colangelo, S. Lanz and E. Passemar *Proceedings of Science*, arXiv:0910.0765 (2009).
- [3] H. Leutwyler, *Proceedings of Science*, arXiv:0911.1416 (2009).
- [4] Ambrosino *et al.* (The KLOE collaboration), *JHEP*, **Vol 5**, page 006, arXiv:1102.4999 (2008).
- [5] S. Lanz, “Berne-Lund-Valencia Dispersive Treatment of $\eta \rightarrow 3\pi$ ”, talk at International PrimeNet Workshop, Jülich, September 26-28 2011, and contribution to these Proceedings.
- [6] Ambrosino *et al.* (The KLOE collaboration), *Phys. Lett. B*, **Vol 694**, page 16, arXiv:1004.1319 (2010).
- [7] M. Zdrahal, “Prague-Lund-Marseille Dispersive Treatment of $\eta \rightarrow 3\pi$ ”, talk at International PrimeNet Workshop, Jülich, September 26-28 2011, and contribution to these Proceedings.

THE $\eta \rightarrow \pi^+ \pi^- \pi^0$ DECAY WITH WASA-at-COSY

PATRIK ADLARSON*

for the WASA-at-COSY Collaboration

1.1 Introduction

The decay $\eta \rightarrow \pi^+ \pi^- \pi^0$ is important since it allows access to light quark mass ratios. Since electromagnetic corrections are small [1, 2] this decay is a probe for the strong isospin violation. The calculated tree level decay width, $\Gamma_{tree} \approx 70$ eV [3], deviates more than a factor of four from the PDG value $\Gamma = 296 \pm 16$ [4]. Higher order diagrams are needed which take into account $\pi\pi$ final state interactions [5, 6, 7]. Alternatively, $\pi\pi$ final state re-scattering can be implemented in dispersive approaches [8, 9, 10, 11, 12] as well as other approaches [13]. The decay width scales as

$$\Gamma = \left(\frac{Q_D}{Q} \right)^4 \bar{\Gamma}, \quad (1.1)$$

where $Q^2 = (m_s^2 - \hat{m}^2)/(m_d^2 - m_u^2)$, $\hat{m} = \frac{1}{2}(m_u + m_d)$, and the decay width $\bar{\Gamma}$ and $Q_D = 24.2$ are calculated in the Dashen limit [14]. Q gives access to light quark mass ratios. The ratios serve also as an important input for lattice QCD [15]. To derive Q , $\bar{\Gamma}$ has to be known reliably from theory which can be tested by comparing with the experimental Dalitz plot distributions. As Dalitz plot variables

$$x = \sqrt{3} \frac{T_+ - T_-}{Q_\eta}, \quad y = \frac{3T_0}{Q_\eta} - 1. \quad (1.2)$$

are used. Here T_+ , T_- and T_0 denote the kinetic energies of π^+ , π^- and π^0 in the η rest frame, and Q_η is the sum of the three kinetic energies. The standard way to parametrize the Dalitz plot density is a polynomial expansion around $x = y = 0$

$$|A(x, y)|^2 \propto 1 + ay + by^2 + dx^2 + fy^3 + gx^2y + \dots \quad (1.3)$$

where a, b, \dots, g are called the Dalitz Plot parameters. The most precise experimental result is based on a Dalitz plot containing $1.34 \cdot 10^6$ events obtained by KLOE [16]. Parameters b and f in [16] deviate significantly from ChPT predictions. Independent measurements are therefore important and WASA-at-COSY [17] aims at providing two independent data sets with η produced in pp and pd reactions.

1.2 Experiment

In 2008 and 2009 WASA-at-COSY collected $1 \cdot 10^7$ and $2 \cdot 10^7$ η mesons respectively, in the reaction $pd \rightarrow {}^3\text{He}X$ at a kinetic beam energy of 1 GeV. The missing mass with respect to ${}^3\text{He}$ is used to tag the η in the reaction $pd \rightarrow {}^3\text{He}X$. To obtain $\eta \rightarrow \pi^+ \pi^- \pi^0$ candidates, at least two particles of opposite charge and at least two photons with an invariant mass close to π^0 are required. To further reduce time coincidental events, cuts on vertices and timing requirements are included. To reduce background channels, mainly coming from $pd \rightarrow {}^3\text{He}\pi\pi$ reactions, conditions on the missing mass calculated for ${}^3\text{He}\pi^+\pi^-$, ${}^3\text{He}\pi^0$ and $\pi^+\pi^-$ are applied. The preliminary analysis gives 260 000 $\eta \rightarrow \pi^+ \pi^- \pi^0$ candidates from the 2008 data sample. The majority of the events populating the Dalitz plot is ${}^3\text{He}\pi^+\pi^- \pi^0$ and $\eta \rightarrow \pi^+ \pi^- \pi^0$. The η content in each Dalitz plot bin is obtained by performing a four-degree polynomial fit over the direct 3π background and the fitted polynomial is subtracted from the signal region. The number of η events in each bin is corrected for acceptance.

*Institute for Physics and Astronomy, Uppsala University, Uppsala, 751 20, Sweden, patrik.adlarson@fysast.uu.se

1.3 Result

The preliminary acceptance corrected experimental results with statistical errors for the x , y projections of the Dalitz plot are compared in Fig. 1.1 to the distributions of the $\eta \rightarrow \pi^+\pi^-\pi^0$ with Monte Carlo weighted with the set of Dalitz plot parameters calculated for the leading order (LO) in ChPT (solid blue line), next-to-next-to-leading order (NNLO) (dashed-dotted green line) and the central values obtained by KLOE (dashed red line). The Monte Carlo results have been normalized to the WASA experimental data. From the preliminary Dalitz plot projections the WASA data points are in reasonable agreement with the KLOE experimental result. The work on the pd data will be continued in order to obtain the Dalitz plot parameters for $\eta \rightarrow \pi^+\pi^-\pi^0$. An effort will be made to understand the systematical effects.

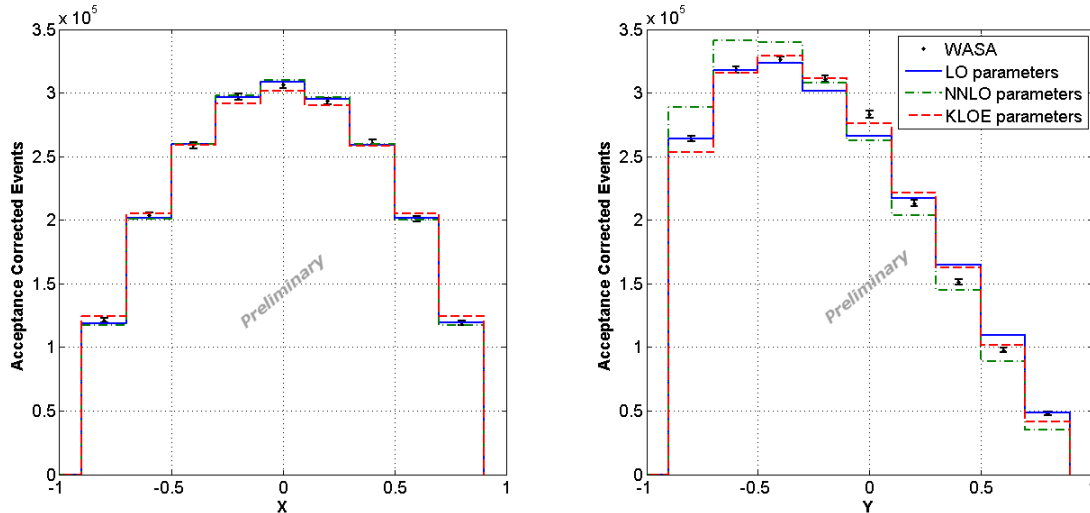


Figure 1.1: Acceptance corrected data points with statistical errors, projected on x (**left**) and y (**right**), compared to Monte Carlo weighted with the Dalitz plot parameters for the leading order calculation (LO) in ChPT (solid blue line), next-to-next-to-leading order (NNLO) (dashed-dotted green line) and the central values obtained by KLOE (dashed red line). The Monte Carlo results are normalized to the experimental data.

Acknowledgements

This publication has been supported by the European Commission under the 7th Framework Programme through the 'Research Infrastructures' action of the 'Capacities' Programme. Call: FP7-INFRASTRUCTURES-2008-1, Grant Agreement N. 227431.

Bibliography

- [1] D.G. Sutherland, *Phys Lett* **23**, 384, (1966).
- [2] C. Ditsche, B. Kubis, U-G. Meißner, arXiv:0910.0210v1 [hep-ph], (2009)
- [3] W.A. Bardeen, *et al.*, *Phys Rev Lett* **18**, 1170, (1967).
- [4] K.Nakamura *et al.*, *J Phys G* **37**, 075021, (2010).
- [5] C. Roiesnel, T. Truong, *Nucl Phys B* **187**, 293, (1981).
- [6] J. Gasser, H. Leutwyler, *Nucl Phys B* **250**, 539, (1985) .
- [7] J.Bijnens, K.Ghorbani, *JHEP* **11**, 030, (2007).
- [8] A.Anisovich, H.Leutwyler, *Phys Lett B* **375**, 335, (1996).

- [9] J.Kambor, C.Wiesendanger, D.Wyler, *Nucl Phys B* **465**, 215, (1996).
- [10] J.Bijnens, J.Gasser, *Phys Scripta* **T99**, 34, (2002).
- [11] G.Colangelo, S.Lanz, E.Passemar, *PoS CD09* **047**,(2009), arXiv:0910.0765v1 [hep-ph].
- [12] K.Kampf, M.Knecht, J.Novotný, M.Zdráhal, arXiv:1103.0982v1 [hep-ph] (2011).
- [13] S.P. Schneider, B.Kubis, C.Ditsche, *JHEP* **1102**, 028, 201 (2011), arXiv:1010.3946v2.
- [14] R. Dashen, *Phys Rev* **183**, 1245, (1969).
- [15] G.Colangelo, *et al.*, arXiv:1011.4408v2 [hep-lat], (2010).
- [16] F. Ambrosini *et al* (KLOE Collab.), *JHEP* **05**, 006, (2008).
- [17] H. H. Adam *et al.*, arXiv:0411038 [nucl-ex] (2004).

BERNE-LUND-VALENCIA

DISPERSIVE TREATMENT OF $\eta \rightarrow 3\pi$ *

STEFAN LANZ[†]

The decay $\eta \rightarrow 3\pi$ is of particular theoretical interest because it can only proceed through isospin breaking. If the strongly suppressed electromagnetic contributions are neglected, the decay amplitude is proportional to $(m_u - m_d)$ or, alternatively, to the quark mass double ratio

$$Q^2 = \frac{m_s^2 - \hat{m}^2}{m_d^2 - m_u^2}, \quad \text{with} \quad \hat{m} = \frac{1}{2}(m_u + m_d). \quad (1.1)$$

Furthermore, this process involves two theoretical puzzles. The first one is the fact that the predictions for the decay width from current algebra, but also from one-loop chiral perturbation theory (χ PT), fail to reproduce the experimental value. It is understood that this is due to large final state rescattering effects that can be ideally treated using dispersion relations. Gasser and Leutwyler, having included one final state rescattering process in the decay amplitude [1], found for the decay width of the charged channel $\Gamma_c = 160 \pm 50$ eV. This was in perfect agreement with the then-current PDG average $\Gamma_c = 197 \pm 29$ eV and the case seemed to be settled. However, the authors already pointed out a new experiment hinting at a larger decay width, which would “resurrect the problem” they “claim[ed] to solve”. Figure 1.1 clearly shows that over the following years, the PDG average grew out of the error bars of the one-loop prediction. The second puzzle is related to the slope parameter α in the neutral channel, where χ PT, but also an older dispersive analysis [2], fail to reproduce the experimental finding.

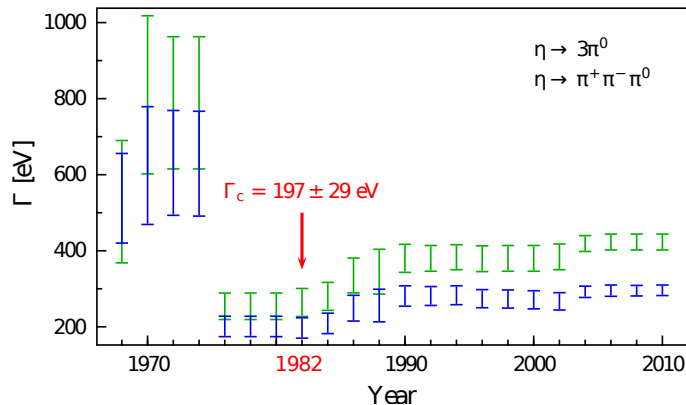


Figure 1.1: PDG average for the decay width of the two $\eta \rightarrow 3\pi$ channels since 1968. Gasser and Leutwyler used the value for the charged channel from 1982.

In 1996 two dispersive analyses of $\eta \rightarrow 3\pi$ have been published [2, 3]. Our analysis follows closely the method proposed in the second reference, where a detailed description and further references can be found. Many developments in recent years, as well as current experimental and theoretical activity by other groups, have made a new analysis worthwhile. The inputs that the dispersive analysis relies on have been improved considerably: several groups have published accurate descriptions of the $\pi\pi$ scattering phase shifts [4, 5, 6], and a modern precision measurement of $\eta \rightarrow 3\pi$ is available [7], which can be used in order to fix the subtraction constants. Even more experimental data is to be expected in the near future [8]. In addition, several theoretical works on this decay have appeared in the last few years (e.g., [9, 10, 11, 12]). In particular, there is also an analytical dispersive treatment [13] that was presented at this workshop.

*in collaboration with G. Colangelo, H. Leutwyler and E. Passemar

[†]Department for Astronomy and Theoretical Physics, Lund University, Sölvegatan 14A, S-223 62 Lund, Sweden; stefan.lanz@thep.lu.se

The dispersive analysis relies on a decomposition of the amplitude into isospin amplitudes $M_I(s)$ that are functions of one variable only,

$$M(s, t, u) = M_0(s) + (s - u)M_1(t) + (s - t)M_1(u) + M_2(t) + M_2(u) - \frac{2}{3}M_2(s). \quad (1.2)$$

From unitarity and analyticity follow dispersion relations for the functions $M_I(s)$,

$$M_0(s) = \Omega_0(s) \left\{ \alpha_0 + \beta_0 s + \gamma_0 s^2 + \frac{s^2}{\pi} \int_{4m_\pi^2}^{\infty} \frac{ds'}{s'^2} \frac{\sin \delta_0(s') \hat{M}_0(s')}{|\Omega_0(s')|(s' - s - i\epsilon)} \right\}, \quad (1.3)$$

and similarly for $M_1(s)$ and $M_2(s)$. The functions $\hat{M}_I(s)$ are angular averages over all of the M_I such that the dispersion relations are coupled. The Omnès function is given by

$$\Omega_I(s) = \exp \left\{ \frac{s}{\pi} \int_{4m_\pi^2}^{\infty} \frac{\delta_I(s')}{s'(s' - s)} ds' \right\}. \quad (1.4)$$

The dispersion relations contain a total number of four subtraction constants: α_0 , β_0 and γ_0 in the equation for M_0 and one more, β_1 , in the equation for M_1 . These are left free by the dispersion relations and have to be determined otherwise. The dispersion relations are solved numerically by an iterative procedure, starting at some initial configuration for the $M_I(s)$. If the subtraction constants are determined by a matching to the one-loop result from χ PT (as in Ref. [3]), it turns out that there is a clear deviation from the experimental result in Ref. [7] for large s (see Fig. 1.2). Alternatively, we can determine the subtraction constants by a combined fit to the measured Dalitz plot and to one-loop χ PT around the Adler zero of the amplitude, where the series is expected to converge best. Since the amplitude is proportional to Q^{-2} , its normalisation cannot be fixed from the experimental data. For this, Chiral Perturbation Theory remains the only source of information. The results from a preliminary fit are shown in Fig. 1.2. As expected, these curves agree well with the result from KLOE.

Comparing the decay width that is calculated from the dispersive amplitude with the present PDG value of $\Gamma_c = 296 \pm 16$ eV, we can extract a value for Q . Using the subtraction constants from the pure matching to one-loop we get $Q = 22.7 \pm 0.7$, thus updating the analysis from Ref. [3]. The preliminary result using the subtraction constants from the fit to the KLOE data is $Q = 21.3 \pm 0.6$. In Fig. 1.3, these results are compared to a number of other values for Q from the literature. Note, in particular, the rather strong disagreement with the result from the analytic dispersive calculation by Kampf et al. The origin of the discrepancy is not yet fully understood, but it lies in the different procedure that is used in order to fix the normalisation, since Q is very sensitive to the latter. While we fit to the one-loop amplitude along the line $s = u$ in the vicinity of the Adler zero, the authors of Ref. [13] fit along the line $t = u$. Doing the same with our dispersive representation results in a very strong violation of the Adler zero and is thus not a viable course.

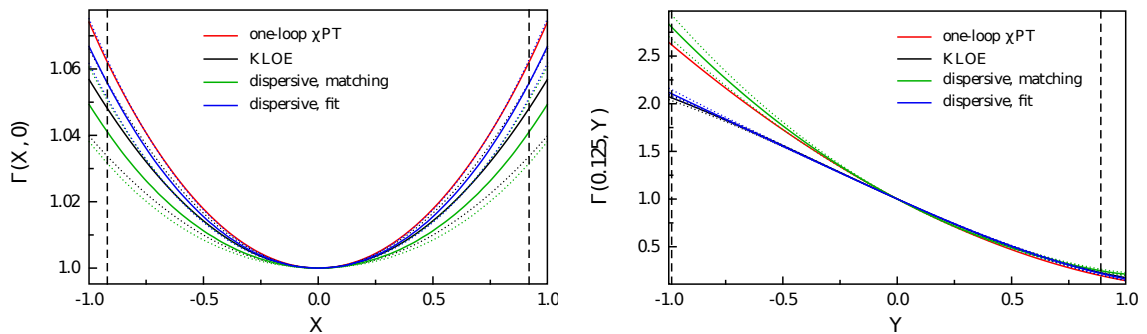


Figure 1.2: The squared amplitude for the decay $\eta \rightarrow \pi^0 \pi^+ \pi^-$ along the lines $Y = 0$ (left) and $X = 0.125$ (right). X and Y are the usual Dalitz plot variables, the dashed lines represent the limits of the physical region. The uncertainty band is marked by the dotted lines. One can clearly see the disagreement between the dispersive result that relies only on one-loop χ PT and experiment for $Y < 0$ (which corresponds to large s).

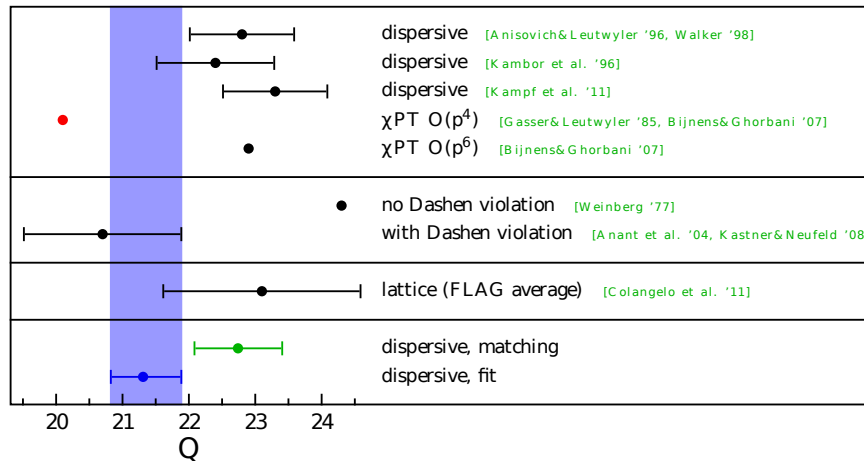


Figure 1.3: Comparison of several results for the quark mass ratio Q . The two last dots represent our preliminary results.

For the slope parameter in the neutral channel, we get $\alpha = -0.045 \pm 0.01$, in only mild disagreement with the PDG average. This value is in excellent agreement with the finding of Kampf et al., again hinting that the discrepancy in Q is not due to the shape but to the normalisation of the amplitude, since α is independent thereof.

Note that all results presented here are preliminary. Last refinements on the numerical analysis are in progress and the final results will be made available soon.

Acknowledgement

I would like to thank the organisers for an interesting workshop and Johan Bijmens, Karol Kampf, Bastian Kubis, Sebastian Schneider, and Martin Zdráhal for discussions. This work is supported by the Swiss Science Foundation and in part by the European Community-Research Infrastructure Integrating Activity “Study of Strongly Interacting Matter” (HadronPhysics2, Grant Agreement n. 227431) and the Swedish Research Council grants 621-2008-4074 and 621-2010-3326.

Bibliography

- [1] J. Gasser and H. Leutwyler, *Nucl. Phys.* **B250** (1985) 539.
- [2] J. Kambor et al., *Nucl. Phys.* **B465** (1996) 215–266, [[hep-ph/9509374](#)].
- [3] A. V. Anisovich and H. Leutwyler, *Phys. Lett.* **B375** (1996) 335–342, [[hep-ph/9601237](#)].
- [4] B. Ananthanarayan et al., *Phys. Rept.* **353** (2001) 207–279, [[hep-ph/0005297](#)].
- [5] S. Descotes-Genon et al., *Eur. Phys. J.* **C24** (2002) 469–483, [[hep-ph/0112088](#)].
- [6] R. Kaminski et al., [arXiv:0905.2139](#).
- [7] **KLOE** Collaboration, F. Ambrosino *et. al.*, *JHEP* **05** (2008) 006, [[arXiv:0801.2642](#)].
- [8] See, e.g., the posters by L. C. Balkeståhl and P. Adlarson at this workshop.
- [9] J. Bijmens and K. Ghorbani, *JHEP* **11** (2007) 030, [[arXiv:0709.0230](#)].
- [10] C. Ditsche et al., *Eur. Phys. J.* **C60** (2009) 83–105, [[arXiv:0812.0344](#)].
- [11] S. P. Schneider et al., *JHEP* **02** (2011) 028, [[arXiv:1010.3946](#)].
- [12] M. Kolesár, [arXiv:1109.0851](#). Talk by M. Kolesár at this workshop.
- [13] K. Kampf et al., [arXiv:1103.0982](#). Talk by M. Zdráhal at this workshop.

PRAGUE-LUND-MARSEILLE (ANALYTICAL) DISPERSIVE APPROACH TO $\eta \rightarrow 3\pi$

MARTIN ZDRÁHAL*

1.1 Introduction

As is obvious from the number of contributions dealing with $\eta \rightarrow 3\pi$ decays presented in this workshop, these processes in recent years attracted and still attract both theoreticians and experimentalists. The main reasons are the following. These processes proceed via isospin breaking effects. Moreover, since the electromagnetic contribution to them is strongly suppressed, to a good approximation they are proportional to $(m_u - m_d)$ mass difference and thus by comparing the result of measurement of their decay rate with the theoretically predicted ones we have a direct method for determination of this quantity, in our work appearing as the quark mass ratio $R = \frac{m_s - \hat{m}}{m_d - m_u}$, where $\hat{m} = \frac{1}{2}(m_u + m_d)$. Secondly, recent measurements (cf. e.g. [1]) of the neutral decay $\eta \rightarrow 3\pi^0$ start to be precise enough to observe the effect of cusp occurring in this decay. Finally, there is still a theoretical challenge to explain satisfactorily the observed discrepancy between the experimentally measured Dalitz plot parameters describing the energy dependence of the amplitudes and their values predicted by the two-loop computation in the framework of chiral perturbation theory (ChPT) [2].

This has inspired various studies exploring possible explanations of the discrepancy [3], namely higher order final state rescatterings, influence of slow convergence of $\pi\pi$ scattering or of $\eta \rightarrow 3\pi$ amplitude itself, unexpectedly large electromagnetic contributions, effects of resonances or with that connected possibility of incorrectly determined next-to-next-to-leading-order (NNLO) low-energy constants of ChPT C_i s. On the experimental side there is substantial activity as well (for instance KLOE and WASA-at-COSY at this workshop [4] promised new data on charged decay, for which there exists currently only one precise analysis on at least 4 Dalitz plot parameters, [5]).

The complication of those analyses which are trying to avoid the above mentioned possible problems of ChPT by using alternative approaches is that currently there exists no such alternative containing explicitly quark masses. This means that even if one found using them a correct description of the energy dependence of the η decays, in order to extract any information on the quark masses (i.e. to fix the normalization), one unavoidably needs to match it back to ChPT. In the case one used in his approach different assumptions than those of ChPT, this matching brings another sources of errors into the game.

1.2 Analytic dispersive parametrization

For the task of finding the correct value of R taking all this into account, we have employed in [6] our analytic dispersive parametrization valid to two-loop order, which is constructed using just basic assumptions of quantum field theories together with some observed hierarchy of various contributions to the amplitude and therefore can reproduce very well also the NNLO chiral amplitude. It is possible to include full isospin breaking effects connected with different masses of charged and neutral pions but at the current level of precision we work in the limit $m_{\pi^\pm} = m_{\pi^0}$. In that limit the neutral decay is connected with the charged one and the parametrization of the charged decay is in this case in the form

$$M_x(s, t, u) = A_x M_\eta^2 + B_x(s - \bar{s}) + C_x(s - \bar{s})^2 + D_x[(t - \bar{s})^2 + (u - \bar{s})^2] + E_x(s - \bar{s})^3 + F_x[(t - \bar{s})^3 + (u - \bar{s})^3] + U(s, t, u), \quad (1.1)$$

where the unitarity part $U(s, t, u)$ contains the same parameters A_x, B_x, C_x, D_x together with a few additional parameters describing $\pi\pi$ scattering (which are held fixed) and is given analytically.

*IPNP, Faculty of Mathematics and Physics, Charles University in Prague, zdrahal@ipnp.mff.cuni.cz

Using this parametrization and the data for charged decay from KLOE [5], we perform the following two distinct analyses.

1.3 Analysis I: Correcting ChPT $\eta \rightarrow 3\pi$ result

By comparing the values of Dalitz plot parameters from the experimental determination with their predictions from NNLO ChPT, we have found that despite the discrepancy for the individual parameters, they fulfill two relations which are valid in the case the imaginary part of the chiral amplitude is determined correctly (the third relation which is simply the value of the neutral parameter β has not been experimentally measured yet). This means that the data indicate the possibility that all the difference between the physically measured amplitude and the one stemming from the ChPT computation can be described by a small real polynomial, i.e. it can also be included into the values of the parameters C_i . This inspired our first analysis, where we have added such polynomial to our parametrization of the ChPT amplitude and fitted it from the KLOE data. From that one could extract constraints on such phenomenological values of C_i and more importantly for our task we have obtained corrected value of $R = 37.7 \pm 2.9$, where the error is estimated from the (slow) convergence of chiral expansion in the first leading orders.

1.4 Analysis II: Direct fit to experimental $\eta \rightarrow 3\pi$ data

Our second analysis resigned on explaining the origin of the Dalitz plot discrepancy and instead assumed that independently on the way one obtained the correct amplitude from QFT computations, it would fulfill the general properties we have employed in the construction of our parametrization, i.e. it will be reproduced well by our parametrization. We have therefore fitted the experimental data on the parametrization.

As was pointed out in the introduction, in order to obtain any information on the quark masses, we need to fix the normalization of the amplitude by matching to ChPT. Thanks to the fact we have analytic expressions, it is sufficient to find just one point where we perform the matching, i.e. the point where the chiral expansion of the amplitude converges fast. However, since there is no theoretical argument that would choose one such point for the matching, we have used the assumption that if such point exists, it will not be an isolated point but a region where the behavior of the NNLO chiral amplitude and the behavior of the amplitude fitted from data would be similar and also various chiral orders behave in that region well. We have found a prescription for such matching fulfilling these requirements and obtained as a result of this analysis $R = 37.8 \pm 3.3$, where the error is fully dominated by the error of the fit to KLOE data.

1.5 Conclusions

We have used two analyses based on different assumptions, which can be however fulfilled simultaneously by the genuine physical amplitude. Since both of the analyses lead to the compatible values for R , we expect that they provide us with some information about the amplitudes and also that the determined value of R is reasonable.

In [7] we have shown how one can combine this determination with the isospin symmetric studies on lattice and those using sum-rules techniques in order to obtain individual quark masses. For example using FLAG [8] values, we obtain

$$m_u = 2.23(13) \text{ MeV}, \quad m_d = 4.63(16) \text{ MeV}, \quad (1.2)$$

where these values are taken in the \overline{MS} renormalization scheme at $\mu = 2 \text{ GeV}$.

Let us conclude with the comment that it will be very important in the forthcoming experimental measurements of the charged $\eta \rightarrow 3\pi$ decay to verify the validity of our assumptions since the current analysis is based on only one experimental information on 5 Dalitz plot parameters which is at our disposal [5].

Bibliography

- [1] S. Prakhov et al. (Crystal Ball at MAMI), *Phys. Rev.* **C79**, 035204, (2009).
- [2] J. Bijnens and K. Ghorbani, *JHEP* **11**, 030, (2007).
- [3] G. Colangelo, S. Lanz, E. Passemar, *PoS CD09*, 047, (2009);
S. P. Schneider, B. Kubis, C. Ditsche, *JHEP* **1102**, 028, (2011);
A. Nehme, arXiv:1106.3491 [hep-ph], (2011);
M. Kolesár, arXiv:1109.0851 [hep-ph], (2011).
- [4] *See contributions of L. Caldeira Balkeståhl and P. Adlarson in these proceedings.*
- [5] KLOE Collaboration, F. Ambrosino et al., *JHEP* **05**, 006, (2008).
- [6] K. Kampf, M. Knecht, J. Novotný, M. Zdráhal, arXiv:1103.0982 [hep-ph], (2011).
- [7] M. Zdráhal, arXiv:1109.1835 [hep-ph], (2011).
- [8] G. Colangelo, et al., *Eur. Phys. J.* **C71**, 1695, (2011). [arXiv:1011.4408 [hep-lat]].

$\eta \rightarrow 3\pi$ IN RESUMMED χ PT: DALITZ PLOT PARAMETERS

MARIÁN KOLESÁR^{*†}, JIŘÍ NOVOTNÝ^{*}
AND SÉBASTIEN DESCOTES-GENON[‡]

We analyze the Dalitz plot parameters of $\eta \rightarrow 3\pi$ decay in the framework of resummed chiral perturbation theory. This approach allows us to keep the uncertainties in the NNLO and higher orders under better control and estimate their influence. The compatibility of assumption of reasonably small higher order remainders with experimental data and NNLO standard χ PT results is investigated. We calculate the effect of lowest order resonance exchange and $\pi\pi$ rescattering bubble corrections up to three loops.

The Dalitz plot parameters are usually defined as:

$$\eta \rightarrow \pi^0 \pi^+ \pi^- : |A|^2 = A_0^2(1 + ay + by^2 + dx^2 + \dots) \quad (1.1)$$

$$\eta \rightarrow 3\pi^0 : |\bar{A}|^2 = \bar{A}_0^2(1 + \alpha z + \dots) \quad (1.2)$$

where $x \sim u - t$, $y \sim s_0 - s$, $z \sim x^2 + y^2$ and s_0 is the Dalitz plot center $s_0 = 1/3(M_\eta^2 + 3M_\pi^2)$. There is recent experimental information available [1, 2, 3, 4, 5, 6, 7, 8, 9], results from collaborations producing values for both channels can be found in table 1.1, along with NNLO χ PT results [10].

As can be seen, a discrepancy can be suspected for the charged decay parameter b and the neutral decay parameter α . Our aim is to try to understand whether the theory, by which we mean χ PT as a low energy representation of QCD, really does have difficulties explaining the data and if so, try to identify the source of the problem.

There is a long standing suspicion that chiral perturbation theory might possess a slow or irregular convergence in the case of the three quark flavor series [11]. An alternative approach, dubbed resummed χ PT [12, 13], was developed in order to express standard assumptions in terms of parameters and uncertainty bands. The procedure can be very shortly summarized as:

- standard χ PT Lagrangian and power counting
- possible irregularities in the expansion assumed
- only expansions derived directly from the generating functional trusted
- explicitly to NLO, higher orders collected in remainders
- remainders not neglected, treated as sources of error
- manipulations done in non-perturbative algebraic way

Our calculation closely follows the procedure outlined in [15], more details can be found in [16]. A comprehensive work is in preparation [17].

In accord with the method, leading order low energy constants (LECs) are expressed in terms of convenient free parameters

$$Z = \frac{F_0^2}{F_\pi^2}, \quad X = \frac{2F_0^2 B_0 \hat{m}}{F_\pi^2 M_\pi^2}, \quad r = \frac{m_s}{\hat{m}}, \quad R = \frac{(m_s - \hat{m})}{(m_d - m_u)}, \quad (1.3)$$

^{*}Institute of Particle and Nuclear Physics, Charles University, Prague

[†]kolesar@ipnp.troja.mff.cuni.cz

[‡]Laboratoire de Physique Théorique, Univ.Paris-Sud

	a	b	d	α
Crystal Barrel [1, 2]	-1.22 ± 0.07	0.22 ± 0.11	0.06 ± 0.04	-0.052 ± 0.020
KLOE [3, 4]	-1.090 ± 0.020	0.124 ± 0.012	0.057 ± 0.017	-0.0301 ± 0.0050
NNLO χ PT [10]	-1.271 ± 0.075	0.394 ± 0.102	0.055 ± 0.057	$+0.013 \pm 0.032$

Table 1.1: Some of the available experimental and χ PT results.

where $\hat{m}=(m_u + m_d)/2$. To first order in isospin breaking the Dalitz plot parameters do not depend on R . At next-to-leading order, the LECs L_4 - L_8 are algebraically reparametrized using chiral expansions of two point Green functions. The $O(p^6)$ and higher order LECs, notorious for their abundance, are collected in a relatively smaller number of higher order remainders.

We use several approaches to deal with the remainders. The first one is based on general arguments about the convergence of the chiral series [12], which leads to

$$G = G^{(2)} + G^{(4)} + \Delta_G^{(6)}, \quad \Delta_G^{(6)} \sim \pm 0.1G, \quad (1.4)$$

where G stands for any of our 2- or 4-point Green functions, which generate the remainders. This is in principle an assumption. Hence we test the compatibility of this assumption of a reasonably good chiral convergence of trusted quantities with experimental data in a statistical sense.

The framework of resummed χ PT is well suited to include additional information about higher orders from various sources [15]. An independent estimate of the remainders can on one side be an important check of the validity of the statistical remainder estimate or could try to explain any deviations from this assumption. Here we employ a specific higher order calculation, namely 3-loop bubble contributions to final state $\pi\pi$ rescattering and an estimate of the influence of the lowest lying resonances using resonance chiral theory [14].

Using the approach outlined above, we have found the experimental values consistent with the assumption of small higher order remainders for the charged decay parameters. We cannot confirm the suspected discrepancy in the case of parameter b , as small uncertainties in higher orders could accommodate the difference.

In the case of the neutral decay parameter α , we confirm the positive-sign prediction of χ PT and find the experimental value incompatible with the assumption of good convergence properties in the center of the Dalitz plot for any scenario of spontaneous chiral symmetry breaking controlled by the free parameters X , Z and r .

Contributions from resonance exchange have turned out to be small. On the other hand, $\pi\pi$ rescattering might explain the discrepancy in α , especially for low values of the pseudoscalar decay constant in the chiral limit. That could signal a failure of convergence of chiral series already at around 500MeV.

Bibliography

- [1] Crystal Barrel Collaboration, *Phys. Lett.*, **B 417**, 197, (1998).
- [2] Crystal Barrel Collaboration, *Phys. Lett.*, **B 417**, 193, (1998).
- [3] KLOE Collaboration, *JHEP*, **05**, 006, (2008).
- [4] KLOE Collaboration, *Phys.Lett.*, **B 694**, 16, (2010).
- [5] Crystal Ball Collaboration, *Phys. Rev. Lett.*, **87**, 192001, (2001).
- [6] M. Bashkanov et al., *Phys. Rev.*, **C 76**, 048201, (2007).
- [7] WASA-at-COSY Collaboration, *Phys. Lett.*, **B 677**, 24, (2009).
- [8] Crystal Ball at MAMI Coll., *Eur. Phys. J.*, **A 39**, 169, (2009).
- [9] Crystal Ball at MAMI Coll., *Phys. Rev.*, **C 79**, 035204, (2009).
- [10] J. Bijnens and K. Ghorbani, *JHEP*, **11**, 030, (2007).
- [11] S. Descotes-Genon, L. Girlanda, J. Stern, *JHEP*, **0001**, 041, (2000).
- [12] S. Descotes-Genon et al., *Eur. Phys. J.*, **C 34**, 201, (2004).
- [13] S. Descotes-Genon, *Eur.Phys.J.*, **C 52**, 141, (2007).
- [14] G. Ecker et al., *Nucl.Phys.*, **B 321**, 311, (1989).
- [15] M. Kolesár, J. Novotný, *Eur.Phys.J.*, **C 56**, 231, (2008).
- [16] M. Kolesár, *arXiv:1109.0851*.
- [17] M. Kolesár, J. Novotný, S. Descotes-Genon, *in preparation*.

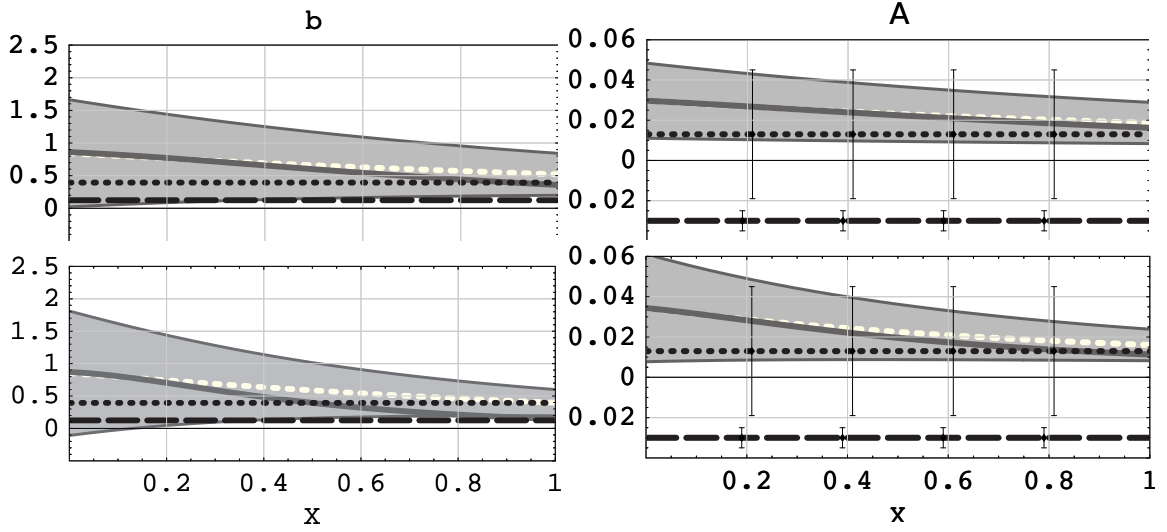


Figure 1.1: Dalitz plot parameters b and α at $r=25$: top $Z=1$, bottom $Z=0.5$. Horizontal lines: dashed - KLOE measurement [3]; dotted - NNLO χ PT [10]. Light band - statistical remainder estimate. Dark solid line - result including lowest lying resonance multiplets.

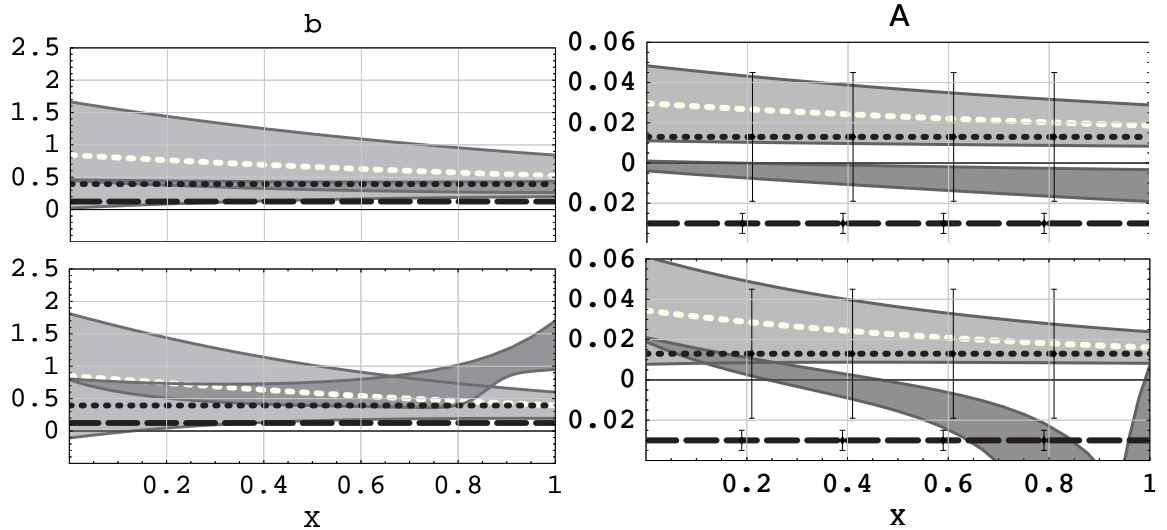


Figure 1.2: Dalitz plot parameters b and α at $r=25$: top $Z=1$, bottom $Z=0.5$. Horizontal lines: dashed - KLOE measurement [3]; dotted - NNLO χ PT [10]. Light band - statistical remainder estimate. Dark band - result including $\pi\pi$ rescattering, depending on ren.scale $\mu=0.5\div 1\text{GeV}$

MODEL-INDEPENDENT APPROACH TO $\eta \rightarrow \pi^+ \pi^- \gamma$ AND $\eta' \rightarrow \pi^+ \pi^- \gamma$

FELIX STOLLENWERK^{*†}

1.1 Introduction

We present a new, model-independent method [1] to analyze radiative decays of mesons to a vector, isovector pair of pions of invariant mass square below the first significant $\pi\pi$ threshold in the vector channel. It is based on a combination of chiral perturbation theory and dispersion theory. This allows for a controlled inclusion of resonance physics without the necessity to involve models, like vector meson dominance, explicitly.

1.2 The approach

For the radiative decays at hand, there is a significant deviation between the predictions [2] of chiral perturbation theory (ChPT) and data, the source of which is mostly the non-perturbative $\pi\pi$ final state interaction. Those are universally collected in the pion vector form factor $F_V(s_{\pi\pi})$, whose analytic properties can be exploited in the form of a dispersion relation to give

$$F_V(s_{\pi\pi}) = \exp \left(\frac{1}{6} s_{\pi\pi} \langle r^2 \rangle + \frac{s_{\pi\pi}^2}{\pi} \int_{4m_\pi^2}^{\infty} ds \frac{\delta_{11}(s)}{s^2(s - s_{\pi\pi} - i\epsilon)} \right), \quad (1.1)$$

where $\langle r^2 \rangle$ and $\delta_{11}(s)$ denote the mean square charge radius of the pion and the elastic $\pi\pi$ phase shift in the vector–isovector channel, respectively, and $s_{\pi\pi}$ is the invariant pion mass.

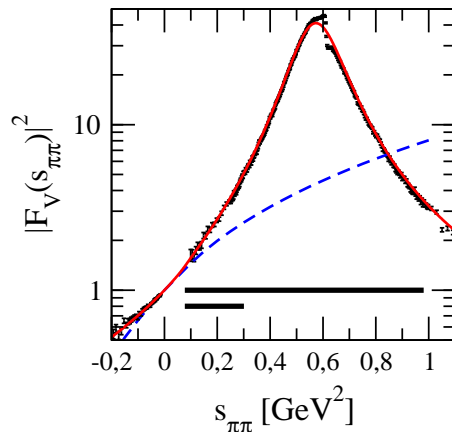


Figure 1.1: The (red) solid band shows the form factor derived from Eq. (1.1), the (blue) dashed line the result from one-loop ChPT — both with identical values for the pion radius. The time-like data are from Refs. [3, 4], whereas the space-like data are from Ref. [5]. The short (long) thick, horizontal bar denotes the kinematic range covered in the decay of the η (η'). In the η range, the form factor can be approximated by $|F_V(s_{\pi\pi})| = 1 + (2.12 \pm 0.01)s_{\pi\pi} + (2.13 \pm 0.01)s_{\pi\pi}^2 + (13.80 \pm 0.14)s_{\pi\pi}^3$.

Eq. (1.1) fixes the form factor only up to a multiplicative function without right-hand cuts. As the transition amplitude features the same analytic structure as $F_V(s_{\pi\pi})$ apart from a kinematically and chirally suppressed left-hand cut, we may factorize the amplitude according to

$$\frac{d\Gamma}{ds_{\pi\pi}} \sim |A P(s_{\pi\pi}) F_V(s_{\pi\pi})|^2, \quad (1.2)$$

^{*}Institut für Kernphysik (Theorie), Institute for Advanced Simulation and Jülich Center for Hadron Physics, Forschungszentrum Jülich, D-52425 Jülich, Germany; f.stollenwerk@fz-juelich.de

[†]in collaboration with Christoph Hanhart, Andrzej Kupsc, Ulf-G. Meißner and Andreas Wirzba

and expand $P(s_{\pi\pi})$ in a Taylor series around $s_{\pi\pi} = 0$:

$$P(s_{\pi\pi}) = 1 + \alpha^{(\prime)} s_{\pi\pi} + \mathcal{O}(s_{\pi\pi}^2) . \quad (1.3)$$

Assuming that the universal part $F_V(s_{\pi\pi})$ comprises *all* non-perturbative effects, the reaction specific part $AP(s_{\pi\pi})$ should be accessible to a perturbative treatment. Indeed, we find that a linear polynomial (1.3) with

$$\alpha = (1.96 \pm 0.27 \pm 0.02) \text{ GeV}^{-2} ; \quad \alpha' = (1.80 \pm 0.49 \pm 0.04) \text{ GeV}^{-2} \quad (1.4)$$

is already sufficient to describe spectral decay data, see Fig. 1.2. In principle, $\rho-\omega$ mixing distorts the η' spectrum. If one assumes the mixing strength to be identical to that in the vector form factor (based on the quark model the effect is much smaller), one finds the wiggly (green) line. Clearly, the data is not yet sufficient to extract information on the magnitude of the effect.

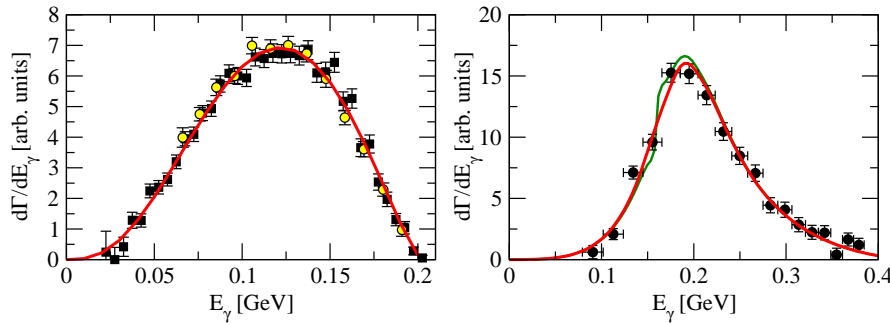


Figure 1.2: Experimental data and error weighted fits for η (left, data are from Ref. [6] (filled squares) and Ref. [7] (open circles)) and η' (right, data are from Ref. [8]) to $\pi^+\pi^-\gamma$ according to Eqs. (1.2) and (1.3) with $s_{\pi\pi} = m_{\eta^{(\prime)}}(m_{\eta^{(\prime)}} - 2E_\gamma)$. The wiggly (green) line in the right panel denotes the possible impact of $\rho-\omega$ mixing under the assumption that it appears here with the same strength as in F_V .

The postulated decay amplitude (1.2) can be matched to one-loop $U(3)$ extended ChPT. Concerning the $s_{\pi\pi}$ -dependent part, this connects the slope parameters $\alpha^{(\prime)}$ to the low energy constant a_2 giving

$$a_2^\eta = 9.70 \pm 0.7 ; \quad a_2^{\eta'} = 9.23 \pm 1.4 .$$

Thus, the data sets are consistent with the assumption that the only non-perturbative part of the amplitude originates from the pion vector form factor, and Eq. (1.2) provides a controlled way to disentangle perturbative and non-perturbative effects in order to methodically extend perturbative calculations to the resonance region. By invoking chiral Ward identity and large N_c arguments, essentially half of the parameter $\alpha^{(\prime)}$ can be physically interpreted. Further possible ways of interpretation are subject of current research.

Bibliography

- [1] F. Stollenwerk, C. Hanhart, A. Kupsc, U.-G. Meißner and A. Wirzba, arXiv:1108.2419 [nucl-th].
- [2] J. Bijnens, A. Bramon, F. Cornet, *Phys. Lett. B* **237**, 488, (1990).
- [3] B. Aubert et al. [BABAR Collaboration], *Phys. Rev. Lett.* **103**, 231801, (2009).
- [4] F. Ambrosio et al. [KLOE Collaboration], *Phys. Lett. B* **700**, 102, (2011).
- [5] S.R. Amendolia et al. [NA7 Collaboration], *Nucl. Phys. B* **277**, 168, (1986).
- [6] P. Adlarson et al. [WASA-at-COSY Collaboration], arXiv:1107.5277v1 [nucl-ex].
- [7] M. Gormley et al., *Phys. Rev. D* **2**, 501, (1970).
- [8] A. Abele, et al. [CRYSTAL BARREL Collaboration], *Phys. Lett. B* **402**, 195 (1997).

STUDY OF $\eta \rightarrow \pi^+\pi^-\gamma$ DECAY

CAMILLA DI DONATO*

for the KLOE and KLOE-2 Collaborations

1.1 Introduction

We measured the ratio $R_\eta = \Gamma(\eta \rightarrow \pi^+\pi^-\gamma)/\Gamma(\eta \rightarrow \pi^+\pi^-\pi^0)$, analyzing an integrated luminosity of 558 pb^{-1} , collected by KLOE at the DAΦNE e^+e^- collider. The $\eta \rightarrow \pi^+\pi^-\gamma$ process is supposed to proceed both via a resonant contribution, mediated by the ρ meson, and a non resonant direct term, connected to the box anomaly. The presence of the direct term affects the partial width value.

The Chiral Perturbation Theory (ChPT) provides accurate description of interactions and decays of light mesons [1]. The decays $\eta \rightarrow \pi^+\pi^-\gamma$ and $\eta' \rightarrow \pi^+\pi^-\gamma$ are expected to get contribution from the anomaly accounted for by the Wess Zumino Witten (WZW) term into the ChPT Lagrangian [2]. According to effective theory [2] the contribution of the direct term should be present together with VMD. In case of $\eta \rightarrow \pi^+\pi^-\gamma$ the ρ contribution is not dominant, this makes the partial width sensitive to the presence of the direct term, while in case of $\eta' \rightarrow \pi^+\pi^-\gamma$ the partial width is dominated by the resonance and the direct term effect should be visible in the dipion invariant mass distribution. The present world average of the $\eta \rightarrow \pi^+\pi^-\gamma$ partial width, $\Gamma(\eta \rightarrow \pi^+\pi^-\gamma) = (60 \pm 4) \text{ eV}$ [3], provides strong evidence in favour of the box anomaly, compared with value expected with and without the direct term, respectively $(56.3 \pm 1.7) \text{ eV}$ and $(100.9 \pm 2.8) \text{ eV}$ [2]. Recently CLEO [4] has measured the ratio $R_\eta = 0.175 \pm 0.007_{stat} \pm 0.006_{syst}$, which differs by more than 3σ from the average result of previous measurement [5, 6], $R_\eta = 0.207 \pm 0.004$ [7]. Here we present a new measurement with the highest statistics and the smallest systematic error ever achieved.

1.2 Event selection

The analysis has been performed using 558 pb^{-1} of the 2004-2005 data set acquired by KLOE at the DAΦNE e^+e^- collider ($\sqrt{s} \simeq 1.02 \text{ GeV}$). The final state under study is $\pi^+\pi^-\gamma\gamma$, since the η mesons are produced together with a monochromatic recoil photon ($E_\gamma = 363 \text{ MeV}$) through the radiative decay $\phi \rightarrow \eta\gamma$. In the considered data sample about $\simeq 25 \times 10^6$ η 's are produced. The main background comes from $\phi \rightarrow \pi^+\pi^-\pi^0, \pi^0 \rightarrow \gamma\gamma$ decaying to the same final state. Other backgrounds are $\phi \rightarrow \eta\gamma \rightarrow \pi^+\pi^-\pi^0 \rightarrow \pi^+\pi^-3\gamma$ with one photon lost, and $\phi \rightarrow \eta\gamma, \eta \rightarrow e^+e^-\gamma$ when both electrons are mis-identified as pions.

As first step of the analysis, a preselection is performed, requiring at least two tracks with opposite charge pointing to the interaction point (IP) and at least two neutral clusters in time (not associated to any track), having energy $E_{cl} \geq 10 \text{ MeV}$ and polar angle in the range $(23^\circ - 157^\circ)$. Tracks are sorted according to the distance of the point of closest approach from the IP. The first two tracks are selected. We require the most energetic cluster (γ_ϕ) to have $E_{cl} > 250 \text{ MeV}$ and we identify it as the photon recoiling against the η in the $\phi \rightarrow \eta\gamma$ decay. Moreover we ask for γ_ϕ inside the calorimeter barrel ($55^\circ - 125^\circ$), to avoid effects of cluster merging between barrel and end-caps of the calorimeter. Other cuts are imposed to clean up the sample; cut on cluster-track collinearity and identification by time of flight (TOF) are used to reject electrons. The cut effectively rejects Bhabha background and other processes with electrons in the final state. To select η decays we exploit the $\phi \rightarrow \eta\gamma$ two body decay kinematic computing the γ_ϕ energy, using only the γ_ϕ polar angle:

$$\vec{p}_\phi = \vec{p}_\eta + \vec{p}_\gamma \quad E_{\gamma_\phi} = \frac{m_\phi^2 - m_\eta^2}{2(E_\phi - |\vec{p}_\phi| \cos\varphi)}$$

where φ is the angle between the average ϕ -meson momentum measured run by run with high accuracy and γ_ϕ . This allows us to improve the energy measurement of the recoil photon to 0.1%.

*INFN Naples, camilla.didonato@na.infn.it

We can determine the direction of the photon from η decay using ϕ and π -mesons information:

$$\vec{p}_{\gamma\eta} = \vec{p}_\phi - \vec{p}_{\pi^+} - \vec{p}_{\pi^-} - \vec{p}_{\gamma\phi}$$

The photon direction is compared with the direction of each neutral cluster, $\Delta\varphi = \varphi^{\text{clu}} - \varphi_{\gamma\eta}$. If no cluster within $\Delta\varphi < 8.5^\circ$ is found the event is rejected. The cluster with the minimum value of $\Delta\varphi$ is selected for further analysis. In order to reject the $\phi \rightarrow \pi^+\pi^-\pi^0$ background, the angle between the two photons in the π^0 reference frame, evaluated using the ϕ and the π -mesons momenta, is calculated and rejected with an angular cut $\varphi_{\gamma\gamma}^{\pi^+\pi^-\gamma} < 165^\circ$; in order to reduce the systematics the angle is evaluated in the transverse plane. Finally we select events requiring $539.5 \text{ MeV} < M_{\pi^+\pi^-\gamma} < 554.5 \text{ MeV}$ (Fig. 1.1).

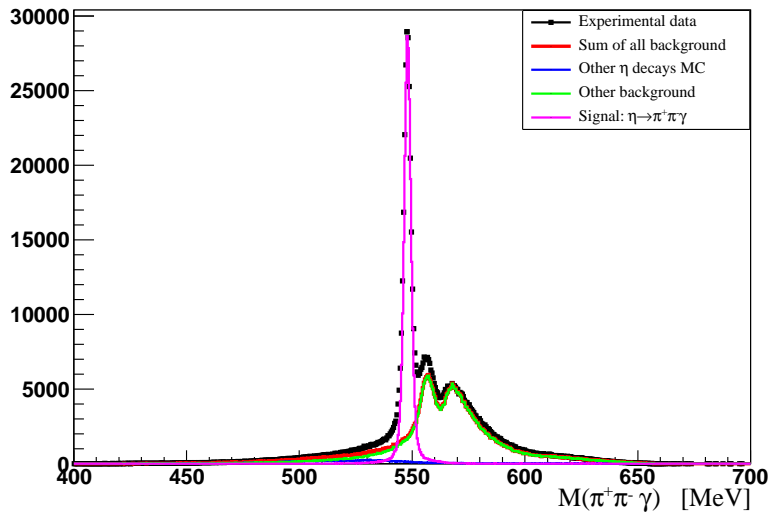


Figure 1.1: The $\pi^+\pi^-\gamma\eta$ invariant mass distribution: Data-MC comparison. Dots are data, Magenta is MC signal $\eta \rightarrow \pi^+\pi^-\gamma$, Red is all MC background contribution

1.2.1 Normalization Sample: $\eta \rightarrow \pi^+\pi^-\pi^0$

The process $\phi \rightarrow \eta\gamma$ with $\eta \rightarrow \pi^+\pi^-\pi^0$ represents a good control sample, due to the similar topology. Moreover the ratio $\Gamma(\eta \rightarrow \pi^+\pi^-\gamma)/\Gamma(\eta \rightarrow \pi^+\pi^-\pi^0)$ is not affected by the uncertainties on the luminosity, the $\phi \rightarrow \eta\gamma$ partial width and the ϕ production cross section cancel in the ratio. We use the same preselection as for the $\eta \rightarrow \pi^+\pi^-\gamma$ signal and calculate the missing four-momentum:

$$\mathbb{P}_{\text{miss}} = \mathbb{P}_\phi - \mathbb{P}_{\pi^+} - \mathbb{P}_{\pi^-} - \mathbb{P}_{\gamma\phi}$$

where the variables in the formula represent the four-momenta of the ϕ meson and the products of the decays. For the $\eta \rightarrow \pi^+\pi^-\pi^0$ signal, the missing mass peaks at the π^0 mass value and we select events with $|M_{\text{miss}} - m_{\pi^0}| < 15 \text{ MeV}$. The remaining background is rejected very efficiently by using an angular cut applied to the two photons from the π^0 decay, $\varphi_{\gamma\gamma}^{3\pi} > 165^\circ$; the angle is evaluated in the transverse plane. We select $N(\eta \rightarrow \pi^+\pi^-\pi^0) = 1115805 \pm 1056$, with a selection efficiency of $\varepsilon = 0.2276 \pm 0.0002$ and a background contamination of 0.65%.

1.3 Results

The total selection efficiency of the $\eta \rightarrow \pi^+\pi^-\gamma$ signal is $\varepsilon = 0.2131 \pm 0.0004$. Background contribution and the signal amount in the final sample are evaluated with a fit to the $E_{\text{miss}} - P_{\text{miss}}$ distribution of the $\pi^+\pi^-\gamma\phi$ system with the shapes from remaining background and signal MC in the range $|E_{\text{miss}} - P_{\text{miss}}| < 10 \text{ MeV}$. We find $N(\eta \rightarrow \pi^+\pi^-\gamma) = 204950 \pm 450$ with a background contamination of 10%. Combining our results we obtain the ratio:

$$R_\eta = \frac{\Gamma(\eta \rightarrow \pi^+\pi^-\gamma)}{\Gamma(\eta \rightarrow \pi^+\pi^-\pi^0)} = 0.1838 \pm 0.0005_{\text{stat}} \pm 0.0030_{\text{syst}} \quad (1.1)$$

Source of uncertainty	Relative error
$\varphi_{\gamma\gamma}^{\pi^+\pi^-\gamma} < 165^\circ \pm 2^\circ$	$\pm 0.6\%$
$\Delta\varphi > 8.5^\circ \pm 2^\circ$	$\pm 0.4\%$
$ M_{\pi^+\pi^-\gamma} - M_\eta < 7.5 \text{ MeV} \pm 2 \text{ MeV}$	$\pm 0.6\%$
$ M_{miss} - M_{\pi^0} < 15 \text{ MeV} \pm 4 \text{ MeV}$	$\pm 0.4\%$
$\varphi_{3\pi}^{\pi^+\pi^-\gamma} > 165^\circ \pm 2^\circ$	$\pm 0.1\%$
$E_{min}^\gamma > 10 \text{ MeV} \pm 2 \text{ MeV}$	$\pm 0.1\%$
$E_{clu}^\gamma > 250 \text{ MeV} \pm 4 \text{ MeV}$	$\pm 0.1\%$
Fit $E_{miss} - P_{miss}$	$\pm 0.6\%$
Total	1.6%

Table 1.1: Summary table of systematic uncertainties.

to be compared with world average value $\Gamma(\eta \rightarrow \pi^+\pi^-\gamma)/\Gamma(\eta \rightarrow \pi^+\pi^-\pi^0) = 0.202 \pm 0.007$ [3]. Our result is in agreement with a recent CLEO [4] measurement, which differs by more 3σ from the average of previous results [5, 6, 7].

The systematic uncertainties due to analysis cuts have been evaluated by varying the cuts on all variables and re-evaluating the branching ratios. The relative variation for each source of systematic is in Tab. 1.1. The total error is taken as the quadratic sum of all contributions.

The $M_{\pi^+\pi^-}$ dependence of decay width has been parameterized in different approaches, in which VMD has been implemented in effective Lagrangians [2, 8]. Preliminary comparison between dipion invariant mass, with the most simple approach as from [8], shows a good agreement with data. Fit with model independent parameterizations, as from [9], is in progress.

1.4 Conclusions

Using a data sample corresponding to an integrated luminosity of 558 pb^{-1} , we select 204950 $\eta \rightarrow \pi^+\pi^-\gamma$ events and 1115805 $\eta \rightarrow \pi^+\pi^-\pi^0$, from the $\phi \rightarrow \eta\gamma$ decays. The corresponding width ratio is: $R_\eta = 0.1838 \pm 0.0005_{stat} \pm 0.0030_{syst}$. Our measurement is in agreement with the most recent result from CLEO [4], which is $R_\eta = 0.175 \pm 0.007_{stat} \pm 0.006_{syst}$. Combining our measurement with the world average value $\Gamma(\eta \rightarrow \pi^+\pi^-\pi^0) = (295 \pm 16) \text{ eV}$ [3], we get $\Gamma(\eta \rightarrow \pi^+\pi^-\gamma) = (54.2 \pm 0.3) \text{ eV}$, which is in agreement with the value expected taking into account the direct term [2], providing a strong evidence in favour of the box anomaly.

Bibliography

- [1] J. Gasser, H. Leutwyler, *Nucl. Phys.* **B 250**, 465, 1985.
- [2] M. Benayoun et al., *Eur. Phys. J.* **C 31**, 525-547, 2003.
- [3] K. Nakamura et al. (Particle Data Group), *Review of Particle Physics*, *J. Phys.* **G37**, 075021, 2010.
- [4] A. Lopez et al., *Phys. Rev. Lett.* **99**, 122001, 2007.
- [5] M. Gormley et al., *Phys. Rev.* **D 2**, 501, 1970.
- [6] J. C. Layter et al., *Phys. Rev.* **D 7**, 2565, 1973.
- [7] W.-M. Yao et al. (Particle Data Group), *Review of Particle Physics*, *J. Phys.* **G33**, 1, 2006.
- [8] C. Picciotto, *Phys. Rev.* **D 45**, 1569, 1992.
- [9] F. Stollenwerk, C. Hanhart, A. Kupsc, U.-G. Meißner, A. Wirzba, *arXiv: 1108.2419 nucl-th*

IN SEARCH OF THE BOX ANOMALY BY STUDYING $\eta \rightarrow \pi^+\pi^-\gamma$

DANIEL LERSCH*

for the WASA-at-COSY-Collaboration

1.1 Introduction & motivation

The decay channel $\eta \rightarrow \pi^+\pi^-\gamma$ provides the opportunity to study QCD anomalies at the chiral limit. The decay width and the shape of the E_γ -distribution of this channel are sensitive to the

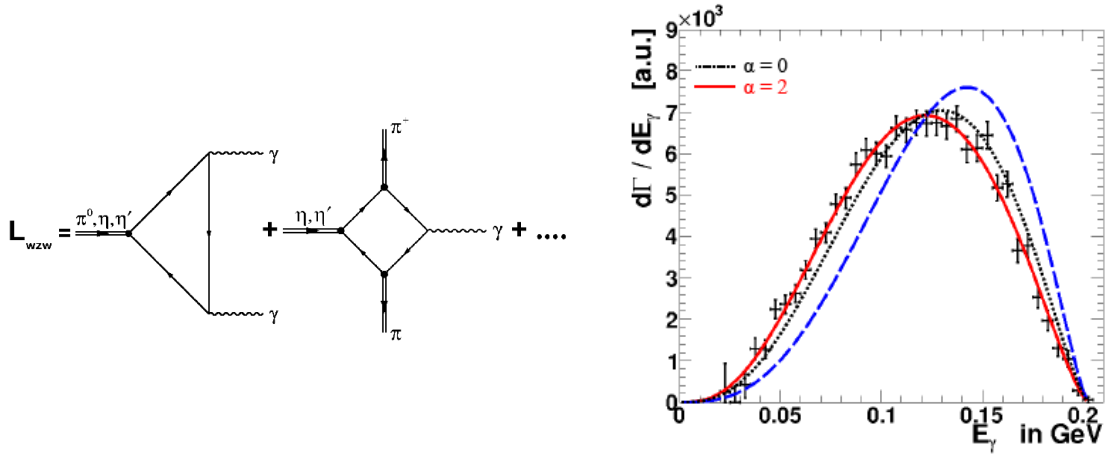


Figure 1.1: Left: Wess-Zumino-Witten-Lagrangian (L_{WZW}) including the triangle anomaly (first) and box anomaly (second) term [1]. Right: Measured E_γ distribution for the reaction: $pd \rightarrow {}^3\text{He}[\eta \rightarrow \pi^+\pi^-\gamma]$ [4]. The measurement has been performed with high statistics and was fully efficiency corrected. The measured E_γ distribution is described by multiplying the simplest gauge invariant matrix element (blue curve) with a form factor (dashed and red curve) which depends on a single parameter α [5].

box anomaly term which is part of the Wess-Zumino-Witten-Lagrangian (see Fig. 1.1). However, the theoretically predicted decay width and E_γ -distribution do not agree with the experimental results, if final state interactions are not included by unitarized extensions of the L_{WZW} . The experimental observables for testing these extensions are (i) the branching ratio [2, 3] or (ii) the distribution of the single photon energy [3]. A recent measurement of the photon energy (see Fig. 1.1) with the WASA detector can be found in [4].

The aim of this work is to measure the branching ratio and the single photon energy distribution in one experiment using the reaction: $pp \rightarrow pp[\eta \rightarrow \pi^+\pi^-\gamma]$. The data have been acquired during an 8 week experiment in spring 2010. At least 10^6 $\eta \rightarrow \pi^+\pi^-\gamma$ events are expected.

The WASA detector (see poster by F. Goldenbaum) is divided into two parts: the forward detector and the central detector.

Scattered projectiles or charged recoil particles are identified in the forward detector, a tracking detector with a set of range hodoscopes, which uses the $\frac{dE}{E}$ -method for particle identification and reconstruction.

Decay products are measured with the central detector. Charged particles are identified by inspecting the deposited energy as function of the momentum as measured with a tracking device in a magnetic field. Neutral particles are detected in the calorimeter.

*IKP1 Forschungszentrum Juelich, Germany, d.lersch@fz-juelich.de

1.2 Data analysis

As a first step, the reaction $\eta \rightarrow \pi^+\pi^-\pi^0$ has been analysed. On the one hand this reaction is important for the determination of $\frac{\Gamma(\eta \rightarrow \pi^+\pi^-\gamma)}{\Gamma(\eta \rightarrow \pi^+\pi^-\pi^0)}$, on the other hand it contributes to the background. The π^0 is also used for monitoring the calorimeter calibration. 5% of the available preselected data have been analysed with the recent analysis chain.

The missing mass spectrum deduced from two protons is shown in Fig. 1.2. The η -peak is visible, along with background, from direct pion production. The following cuts on the invariant and missing mass spectra of the decay products were employed to extract the η -signal from the direct pion background: (i) The invariant mass of two photons had to be within a 0.11 GeV/ c^2 window around the π^0 -mass (ii) The missing mass deduced from two photons had to be larger than the rest mass of the two charged pions (iii) The missing mass squared deduced from the two charged pions had to be positive.

The energy and momentum balance (Fig. 1.2 right) is used to check the effect of each cut and investigate the background contributions.

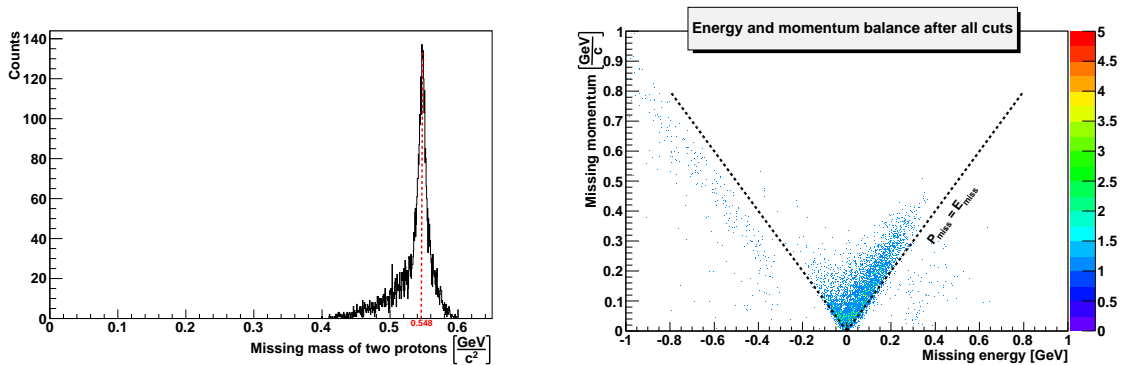


Figure 1.2: Left: Missing mass deduced from the initial state and the two final state protons. The red line indicates the η -mass at 0.548 GeV/ c^2 . This spectrum is obtained after proton reconstruction and applying the cuts mentioned above. Right: Plot of the missing momentum as function of the missing energy (derived by the momentum/energy of all initial and final particles in the reaction).

1.3 Summary & outlook

The η -peak is clearly visible after applying cuts on invariant and missing mass related to the decay products. Background channels shall be identified in a second step using Monte Carlo simulations and analysing more data runs.

The goal is to investigate the reaction $\eta \rightarrow \pi^+\pi^-\gamma$ and to determine the branching ratio.

Acknowledgements

This publication has been supported by the European Commission under the 7th Framework Programme through the ‘Research Infrastructures’ action of the ‘Capacities’ Programme. Call: FP7-INFRASTRUCTURES-2008-1, Grant Agreement N. 227431.

Bibliography

- [1] Wess, Zumino, *Phys. Lett.*, **B37**, 95, (1971), Witten, *Nucl. Phys.*, **B223**, 422, (1983).
- [2] CLEO Collaboration, *Phys. Rev. Lett.*, **99**, 122001, (2007).
- [3] KLOE Collaboration, F.Ambrosio et al., arXiv:1107.5733 [hep-ex].
- [4] WASA Collaboration, P.Adlarson et al., arXiv:1107.5277v1 [nucl-ex].
- [5] F.Stollenwerk et al., arXiv:1108:2419 [nucl-th].

RADIATIVE DECAYS OF PSEUDOSCALARS AND VECTORS

CARLA TERSCHLÜSEN^{*†} and STEFAN LEUPOLD^{*}

1.1 Introduction

Due to the running coupling constant in QCD, one cannot use perturbation theory for the low-energy regime. Instead one can use effective theories with hadrons instead of quarks as relevant degrees of freedom. We use a new counting scheme [1] which treats both vector mesons (V) and pseudoscalar mesons (P) as soft, i.e. of the order of a typical momentum q :

$$m_V, m_P, \partial_\mu \sim q. \quad (1.1)$$

In addition, we use large- N_c arguments (with N_c denoting the number of colors) to suppress additional flavor traces. We will use this counting scheme to describe radiative decays into dileptons (l^+l^-). A more detailed introduction is given in these proceedings in [2].

1.2 Decays $V \rightarrow Pl^+l^-$ and $P \rightarrow Vl^+l^-$

Using the counting scheme (1.1), the leading-order Lagrangian for the decays $V \rightarrow Pl^+l^-$ and $P \rightarrow Vl^+l^-$ can be determined as

$$\begin{aligned} \mathcal{L}_{\text{vec.}} = & -\frac{1}{16f} h_A \varepsilon^{\mu\nu\alpha\beta} \text{tr} \left\{ [V_{\mu\nu}, \partial^\tau V_{\tau\alpha}]_+ \partial_\beta \Phi \right\} - \frac{1}{16f} b_A \varepsilon^{\mu\nu\alpha\beta} \text{tr} \left\{ [V_{\mu\nu}, V_{\alpha\beta}]_+ [\Phi, \chi_0]_+ \right\} \\ & - \frac{m_V^2}{4f} n_A \varepsilon^{\mu\nu\alpha\beta} \text{tr} \{ V_{\mu\nu} V_{\alpha\beta} \} \eta_1 - \frac{e_V m_V}{4} \text{tr} \{ V^{\mu\nu} Q \} \partial_\mu A_\nu. \end{aligned} \quad (1.2)$$

Thereby, $\chi_0 = \text{diag} \{ m_\pi^2, m_\pi^2, m_K^2 \}$, $Q = \text{diag} \{ 2/3, -1/3, -1/3 \}$ and the matrices $V_{\mu\nu}$ and Φ describe the vector mesons (represented by antisymmetric tensor fields) and the pseudoscalar mesons, respectively, i.e.

$$V_{\mu\nu} := \begin{pmatrix} \rho_{\mu\nu}^0 + \omega_{\mu\nu} & \sqrt{2}\rho_{\mu\nu}^+ & \sqrt{2}K_{\mu\nu}^+ \\ \sqrt{2}\rho_{\mu\nu}^- & -\rho_{\mu\nu}^0 + \omega_{\mu\nu} & \sqrt{2}K_{\mu\nu}^0 \\ \sqrt{2}K_{\mu\nu}^- & \sqrt{2}K_{\mu\nu}^0 & \sqrt{2}\phi_{\mu\nu} \end{pmatrix}, \quad (1.3)$$

$$\Phi := \begin{pmatrix} \pi^0 + \frac{1}{\sqrt{3}}\eta_8 & \sqrt{2}\pi^+ & \sqrt{2}K^+ \\ \sqrt{2}\pi^- & -\pi^0 + \frac{1}{\sqrt{3}}\eta_8 & \sqrt{2}K^0 \\ \sqrt{2}K^- & \sqrt{2}K^0 & -\frac{2}{\sqrt{3}}\eta_8 \end{pmatrix} + \sqrt{\frac{2}{3}} \eta_1 I_{3 \times 3}. \quad (1.4)$$

All three terms proportional to h_A , b_A and n_A are of order q^2 : The h_A term because of the two derivatives, the b_A term because of the quark-mass insertion proportional to χ_0 and the n_A term because of the separate traces (note that η_1 is proportional to $\text{tr}\{\Phi\}$). Obviously, this leading-order Lagrangian (1.2) allows only for an indirect decay via a virtual vector meson. Furthermore, for the description of η and η' mesons one has to take η - η' mixing into account,

$$\eta = \cos\theta \eta_8 - \sin\theta \eta_1, \quad (1.5)$$

$$\eta' = \sin\theta \eta_8 + \cos\theta \eta_1 \quad \text{with } \theta \approx -20^\circ. \quad (1.6)$$

The decay of the virtual photon into a dilepton is described by usual QED.

^{*}Uppsala University

[†]carla.terschluesen@physics.uu.se

1.2.1 Parameter determination

To determine the parameters h_A , b_A and n_A , the partial-decay widths for the two-body decays

$$\omega \rightarrow \pi^0 \gamma, \quad \omega \rightarrow \eta \gamma, \quad \phi \rightarrow \eta \gamma, \quad \phi \rightarrow \eta' \gamma, \quad \eta' \rightarrow \omega \gamma \quad (1.7)$$

are compared to experimental data. First, the value h_A is mainly determined via the decay $\omega \rightarrow \pi^0 \gamma$ and, therefore, is fixed as

$$h_A = 2.32 \quad (1.8)$$

as in previous calculations [3]. The parameters b_A and n_A are then determined such that all considered two-body widths are approximately equally well described. It turns out that one does not find fixed values for this parameters but intervals

$$b_A \in [0, 0.19], \quad n_A \in [0, 0.05]. \quad (1.9)$$

For decays into dileptons no additional parameters are needed and we have predictive power.

1.2.2 Results

In Fig. 1.1, the form factors for the transition $\omega \rightarrow \pi^0$ and $\eta' \rightarrow \omega$ are plotted (solid lines). Both are compared to the standard vector meson dominance (VMD) form factors (dashed lines). For both transitions, there is a deviation from VMD visible. Whereas the $\omega \rightarrow \pi^0$ form factor is mainly determined by the term proportional to h_A , there is a sizable influence of b_A and n_A on the $\eta' \rightarrow \omega$ form factor yielding a larger uncertainty compared to $\omega \rightarrow \pi^0$. Obviously, data taken by the NA60 collaboration for the $\omega \rightarrow \pi^0$ transition form factor [4] is much better described with our approach than with standard VMD. Additionally, the calculated results for the integrated rates are within acceptable intervals and agree well with the available experimental data [5] if existent:

$$\begin{aligned} \Gamma_{\omega \rightarrow \pi^0 \mu^+ \mu^-} / \Gamma_{\omega \rightarrow \pi^0 \gamma} &\in [1.36, 1.37] \cdot 10^{-3}, & \Gamma_{\omega \rightarrow \pi^0 \mu^+ \mu^-}^{\text{exp}} / \Gamma_{\omega \rightarrow \pi^0 \gamma}^{\text{exp}} &= (1.57 \pm 0.54) \cdot 10^{-3}, \\ \Gamma_{\omega \rightarrow \pi^0 e^+ e^-} / \Gamma_{\omega \rightarrow \pi^0 \gamma} &\in [9.68, 9.70] \cdot 10^{-3}, & \Gamma_{\omega \rightarrow \pi^0 e^+ e^-}^{\text{exp}} / \Gamma_{\omega \rightarrow \pi^0 \gamma}^{\text{exp}} &= (9.30 \pm 1.04) \cdot 10^{-3}, \\ \Gamma_{\eta' \rightarrow \omega e^+ e^-} / \Gamma_{\eta' \rightarrow \omega \gamma} &\in [6.82, 6.84] \cdot 10^{-3}. & & \end{aligned} \quad (1.10)$$

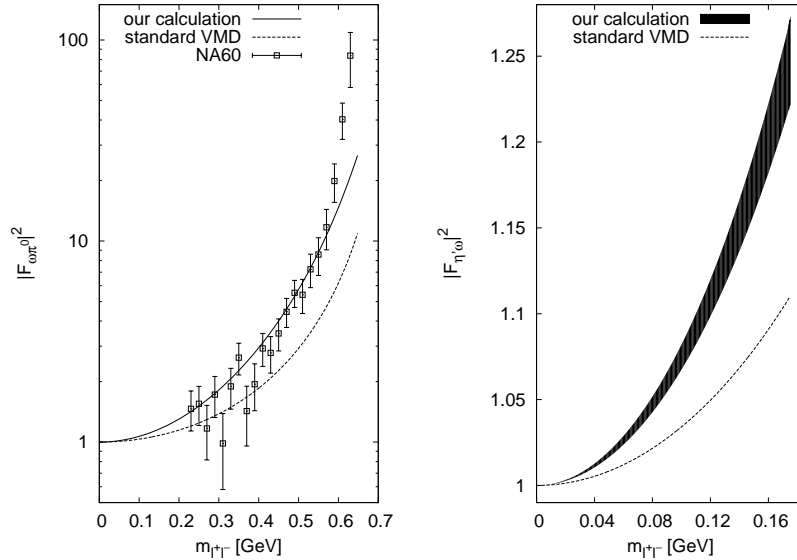


Figure 1.1: **Left-hand side:** $\omega \rightarrow \pi^0$ form factor compared to dimuon data taken by the NA60 collaboration [4]. **Right-hand side:** $\eta' \rightarrow \omega$ transition form factor.

1.3 Decay $P \rightarrow \gamma l^+ l^-$

For the transition of a pseudoscalar meson into a (real) photon, we use a more phenomenological approach by including the Wess-Zumino-Witten action [6]. On the one hand, a pseudoscalar meson can decay into two (real or virtual) photons via two virtual vector mesons. In the counting scheme

(1.1), this is in leading order described by the Lagrangian \mathcal{L}_{vec} . (1.2). On the other hand, the leading-order ChPT Lagrangian, the effective Wess-Zumino-Witten Lagrangian [6]

$$\mathcal{L}_{\text{WZW}} = \frac{3e^2}{8\pi^2 f} \varepsilon^{\mu\nu\alpha\beta} \text{tr} \{ Q^2 \Phi \} \partial_\mu A_\alpha \partial_\nu A_\beta + \mathcal{O}(\Phi^2), \quad (1.11)$$

allows for direct decays. Formally, this term is of order q^4 in our counting scheme (1.1) but nevertheless important as the low-energy leading-order term. Furthermore, the relative sign between both Lagrangians was fixed as negative by comparing the calculated $\eta \rightarrow \gamma$ transition form factor to experimental data.

The $\eta \rightarrow \gamma$ transition form factor is plotted on the left-hand side in Fig. 1.2 (solid line) in comparison to the standard VMD calculation (dashed line) and data taken by the NA60 collaboration for the decay into a dimuon [4]. There is nearly no deviation between the two form factors visible, both describe the data very well. On the right-hand side in Fig. 1.2, the $\eta' \rightarrow \gamma$ transition form factor is plotted (solid line). Again, it is compared to the standard VMD calculation (dashed line). Here, a small deviation between our calculation and standard VMD is visible. Note that both ρ^0 and ω are visible in this form factor.

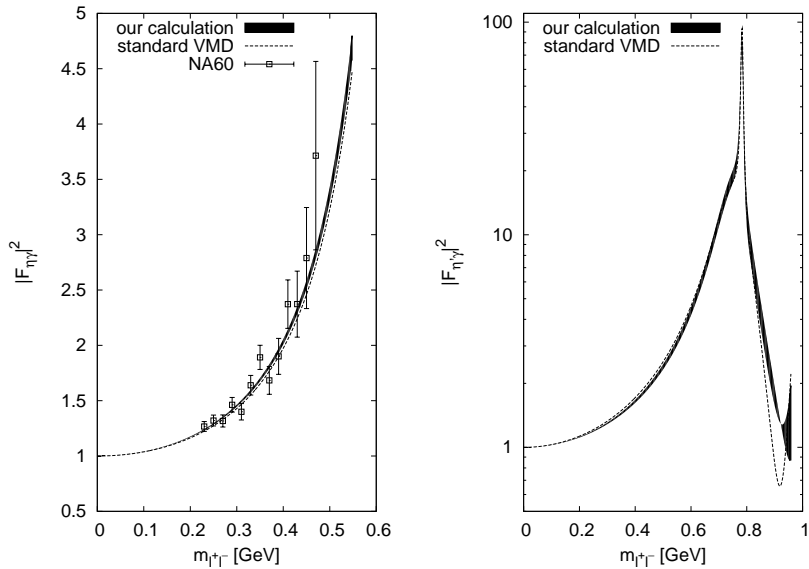


Figure 1.2: **Left-hand side:** $\eta \rightarrow \gamma$ form factor in comparison to dimuon data taken by the NA60 collaboration [4]. **Right-hand side:** $\eta' \rightarrow \gamma$ form factor.

1.4 Summary and outlook

The counting scheme (1.1) was used to calculate transition form factors in leading order. Thereby, the $\omega \rightarrow \pi^0$ form-factor data was much better described than with standard VMD, the $\eta \rightarrow \gamma$ form-factor data as good as with standard VMD. The presented partial decay widths are within acceptable intervals and agree well with the available experimental data. As a next step, next-to-leading order calculations have to be performed.

Bibliography

- [1] M. F. M. Lutz and S. Leupold, *Nucl. Phys.*, **A813**, 96, (2008).
- [2] C. Terschläusen and S. Leupold, in these proceedings.
- [3] C. Terschläusen and S. Leupold, *Phys. Lett.*, **B691**, 191, (2010).
- [4] R. Araldi et al., *Phys. Lett.*, **B677**, 260, (2009).
- [5] K. Nakamura et al., *J. Phys.*, **G37**, 075021, (2010)
- [6] S. Scherer, *Adv. Nucl. Phys.*, **27**, 277, (2003).

π^0 DECAYS MEASURED WITH WASA-at-COSY

CARL-OSCAR GULLSTRÖM*
for the WASA-at-COSY Collaboration

1.1 Introduction

π^0 is the lightest known hadron and can only decay via the electromagnetic interaction. The most common decay is into 2γ (BR 98.82 %) but the interesting physics occurs when decays include leptons. The aim for WASA-at-COSY is to measure the decays $\pi^0 \rightarrow e^+e^-\gamma$, $\pi^0 \rightarrow e^+e^-e^+e^-$ and $\pi^0 \rightarrow e^+e^-$. In $\pi^0 \rightarrow e^+e^-\gamma$ (BR 1.2%) and $\pi^0 \rightarrow e^+e^-e^+e^-$ (BR $3 \cdot 10^{-5}$) the transition form factor reveals the electromagnetic structure of the decaying meson. The e^+e^- mass distribution probe the existence of a new hypothetical boson that couples to the virtual photon [1]. The current upper limit for $\pi^0 \rightarrow e^+e^-\gamma$ is set by the SINDRUM collaboration [2] based on 100.000 events above 25 MeV e^+e^- invariant mass. For $\pi^0 \rightarrow e^+e^-$ the KTeV Collaboration found 795 events in $K_L \rightarrow 3\pi^0$ [3]. They measured a BR of $(7.49 \pm 0.29) \times 10^{-8}$ which exceeds the standard model prediction $(6.23 \pm 0.09 \times 10^{-8})$ [4]. This leads to some speculation about new physics. One promising theory is a new boson U that couples both to quarks and leptons [5]. Excess positrons from the U boson could also explain the intensity and shape of the 511 keV line from the galactic center [6].

1.2 Analysis

During spring 2010 a one week test measurement has been performed with WASA-at-COSY in Jülich. In the experiment proton-proton collisions were used as π^0 sources. The kinetic beam energy was set to 550 MeV in order to maximize the π^0 cross section below threshold for two pion production. The advantage of excluding π^- production is a clean e^- sample for negatively charged tracks.

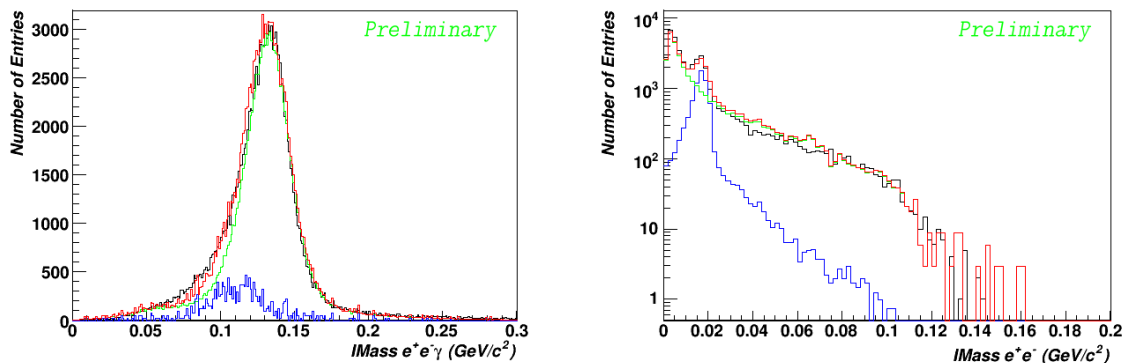


Figure 1.1: Left: Invariant mass distribution of $e^+e^-\gamma$. Right: Invariant mass of e^+e^- pair from the $e^+e^-\gamma$ peak. Black: Data; Green: MC $\pi^0 \rightarrow e^+e^-\gamma$; Blue: Background from pair production in the detector $\pi^0 \rightarrow (\gamma \rightarrow e^+e^-)\gamma$; Red: Total MC sample $\pi^0 \rightarrow e^+e^-\gamma$.

1.2.1 $\pi^0 \rightarrow e^+e^-\gamma$

In $\pi^0 \rightarrow e^+e^-\gamma$ 1.5 million reconstructed $e^+e^-\gamma$ events are available. Out of those 50% is background from external conversion of one photon in the $\pi^0 \rightarrow 2\gamma$ decay. The main cut for reducing such events is the vertex cuts since the main part of the photons convert at the beamtube 30 mm from the interaction point. After cuts 40.000 $\pi^0 \rightarrow e^+e^-\gamma$ events are left with low background and high invariant mass resolution ($\sim 4\%$). The Dalitz distribution in Fig. 1.1 shows no U boson peak

*Department of Physics and Astronomy, Uppsala University, carl-oscar.gullstrom@physics.uu.se

and follows the existing $\pi^0 \rightarrow e^+e^-\gamma$ transition formfactor. Tighter vertex cuts at the expense of efficiency are possible to exclude the pair production peak at 20 MeV, so that an upper limit of U-boson exclusion could be set in this region.

1.2.2 $\pi^0 \rightarrow e^+e^-$

In order to identify the $\pi^0 \rightarrow e^+e^-$ candidates in the high-energy tail of the $\pi^0 \rightarrow e^+e^-\gamma$ events one needs good momentum resolution. The vertex points serve as a check how well momentum was reconstructed by the central tracker. If the curvature is bad also the point of closest approach to the center is bad. To reach the desired resolution even tighter cuts are set than in the $\pi^0 \rightarrow e^+e^-\gamma$ case. Fig. 1.2 shows a peak of 20 $\pi^0 \rightarrow e^+e^-$ event candidates. MC simulations show that there should be about 25 % background from $\pi^0 \rightarrow e^+e^-\gamma$ with a lost photon. The external conversion is completely removed in this region by the vertex cut.

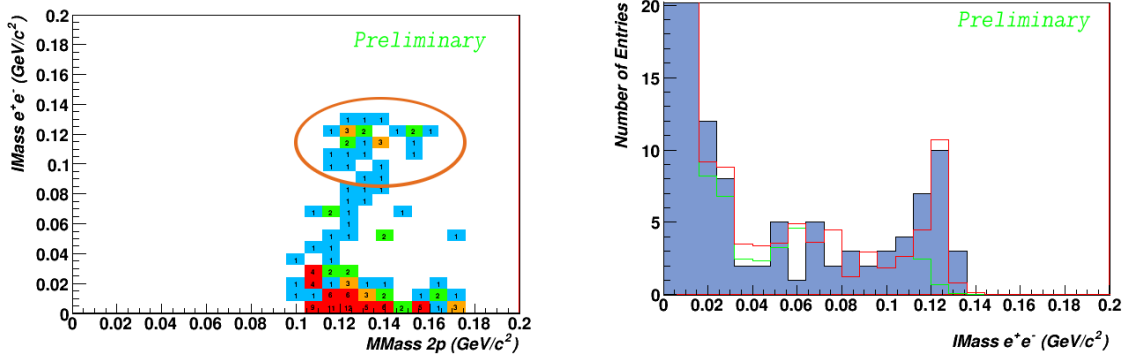


Figure 1.2: Left: Missing mass of 2 protons in the Forward Detector *vs.* invariant mass of e^+e^- pair. Right: invariant mass of e^+e^- pair in the central detector. Blue filled: Data; Green: MC $e^+e^-\gamma$ background; Red: MC simulation of $\pi^0 \rightarrow e^+e^-$ plus $e^+e^-\gamma$ and pair production background.

1.3 Conclusion and Outlook

For the one week test run we reconstructed 40.000 $\pi^0 \rightarrow e^+e^-\gamma$. This data could be used to extend the upper limit on U Boson searches to lower masses. No deviation from the π^0 transition form factor has been found. The 15 event candidates of $\pi^0 \rightarrow e^+e^-$ after background subtraction motivate a longer production run in the future. The test run has not been optimized with respect to trigger and calibration and hence it is possible to reach 50 $\pi^0 \rightarrow e^+e^-$ events per week.

Bibliography

- [1] M. Reece and L.-T. Wang JHEP 07.051 (2009).
- [2] R. Meijer Drees et al. (SINDRUM 1 Collaboration), Phys.Rev.Lett. 68(1992) 3845.
- [3] E. Abouzaid *et. al*, Phys. Rev. D **75** (2007) 012004.
- [4] A. Dorokhov, M. A. Ivanov, Phys. Rev. D **75** (2007) 114007.
- [5] C. Boehm and P.Fayet, Nucl. Phys. B **683** (2004) 219.
- [6] Y Kahn, M. Schmitt, T.M.P. Tait, Phys. Rev. D 78 (2008) 115002.

STUDY OF THE $\eta \rightarrow e^+e^-\gamma$ DECAY

MALGORZATA HODANA*^{†‡} and PAWEŁ MOSKAL*[†]
for the WASA-at-COSY Collaboration

1.1 Introduction

Since the η meson is a short-lived, neutral particle, it is not possible to investigate its structure via the classical method of particle scattering. To learn about its quark wave function, one studies the decay processes of this meson, in which a pair of photons is produced, at least one of them being virtual. The virtual photons have a non-zero mass and convert into lepton-antilepton pairs. The squared four-momentum transferred by the virtual photon corresponds to the squared invariant mass of the created lepton-antilepton pair. Therefore, information about the quarks' spatial distribution inside the meson can be achieved from the lepton-antilepton invariant mass distributions by comparison of empirical results with predictions, based on the assumption that the meson is a point-like particle. The latter can be obtained from the theory of Quantum Electrodynamics. The deviation from the expected behaviour in the leptonic mass spectrum expose the inner structure of the meson. This deviation is characterized by a form factor. It is currently not possible to precisely predict the dependence of the form factor on the four-momentum transferred by the virtual photon in the framework of Quantum Chromodynamics. Therefore, to perform calculations, assumptions about the dynamics of the investigated decay are needed.

The knowledge of the form factors is also important in studies of the muon anomalous magnetic moment, $a_\mu = (g_\mu - 2)/2$, which is the most precise test of the Standard Model and, as well, may be an excellent probe of new physics. The theoretical error of calculation of a_μ is dominated by hadronic corrections and therefore limited by the accuracy of their determination. At present, the discrepancy between the a_μ prediction based on the Standard Model [1] and its experimental value is $(28.7 \pm 8.0) \cdot 10^{-10}$ (3.6σ) [2].

The aim of the data analysis is the investigation of the electromagnetic structure of the η meson by determining the transition form factor using the $\eta \rightarrow e^+e^-\gamma$ decay mode. The probability of creation of a dielectron pair in considered decay is proportional to the probability of emission of a virtual photon with a time-like four-momentum. The square of this four-momentum vector is equal to the square of the mass of created e^+e^- pair. By studying the probability of given decay as a function of the dilepton pair mass, one obtains information about the hadron-photon transition and hence about the electromagnetic structure of decaying neutral meson [3].

1.2 Current status of the analysis

Data were collected using the $pd \rightarrow {}^3\text{He}\eta$ reaction at proton beam momentum of 1.69 GeV/c. The experiment was performed using the WASA-at-COSY detector [4] in November 2008. Data collected during 4 weeks, yielded approximately 10 million η mesons tagged by the ${}^3\text{He}$ ions measured in the Forward Detector.

The event selection in the Central Detector aims at choosing the decay channel of interest. We demand (i) that two tracks corresponding to oppositely charged particles are reconstructed and, (ii) that at least one neutral particle was registered and, (iii) that the signals are correlated in time with signals observed in the Forward Detector within a 12 ns and a 31 ns window for charged and neutral tracks, respectively. The energy deposited by a neutral particle (E_γ) is demanded to drop linearly with increasing opening angle with the nearest charged particle (Ω) starting from 100 MeV for $\Omega = 0^\circ$ and having $E_\gamma = 0$ MeV for $\Omega = 180^\circ$. Additionally, in the η centre of mass system, there has to be only one such neutral candidate, forming with a lepton pair a $\Delta\phi$ angle in the range from 60° to 300° . The identification of electrons is achieved using energy-momentum plot as shown in Fig. 1.1 (right). An additional restriction is imposed on the missing mass of the

*Institute of Physics, Jagiellonian University, PL-30-059 Cracow

[†]IKP1, Forschungszentrum Jülich, Germany

[‡]m.hodana@fz-juelich.de

$pd \rightarrow Xe^+e^-\gamma$ in the range of $2.66 - 2.87 \text{ GeV}/c^2$, further reducing background coming from η decay channels with pions. The efficiency of suppression of the $\eta \rightarrow \pi^+\pi^-\gamma$ and $\eta \rightarrow \pi^+\pi^-\pi^0$ can be seen in Fig. 1.2.

Despite of asking in the analysis for events with two oppositely charged particles, there is a large background coming from the $\eta \rightarrow \gamma\gamma$ decay channel (the one with the highest branching ratio). Since photons may undergo conversion at the beam pipe, the η meson decaying to two photons, may give the same signature at the end as the decay of interest. One can see that in Fig. 1.2 (left) which shows the $M_{e^+e^-}$ spectra from experiment and simulations before applying cut on photon's conversion. In order to suppress background from $\eta \rightarrow \gamma\gamma$ decay, where one of photons undergoes conversion into e^+e^- pair in the beam pipe, the radius of point of closest approach (R_{CA}) is used as presented in Fig. 1.1 (left).

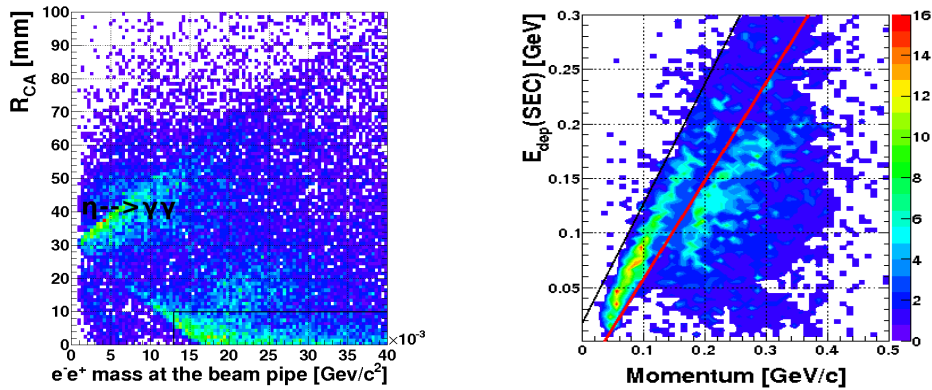


Figure 1.1: Left: experimental distribution of the radius of the point of the closest approach between two helices as a function of the e^+e^- mass (taken from the leptons' three momenta calculated at the beam pipe). The x-axis is zoomed in to see events from the $pd \rightarrow \gamma\gamma$ reaction. The region outside the black lines is discarded from further analysis. Right: experimental spectrum of the energy deposited in the Electromagnetic Calorimeter as a function of particles' momenta. Electrons arrange themselves on the band, along the momentum- E_{dep} diagonal (between black and red lines).

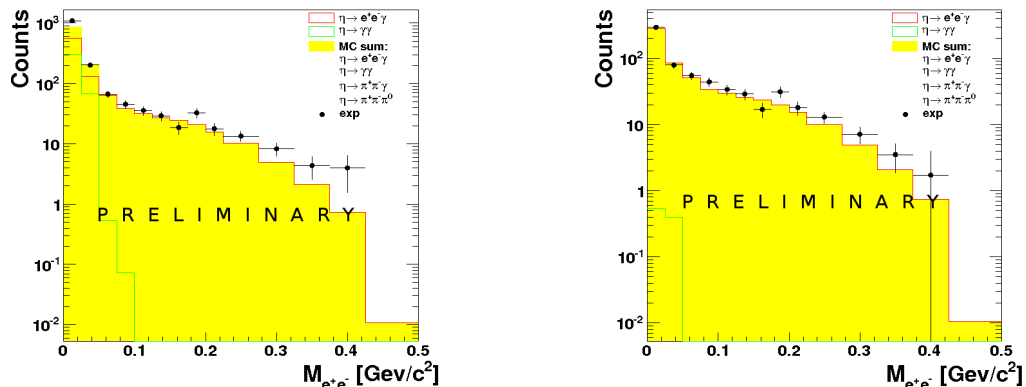


Figure 1.2: The $M_{e^+e^-}$ spectra from the simulations, and the experiment (after prompt pion background subtraction), before applying the cut on the photon conversion (left) and with this cut (right). The spectra are not acceptance corrected.

The $M_{e^+e^-}$ spectrum after selection of $\eta \rightarrow e^+e^-\gamma$ decay channel as described above is shown in Fig. 1.2 (right). Approximately 700 events of $\eta \rightarrow e^+e^-\gamma$ has been reconstructed. The extraction of the transition form factor and the systematic studies are in progress.

Acknowledgements

This publication has been supported by COSY-FFE and by the European Commission under the 7th Framework Programme through the Research Infrastructures action of the Capacities Programme, Call: FP7-INFRASTRUCTURES-2008-1, Grant Agreement N. 227431 and by the Polish Ministry of Science and Higher Education under grants No. 2861/B/H03/2010/38 and 0320/B/H03/2011/40.

Bibliography

- [1] Bennett, G.W. et al., *Phys.Rev.*, **D73** , 072003, (2006).
- [2] Davier, Michel and Hoecker, Andreas and Malaescu, Bogdan and Zhang, Zhiqing, *Eur.Phys.J.*, **C71**, 1515, (2011).
- [3] L. G. Landsberg, *Physics Reports*, **128** (6), p.301-376, (Nov 1985).
- [4] Adam, H. H. and others, nucl-ex/0411038, (2004).

ANALYSIS OF THE DOUBLE DALITZ DECAY

$$\eta \rightarrow e^+ e^- e^+ e^-$$

PATRICK WURM*

for the WASA-at-COSY Collaboration

1.1 Introduction

The Wide Angle Shower Apparatus (WASA) is a large-acceptance detector to study the decay channels of light mesons [1, 2]. It is operated at the Cooler Synchrotron COSY Jülich.

A large number of η mesons is being produced in proton-deuteron and proton-proton collisions. The data permit the study of very rare η -decay channels, like the double Dalitz decay, where the η meson decays via two virtual photons into two electron-positron pairs.

So far, the only published value for the branching ratio is $\mathcal{BR} = (2.4 \pm 0.2_{\text{stat}} \pm 0.1_{\text{syst}}) \times 10^{-5}$ [3]. One objective of the WASA-at-COSY experiment is to determine a value for this branching ratio. A first analysis is based on a $pd \rightarrow {}^3\text{He}\eta$ beam time from 2008, which comprises approximately 10^7 η mesons [4]. The analysis presented here is based on a total amount of 3×10^7 η mesons, which includes additional 2×10^7 η mesons, which have been produced using the same reaction in 2009.

1.2 Analysis chain

In the production reaction $pd \rightarrow {}^3\text{He}\eta$ the η meson is tagged by the ${}^3\text{He}$ nuclei, measured in forward tracking detectors and an arrangement of hodoscopes. ${}^3\text{He}$ can be identified with the $\Delta E - E$ method, where the energy deposit in a thin plastic scintillator is plotted versus the energy deposit in the stopping layer of the hodoscope. The ${}^3\text{He}$ -missing mass distribution is used as a monitoring spectrum to count the number of η events after every cut.

The central part of the detector is used to reconstruct and identify the η -decay products. First, it is checked if the event has two or more positively and negatively charged particles. The charge of a particle is determined by the curvature of the track helix. The helix is measured by a Mini Drift Chamber, embedded in a solenoid magnet.

Due to the large amount of pions, an effective method to distinguish electrons (positrons) and pions must be found. WASA provides particle identification with the momentum information, which is measured by the Mini Drift Chamber, combined with the energy deposit in a Plastic Scintillator Barrel and in an Electromagnetic Calorimeter. Fig. 1.1 shows the electron (positron) and pion bands.

The decision, whether the particle is an electron (positron) or a pion, is based on an artificial neural network implemented in ROOT [5]. After the particle identification, an event candidate must have at least two electrons and two positrons. Out of these tracks all possible pair-combinations are build, which can be the decay product of one of the two virtual photons. In the following, each combination is evaluated to be a double Dalitz decay event.

To get rid of pions which have been misidentified as electrons (positrons), the opening angle between the supposed electron and the positron from the same virtual photon is checked. In case of an electron-positron pair it has to peak at small values.

Another source of background are events, where a photon converts into an electron-positron pair. In case of the single Dalitz decay $\eta \rightarrow e^+ e^- \gamma$, there is the same number of electrons and positrons in the final state as in case of the double Dalitz decay. To suppress such events, the distance between the point of closest approach of the positively and negatively charged particle and the beam center is analyzed as a function of the invariant mass of the lepton-pair, calculated from

*Institut für Kernphysik (IKP) and Jülich Center for Hadron Physics (JCHP), Forschungszentrum Jülich, Germany, p.wurm@fz-juelich.de

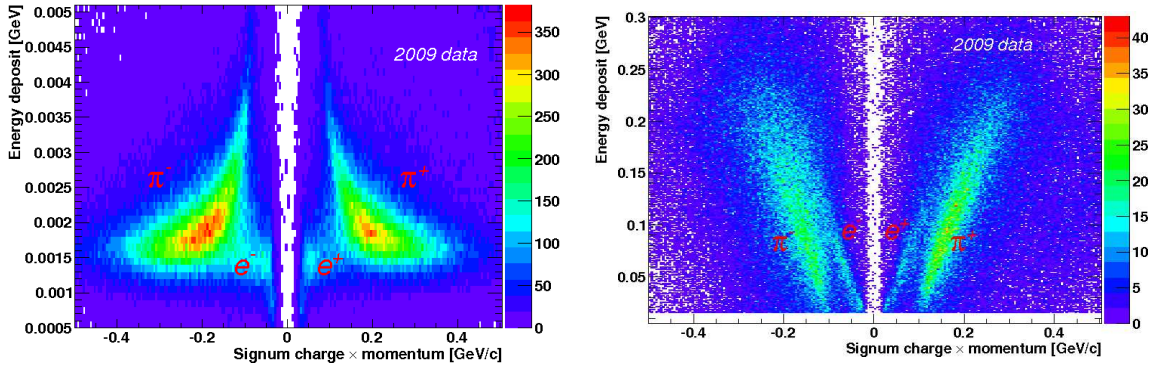


Figure 1.1: Energy deposit in the central part of WASA against the momentum of a particle times its charge. Left: Plastic Scintillator Barrel. Right: Electromagnetic Calorimeter.

their four-vectors at the beam pipe. For conversion events, the invariant mass is zero, since the lepton-pair comes from a real photon. The radius of the closest approach peaks around 30 mm, since this is the radius of the beam pipe. The left panel of Fig. 1.2 shows the distribution for simulated conversion events and for signal events, and the right panel shows the distribution from the data.

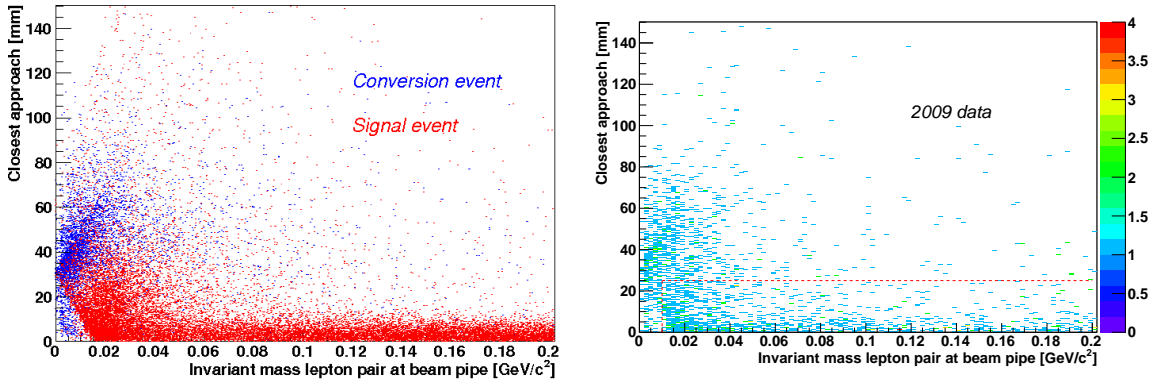


Figure 1.2: Radius of the closest approach of the positively and negatively charged particle against the invariant mass calculated from their four-vectors at the beam pipe. Left: Simulation. Right: 2009 data. The dashed line in denotes the used cut.

After all these cuts the signal to background ratio for η events is $\approx 2/1$, where the main background channels are $\eta \rightarrow \pi^0\pi^0\pi^0$ and $\eta \rightarrow \pi^+\pi^-\pi^0$.

1.3 Results

Fig. 1.3 shows the development of the ${}^3\text{He}$ -missing mass distribution for the 2009 data after each cut. The remaining background events are mainly from direct pion production. To get rid of those events the final ${}^3\text{He}$ -missing mass distribution is fitted with a polynomial function for the direct pion background and a Gaussian function for the η signal. Fig. 1.4 shows the ${}^3\text{He}$ -missing mass distribution from the 2008 and 2009 data after subtracting the direct pion background. After subtracting the background from η decays besides the double Dalitz decay, 52 ± 13 events remain in the distribution.

The combined result from the analysis presented in Ref. [4] and from the analysis, which is presented here, is $\mathcal{BR} = (3.0 \pm 0.8_{\text{stat}} \pm 0.7_{\text{syst(norm.)}}) \times 10^{-5}$ (preliminary), which is in agreement with the value from Ref. [3]. The systematic error comes from the branching ratio calculation based on two different normalization channels, e.g. $\eta \rightarrow e^+e^-\gamma$ and $\eta \rightarrow \pi^+\pi^-e^+e^-$.

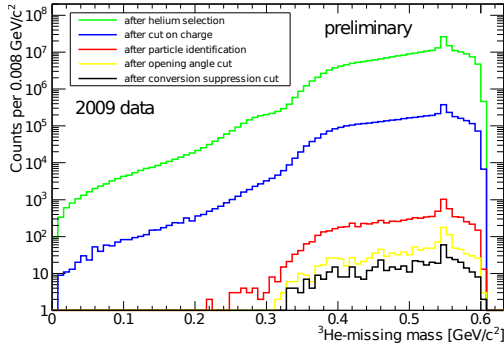


Figure 1.3: Development of the ${}^3\text{He}$ -missing mass distribution (2009 data).

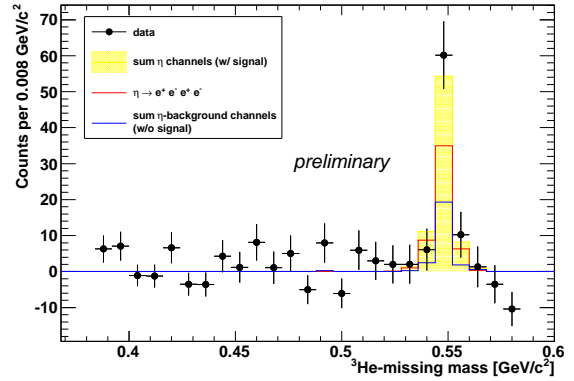


Figure 1.4: Final ${}^3\text{He}$ -missing mass distribution after direct pion background subtraction (2008 and 2009 data).

1.4 Outlook

As a next step the systematic error, which is approximately on the same order of magnitude as the statistical uncertainty, has to be studied in more detail.

The statistics can be improved with $pp \rightarrow pp\eta$ reactions, where WASA-at-COSY has already measured $> 10^8$ η mesons. On the one hand the production cross section is in this reaction around twenty times larger compared with the $pd \rightarrow {}^3\text{He}\eta$ production reaction, but on the other hand there is also a larger contribution from direct pions.

Bibliography

- [1] H. H. Adam et al. (WASA-at-COSY Collaboration), arXiv:nuclex/0411038, (2004)
- [2] C. Bargholtz et al., *Nucl. Instrum. Meth. A*, **594**, 339-350, arXiv:nucl-ex/0803.2657, (2008)
- [3] KLOE Collaboration and KLOE-2 Collaboration, arXiv: 1105.6067, (2011)
- [4] L. Yurev, Study of the decay $\eta \rightarrow e^+e^-e^+e^-$ with WASA-at-COSY, PhD thesis, (2011)
- [5] R. Brun et al., Proc. AIHENP'96 Workshop, Lausanne, Sep. 1996, *Nucl. Inst. and Meth. in Phys. Res. A*, **389**, 81-86, (1997)

DETERMINATION OF THE ELECTROMAGNETIC η TRANSITION FORM FACTOR

*VOLKER METAG**
for the A2 Collaboration

The viewgraph of this presentation can be found at:
http://www2.fz-juelich.de/ikp/primenet/2011_Workshop_Juelich/talks/Metag_Juelich-11_eta-FF_s_print.pdf

*II. Physikalisches Institut, Universität Giessen, Volker.Metag@exp2.physik.uni-giessen.de

DALITZ DECAY OF THE ω MESON

FARHA ANJUM KHAN*

for the WASA-at-COSY collaboration

1.1 Introduction

Our motivation is to measure the electromagnetic transition form factor of the ω meson Dalitz decay $\omega \rightarrow \pi^0 e^+ e^-$. The differential decay width at the vertex of the ω -pion-transition can be described as a product of the differential decay width for point like - particles (a function of invariant mass of dilepton) and the transition form factor, where the form factor is the description of the electromagnetic structure arising at the transition point. The form factor is a function of q^2 where q is the transferred four momentum of the dileptons equivalent to their invariant mass. In this Dalitz decay, the ω vector meson decays into a pseudoscalar meson π^0 and a dilepton. According to the VMD (Vector Meson Dominance) assumption this decay occurs via a virtual ρ meson, $m_\omega \approx m_\rho = 0.77$ GeV, thus a resonance at $m_\gamma^* = \sqrt{q^2} = m_\rho$. Experimentally, the form factor is determined by comparing the dilepton invariant mass spectrum with the point-like Quantum Electrodynamics prediction.

The issue is that the transition form factor for the ω meson does not agree with VMD predictions compared to other meson decays involving dileptons; for example, $\pi^0 \rightarrow \gamma^0 e^+ e^-$ and $\eta \rightarrow \gamma^{01+1-}$ are consistent with VMD predictions. However, even extensions of VMD do not seem to work for the ω meson. There is agreement when the decays of narrow light vector mesons into pseudoscalar mesons and dileptons are calculated to leading order by treating pseudoscalar and vector mesons on equal footing. These theoretical efforts can attempt to go beyond VMD in a systematic way and are in need of further experimental input [1]. Experiments have been performed and results for the ω meson form factor measured from $\mu^+ \mu^-$ are found in the 1986 review by L.G.Landsberg [2] which shows disagreement with calculations. Recently, the NA60 collaboration has claimed to have confirmed the old data [3]. It would be useful to have data with $e^+ e^-$ as an additional experimental approach giving access to smaller virtual photon masses including the full reconstruction of the decaying meson.

Two sets of experiments have been performed with the WASA detector at COSY using two different reaction mechanism. The intention is to compare the quality of the data between pd and pp reactions, in the sense of a feasibility and background study for $\omega \rightarrow e^+ e^- \pi^0$ decays. For $p + d \rightarrow {}^3\text{He} + \omega$ 20 TB of data have been recorded during 12 days of beamtime at two different beam kinetic energies 1.5 GeV and 1.45 GeV. The excess energies are 88 MeV and 63 MeV, respectively. This reaction has a smaller cross section and smaller background than the p+p reaction. The cross section at 1.45 GeV is $83.6 \pm 1.5 \pm 2.2$ nb [4]. The two beam energies have been selected to improve the background subtraction. The pilot experiment for the $p + p \rightarrow p + p + \omega$ reaction has been performed for 11 days at 2.063 GeV beam kinetic energy, 60 MeV excess energy and 18TB of data have been recorded. This reaction has a bigger cross section and significantly more background than p+d. The cross section for this reaction at 2.063 GeV of beam kinetic energy is $5.7 \pm 0.6 \pm 0.8 \pm 0.9 \mu\text{b}$ [5]. The bigger background makes the online and offline event selection more challenging.

1.2 Preliminary analysis

The first analysis is being performed using the p d induced reaction. A preselection, i.e. a subset of acquired data is used for the analysis. The preselection of the p+d reaction was based on the ${}^3\text{He}$ selection by extracting those events where ${}^3\text{He}$ was formed. Particles emitted in the forward direction i.e. ${}^3\text{He}$, can be detected in the forward detection system that includes tracking detectors and range hodoscopes using the ΔE -E method. The decay particles i.e. e^+, e^-, γ can be identified in the central part of the detector. The central detector consists of a mini drift chamber operated in the field of a superconducting solenoid, a plastic scintillator barrel and an electromagnetic

*IKP and JCHP, Forschungszentrum Jülich, Germany, f.khan@fz-juelich.de

calorimeter. We aim to analyse $\omega \rightarrow \gamma^* \pi^0 \rightarrow e^+ e^- \pi^0$ but start with the real photon case $\omega \rightarrow \gamma \pi^0$ which is one of our reference channels. For $\omega \rightarrow \gamma \pi^0 \rightarrow \gamma \gamma \gamma$, the π^0 is reconstructed via the two decay photons. ω mesons can be tagged via the missing mass deduced from the ${}^3\text{He}$ detected in forward direction $M_\omega = \sqrt{(E_p + E_d - E_{\text{He}})^2 - (P_p - P_{\text{He}})^2}$. The ω is also fully reconstructed with the invariant mass $M_{\pi^0 \gamma} = \sqrt{(E_{\pi^0} + E_\gamma)^2 - (P_{\pi^0} + P_\gamma)^2}$. A peak is expected at the ω mass $0.782 \text{ GeV}/c^2$ in both spectra. A two-dimensional spectrum is shown on the left panel of Figure 1. In this histogram one can see an enhancement at the ω mass indicated by the black lines. The background comes from multi pion production. The projection of the spectra is shown on the right panel of Figure 1, one can see a peak at the ω mass (red line) for both energies of the p+d data set. In this histogram one can see an enhancement at the ω mass indicated by black lines. The black dashed line corresponds to $1.5 \text{ GeV}/c^2$ and the blue line correspond $1.45 \text{ GeV}/c^2$ beam kinetic energy. One can see the ω peak at the same point for both energies but with different background features. This will allow to have a better understanding of the background.

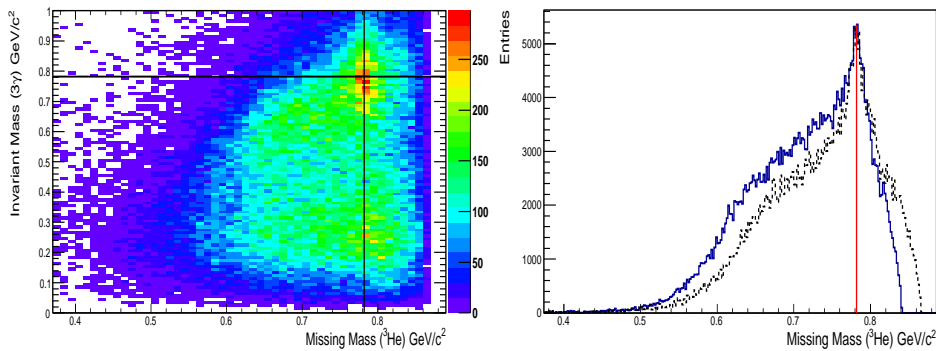


Figure 1.1: The left panel shows the invariant mass vs missing mass plot. The intersection of the two black lines indicate the location of ω peak. The figure on the right panel is the projection for invariant masses above $0.5 \text{ GeV}/c^2$. This figure shows the peak at $0.782 \text{ GeV}/c^2$ (red line) for both energies. The black dashes correspond to $1.5 \text{ GeV}/c^2$ and the blue histogram corresponds to the $1.45 \text{ GeV}/c^2$ data set, showing the two phase space regions and the different position of the peak relative to the background.

For fast analysis we need preselected data for p+p reaction as well. The preselection has been started and data is saved into four different streams, using dedicated experiment triggers and extracting those events where at least two proton tracks were found. Central detector conditions for the four streams are:

stream1: at least 3 neutral tracks in central detector ($\gamma\pi^0$)

stream2: at least 2 charged tracks and at least 2 neutral tracks in central detector ($e^+e^-\pi^0$, and other decays with similar topology)

stream3: at least 2 charged in central detector

stream4: exactly 2 neutral tracks in central detector (background studies)

The goal of the analysis is to find the event candidates in the p+d reaction and compare with the p+p reaction and then decide which reaction can be used for the production beamtime.

Bibliography

- [1] C. Terschluesen, St.Leupold, *arXiv:1003.1030v1 [hep-ph]*.
- [2] L.G. Landsberg, *Phys. Rept.*, **128**, 301, (1985).
- [3] NA60 Collaboration (R. Arnaldi et al.), *Phys. Lett. B*, **677**, 260, (2009).
- [4] K. Schonning et al. CELSIUS/WASA Collaboration, *Phys. Rev. C*, **79**, 044002, (2009).
- [5] S. Barsov et al., *Eur. Phys. J. A*, **31**, 95, (2007).

STUDY OF THE $\phi \rightarrow \eta e^+ e^-$ DECAY AT KLOE

JAROSLAW ZDEBIK*
for the KLOE-2 Collaboration

1.1 Introduction

The analysis of $\phi \rightarrow \eta e^+ e^-$ decay is interesting from several points of view. The structure of ϕ and η mesons and underlying quark dynamics in the transition region can be extracted from $e^+ e^-$ invariant mass spectrum. By comparing the experimentally measured spectrum of the lepton pair with QED calculations for pointlike particles, it is possible to determine transition form factor in the time-like region of momentum transfer [1].

The only one measurement of the form factor comes from SND collaboration is not in good agreement with predictions from the Vector Meson Dominance (VMD) framework [1, 2]. The form factor is often parametrized in one-pole approximation:

$$F_{\phi\eta}(q^2) = \frac{1}{1 - q^2/\Lambda^2}. \quad (1.1)$$

where $q = M_{ee}$ and Λ is a free parameter.

The theoretical calculation for Λ is 1.0 GeV (VMD), which the value measured by SND is 0.5 ± 0.1 GeV [3]. Also is interesting to compare experimental results with another theoretical models [4]. In this paper preliminary results of the investigation of the $\phi \rightarrow \eta e^+ e^-$ decay at KLOE are presented.

Additional goal of this work is also to understand the signature of this channel in the KLOE detector, since it is the main and nonreductive background for dark matter particles searches [5, 6].

1.2 The KLOE detector

The KLOE (**K**long **E**xperiment) detector is installed at the interaction point of the electron and positron beams of the DAΦNE (**D**ouble **A**nnular ϕ -factory for **N**ice **E**xperiments) collider operating in the Laboratori Nazionali di Frascati (LNF).

DAΦNE is an $e^+ e^-$ collider running at a center of mass energy of ~ 1020 MeV (the mass of the ϕ meson). The positron and electron beams collide at an angle of π -(25 mrad), producing ϕ mesons nearly at rest. At the interaction point (IP) the beam pipe has the shape of a sphere which is made of a beryllium-aluminium alloy with 10 cm diameter and 50 μm thickness [6].

This detector was fully constructed by the end of the year 1998 [7]. It consists of two main subsystems: an electromagnetic calorimeter and a large drift chamber. The drift chamber and the calorimeter are inside a superconducting coil which produces a 0.57 T magnetic field parallel to the beam axis.

Energy and time resolutions for calorimeter are $\sigma_E/E = 5.7\%/\sqrt{E}$ (GeV) and $\sigma_t = 57$ ps/ \sqrt{E} (GeV) \oplus 100 ps, respectively. For the drift chamber, the spatial resolutions are $\sigma_{xy} \sim 150$ μm and $\sigma_z \sim 2$ mm. The momentum resolution is $\sigma(p_\perp)/p_\perp \approx 0.4\%$. Vertices are reconstructed with a spatial resolution of ~ 3 mm.

*Institute of Physics, Jagiellonian University, Cracow, Poland, zdebik.jaroslaw@gmail.com

1.3 Event Selection

The analysis of the $\phi \rightarrow \eta e^+ e^-$ decay with subsequent, $\eta \rightarrow \pi^+ \pi^- \pi^0$, has been performed on 1.52 fb^{-1} of the KLOE dataset. The signal Monte Carlo (MC) simulation has been produced with $d\Gamma(\phi \rightarrow \eta e^+ e^-)/dq$ weighted according to Vector Meson Dominance model [1], using the form factor parametrization from the SND experiment [3]. Data-MC corrections for cluster energies and tracking efficiency, evaluated with radiative Bhabha events and $\phi \rightarrow \rho\pi$ samples respectively, have been applied [6].

The first step of the analysis was preselection of events, that have to satisfy the following criteria:

1. two positive and two negative tracks with point of closest approach to the beam line inside a cylinder around the interaction point (IP), with transverse radius $R=4 \text{ cm}$ and length $Z=20 \text{ cm}$;
2. two energy clusters in calorimeter with $E > 7 \text{ MeV}$ not associated to any track, in an angular acceptance $|\cos\theta_\gamma| < 0.92$ and in the expected time window for a photon ($|T_\gamma - R_\gamma/c| < \text{MIN}(5\sigma_t, 2 \text{ ns})$);
3. best $\pi^+ \pi^- \gamma\gamma$ match to the η mass with the pion hypothesis to assign π^\pm tracks; the other two tracks are then assigned to e^\pm ;
4. loose cuts on η and π^0 invariant masses ($495 < M_{\pi^+ \pi^- \gamma\gamma} < 600 \text{ MeV}$, $70 < M_{\gamma\gamma} < 200 \text{ MeV}$).

After this preselection, a clear peak corresponding to $\phi \rightarrow \eta e^+ e^-$ events is observed in the distribution of the recoil mass to the $e^+ e^-$ pair (Fig. 1.1). The second peak at $\sim 590 \text{ MeV}$ is due to $\phi \rightarrow K_S K_L$, $K_S \rightarrow \pi^+ \pi^-$ events with a wrong mass assignment. Events in the $535 < M_{\text{recoil}}(ee) < 560 \text{ MeV}$ window are retained for further analysis.

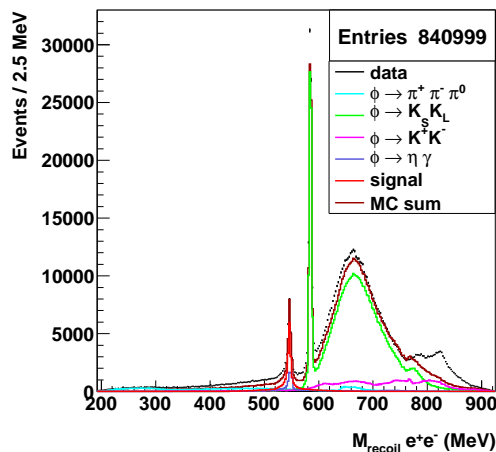


Figure 1.1: Recoiling mass against the $e^+ e^-$ pair for the data sample and MC events after preselection.

The next selection level was performed taking into account the information from the signal channel MC simulation. After the preselection, the remaining background contamination mainly comes from $\phi \rightarrow \eta\gamma$ reaction and events which have more than two charged pions in the final state.

The background, due to $\phi \rightarrow \eta\gamma$ events with photon conversion on beam pipe (BP) or drift chamber walls (DCW), is rejected by tracing back the tracks of the e^+ , e^- candidates and reconstructing their invariant mass (M_{ee}) and distance (D_{ee}) at the BP/DCW surfaces. As both quantities are small in case of photon conversions, $\phi \rightarrow \eta\gamma$ background is removed by rejecting events with: $M_{ee}(BP) < 10 \text{ MeV}$ and $D_{ee}(BP) < 2 \text{ cm}$, $M_{ee}(DCW) < 80 \text{ MeV}$ and $D_{ee}(DCW) < 10 \text{ cm}$. The second relevant background, originated from $\phi \rightarrow K\bar{K}$ decays surviving analysis cuts, has more than two charged pions in the final state and is suppressed using time-of-flight (ToF) to the calorimeter. When an energy cluster is connected to a track, the arrival time to the calorimeter is evaluated both using the calorimeter timing (T_{cluster}) and the track

trajectory ($T_{\text{track}} = L_{\text{track}}/\beta c$). The $\Delta T = T_{\text{track}} - T_{\text{cluster}}$ variable is then evaluated for both electron (ΔT_e) and pion (ΔT_π) mass hypotheses. Events with an e^+ , e^- candidate outside a 3σ 's window on the ΔT_e variables are rejected. The distribution of invariant mass of e^-e^+ pair after all analysis cuts is reported in Fig. 1.2.

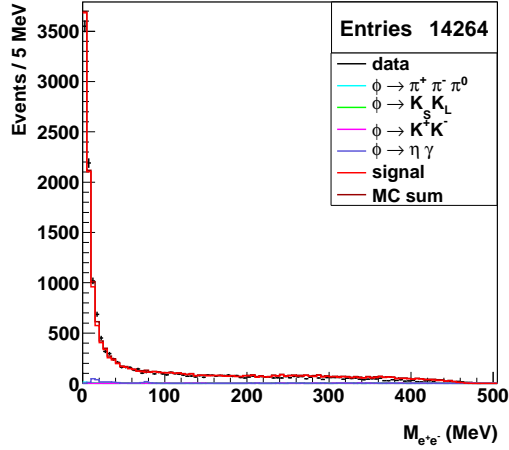


Figure 1.2: Distribution of the e^+e^- invariant mass spectra for the process $\phi \rightarrow \eta e^+e^-$ with $\eta \rightarrow \pi^+\pi^-\pi^0$ decay chain.

After all selection cuts the contamination coming from background events is less than 5% in the final sample and more than 14000 events of $\phi \rightarrow \eta e^+e^-$ reaction we reconstructed. The statistics is almost two orders of magnitude larger than in any previous measurement.

1.4 Preliminary Results

A fit to the invariant mass distribution corrected with acceptance and background subtracted was done using parametrization from Ref. [1].

$$\frac{d\Gamma(\phi \rightarrow \eta e^+e^-)}{dq^2} = \frac{\alpha}{3\pi} \frac{|F_{\phi\eta}(q^2)|^2}{q^2} \sqrt{1 - \frac{4m^2}{q^2}} \left(1 + \frac{2m^2}{q^2}\right) \times \left[\left(1 + \frac{q^2}{m_\phi^2 - m_\eta^2}\right)^2 - \frac{4m_\phi q^2}{(m_\phi^2 - m_\eta^2)^2} \right]^{\frac{3}{2}} \quad (1.2)$$

Free parameters of the fit are Λ (reported in Eq. 1) and an overall normalization factor. The fit result is shown in Fig. 1.3.

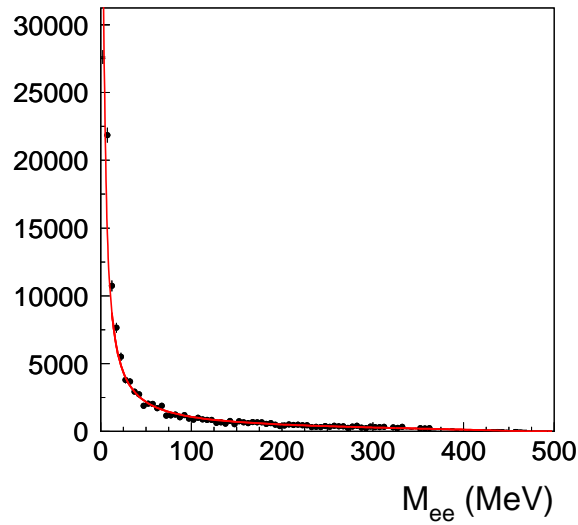


Figure 1.3: Fit to the e^+e^- invariant mass distribution corrected with acceptance and background subtracted.

The achieved statistical error from the fit for Λ is about 0.005 GeV. The evaluation of systematic errors and implementation of the smearing matrix into fit procedure is in progress.

Bibliography

- [1] L.G. Landsberg, *Phys. Rep.*, **128**, 301, (1985).
- [2] A. Faessler, C. Fuchs, M.I. Krivoruchenko, *Phys. Rev.*, **C 61**, 035206, (2000).
- [3] M.N. Achasov et al., *Phys. Lett.*, **B 504**, 275, (2001).
- [4] C. Terschlüsen, S. Leupold, *Phys. Lett.*, **B 691**, 191, (2010).
- [5] C. Boehm, P. Fayet, *Nucl. Phys.*, **B 683**, 219, (2004).
- [6] F. Archilli et. al, e-Print: arxiv 1110.0411, (2011). Submitted to *Phys. Lett.*, **B**.
- [7] F. Bossi et. al., *Nuovo Cimento*, **031**, 531, (2008).

ELECTROMAGNETIC TRANSITION FORM FACTORS OF PSEUDOSCALAR AND VECTOR MESONS

CARLA TERSCHLÜSEN^{†} and STEFAN LEUPOLD^{*}*

1.1 Introduction

The aim of this contribution is the description of two kinds of decays,

- light vector meson (ρ, ω, K^*, ϕ) into a light pseudoscalar meson (π, K, η, η') and a dilepton,
- pseudoscalar meson into a photon and a dilepton.

Both processes might contain intermediate vector mesons.

The most general transition form factor for a decay including a virtual vector meson with mass m is given as

$$F_{\text{gen.}}(q) = g_0 \frac{m^2}{m^2 - q^2} + (1 - g_0) + g_1 \frac{q^2}{m^2} + g_2 \frac{q^4}{m^4} + \dots \quad (1.1)$$

with q^2 denoting the square of the invariant mass of the dilepton. In general, this form factor is an infinite series. Therefore, the parameters cannot be fixed. Progress can be made if it is possible to introduce a power counting scheme which orders the coupling constants g_0, g_1, g_2, \dots according to their importance. Therewith, it is possible to perform calculations up to a given order with a finite number of parameters. Additionally, one will be able to improve the results systematically by adding the next order.

Due to the running coupling constant in QCD, perturbation theory can only be used for high but not for low energies. A possible solution are effective theories which take hadrons instead of quarks as relevant degrees of freedom. The effective theory called Chiral perturbation theory (ChPT) [1] takes the light pseudoscalar mesons as relevant degrees of freedom and treats all other mesons, in particular the vector mesons as heavy. Therefore, it is not applicable for the energy range of the hadronic resonances.

We are using a new counting scheme [2] which treats the masses of both light vector and pseudoscalar mesons as soft, i.e. of the order of a typical momentum q . For decays, all involved momenta are smaller than the mass of the decaying particle and, hence, also of the order of q ,

$$m_V, m_P, \partial_\mu \sim q. \quad (1.2)$$

In ChPT, the range of applicability, i.e. the range for q is limited (on tree level) by the not-considered mesons, in practice by m_V , and (for loops) by the scale $4\pi f$, where f denotes the pion decay constant. In the scheme of [2], where vector mesons are included and where two-particle reducible diagrams (rescattering processes) are resummed, it is suggestive that the range of applicability can be pushed to larger energies. Next-to-leading-order calculations are necessary to assess this proposition. At present, phenomenological consequences are worked out in leading order and compared to data.

1.2 Decay of a light vector meson into a pseudoscalar meson and a dilepton

Using the counting scheme (1.2), one can determine the leading-order Lagrangian for the decay of a vector meson into a pseudoscalar meson and a (real or virtual) photon,

^{*}Uppsala University

[†]`carla.terschluesen@physics.uu.se`

$$\begin{aligned} \mathcal{L}_{\text{vec.}} = & -\frac{1}{16f} h_A \varepsilon^{\mu\nu\alpha\beta} \text{tr} \left\{ [V_{\mu\nu}, \partial^\tau V_{\tau\alpha}]_+ \partial_\beta \Phi \right\} - \frac{1}{16f} b_A \varepsilon^{\mu\nu\alpha\beta} \text{tr} \left\{ [V_{\mu\nu}, V_{\alpha\beta}]_+ [\Phi, \chi_0]_+ \right\} \\ & - \frac{e_V m_V}{4} \text{tr} \{ V^{\mu\nu} Q \} \partial_\mu A_\nu. \end{aligned} \quad (1.3)$$

Thereby, $V_{\mu\nu}$ describes the vector mesons in antisymmetric tensor representation and Φ the pseudoscalar mesons,

$$V_{\mu\nu} := \begin{pmatrix} \rho_{\mu\nu}^0 + \omega_{\mu\nu} & \sqrt{2}\rho_{\mu\nu}^+ & \sqrt{2}K_{\mu\nu}^+ \\ \sqrt{2}\rho_{\mu\nu}^- & -\rho_{\mu\nu}^0 + \omega_{\mu\nu} & \sqrt{2}K_{\mu\nu}^0 \\ \sqrt{2}K_{\mu\nu}^- & \sqrt{2}K_{\mu\nu}^0 & \sqrt{2}\phi_{\mu\nu} \end{pmatrix}, \quad (1.4)$$

$$\Phi := \begin{pmatrix} \pi^0 + \frac{1}{\sqrt{3}}\eta_8 & \sqrt{2}\pi^+ & \sqrt{2}K^+ \\ \sqrt{2}\pi^- & -\pi^0 + \frac{1}{\sqrt{3}}\eta_8 & \sqrt{2}K^0 \\ \sqrt{2}K^- & \sqrt{2}K^0 & -\frac{2}{\sqrt{3}}\eta_8 \end{pmatrix} + \sqrt{\frac{2}{3}} \eta_1 I_{3 \times 3}. \quad (1.5)$$

Furthermore, $\chi_0 = \text{diag} \{m_\pi^2, m_\pi^2, m_K^2\}$, $Q = \text{diag} \{2/3, -1/3, -1/3\}$ and A_ν denotes the photon field. Note that strictly speaking the non-Goldstone boson η_1 was not included in the scheme of [2].

The first two terms in (1.3) describe the decay of a vector meson into a pseudoscalar meson and a virtual vector meson, the last term the decay of the virtual vector meson into a photon. The decay of the photon into a dilepton is described by usual QED. Obviously, the counting scheme (1.2) allows in leading order only for decays via virtual mesons. Additionally, the parameters h_A and b_A can be fixed by comparing the calculated results of two-body decays into real photons to experimental data. There are no additional parameters needed to describe the decays into dileptons so that our calculations for such decays are real predictions.

If the decay can happen only via one type of virtual vector meson with mass m , the standard vector-meson dominance (VMD) form factor equals

$$F_{\text{VMD}}(q) = \frac{m^2}{m^2 - q^2}. \quad (1.6)$$

Our form factor calculated with (1.3) gets an additional non-VMD term,

$$F(q) = g_0 \frac{m^2}{m^2 - q^2} + (1 - g_0). \quad (1.7)$$

On the left-hand side of Fig. 1.1, the $\omega \rightarrow \pi^0$ transition form factor is plotted [3] (solid line) in comparison to the standard VMD form factor (dashed line) and data taken by the NA60 collaboration for the decay into a dimuon [4]. Obviously, the standard VMD form factor fails to describe the data whereas our calculation misses only the last three data points. In the middle of Fig. 1.1, the $\phi \rightarrow \eta$ transition form factor is plotted [3] (solid line). Hereby, the physical η meson is approximated by the octet state η_8 . Again, it is compared to the standard VMD form factor (dashed line) and data taken at the VEPP-2M detector for the decay into a dielectron [5]. Due to the relatively large error bars there is no assessment possible which form factor describes the data better. In the near future better data are expected from KLOE¹.

1.3 Decay of a light pseudoscalar meson into a photon and a dilepton

As a more phenomenological approach for the decay of a light pseudoscalar meson into two (real or virtual) photons, we take both our Lagrangian (1.3) describing the decay via two virtual vector mesons and the Wess-Zumino-Witten Lagrangian [1]

$$\mathcal{L}_{\text{WZW}} = \frac{3e^2}{8\pi^2 f} \varepsilon^{\mu\nu\alpha\beta} \text{tr} \{ Q^2 \Phi \} \partial_\mu A_\alpha \partial_\nu A_\beta + \mathcal{O}(\Phi^2) \quad (1.8)$$

¹See the contribution by Jaroslaw Zdebek in these proceedings.

which describes the direct decay into two photons. Additionally, the η - η' mixing is given by

$$\eta = \cos \theta \eta_8 - \sin \theta \eta_1 \quad \wedge \quad \eta' = \sin \theta \eta_8 + \cos \theta \eta_1 \quad (1.9)$$

with the mixing angle $\theta \approx -19.5^\circ$.

The $\eta \rightarrow \gamma$ transition form factor is plotted on the right-hand side of Fig. 1.1 (solid line) in comparison to the standard VMD form factor² (dashed line) and data taken by the NA60 collaboration for the decay into a dimuon [4]. Here, the form factors are on top of each other and describe the data equally well.

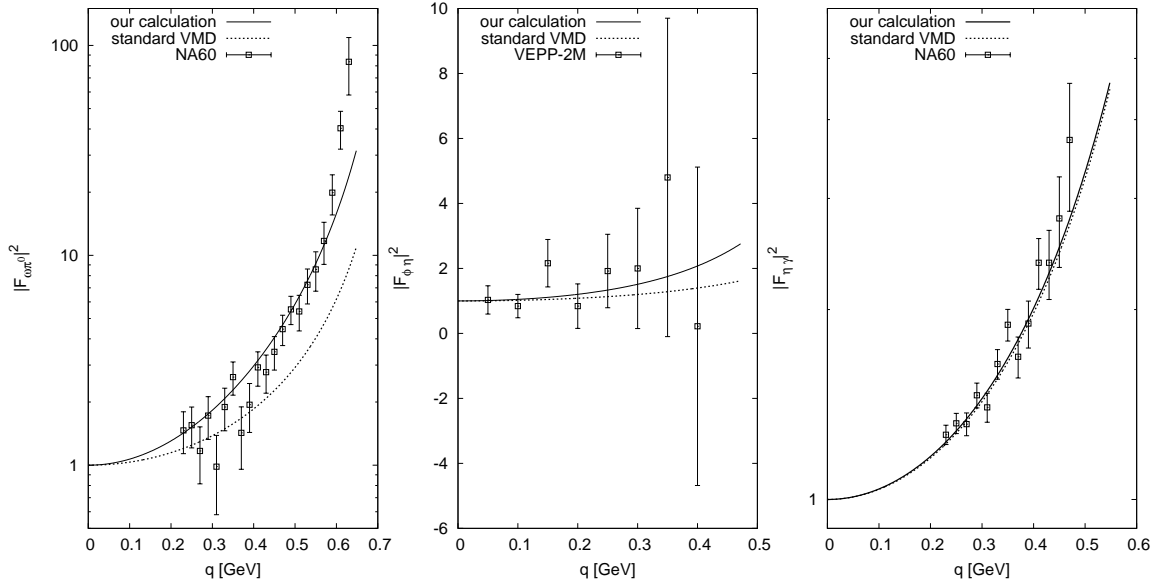


Figure 1.1: **Left-hand side:** $\omega \rightarrow \pi^0$ form factor compared to dimuon data taken by the NA60 collaboration [4]. **Middle:** $\phi \rightarrow \eta$ form factor compared to dielectron data taken at the VEPP-2M detector [5]. **Right-hand side:** $\eta \rightarrow \gamma$ form factor compared to dimuon data taken by the NA60 collaboration [4]. The first two results are published in [3].

1.4 Summary and outlook

Using a new counting scheme (1.2) we were able to determine the leading-order Lagrangian for the decays $V \rightarrow Pl^+l^-$ and for the vector part of the decay $P \rightarrow \gamma l^+l^-$. The form factors for the transitions $\omega \rightarrow \pi^0$, $\phi \rightarrow \eta$ and $\eta \rightarrow \gamma$ describe the experimental data very well, especially the $\omega \rightarrow \pi^0$ transition is much better described than with standard VMD. Additionally, we were able to describe the partial decay widths very well [3]. As a next step, next-to-leading order calculations have to be performed.

Bibliography

- [1] S. Scherer, *Adv. Nucl. Phys.*, **27**, 277, (2003).
- [2] M. F. M. Lutz and S. Leupold, *Nucl. Phys.*, **A813**, 96, (2008).
- [3] C. Terschläusen and S. Leupold, *Phys. Lett.*, **B691**, 191, (2010).
- [4] R. Araldi et al., *Phys. Lett.*, **B677**, 260, (2009).
- [5] M. N. Achasov et al., *Phys. Lett.*, **B504**, 275, (2001).

²The decay $\eta \rightarrow \gamma l^+l^-$ can happen via all three neutral light vector mesons and, therefore, the standard VMD form factor is more complicated than for the case of only one type of possible virtual meson.

INVESTIGATION OF $\omega \rightarrow \pi^+\pi^-\pi^0$ WITH WASA-AT-COSY

LENA HEIJKENSKJÖLD* AND SIDDESH SAWANT†
for the WASA-at-COSY Collaboration

1.1 Introduction

The WASA-at-COSY collaboration has recently performed experiments dedicated to studies of the ω meson decays. One of the decay channels that will be under detailed investigations is the most probable decay of the ω meson into $\pi^+\pi^-\pi^0$. The goal of this experiment is the investigation of the ω decay mechanism to three pions. This information may be gained from a comparison of the density distribution in Dalitz plot with appropriate theoretical predictions. To reach this goal a high statistics experimental Dalitz plot distribution is necessary. Measurements of the Dalitz plot for $\omega \rightarrow \pi^+\pi^-\pi^0$ decay have been done before in experiments on the determination of the spin and parity of the ω meson [1]. However, the statistics of existing measurements is limited to about 4600 $\omega \rightarrow 3\pi$ events. The WASA-at-COSY experiment has produced a higher amount of fully reconstructed $\omega \rightarrow 3\pi$ events using proton-proton and proton-deuteron collisions.

The decay mechanism was considered within Vector Meson Dominance model as proceeding via the $\rho\pi$ intermediate state [2]. More recent predictions base on a counting scheme for flavor-SU(3) systems of Goldstone bosons and light vector mesons [3]. The importance of the $\pi\pi$ final state interaction is also considered [4]. However, the expected deviations from Vector Meson Dominance model are small.

1.2 WASA-at-COSY

The experiments have been performed with the WASA detector setup at COSY [5]. COSY (COoler SYNchrotron) is a synchrotron and storage ring which can provide a beam of (un)polarized protons or deuterons with a momentum range of 600-3700 MeV/c.

WASA (Wide Angle Shower Apparatus) is a nearly 4π detector optimised for studying production and decay of light mesons. A unique pellet generator provides frozen pellets of hydrogen and deuterium as a fixed target. The central part of WASA can detect both charged and neutral particles while the forward detector is designed to detect scattered projectiles and charged recoil particles like protons, deuterons and He nuclei.

1.3 The current analyses

In spring 2011, WASA-at-COSY collected data of ω production in proton beam on proton target (p-p) collisions ($p+p \rightarrow p+p+\omega$) at $T_p=2.063$ GeV and in proton beam on deuteron target (p-d) collisions ($p+d \rightarrow {}^3\text{He}+\omega$) at $T_p=1.45$ GeV and $T_p=1.5$ GeV. The corresponding excess energies are 60 MeV for the p-p reaction and 63 MeV and 88 MeV for the p-d reaction, respectively. These two reaction have complementary advantages and drawbacks, which are summarised in Tab. 1.1.

1.3.1 First preliminary results

Preliminary analyses have been performed on both data sets. In these analyses the protons or the ${}^3\text{He}$ particles are identified in the forward part of WASA using the $\Delta E/E$ technique. The decay products of the ω are detected in the central part of WASA. For charged pions, the charge and momentum are reconstructed using information from the central mini drift chamber placed in the solenoid magnetic field. The π^0 is reconstructed using the energy deposit and angle in the central calorimeter of the two photons.

In presented analysis 11% for the p-d data and 15% for the p-p data of the detected events have been analysed. On the left panel of Fig. 1.1, which shows the missing mass of the ${}^3\text{He}$ detected

*Uppsala University, lena.heijkenskjoeld@physics.uu.se

†Indian Institute of Technology Bombay, sawantsiddhesh08@gmail.com

Table 1.1: The table displays the advantages and drawbacks of the two production reactions.

Reaction	Advantage	Drawback
p-p	Higher production cross section, at $T_p = 2.063$ GeV $\sigma_{\text{tot}} = 5.7 \mu\text{b}$ [6].	Fast protons, majority punches through forward part of detector. Requires elaborate trigger.
p-d	Simple triggering on ${}^3\text{He}$. ${}^3\text{He}$ stops in forward part of detector. Advantageous for tagging.	Lower production cross section, at $T_p = 1.45$ GeV $\sigma_{\text{tot}} = 83.6$ nb [7].

for $p + d \rightarrow {}^3\text{He} + \pi^+ + \pi^- + \pi^0$, a peak at the value of ω mass is clearly visible. In the middle plot of Fig. 1.1 the three pion invariant mass versus the missing mass of two protons detected for $p + p \rightarrow p + p + \pi^+ + \pi^- + \pi^0$ reaction is presented. By putting a cut shown in the figure on the invariant mass of three pions around the ω meson mass, the missing mass of two protons (right plot in Fig. 1.1) does not show a clear peak but only a shoulder at the value of ω mass. This suggests a small ω meson signal hidden under the three pion background.

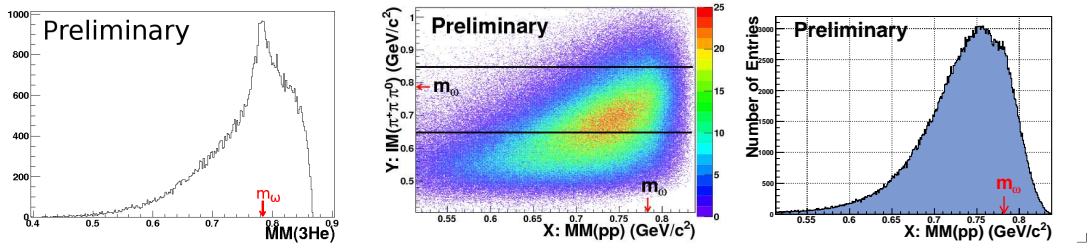


Figure 1.1: **Left:** The missing mass deduced from the ${}^3\text{He}$ in the p-d data at $T_p = 1.5$ GeV. **Middle:** The invariant mass of three pions versus the missing mass from the protons in the p-p data. Black lines show the cut on the invariant mass of $\pi^+\pi^-\pi^0$. **Right:** The missing mass from the protons in the p-p data after the cut on the invariant mass of the three pions.

1.3.2 Outlook

In order to extract the ω signal, the next steps in the analyses would be fine tuning of energy calibration of all detectors. Then the kinematic fitting method will be applied to improve overall resolution. These steps should allow to obtain the best signal to background ratio and properly select the ω signal.

Bibliography

- [1] M. L. Stevenson et al., *Phys. Rev.*, **125**, 687, (1962)
- [2] M. Gell-Mann, D. Sharp, W. G. Wagner, *Phys. Rev. Lett.* **8** (1962) 261.
- [3] S. Leupold, M.F.M. Lutz, *Eur. Phys. J. A*, **39**, 205, (2009).
- [4] Contribution to these proceedings by F. Niecknig, S. Schneider, B. Kubis, Universität Bonn
- [5] H. H. Adam et al., arXiv:nucl-ex/0411038
- [6] S. Barsov et al., *Eur. Phys. J. A*, **31**, 95, (2007)
- [7] K. Schönning et al. CELSIUS/WASA Collaboration, *Phys. Rev. C*, **79**, 044002, (2009)

DISPERSIVE ANALYSES OF $\omega/\phi \rightarrow 3\pi$ AND $\eta' \rightarrow \eta\pi\pi$

SEBASTIAN P. SCHNEIDER[†], FRANZ NIECKNIG*[‡] AND BASTIAN KUBIS**

1.1 Introduction

The advent of high-statistics measurements of hadronic three-body decays calls for equally accurate theoretical descriptions. In this context rescattering effects between decay products play a very important role if one aspires to perform precision amplitude analyses. While perturbative approaches, such as chiral perturbation theory or non-relativistic approaches, implement final-state interactions up to a certain order in a small power-counting parameter and are restricted to a low-energy regime, dispersive approaches resum hadronic rescattering up to all orders and thus allow for an extension to higher energies. While the groundwork for dispersive analyses of hadronic three-body decays has been laid long ago [1], high-accuracy parameterizations of phase-shifts and sufficient computational power, which are necessary for such an enterprise, have only recently become available.

We apply the dispersive approach to two specific examples. $\omega/\phi \rightarrow 3\pi$ is the simplest imaginable system in which three-body effects in hadronic rescattering can be studied, due to the fact that the decaying particles are of vector type. If one neglects contributions from F- and higher partial waves, the system is completely determined by P-wave interactions. In the case of $\phi \rightarrow 3\pi$ the phase space is sufficiently large to study three-body effects on the ρ -resonance. With its large existing (ϕ : KLOE/CMD-2 [2, 3]) and upcoming (ω : WASA-at-COSY) data base $\omega/\phi \rightarrow 3\pi$ provides an ideal testing ground for the approach.

$\eta' \rightarrow \eta\pi\pi$ on the other hand is one of the very few processes in which effects from $\pi\eta$ scattering might be studied, in the hope of gathering information on $\pi\eta$ phase shifts. Additionally, the neutral channel $\eta' \rightarrow \eta\pi^0\pi^0$ exhibits a cusp effect that may allow for a determination of $\pi\pi$ S-wave scattering lengths [4]. Finally, recent and upcoming experimental efforts from various collaborations (BES-III, WASA-at-COSY, ELSA, CB-AT-MAMI-C) call for a renewed analysis.

1.2 The framework

The goal of the dispersive approach is to relate the decay amplitudes to a set of integral equations derived from the fundamental principles of unitarity and maximal analyticity, which are then solved numerically. We follow a Khuri–Treiman type dispersion relation ansatz [1], where the dispersive result for two-body scattering is linked to the three-body decay by analytic continuation in the mass of the decaying particle and the center-of-mass energy.

1.2.1 Decay amplitude for $\omega/\phi \rightarrow \pi^0\pi^+\pi^-$

In the following we resort to the standard Mandelstam representation for three-body decays, $s = (p_{\pi^-} + p_{\pi^+})^2$, $t = (p_{\pi^-} + p_{\pi^0})^2$, $u = (p_{\pi^+} + p_{\pi^0})^2$ with $s + t + u = 3s_0 \equiv M_V^2 + 3M_\pi^2$, where $M_V = M_{\omega/\phi}$ is the mass of the decaying vector meson. The process is of odd intrinsic parity and we may decompose the amplitude $\mathcal{M}(s, t, u)$ according to

$$\mathcal{M}(s, t, u) = \epsilon_{\mu\nu\alpha\beta} n^\mu p_{\pi^+}^\nu p_{\pi^-}^\alpha p_{\pi^0}^\beta \mathcal{F}(s, t, u) , \quad (1.1)$$

where n^μ is the polarization vector of the decaying ω/ϕ . Due to Bose symmetry only odd angular momenta contribute in the partial-wave expansion of $\mathcal{F}(s, t, u)$. We restrict our analysis to P-wave contributions only, since the effects of F- and higher partial waves are expected to be significantly

*Helmholtz-Institut für Strahlen- und Kernphysik and Bethe Center for Theoretical Physics, Universität Bonn

[†]Talk; schneider@hiskp.uni-bonn.de

[‡]Poster; niecknig@hiskp.uni-bonn.de

suppressed. The P-wave part of the amplitude can be decomposed into a sum of single-variable amplitudes $\mathcal{F}(s)$ (compare [5]),

$$\mathcal{F}(s, t, u) = \mathcal{F}(s) + \mathcal{F}(t) + \mathcal{F}(u) . \quad (1.2)$$

Imposing unitarity and elastic final-state interactions provides us with the discontinuity of $\mathcal{F}(s)$ [6],

$$\text{disc } \mathcal{F}(s) = 2i[\mathcal{F}(s) + \hat{\mathcal{F}}(s)]e^{-i\delta_1(s)} \sin(\delta_1(s)) , \quad (1.3)$$

where $\mathcal{F}(s) + \hat{\mathcal{F}}(s)$ is the P-wave projection of $\mathcal{F}(s, t, u)$ and $\delta_1(s)$ the $\pi\pi$ P-wave phase shift taken from phenomenology [7, 8]. The inhomogeneity $\hat{\mathcal{F}}(s)$ is given as

$$\begin{aligned} \hat{\mathcal{F}}(s) &= 3\langle(1-z^2)\mathcal{F}\rangle , \quad \langle z^n f \rangle = \frac{1}{2} \int_{-1}^1 dz z^n f \left(\frac{3s_0 - s + z\kappa(s)}{2} \right) , \\ \kappa(s) &= \sqrt{1 - \frac{4M_\pi^2}{s}} \sqrt{((M_V + M_\pi)^2 - s)((M_V - M_\pi)^2 - s)} . \end{aligned} \quad (1.4)$$

To solve for the amplitude we use a product ansatz $\mathcal{F}(s) = \Omega(s)\phi(s)$ where $\Omega(s)$ is the well-known Muskhelishvili–Omnès (MO) solution to the homogeneous equation $\hat{\mathcal{F}}(s) = 0$ [9]. For $\mathcal{F}(s)$ we thus obtain

$$\mathcal{F}(s) = \Omega(s) \left\{ \alpha + \frac{s}{\pi} \int_{4M_\pi^2}^{\infty} \frac{ds'}{s'} \frac{\hat{\mathcal{F}}(s') \sin(\delta(s'))}{|\Omega(s')|(s' - s)} \right\} , \quad \Omega(s) = \exp \left\{ \frac{s}{\pi} \int_{4M_\pi^2}^{\infty} \frac{ds'}{s'} \frac{\delta(s')}{(s' - s)} \right\} . \quad (1.5)$$

The subtraction constant α is fixed by the partial decay width. The number of subtractions is chosen such that the dispersion integral is guaranteed to converge. The issue of performing the double integration correctly in view of the analytic continuation in M_V and s will not be discussed here. We refer to [10] and references therein.

1.2.2 $\eta' \rightarrow \eta\pi\pi$

Similarly to the $\omega/\phi \rightarrow 3\pi$ case we can decompose the full amplitude into isospin components,

$$\mathcal{M}(s, t, u) = \mathcal{M}_0^{\pi\pi}(s) + \mathcal{M}_0^{\pi\eta}(t) + \mathcal{M}_0^{\pi\eta}(u) , \quad (1.6)$$

with the amplitudes of the $\pi\pi$ S-wave $\mathcal{M}_0^{\pi\pi}$ and the $\pi\eta$ S-wave $\mathcal{M}_0^{\pi\eta}$. We neglect the exotic $\pi\eta$ P-wave throughout. The set of integral equations can be obtained analogously as before,

$$\begin{aligned} \mathcal{M}_0^{\pi\pi}(s) &= \Omega_0^{\pi\pi}(s) \left\{ a_0 + b_0 s + c_0 s^2 + \frac{s^3}{\pi} \int_{4M_\pi^2}^{\infty} \frac{ds'}{s'^3} \frac{\sin \delta_0^{\pi\pi}(s') \hat{\mathcal{M}}_0^{\pi\pi}(s')}{|\Omega_0^{\pi\pi}(s')|(s' - s - i\epsilon)} \right\} , \\ \mathcal{M}_0^{\pi\eta}(t) &= \Omega_0^{\pi\eta}(t) \left\{ a_1 + \frac{t^2}{\pi} \int_{t_\eta}^{\infty} \frac{dt'}{t'^2} \frac{\sin \delta_0^{\pi\eta}(t') \hat{\mathcal{M}}_0^{\pi\eta}(t')}{|\Omega_0^{\pi\eta}(t')|(t' - t - i\epsilon)} \right\} , \quad t_\eta = (M_\eta + M_\pi)^2 . \end{aligned} \quad (1.7)$$

We fix the $\pi\eta$ phase shift $\delta_{\pi\eta}$ using a simplified unitarization model. The subtraction constants are matched to Resonance Chiral Theory (RChT, see [11]), using a narrow-width-resonance approximation for the Omnès function $\Omega(s) \rightarrow M_S^2/(M_S^2 - s)$. This is by no means a perfect method to fix the subtraction constants, since obviously the $\pi\pi$ S-wave is not well-described by a resonance approximation. An alternative would be to match to large- N_C chiral perturbation theory. In this case, however, it is not clear how to properly treat resonance contributions in the low-energy constants.

1.3 Preliminary numerical results

The integral equations are solved numerically by an iterative procedure. We start out with an arbitrary input function and calculate the inhomogeneity $\hat{\mathcal{F}}(s)$. The single-variable amplitude is then calculated from this inhomogeneity, which is in turn used as input for the following iteration step. We repeat the procedure until convergence is reached up to satisfactory accuracy.

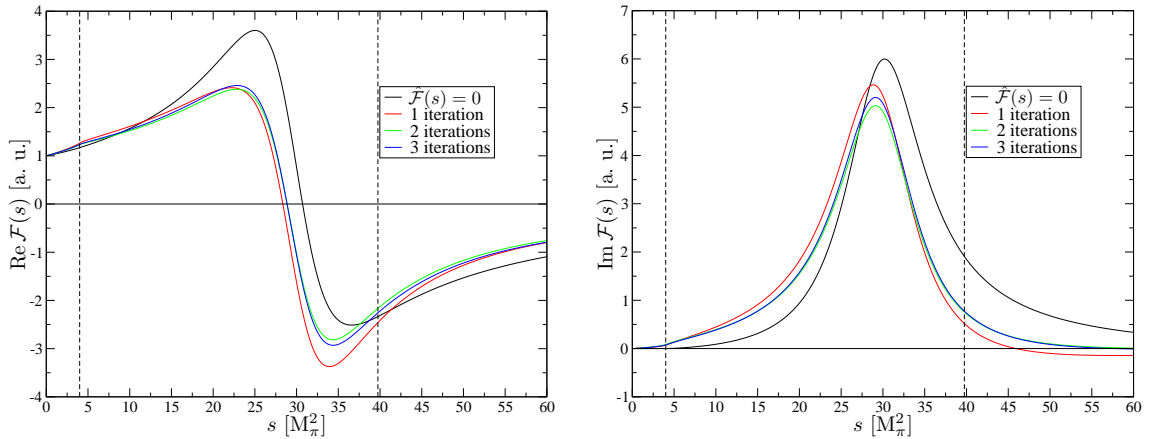


Figure 1.1: Successive iterations steps of real (left) and imaginary (right) part of the amplitude $\mathcal{F}(s)$ for $\phi \rightarrow 3\pi$. The dashed lines denote the physical region of the decay.

1.3.1 $\phi/\omega \rightarrow 3\pi$ amplitudes and Dalitz plot

To illustrate the convergence of the iteration procedure the $\phi \rightarrow 3\pi$ amplitude $\mathcal{F}(s)$ is plotted after each iteration step in Fig. 1.1. We have chosen the MO function as the starting point for the iteration. It should be mentioned that the final result of the iteration is independent of the specific choice of the starting point; however, choosing the MO function allows us to quantify crossed-channel rescattering effects in a plausible way. We find that these effects are sizable and from the point of view of precision analyses certainly not negligible. As seen in Fig. 1.1, convergence of the amplitude is reached after three iterations; for $\omega \rightarrow 3\pi$ (not shown here), this is the case after two iterations.

For a three-body decay, the Dalitz plot distribution is of particular interest. The Dalitz plot is a two-dimensional scatter plot in terms of two kinematic variables; in the case of $\phi/\omega \rightarrow 3\pi$ it is common practice to use $x = (t - u)/(2M_V)$ and $y = [(M_V - M_\pi)^2 - s]/(2M_V)$. The *normalized* Dalitz plot is shown in Fig. 1.2; we note that it is independent of the subtraction constant, so that Fig. 1.2 is free from any input aside from the $\pi\pi$ P-wave phase shift, which is well-established up to roughly 1.2 GeV.

The $\omega \rightarrow 3\pi$ Dalitz plot is a relatively smooth distribution, which rises from the center to its border. The outer corners show a maximum increase of roughly 20% with respect to the center. In contrast, the $\phi \rightarrow 3\pi$ Dalitz plot exhibits significantly more structure. From its center the Dalitz plot rises towards the bands created by the ρ resonance, and then steeply falls off towards the outer corners. The profile of the $\phi \rightarrow 3\pi$ Dalitz plot seems to agree qualitatively with the one shown in [2]; for an in-depth analysis, closer comparison to the data is certainly required.

Finally we wish to study the effects of crossed-channel rescattering on the Dalitz plot distribution. For that purpose, we follow two different approaches to fix the subtraction constant. First we assume that the subtraction constant is given by some independent method, and we are interested in what bearings the crossed-channel effects have on both the overall shape of the Dalitz plot

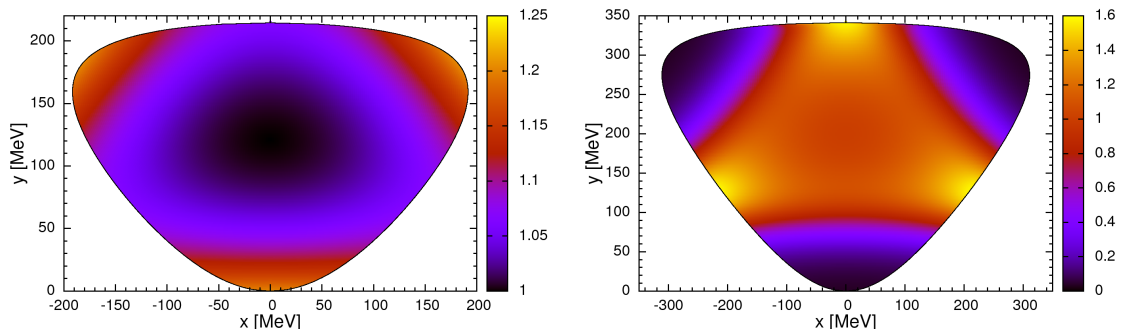


Figure 1.2: Normalized Dalitz plot for $\omega \rightarrow 3\pi$ (left) and $\phi \rightarrow 3\pi$ (right).

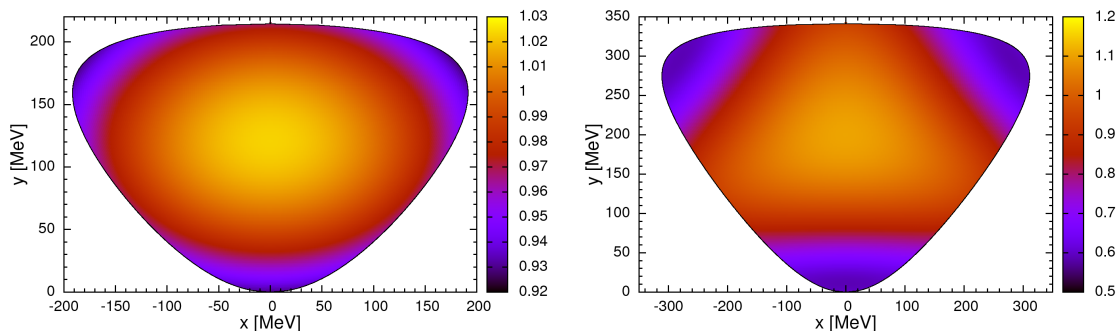


Figure 1.3: $|\mathcal{F}_{\text{full}}|^2/|\mathcal{F}_{\hat{\mathcal{F}}=0}|^2$ for $\omega \rightarrow 3\pi$ (left) and $\phi \rightarrow 3\pi$ (right). The subtraction constant is fixed so that it reproduces the decay width before and after the iteration.

and the partial decay width. We fix the subtraction constant from the experimental decay width for the case $\hat{\mathcal{F}} = 0$. The effect on the decay width in both processes amounts to roughly 20%. However, while the partial width of $\omega \rightarrow 3\pi$ sees an increase, it suffers a decrease in $\phi \rightarrow 3\pi$. The same qualitative behaviour shows up in the Dalitz plot distribution.

In our second approach, we match the subtraction constant to reproduce the experimental decay width in both cases, that is with and without crossed-channel rescattering effects included. We then study the effects on the profile of the Dalitz plot. The result of this approach is shown for both $\omega \rightarrow 3\pi$ and $\phi \rightarrow 3\pi$ in Fig. 1.3. One observes that the effects of crossed-channel rescattering are to a large degree absorbed in the partial width. The overall behavior is very similar: in both processes one observes an increase from the outer corners to the center of the Dalitz plot. It is noteworthy that the ρ resonance bands in $\phi \rightarrow 3\pi$ are left relatively untouched.

For a rough error estimate we have varied the cutoff in both the integral of the MO function and the dispersion integral. Further we have varied between two sets of phenomenological representations of the $\pi\pi$ P-wave phase shifts [7, 8]. We found that these effects are small and certainly not comparable to the sizable crossed-channel effects.

1.3.2 $\eta' \rightarrow \eta\pi\pi$ Dalitz plot

The $\eta' \rightarrow \eta\pi\pi$ amplitude exhibits a similar convergence behavior as $\phi \rightarrow 3\pi$. Crossed-channel effects are sizable and convergence is reached only after three iterations. It is also interesting to study the effects of crossed-channel rescattering on the Dalitz plot, more specifically the Dalitz plot parameters. Slightly different conventions for the Dalitz plot variables in $\eta' \rightarrow \eta\pi\pi$ as opposed to $\omega/\phi \rightarrow 3\pi$ are used, namely

$$y = \frac{(M_\eta + 2M_\pi)(M_{\eta'} - M_\eta)^2 - s}{2M_{\eta'}M_\pi(M_{\eta'} - M_\eta - 2M_\pi)} - 1, \quad x = \frac{\sqrt{3}(t - u)}{2M_{\eta'}(M_{\eta'} - M_\eta - 2M_\pi)}, \quad (1.8)$$

where s and t are defined analogously as before. The amplitude squared can then be expanded around the center of the Dalitz plot in terms of x and y according to

$$|\mathcal{M}(x, y)|^2 = |\mathcal{N}|^2 \{1 + ay + by^2 + dx^2\}, \quad (1.9)$$

neglecting terms of cubic order and higher, where \mathcal{N} is the overall normalization and a , b and d are the Dalitz plot parameters. A term $\propto x$ is forbidden by C-parity. Table 1.1 shows the parameters as determined by our procedure. The following comments are in order: we matched

	RChT [11]	$\hat{\mathcal{M}} = 0$	full	VES Collaboration [12]
a	-0.119	-0.239	-0.478	$-0.127 \pm 0.016 \pm 0.008$
b	+0.001	-0.025	+0.053	$-0.106 \pm 0.028 \pm 0.014$
d	-0.056	-0.023	-0.043	$-0.082 \pm 0.017 \pm 0.008$

Table 1.1: Determination of the $\eta' \rightarrow \eta\pi\pi$ Dalitz plot parameters by RChT, the pure MO solution ($\hat{\mathcal{M}} = 0$), the full dispersive result and the experimental measurement by the VES collaboration.

the dispersive representation to RChT in the limit $\Omega(s) \rightarrow M_S^2/(M_S^2 - s)$. This is not fulfilled well by the $\pi\pi$ S-wave, which manifests itself in large modifications of the parameter a from the RChT result to the MO solution. From that vantage point, if the RChT result is already in marginal agreement with experiment, one cannot expect the outcome of the full analysis to be close to the measured parameters, especially if the crossed-channel rescattering corrections are as large as evidenced in the table. Certainly the matching procedure and thus the determination of the subtraction constants is still the weakest link in our analysis and requires further improvement.

Finally, while we do observe effects of $\pi\eta$ phase shifts on the Dalitz plot parameter d , these are not large enough to extract precision information about $\pi\eta$ scattering, especially if the subtraction constants are not under control.

Bibliography

- [1] N. N. Khuri, S. B. Treiman, *Phys. Rev.* **119**, 1115 (1960).
- [2] A. Aloisio *et al.* [KLOE Collaboration], *Phys. Lett.* **B561**, 55 (2003) [Erratum-ibid. **B609**, 449 (2005)] [arXiv:hep-ex/0303016].
- [3] R. R. Akhmetshin *et al.*, *Phys. Lett.* **B642**, 203 (2006).
- [4] B. Kubis, S. P. Schneider, *Eur. Phys. J.* **C62**, 511 (2009).
- [5] J. Stern, H. Sazdjian, N. H. Fuchs, *Phys. Rev.* **D47**, 3814 (1993) [arXiv:hep-ph/9301244].
- [6] K. M. Watson, *Phys. Rev.* **95**, 228 (1954).
- [7] I. Caprini, G. Colangelo, H. Leutwyler, in preparation.
- [8] R. García-Martín, R. Kamiński, J. R. Peláez, J. Ruiz de Elvira, F. J. Ynduráin, *Phys. Rev.* **D83**, 074004 (2011) [arXiv:1102.2183 [hep-ph]].
- [9] R. Omnès, *Nuovo Cim.* **8**, 316 (1958).
- [10] J. B. Bronzan, C. Kacser, *Phys. Rev.* **132**, 2703 (1963).
- [11] R. Escribano, P. Masjuan, J. J. Sanz-Cillero, *JHEP* **1105**, 094 (2011) [arXiv:1011.5884 [hep-ph]].
- [12] V. Dorofeev *et al.*, *Phys. Lett.* **B651**, 22 (2007) [arXiv:hep-ph/0607044].

HARD PION CHIRAL PERTURBATION THEORY: WHAT IS IT AND IS IT RELEVANT FOR η' DECAYS?

JOHAN BIJNENS*

1.1 Introduction

In this talk I will try to convince you that we can give predictions from chiral symmetry also for cases where not all pions are soft. This is something I called hard pion Chiral Perturbation Theory (HPChPT) and there have been a few recent papers using this [1, 2, 3, 4, 5].

I will first give a short introduction to effective field theory (EFT) and remind you of the underlying principles of Chiral Perturbation Theory (ChPT). I will remind you of the fact that in ChPT with baryons and other heavy particles a power-counting has been achieved by consistently absorbing the heavy mass dependence into the low-energy-constants (LECs).

The arguments will then be generalized to the case of processes with high energy or hard pions. The arguments also apply to cases where we can treat the strange quark mass as small as well.

After that I will show applications to $K \rightarrow \pi\pi$, to semileptonic decays of pseudo-scalar mesons or to more general vector form-factors and to charmonium decays to two pseudo-scalars.

Unfortunately, there seem to be no η' decays where the present method are applicable.

1.2 Effective field theory and ChPT

The underlying idea of EFT is a general theme in science, restrict yourself to the relevant degrees of freedom. So, in cases where there exists an energy or mass gap we keep only the lower degrees of freedom. Lorentz-invariance and quantum mechanics imply that we are restricted to a field theory but we should build the most general one with our chosen degrees of freedom. We have no predictability left since the most general Lagrangian will have an infinite number of parameters. This can be cured if we find an ordering principle, power-counting, for the importance of terms.

ChPT is “exploring the consequences of the chiral symmetry of QCD and its spontaneous breaking using effective field theory techniques” and was introduced as an EFT in [6, 7]. The degrees of freedom are the Goldstone bosons from the spontaneous breakdown of the global chiral $SU(n)_L \times SU(n)_R$ to the diagonal vector subgroup $SU(n)_V$. That the Goldstone boson interactions vanish at zero momentum allows to construct a consistent power-counting [6].

The basic form of ChPT has since been extended to baryons, mesons and baryons containing a heavy quark, vector mesons, structure functions and related quantities as well as beyond the pure strong interaction by including weak and electromagnetic internal interactions. Many models of alternative Higgs sectors also use the same technology.

1.3 Power-counting and one large scale

In purely mesonic ChPT the power-counting is essentially dimensional counting and this works since all the lines in all diagrams have “small” momenta. Already when discussing baryons, this lead to problems because now there is a large scale, the baryon mass. However, by setting the baryon momentum $p_B = M_B v + k$ with v the baryon four-velocity, a consistent power-counting can be achieved. This works “obviously” since the heavy line goes through the entire diagram and all momenta apart from $M_B v$ are soft as indicated by the thick line in Fig. 1.1(a). The same arguments apply to ChPT for mesons containing a heavy quark. It works because the “soft” stuff can be expanded in “soft/ M_B ” and the remaining M_B dependence can be absorbed in LECs. For vector meson ChPT there is a problem since they can decay. A typical diagram is shown in Fig. 1.1(b). However it was argued that the non-analytic dependence on the light quark mass

*Department of Astronomy and Theoretical Physics, Lund University, Sölvegatan 14A, SE 223 62 Lund, Sweden, bjnens@thep.lu.se

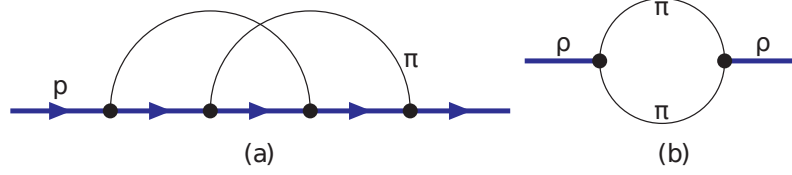


Figure 1.1: (a) A typical baryon ChPT diagram with the baryon going through the entire diagram. (b) An example of a diagram in vector meson ChPT with no continuous vector meson line.

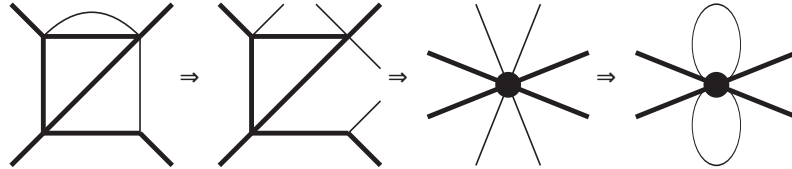


Figure 1.2: The process of cutting the soft lines and reproducing the non-analytic dependence by the diagram on the right. The hard lines are thick, soft lines are shown thin.

could still be obtained, see the discussions in [8]. Again, the underlying idea is that the large M_V allows to expand in “soft/ M_V ” and the remaining M_V dependence is absorbed in the LECs.

1.4 Several large scales or HPChPT

In [1] the authors applied heavy Kaon ChPT to $K_{\ell 3}$ at the endpoint, i.e. the pion is soft, this works as in usual ChPT. They also applied it to the region for small q^2 where the pion has a large momentum and gave arguments based on partial integrations why this would give a correct chiral logarithm. The argument was generalized in [2, 3, 4, 5]. The underlying idea is similar to the previous section. The “heavy/fast/hard” dependence on the soft stuff can always be expanded and the remaining dependence goes into the LECs. That this might be possible follows also from current algebra. Non-analyticities in the light masses come from the soft lines and soft pion couplings are restricted by current algebra via $\lim_{q \rightarrow 0} \langle \pi^k(q) \alpha | O | \beta \rangle = -\frac{i}{F_\pi} \langle \alpha | [Q_5^k, O] | \beta \rangle$. Nothing prevents hard pions to be in the states α or β , so by heavily using current algebra one can get the light quark mass non-analytic dependence

A field theoretic argument is: (1) Take a diagram with a given external and internal momentum configuration. (2) Identify the soft lines and cut them. (3) The resulting part is analytic in the soft stuff, so it can be described by an effective Lagrangian with coupling constants dependent on the external given momenta (Weinberg’s folklore theorem [6]). (4) The non-analytic dependence on the soft stuff is reproduced by loops in the latter Lagrangian. The process is depicted in Fig. 1.2.

The remaining problem is that we have no power-counting. The Lagrangian that reproduces the non-analyticities is fully general. In the HPChPT papers it was shown that for the processes at hand, all higher order terms can be reduced to those with the fewest derivatives thus allowing the light quark mass chiral logarithm to be predicted. The underlying arguments were tested by comparing to a two-loop calculation [4] and by explicitly keeping some higher order terms [2, 3, 4, 5].

1.5 Applications

We have applied the method to $K \rightarrow \pi\pi$ decays [2] where we treat the Kaon as heavy and look for the dependence on the pion mass M^2 . The result is, up to linear in M^2 and higher order:

$$A_0^{NLO}/A_0^{LO} = 1 + (3/8)\hat{A}, \quad A_2^{NLO}/A_2^{LO} = 1 + (15/8)\hat{A}, \quad \hat{A} = -M^2 \ln(M^2/\mu^2)/(16\pi^2 F^2).$$

The scalar and vector form-factors of the pion are known to two-loops in ChPT [9]. HPChPT predicts at large t [4] with $F_V(t, 0)$ and $F_S(t, 0)$, the form-factors at large t in the chiral limit, completely free:

$$F_V(t, M^2) = F_V(t, 0) (1 + \hat{A}), \quad F_S(t, M^2) = F_S(t, 0) (1 + (5/2)\hat{A}).$$

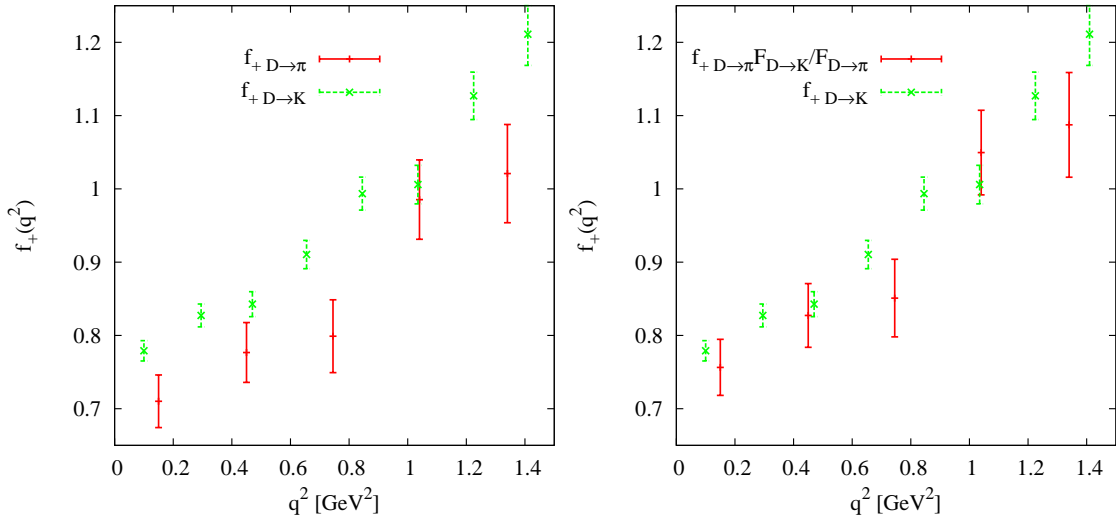


Figure 1.3: The CLEO data on $D \rightarrow \pi$ and $D \rightarrow K$. Form-factors as measured to the left and corrected with the chiral logarithms to the right. Note the improved agreement.

The full two-loop result expanded for large t should have this form and it does with for e.g. F_V

$$F_V(t, 0) = 1 + (t/(16\pi^2 F^2)) (5/18 - 16\pi^2 t_6^r + i\pi/6 - (1/6) \ln(t/\mu^2)) .$$

The first application was semileptonic form-factors in $K_{\ell 3}$. We extended this to $B, D \rightarrow D, \pi, K, \eta$ -decays in [3, 4]. This allowed to test our results experimentally. The form factor $f_+(t)$ as measured by CLEO [10] in $D \rightarrow \pi$ and $D \rightarrow K$ decays are different by about the amount expected from the chiral logarithms as shown in Fig. 1.3. One puzzling observation [4] was that in the limit of a hard pseudo-scalar in the final state the correction was always the same for f_+ and f_- . This is in fact due to the LEET relation [11] which shows that there is only one form-factor in this limit and it is nice to see that our calculation respects this without it being used as input.

A last application was to $\chi_{c0,2} \rightarrow \pi, KK, \eta\eta$ [5]. Here it was found that there were no chiral logarithms to the order considered. Comparing with the known experimental results indeed shows $SU(3)$ breaking to be somewhat smaller than in e.g. F_K/F_π . Details can be found in [5].

Acknowledgments

This work is supported in part by the EU, HadronPhysics2 Grant Agreement n. 227431, and the Swedish Research Council, grants 621-2008-4074 and 621-2010-3326.

Bibliography

- [1] J. M. Flynn and C. T. Sachrajda, *Nucl. Phys. B* **812** (2009) 64 [arXiv:0809.1229 [hep-ph]].
- [2] J. Bijnens and A. Celis, *Phys. Lett. B* **680** (2009) 466 [arXiv:0906.0302 [hep-ph]].
- [3] J. Bijnens and I. Jemos, *Nucl. Phys. B* **840** (2010) 54 [arXiv:1006.1197 [hep-ph]].
- [4] J. Bijnens, I. Jemos, *Nucl. Phys. B* **846** (2011) 145 [arXiv:1011.6531 [hep-ph]].
- [5] J. Bijnens, I. Jemos, arXiv:1109.5033 [hep-ph], to be published in *Eur. Phys. J. A*.
- [6] S. Weinberg, *Physica* **A96** (1979) 327.
- [7] J. Gasser and H. Leutwyler, *Annals Phys.* **158** (1984) 142.
- [8] J. Bijnens, P. Gosdzinsky, P. Talavera, *JHEP* **9801** (1998) 014 [hep-ph/9708232].
- [9] J. Bijnens, G. Colangelo and P. Talavera, *JHEP* **9805** (1998) 014 [arXiv:hep-ph/9805389].
- [10] J. Y. Ge *et al.* [CLEO Coll.], *Phys. Rev. D* **79** (2009) 052010 [arXiv:0810.3878 [hep-ex]].
- [11] J. Charles *et al.*, *Phys. Rev. D* **60** (1999) 014001 [hep-ph/9812358].

HUNTING RESONANCE POLES

PERE MASJUAN*

1.1 Introduction

The non-perturbative regime of QCD is characterized by the presence of physical resonances, complex poles of the amplitude in the transferred energy at higher (instead of the physical one) complex Riemann sheets. From the experimental point of view, one can obtain information about the spectral function of the amplitude through the Minkowsky region ($q^2 > 0$) and also about its low energy region through the experimental data on the Euclidean region ($q^2 < 0$).

In reference [1], the particular case of the $\pi\pi$ Vector Form Factor (VFF) was analyzed using the available Euclidean data and its first and the second derivatives were determined at $q^2 = 0$ with Padé Approximants (PA) centered at the origin trough a fit procedure to that data [1]. In such a way, the vector quadratic radius $\langle r^2 \rangle_V^\pi$ and the curvature c_V^π were extracted from the fit and, as a consequence, a value for the low-energy constant $L_9 = (6.84 \pm 0.07) \cdot 10^{-3}$ was obtained, [1, 2]. Similar ideas are applied in reference [3] to study the pion Transition Form Factor (TFF) and its first (a_π) and second (b_π) derivatives with better precision compared to the current world average result [4]. The implications of these parameters on the π^0 contribution to the hadronic light-by-light scattering to the muon anomalous magnetic moment are also studied showing the relevance of this kind of model-independent methods.

Despite the nice convergence and the systematical treatment of the errors, this procedure does not allow us to obtain properties of the amplitude above the threshold, such as in the case of the $\pi\pi$ VFF, the ρ -meson pole position, or trough the $\pi\pi$ phase shift the σ -pole. The reason is simple: the convergence of a sequence of Padé Approximants centered at the origin of energies ($q^2 = 0$) is limited by the presence of the $\pi - \pi$ production brunch cut: the PA sequence converge everywhere except on the cut [2]. Still, the mathematical Padé Theory, through the Montessus de Ballore theorem, allow us to produce a model independent determination of resonance poles when certain conditions are fulfilled. The most important one is to center our PA sequence above the branch-cut singularity (beyond the first production threshold) instead of at origin of energies ($q^2 = 0$). This small modification also provides the opportunity to use Minkowskian data in our study instead of the Euclidean one. The relevance of this model-independent method to extract resonance poles is clear since does not depend on a particular lagrangian realization or modelization on how to extrapolate from the data on the real energy axis into the complex plane.

The Montessus de Ballore's theorem states that the sequence of one-pole Padé Approximants P_1^N around x_0 ,

$$P_1^N(x, x_0) = \sum_{k=0}^{N-1} a_k (x - x_0)^k + \frac{a_N (x - x_0)^N}{1 - \frac{a_{N+1}}{a_N} (x - x_0)}, \quad (1.1)$$

converges to $F(x)$ in any compact subset of the disk excluding the pole x_p , i.e, $\lim_{N \rightarrow \infty} P_1^N(x, x_0) = F(x)$.

As an extra consequence of this theorem, one finds that the PA pole $x_{PA} = x_0 + \frac{a_N}{a_{N+1}}$ converges to x_p for $N \rightarrow \infty$. Since experiments provide us with values of F_j at different x_j instead of the derivatives of our function, we can use the rational functions P_1^N as fitting functions to the data in a similar way as in Ref. [1, 3] In this way, as N grows P_1^N gives us an estimation of the series of derivatives and the x_p pole position.

For a physical amplitude, the function $F(x)$ (without a right-hand cut) is analytic from $x = -\infty$ up to the first production threshold x_{th} and within the disk $B_{x_{th}}(0)$. In the $\pi\pi$ VFF case, the threshold is found to be at $x_{th} = 4m_\pi^2$, where m_π is the mass of the pion. One can use Padé Approximants in a safe way by using the Montessus' theorem and center the approximants at $x_0 + i0^+$ over the brunch cut between the first and the second production threshold. In the $\pi\pi$

*Departamento de Física Teórica y del Cosmos, Universidad de Granada. Campus de Fuentenueva, E-18071 Granada, Spain. masjuan@ugr.es

Ref.	$M_\rho(\text{MeV})$	$\Gamma_\rho(\text{MeV})$
[7]	762.5 ± 2	142 ± 7
[8]	754 ± 18	148 ± 20
[9]	763.0 ± 0.2	139.0 ± 0.5
[10]	$764.1 \pm 2.7^{+4.0}_{-2.5}$	$148.2 \pm 1.9^{+1.7}_{-5.9}$
this work	763.7 ± 1.2	144 ± 3

Table 1.1: Comparison of different results for the determination of the mass and width of the ρ -meson.

VFF that would correspond to the range between $x_{th} = 4m_\pi^2$ and $\tilde{x}_{th} = 4m_K^2$ (assuming small multipion channels). In such a way we unfold the Second Riemann sheet due to the analytical extension of the function $F(x)$ from the first Riemann sheet at $x + i0^+$ into the second one.

In the case of resonant amplitudes, a single pole appears in the neighborhood of the real x axis in the second Riemann sheet which is related to a hadronic state, a resonance. Once we have unfold the Second Riemann sheet by locating our approximants over the brunch cut, the application of the Montessus' theorem in the disk of convergence (which is the region defined between the thresholds) is straightforward and allows us to locate the position of the resonant pole if lies inside that region. If that is the case, our P_1^N Padé approximant sequence determine systematically its position in a model independent way.

1.2 Application of the method in a physical case

We would like to use the method to analyze the final compilation of ALEPH $\pi\pi$ VFF data for the squared modulus $|F_{\pi\pi}(q^2)|^2$, [5], and the $I = J = 1$ $\pi\pi$ scattering phase-shift $\delta_{\pi\pi}$, identical to the $\pi\pi$ VFF phase-shift in the elastic region $4m_\pi^2 < q^2 < 4m_K^2$ (if multipion channels are neglected), which conforms the range of applicability of our P_1^N sequence (more details can be found in Ref. [6]). For $N \geq 3$ the fit χ^2 already lies within the 68% confidence level (CL) and becomes statistically acceptable. At this point one needs to reach the typical fitting compromise. On one hand the experimental errors have an statistical origin and the contribution of this error increase as one considers higher order P_1^N , with larger number of parameters. On the other hand, the systematic theoretical error decreases as N increases and the PA converges to the actual VFF and the phase-shift. For the ρ -mass determination we have taken $N = 6$ as our best estimate as the new parameters of PA with $N \geq 7$ turn out to be all compatible with zero, introducing no more information with respect to the previous P_1^6 . Furthermore, the model studied in Ref.[6] shows that the theoretical errors for mass and width results are smaller than $10^{-2} - 10^{-3}\text{MeV}$ for $N \geq 6$, being negligible compared to the $\mathcal{O}(1 \text{ MeV})$ experimental errors. This yields to the determination:

$$M_\rho = 763.7 \pm 1.2\text{MeV}, \quad \Gamma_\rho = 144 \pm 3\text{MeV}, \quad (1.2)$$

which is found to be in good agreement with previous determinations using more elaborated and complex procedures and with similar size of uncertainties as shown in Table 1.1.

Similar results are found when analyzing the $\pi - \pi$ phase-shift data for the σ -pole position, yielding in this case

$$M_\sigma = 451 \pm 21\text{MeV}, \quad \Gamma_\sigma = 619 \pm 18\text{MeV}, \quad (1.3)$$

again in good agreement with previous determinations with more complex methods [4].

1.3 Conclusions

We have develop a new model-independent method for extracting resonance poles (mass and width) from physical amplitudes based on the well defined mathematical theory of Padé Approximants which makes use of the Montessus' theorem to unfold de Second Riemann sheet of the desired amplitud to locate the resonant pole in the complex plane. This method systematize the algorithm of extracting the desired resonance pole (or low energy properties of these amplitudes as commented in the introduction) by building up a convergence sequence of those PA which at the very same time provides with a simple way to estimate the systematic errors. Our method has,

however, a larger application since does not rely on a particular lagrangian or in a modelization on how to extrapolate from the data on the real energy axis into the complex plane (such as other methods discussed in Ref. [11]).

In the particular case presented here we have analyzed on one hand the experimental Euclidean data to obtain the first and the second derivatives at $q^2 = 0$ for both the π -VFF and for the π^0 TFF. And on the other hand, also Minkowskian data have been analyzed for $\pi\pi$ -VFF and also $\pi\pi$ -scattering data by a P_1^N Padé Approximant sequence centered between the first and the second production thresholds (in such a way that we can unfold the second Riemann sheet of our amplitude). We have obtained a prediction of the ρ -meson and σ -meson pole positions with compatible accuracy compared to other determinations but with a simpler and systematic method.

Acknowledgments

This work has been supported by MICINN, Spain (FPA2006-05294), the Spanish Consolider-Ingenio 2010 Programme CPAN (CSD2007-00042) and by Junta de Andalucía (Grants P07-FQM 03048 and P08-FQM 101).

Bibliography

- [1] P. Masjuan, S. Peris and J. J. Sanz-Cillero, Phys. Rev. D **78** (2008) 074028 [arXiv:0807.4893 [hep-ph]].
- [2] P. Masjuan and S. Peris, JHEP **0705** (2007) 040 [arXiv:0704.1247 [hep-ph]]; P. Masjuan and S. Peris, Phys. Lett. B **663** (2008) 61 [arXiv:0801.3558 [hep-ph]]; P. Masjuan, Nucl. Phys. Proc. Suppl. **186** (2009) 149 [arXiv:0809.2704 [hep-ph]]; P. Masjuan Queralt, arXiv:1005.5683 [hep-ph].
- [3] P. Masjuan, work in progress.
- [4] K. Nakamura et al.- (Particle Data Group), J. Phys. G **37**, 075021 (2010).
- [5] S. Schael *et al.* [ALEPH Collaboration], Phys. Rept. **421** (2005) 191 [arXiv:hep-ex/0506072].
- [6] J. J. Sanz-Cillero, arXiv:1002.3512 [hep-ph]; P. Masjuan and J. J. Sanz-Cillero, in preparation.
- [7] B. Ananthanarayan, G. Colangelo, J. Gasser and H. Leutwyler, Phys. Rept. **353** (2001) 207 [arXiv:hep-ph/0005297].
- [8] J. R. Pelaez, Mod. Phys. Lett. A **19** (2004) 2879 [arXiv:hep-ph/0411107].
- [9] Z. Y. Zhou, G. Y. Qin, P. Zhang, Z. Xiao, H. Q. Zheng and N. Wu, JHEP **0502** (2005) 043 [arXiv:hep-ph/0406271].
- [10] J. J. Sanz-Cillero and A. Pich, Eur. Phys. J. C **27** (2003) 587 [arXiv:hep-ph/0208199].
- [11] P. Masjuan, J. J. Sanz-Cillero and J. Virto, "Some Remarks on the Pade Unitarization of Low-Energy Amplitudes," Phys. Lett. B **668** (2008) 14 [arXiv:0805.3291 [hep-ph]].

EXPLORING LOW-ENERGY QCD USING A GENERALIZED LINEAR SIGMA MODEL

AMIR H. FARIBORZ*

The decays of η' can provide very useful information on the physics of scalar mesons. For example, the decay $\eta' \rightarrow \eta\pi\pi$ involves intermediate scalar states $f_0(600)$ (or sigma), $f_0(980)$ and $a_0(980)$ as shown in Fig. 1.1. Therefore, at least in principle, such decays can shed light on various aspects of scalar meson. However, in practice, this objective is overshadowed by various uncertainties such as different final state interactions as well as various underlying mixing among scalar states. Nevertheless, one would hope to find useful approximations that could provide some insights into the physics of scalar mesons. The present work summarizes one such approach within the context of a generalized linear sigma model.

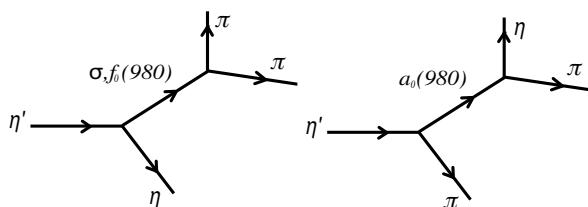


Figure 1.1: Contribution of scalar mesons to decay $\eta' \rightarrow \eta\pi\pi$.

Below 1 GeV, the known scalar states are listed in Fig. 1.2 [1]: the light and broad isosinglet $f_0(600)$ or sigma, followed by isodoublet $K^*(800)$ or kappa meson and the two nearly degenerate states, isosinglet $f_0(980)$ and isotriplet $a_0(980)$. Above 1 GeV, the known scalar states are also listed in Fig. 1.2: The isosinglet state $f_0(1370)$ followed by the isodoublet $K_0^*(1430)$, the isotriplet $a_0(1450)$ and the two isosinglet states $f_0(1500)$ and $f_0(1710)$. There have been numerous works addressing the physics of these illusive states and at times conflicting point of views have surfaced. Of course, getting into the history of these states and various approaches by different investigators is beyond the scope of this short summary and the reader is encouraged to refer to the available literature for details. However, in a nutshell, the scalar states below 1 GeV seem to be close to four-quark states [2] (with some deviations) and those above 1 GeV seem to be close to two-quark states (with some deviations). To generate such deviations from pure four-quark and pure two-quark pictures, it seems natural to investigate a possible underlying mixing among four- and two-quark states. Such a mixing was first investigated within a nonlinear chiral Lagrangian framework in ref. [3] and it was shown that it provides a natural understanding of some of the puzzling aspects of $K_0^*(1430)$ and $a_0(1450)$. The same type of mixing was further extended to the case of isosinglet scalar states below and above 1 GeV (which can also mix with scalar glueballs) in [4], in which again consistent results were obtained and estimates on the quark and glue substructure of the isosinglet scalars were made. Such mixing patterns were further studied within the framework of a generalized linear sigma model which is the topic of the present summary. In this approach, the pseudoscalar mesons below and above 1 GeV (also given in Fig. 1.2) are brought into the picture. The main motivations for using a generalized linear sigma model are: First, it provides an independent check of the results obtained for scalar mixings in the nonlinear chiral Lagrangian approach mentioned above, and tests whether the results obtained are robust, or are artifacts of the framework used. Second, as scalar mesons are probed in various pseudoscalar interactions (such as, for example, $\pi\pi$, πK , and $\pi\eta$ scatterings and decays such as $\eta' \rightarrow \eta\pi\pi$, \dots) it seems important to see what roles (if any) two- and four-quark mixings play in the physics of pseudoscalar mesons, for which, at least for pseudoscalars below 1 GeV, the phenomenology is fairly established, and as a result, allowing pseudoscalars to participate in these mixing patterns can provide a reliable probe into the understanding of the mixing. Third, some of the heavier pseudoscalar states above 1 GeV are

*Department of Engineering, Science and Mathematics, State University of New York Institute of Technology, Utica, New York, U.S.A. fariboa@sunyit.edu

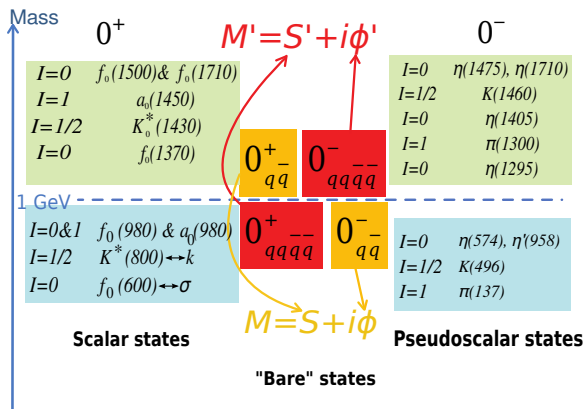


Figure 1.2: Scalars (left) and pseudoscalars (right) below 2 GeV together with their “bare” (unmixed) underlying two- and four-quark mixing nonets (middle).

known to be dubious and speculated to be of a non quark-antiquark nature, therefore, extending the mixing mechanism to the pseudoscalar sector may provide useful insight into the nature of some of the heavier pseudoscalars. A generalized linear sigma model [which is formulated in terms of two scalar meson nonets (a two-quark nonet and a four-quark nonet) and two pseudoscalar meson nonets (a two-quark nonet and a four-quark nonet)] seems to be an appropriate framework for exploring the mixing patterns in both scalar as well as pseudoscalar sectors. The idea of mixing within this framework is investigated in Ref. [5] (and references therein) and the outcome (within the approximation used in [5]) is symbolically summarized in Fig. 1.2. In this approach, it is found that (as expected) the underlying four-quark scalar nonet is lighter than the two-quark scalar nonet, and the situation is reversed for the two pseudoscalar nonets (i.e. the two-quark pseudoscalar nonet tends to become lighter than the four-quark pseudoscalar nonet). This of course agrees with the conventional phenomenology for light pseudoscalars where their properties are understood based on a quark-antiquark picture. Further details can be seen in Ref. [5]. The notation is clarified in Fig. 1.2 in which the chiral nonet M is formed out of quark-antiquark scalar nonet S and quark-antiquark pseudoscalar nonet ϕ (similarly, the chiral nonet M' is formed out of four-quark nonets S' and ϕ'). The general structure of the Lagrangian in terms of M and M' is:

$$\mathcal{L} = -\frac{1}{2}\text{Tr}(\partial_\mu M \partial_\mu M^\dagger) - \frac{1}{2}\text{Tr}(\partial_\mu M' \partial_\mu M'^\dagger) - V_0(M, M') - V_{SB}, \quad (1.1)$$

where $V_0(M, M')$ stands for a function made from $SU(3)_L \times SU(3)_R$ (but not necessarily $U(1)_A$) invariants formed out of M and M' and V_{SB} is the flavor symmetry breaking term. In dealing with this Lagrangian, two approaches have been considered: Approach 1 is based on the underlying chiral symmetry and the resulting generating equations [6]. In this approach no specific choice for the chiral invariant part of V_0 is made, and only the axial anomaly, the V_{SB} and the condensates are modeled. The details of this approach can be found in Ref. [6] and are not discussed here. The main conclusions are: (i) The light pseudoscalars, as expected from conventional phenomenology, remain dominantly close to quark-antiquark states; (ii) The kappa meson tends to become a dominantly four-quark state; and (iii) This approach does not provide any information on a_0 and f_0 systems. To study a_0 and f_0 systems, specific choices for V_0 should be made, and that leads to the second approach which is summarized here. In approach 2, a specific choice for the chiral invariant part of V_0 is made [5] (in addition to modeling the axial anomaly, the V_{SB} and the condensates). The main conclusions are: (i) Again, light pseudoscalars have the tendency of becoming quark-antiquark states; (ii) Light scalars tend to become mainly four-quark states; and (iii) Predictions for various low-energy processes such as $\pi\pi$, πK , $\pi\eta$ scatterings, and decays such as η' decays, semileptonic decays of D_s , \dots can be made. Here, we only give a summary of approach 2. Obviously, there are infinite number of terms that can be written down for V_0 . Up to dimension 4, there are twenty one $SU(3)_L \times SU(3)_R$ invariant terms in V_0 which can be made out of M and M' . To work with such a high number of terms, it seems reasonable to consider an approximation scheme in which V_0 is organized in terms of the number of quark and antiquark lines. In the first approximation attempt: 1) We only consider terms with eight or fewer quark or antiquark lines; 2) We mock up the $U(1)_A$ anomaly exactly; 3) We ignore terms that are not

consistent with OZI rule; and 4) We consider the leading flavor symmetry breaking term that mocks up the quark mass term in the fundamental QCD Lagrangian. These approximations lead to the potential:

$$\begin{aligned}
V = & - c_2 \text{Tr}(MM^\dagger) + c_4^a \text{Tr}(MM^\dagger MM^\dagger) + d_2 \text{Tr}(M'M'^\dagger) + e_3^a (\epsilon_{abc} \epsilon^{def} M_d^a M_e^b M_f^{c\dagger} + \text{h.c.}) \\
& + c_3 \left[\gamma_1 \ln \left(\frac{\det M}{\det M^\dagger} \right) + (1 - \gamma_1) \ln \left(\frac{\text{Tr}(MM'^\dagger)}{\text{Tr}(M'M'^\dagger)} \right) \right]^2 + k_1 [\text{Tr}(AM) + \text{h.c.}]. \quad (1.2)
\end{aligned}$$

where matrix $A = \text{diag. } (A_1, A_2, A_3)$ induces the flavor symmetry breaking and the two- and four-quark condensates of fields S and S' obey $\langle S_a^b \rangle = \delta_a^b \alpha_a$ and $\langle S'^b_a \rangle = \delta_a^b \beta_a$. We assume isospin limit which implies: $A_1 = A_2 \neq A_3$ and $\alpha_1 = \alpha_2 \neq \alpha_3$ and $\beta_1 = \beta_2 \neq \beta_3$. At the level of the approximate potential of Eq. (1.2), altogether, there are 12 unknown parameters $c_2, c_4^a, d_2, e_3^a, c_3, \gamma_1, \alpha_1, \alpha_3, \beta_1, \beta_3, A_1, A_3$ that need to be determined using 12 inputs. We take the following eight experimental inputs: $m[a_0(980)] = 984.7 \pm 1.2 \text{ MeV}$; $m[a_0(1450)] = 1474 \pm 19 \text{ MeV}$; $m[\pi(1300)] = 1300 \pm 100 \text{ MeV}$; $m_\pi = 137 \text{ MeV}$; $F_\pi = 131 \text{ MeV}$; $\frac{A_3}{A_1} = 20 \rightarrow 30$; $\det(M_\eta^2) = \det(M_\eta^2)^{\text{exp}}$; and $\text{Tr}(M_\eta^2) = \text{Tr}(M_\eta^2)^{\text{exp}}$, together with four minimum conditions: $\left\langle \frac{\partial V}{\partial S_1^1} \right\rangle = \left\langle \frac{\partial V}{\partial S_3^3} \right\rangle = \left\langle \frac{\partial V}{\partial S_1^1} \right\rangle = \left\langle \frac{\partial V}{\partial S_3^3} \right\rangle = 0$. These inputs and minimum conditions allow a determination of the Lagrangian parameters and the detailed numerical analysis of this study is given in [5]. The main uncertainties are clearly on $m[\pi(1300)]$ as well as the ratio $\frac{A_3}{A_1}$, and therefore, the results have some variations that reflect these two uncertainties. The work of [5] shows that the underlying mixing among two- and four-quark pseudoscalars does not change the well-established picture of the light pseudoscalars as dominantly being quark-antiquark states (the situation is of course reversed for the heavy pseudoscalars). The present level of this investigation predicts four etas: Two of the predicted etas are below 1 GeV and are close to the physical states $\eta(547)$ and $\eta(958)$. The two heavier etas above 1 GeV may be identified with two of the several physical eta states above 1 GeV. In the work of [5] various scenarios for this identification is studied in detail and the closest agreement corresponds to identifying the two predicted etas above 1 GeV with $\eta(1295)$ and $\eta(1760)$. The situation for scalar mesons is the opposite of pseudoscalars: Those below 1 GeV come out close to four-quark states and those above 1 GeV tend to become more of two-quark states. These natural tendencies for scalar mesons are consistent with those studied within nonlinear chiral Lagrangians described above. Therefore, in summary, it seems that the generalized linear sigma model discussed here is an appropriate framework for learning about scalar and pseudoscalar mesons, and already has provided useful insights into their quark substructure. Further extensions will involve inclusion of higher order terms in the potential [with higher number (more than eight) of underlying quark and antiquark lines]. Also inclusion of glueballs seems to be quite important. Various predictions of the model for several low-energy processes are being currently looked at and will be reported elsewhere. Particularly, the present approach is hoped to provide useful insights into the physics of η' and the eta's above 1 GeV.

The author wishes to thank the organizers of PrimeNet Workshop for a very productive meeting. This work is based on an ongoing collaboration with R. Jora, J. Schechter and M.N. Shahid, and the author thanks collaborators for many helpful discussions. This work has been partially supported by the NSF Grant 0854863 and by a 2011 grant from the Office of the Provost, SUNYIT.

Bibliography

- [1] K. Nakamura et. al.(Particle Data Group), J. Phys. G **37**, 075021 (2010).
- [2] R.L. Jaffe, Phys. Rev. D **15**, 267 (1977).
- [3] D. Black, A. H. Fariborz and J. Schechter, Phys. Rev. D **61** 074001 (2000).
- [4] A.H. Fariborz, Int. J. Mod. Phys. A **19**, 2095 (2004); 5417 (2004); Phys. Rev. D **74**, 054030 (2006).
- [5] A.H. Fariborz, R. Jora and J. Schechter, Phys. Rev. D **79**, 074014 (2009).
- [6] A.H. Fariborz, R. Jora and J. Schechter, Phys. Rev. D **72**, 034001 (2005).

THE η DECAY PROGRAM AT WASA-AT-COSY

DANIEL CODERRE*

for the WASA-at-COSY Collaboration

1.1 Introduction

The η meson provides an excellent laboratory for the study of matter in the low-energy regime. Because all strong and electromagnetic decays of the η are forbidden in the first order, rare processes are accessible which would otherwise be highly suppressed. The measurement of the decays of the η can test fundamental symmetries, probe the structure and dynamics of hadrons, and investigate possible new physics.

A major goal of the WASA-at-COSY experiment is to make precision measurements of η decays. η mesons are produced by impinging a proton beam onto a proton or deuteron target. With the WASA detector, both forward-scattered hadrons and wide-angle decay products of the η can be measured.

WASA has recorded 3×10^7 η mesons in the $pd \rightarrow {}^3He\eta$ reaction. In the $pp \rightarrow pp\eta$ reaction, over 10^8 η mesons have been produced with a trigger biased towards charged decays. Proton-deuteron reactions feature a favorable ratio between η production and background processes, but a lower rate of η production of about $10\eta s^{-1}$. Proton-proton reactions have a factor of ten higher rate of η production but significantly higher background. The two production methods are complementary.

1.2 Current Work on Selected Decay Channels

In the following, the current status of the analysis of selected decay channels will be described.

The decay $\eta \rightarrow \pi^+\pi^-\gamma$ provides the possibility to search for a contribution of the box-anomaly term from the Wess-Zumino-Witten (WZW) Lagrangian [1, 2]. The predicted decay width calculated with chiral perturbation theory is significantly lower than the measured value, partially because the phase space available for this decay is constrained by the mass of the π and is far from the chiral limit. Attempts have been made to include final-state interactions as unitarized extensions to the WZW Lagrangian. In order to test these predictions, both the decay rate and the dynamics of the final state particles can be investigated.

In the WASA measurement, a total of 13960 ± 140 event candidates for this reaction were reconstructed from $pd \rightarrow {}^3He\eta$ data and the shape of the relevant kinematic distributions have been determined [3]. The data deviates from calculations using the simplest gauge-invariant matrix element. For a more realistic description, a form factor as described in [4] has been applied to the prediction of the simplest matrix element. This allows for a model independent description of the distribution with a single free parameter, α . This parameter can be compared to theoretical predictions.

Another aspect of this decay is the measurement of the branching ratio. A value about $3\text{-}\sigma$ lower than the former experimental average was recently measured by the CLEO collaboration and confirmed by the KLOE collaboration [5, 6]. As a next step for this channel, WASA will measure both the branching ratio and the photon-energy dependence in one analysis from high-statistics proton-proton data.

The decay $\eta \rightarrow \pi^+\pi^-e^+e^-$ is a rare decay with a branching ratio of $(2.68 \pm 0.11) \times 10^{-4}$ [7]. One goal of the analysis is to confirm the experimental value of the branching ratio, which has only been measured once with high statistics [8]. This decay is interesting because it may provide a novel test for CP-violation outside of the standard model. It has been shown that the asymmetry of the angle between the electron and π decay planes is sensitive to a contribution of the CP-violating E-1 transition to the decay amplitude [9, 10]. Unlike the reaction $\eta \rightarrow \pi^+\pi^-$, CP-violation in this

*Forschungszentrum Jülich and Ruhr Universität Bochum, d.coderre@fz-juelich.de

system is not suppressed by experimental limit on the electric dipole moment of the neutron. The theoretical upper limit for this asymmetry is about 1%.

So far (230 ± 22) signal event candidates have been identified in proton-deuteron data, shown in Figure 1.1a. This number is consistent with a branching ratio near the measured and predicted values. Systematic studies are currently being performed in order to extract the branching ratio with the lowest possible error. The decay is also being analyzed in proton-proton data where a larger sample of event candidates is visible. The goal is to measure the branching ratio with proton-deuteron data and to subsequently use the proton-proton data to confirm the branching ratio and measure the decay plane asymmetry.

Because it proceeds via two virtual photons, the decay $\eta \rightarrow e^+e^-e^+e^-$ has a very small branching ratio, with a QED prediction of 2.6×10^{-5} . It has been measured only once and the experimental value was found to be within errors of the QED calculation [11].

WASA has measured this decay in the $pd \rightarrow {}^3\text{He}\eta$ reaction. Two independent analyses report (50 ± 14) event candidates. The event sample from one analysis is shown in Figure 1.1b. The branching ratio returned by these two analyses is consistent, allowing WASA to quote a preliminary value of $(3.0 \pm 0.8_{\text{stat}} \pm 0.7_{\text{sys.}(norm)}) \times 10^{-5}$ which is in agreement with theoretical and experimental values. Systematic studies as well as consistency checks between the two analyses are currently being performed.

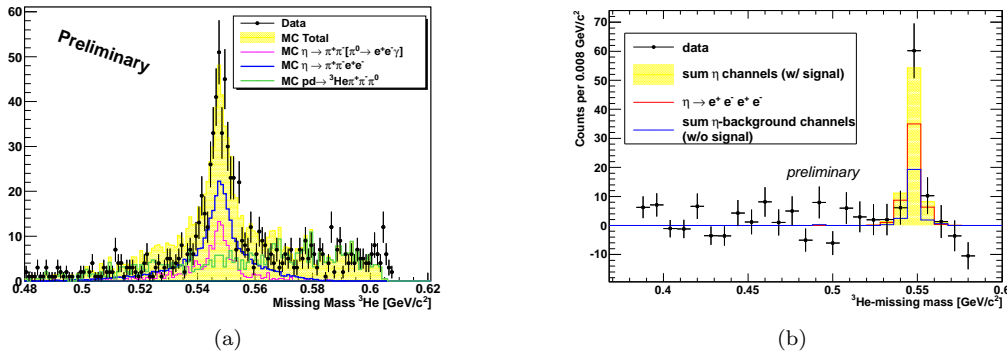


Figure 1.1: Missing Mass of ${}^3\text{He}$ for events satisfying conditions for (a) $\eta \rightarrow \pi^+\pi^-e^+e^-$ and (b) $\eta \rightarrow e^+e^-e^+e^-$.

The decay of η into two electrons is a fourth order electromagnetic process proceeding through two virtual photons and additionally suppressed due to helicity conservation to the order of 10^{-9} . This extremely low branching ratio makes the reaction very sensitive to any processes that could enhance the decay width, including possible effects outside the standard model [12, 13, 14]. Measurements of the closely related $\pi^0 \rightarrow e^+e^-$ decay have found branching ratios above theoretical predictions. Measurements in the η system should be even more sensitive to such effects due to the lower branching ratio predicted by the standard model.

The current experimental upper limit for this decay is 7.7×10^{-5} [7] and was measured by the CELSIUS-WASA collaboration. Using two weeks of data in proton-proton interactions from WASA-at-COSY, a value one order of magnitude lower has been calculated. When considering the full statistics available in the $pp \rightarrow pp\eta$ reaction, it is expected that additional sensitivity can be gained corresponding to at least another order of magnitude improvement. Additionally, a more intelligent trigger has been developed and is being tuned to enable data collection at higher luminosities.

1.3 Conclusion

The WASA-at-COSY collaboration is in the processes of analyzing the large amount of data taken on η decays while simultaneously gearing up for extended production runs to increase statistics for rare processes. Results for some decay channels have been released while several more are at the stage of careful systematic checks.

Additionally, the meson program at WASA-at-COSY is expanding. A pilot run intended to produce large numbers of π^0 mesons in order to measure the very rare $\pi^0 \rightarrow e^+e^-$ decay is currently

being analyzed. Also, the first data on ω decays was taken in proton-deuteron and proton-proton reactions in Spring of 2011.

Acknowledgements

This publication has been supported by COSY-FFE and by the European Commission under the 7th Framework Programme through the 'Research Infrastructures' action of the 'Capacities' Programme. Call: FP7-INFRASTRUCTURES-2008-1, Grant Agreement N. 227431.

Bibliography

- [1] J. Wess, B. Zumino, *Phys. Lett. B*, **37**, 95 (1975).
- [2] E. Witten, *Nucl. Phys. B*, **223**, 422 (1983).
- [3] P. Adlarson et al., *Subm. to Phys. Lett B* arxiv:1107.5277v1 (hep-ex).
- [4] F. Stollenwerk, C. Hanhart, A. Kupsc, U.-G. Meiner, A. Wirzba, arxiv:1108.2419, (nucl-th).
- [5] A. Lopez et al., *Phys. Rev. Lett.*, **99**, 122001 (2007).
- [6] F. Ambrosino et al., arXiv:1107.5733, (hep-ex).
- [7] K. Nakamura et al. (Particle Data Group), *J. of Phys. G37*, 0705021 (2010) and 2011 partial update for the 2012 edition.
- [8] F. Ambrosino et al., *Phys.Lett.B*, **675**, 293, (2009).
- [9] D.N. Gao, *Mod. Phys. Lett. A*, **17**, 1583 (2002).
- [10] C.Q. Geng, J.N. Ng, and T.H. Wu, *Mod. Phys. Lett. A*, **17**, 1489 (2002).
- [11] F. Ambrosino et al., *Phys. Let. B*, **702**, 324 (2011).
- [12] P. Fayet, *Phys.Rev.D*, **74**, 054034 (2006).
- [13] Q.Chang, Y.-D. Yang, *Phys.Lett.B*, **676**, 88 (2009).
- [14] Y. Kahn, M. Schmitt, and T.M.P. Tait, *Phys.Rev.D*, **78**, 115002 (2008).

DECAYS OF LIGHT MESONS IN CLAS

M. AMARYAN[†], C. NEPALI* and M. KUNKEL**
for the CLAS Collaboration

1.1 Introduction

At low energies the coupling constant of Quantum Chromodynamics (QCD) becomes large and renders perturbation theory useless. The phenomenology of the strong interactions in this domain remains one of the major challenges of modern particle physics. Experimental study of decays of light mesons in general and π^0 , η and η' pseudoscalars in particular is a unique way to explore low energy QCD. By comparing data obtained at different facilities like KLOE, CLEO, BES, MAMI, COSY, and CLAS with a predictions of effective field theory at low energy, Chiral Perturbation Theory (ChPT), one can get an insight into the non-perturbative regime of strong interactions and provide important information for a firmer foundation of hadronic physics rooted in the standard model. Until recently the quest for high statistics accurate experimental data was not fulfilled.

In this talk we give a brief overview of experimental data on a decay of light mesons collected with the CLAS setup at JLAB either with unprecedented high statistics or comparable with the worlds highest statistics measurements depending on the decay mode. Below we outline the quality and statistics of available data at CLAS in a different decay channels of light mesons, rather than present results of finalized analyses that are in progress.

1.2 Light mesons in CLAS

The tagged beam of photons produced from 6 GeV CEBAF electron accelerator is used to study photo-production of light mesons from liquid hydrogen target. Until now the main focus of the experiments in CLAS related to light mesons was the study of different aspects of photo-production cross sections aiming to understand mechanism of their production. However as it is shown below the wealth of data allows to make a studies exploiting different decay modes detached from the production vertex and considering decaying mesons as a laboratory by themselves.

Experimental data are presented by accenting on photo-production reactions $\gamma+p \rightarrow p\pi^0(\eta, \eta')$ collected in the following decay modes:

- Dalitz decays $\pi^0(\eta, \eta') \rightarrow e^+e^-\gamma$
- Radiative decays $\eta(\eta') \rightarrow \pi^+\pi^-\gamma$
- Hadronic decays $\eta(\eta') \rightarrow \pi^+\pi^-\pi^0$
- Hadronic decay $\eta' \rightarrow \pi^+\pi^-\eta$

1.2.1 Dalitz decays

The branching ratios of radiative decay of pseudoscalar mesons π^0 and η were measured and are recorded in PDG, however there is only an upper limit quoted for η' . Below in Fig. 1.1 (left panel) we present distribution of the invariant mass of $e^+e^-\gamma$ measured in photoproduction reaction with CLAS. As one can there are clear peaks of all three light pseudoscalar mesons π^0 , η and η' . One of the less studied channel of the $\eta \rightarrow e^+e^-\gamma$ decay allows to extract form factor of η in the timelike region by studying distribution of the invariant mass of e^+e^- pairs presented in Fig. 1.1 (right panel). In both panels in Fig. 1.1 number of events are presented without corrections due to the CLAS acceptance and efficiency.

*Old Dominion University, Norfolk, VA, USA

[†] mamaryan@odu.edu

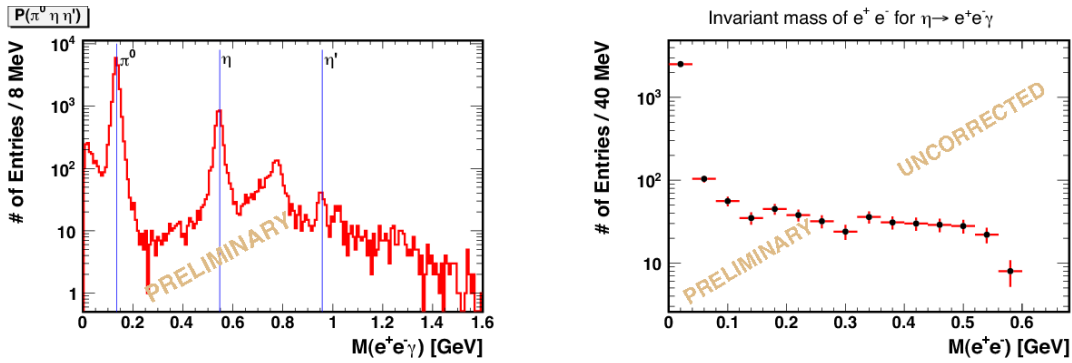


Figure 1.1: (Color online). Left panel: the $e^+e^-\gamma$ invariant mass distribution in the reaction $\gamma + p \rightarrow pe^+e^-\gamma$, the vertical lines show positions of pseudoscalar mesons π^0, η, η' . Right panel: invariant mass of e^+e^- lepton pairs for events under the η peak $M(e^+e^-\gamma) = 0.548 \pm 0.01$ GeV.

1.2.2 Radiative decays

Another very interesting decay of η and η' mesons is their radiative decay $\eta(\eta') \rightarrow \pi^+\pi^-\gamma$. Recent theoretical paper [1] demonstrates that the photon energy distribution from radiative decay of η and η' mesons provides very important test of theoretical models. In Fig. 1.2 (left panel) missing mass of the proton is presented for exclusive reaction $\gamma + p \rightarrow p\pi^+\pi^-\gamma$. In both η and η' peaks a statistics is by more than an order of magnitude higher than existing world data (see [1] and references therein). In Fig. 1.2 (middle (right) panel) distribution of the energy of the photon from the decay of $\eta(\eta')$ in the center-of-mass frame of the parent is presented.

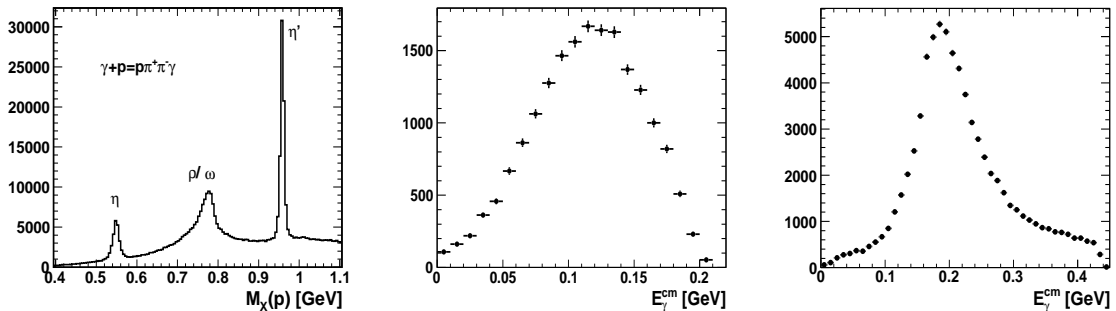


Figure 1.2: Left panel: distribution of missing mass of the proton in exclusive reaction $\gamma + p \rightarrow p\pi^+\pi^-\gamma$. Middle panel: the distribution of the γ energy in the center-of-mass of η . Right panel: same as the middle panel plotted for the η' decay. All three plots show raw number of events before the acceptance and efficiency corrections.

1.2.3 Hadronic decays

In this section we present experimental data for the reaction $\gamma + p \rightarrow p\pi^+\pi^-X(\pi^0(\eta))$, where $\pi^0(\eta)$ are identified via missing mass of proton, π^+ and π^- . In Fig. 1.3 (left panel) a distribution of missing mass of the proton is presented showing clear peaks of η and ω mesons with $\sim 2M$ and $\sim 20M$ events respectively as well as hints of η' and ϕ mesons. To see peaks of η' and ϕ better in Fig. 1.3 (right panel) we plot the same distribution for the range above ω meson. As one can see there we observe one of rare decays $\eta' \rightarrow \pi^+\pi^-\pi^0$ ($\text{Br}=3.6 \times 10^{-3}$) and OZI violating decay $\phi \rightarrow \pi^+\pi^-\pi^0$ ($\text{Br}=15.3\%$) observed for the first time in the photo-production experiments. The photo-production of the latter can be studied to check the influence of meson-baryon interference that might occur in the charge and neutral $K\bar{K}$ decay modes and is absent in this channel.

In Fig. 1.4 (left panel) we present distribution of missing mass of the proton in the reaction $\gamma + p \rightarrow p\pi^+\pi^-\eta$, where η is reconstructed in the missing mass of proton, π^+ and π^- . As one can see there is a clear peak of η' with $\sim 340K$ events which is almost an order of magnitude higher than recent BES [2] data. This will allow to extract coefficients of polynomial distributions of Dalitz plot projections with much higher statistical precision. On the other hand there appears a

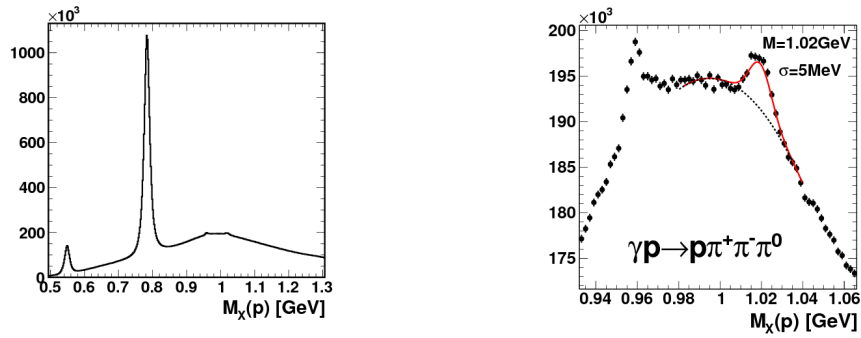


Figure 1.3: Left panel: distribution of missing mass of the proton in the reaction $\gamma + p \rightarrow p\pi^+\pi^-\pi^0$. Right panel: the same for the range of invariant mass above ω meson production.

hint of G-parity decay mode of $\phi \rightarrow \pi^+\pi^-\eta$. In In Fig. 1.4 (right panel) the same distribution is plotted above the η' peak. Here we see clear peak of ϕ meson. This decay mode has never been observed and PDG quotes only an upper limit $\text{Br} < 1.8 \times 10^{-5}$. Theoretical model [3] predicts even smaller upper limit on the order of $\sim 3 \times 10^{-7}$.

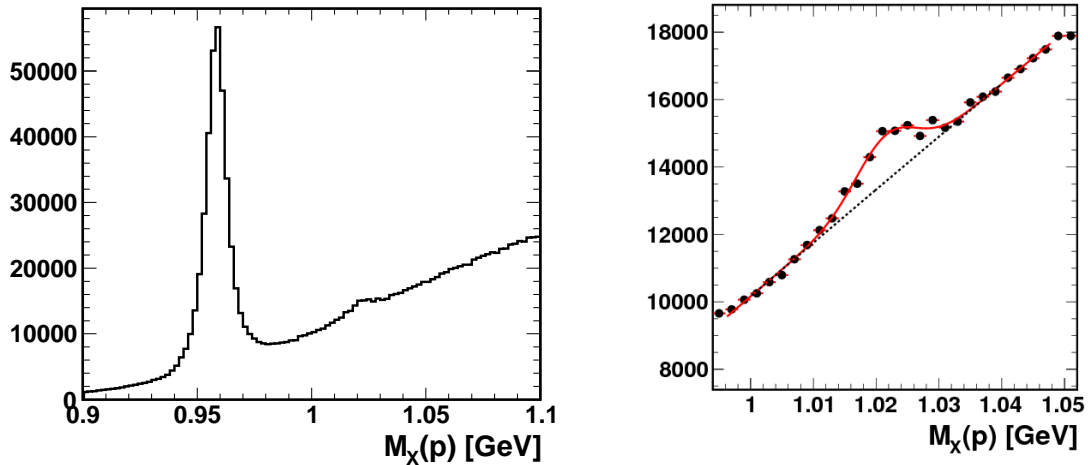


Figure 1.4: Left panel: distribution of missing mass of the proton for the reaction $\gamma + p \rightarrow p\pi^+\pi^-\eta$. Right panel: the same for the range of invariant mass above η' meson production.

1.3 Acknowledgements

We take this opportunity to express our gratitude to organizers for the invitation to give a talk at very fruitful PrimeNet workshop in Jülich and for their kind hospitality. This work is supported by the DOE Grant No. 350314.

Bibliography

- [1] F. Stollenwerk et al., arXiv:1108.2419
- [2] BESIII Collaboration, M. Ablikim et al., *Phys. Rev.*, **D83**, 012003, (2011).
- [3] N.N. Achasov and A.A. Kozhevnikov, *Int.J.Mod.Phys*, **A7**, 4825, (1992).

PSEUDOSCALAR MESON STUDIES WITH CHARM

*JOHAN MESSCHENDORP**

The viewgraph of this presentation can be found at:

http://www2.fz-juelich.de/ikp/primenet/2011_Workshop_Juelich/talks/meschendorp_primenet.pdf

*KVI and University of Groningen, meschendorp@kvi.nl

Meson Production

in photon-induced reactions and from NN collisions
as well as e^+e^- production from pp collisions

STUDY OF η MESON PRODUCTION WITH A POLARIZED PROTON BEAM

IRYNA OZERIANSKA^{*†‡}, PAWEŁ MOSKAL^{†‡} and MALGORZATA HODANA^{†‡}
for the WASA-at-COSY Collaboration

1.1 Introduction

In the low energy regime of Quantum Chromodynamics, the interaction between quarks and gluons cannot be treated perturbatively and so far the understanding of the processes governed by the strong forces is unsatisfactory. Therefore, it is essential to carry out measurements involving the production and decay of hadrons and to interpret them in the framework of effective field theories experiencing recently an enormous development in applications to the description of meson decays and production. In this contribution we concentrate on the η meson. The progress in understanding of the production processes of the η meson will strongly rely on the precise determination of spin and isospin observables. So far these observables have been determined only for few excess energies and with low statistics [1-5].

1.2 Partial waves

For an unambiguous understanding of the production process relative magnitudes from the partial waves contributions must be well established. This may be achieved by the measurement of the analysing power which would enable to perform the partial wave decomposition with an accuracy by far better than resulting from the measurements of the distributions of the spin averaged cross sections [6, 7]. Analysing power A_y may be understood as a measure of the relative deviation between the differential cross section for the experiment with and without polarized beam (σ and σ_0 respectively):

$$\sigma(\theta, \varphi) = \sigma_0(\theta, \varphi) \cdot [1 + A_y(\theta) \cdot P \cdot \cos(\varphi)] \quad (1.1)$$

where P denotes the beam polarization.

1.3 Studies of A_y with the WASA detector at COSY

Using the WASA-at-COSY detector [8] we intend to determine the energy and the angular dependence of $A_y(Q, \theta)$ and the total and differential cross sections for the $\vec{p}p \rightarrow pp\eta$ reaction in the excess energy range from the threshold up to 100 MeV. In November 2010 first measurements for $Q = 15$ MeV and $Q = 72$ MeV have been conducted [9]. From Table 1.1 we can see the beam parameters and the expected number of events for each excess energy.

Q [MeV/c]	P [MeV/c]	$\sigma_{tot}[\mu\text{b}]$	Acceptance	$N_{\eta \rightarrow \gamma\gamma}$	$N_{\eta \rightarrow 3\pi^0}$
15	2026	10^3	0.55	99770	81861
72	2188	$5 \cdot 10^3$	0.63	447739	375580

Table 1.1: Estimate of the number of produced η mesons

Protons from the $\vec{p}p \rightarrow pp\eta$ reaction are registered in the forward part of the detector and photons from the η meson decay are detected in the Electromagnetic Calorimeter of the central part. Simultaneously to the $\vec{p}p \rightarrow pp\eta$ reaction elastically scattered protons were registered. The $\vec{p}p \rightarrow pp$ reaction will be used for monitoring of the polarization degree, luminosity and the detector

*i.ozerianska@gmail.com

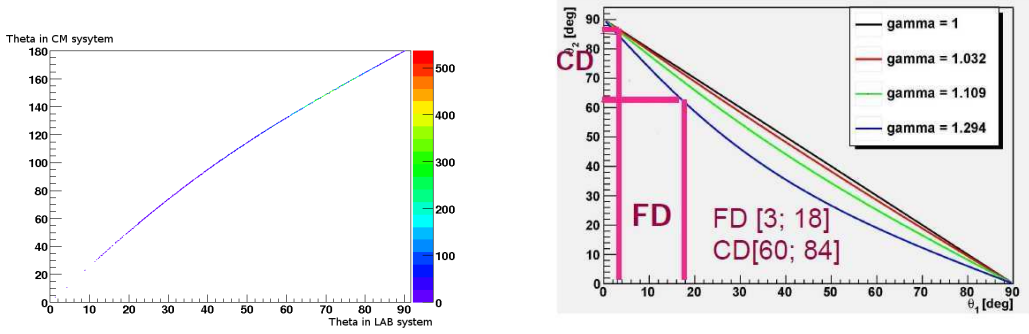
†Institute of Physics, Jagiellonian University, PL-30-059 Cracow

‡Institut für Kernphysik, Forschungszentrum Jülich, 52425 Jülich, Germany

performance. In the case of the $\bar{p}p \rightarrow pp$ reaction one proton is registered in the Forward Detector and the other in the Central Detector.

Within the geometrical acceptance of the Forward Detector (from 3° to 18°), the Central Detector covers proton scattering angle from 60° to 84° . In the center of mass system that corresponds to a scattering angle in the range of 30° to 46° as seen in Fig. 1.1a.

In Fig. 1.1b the scattering angle of one proton is depicted as a function of the scattering angle of the second proton. The first proton is registered in the Central Detector, the second one in the Forward Detector. Colored lines are predictions for different beam momenta. The blue line corresponds to a beam momentum of 2 GeV/c, close to the experimental value.



(a) The scattering angle in the centre of mass system is presented as a function of the scattering angle in the laboratory frame.

(b) The distribution of the scattering angle of proton registered in the Central Detector as a function of the scattering angle of the proton registered in the Forward Detector. For more details see the text.

Figure 1.1: The protons angular distributions in the Monte Carlo simulations of the $pp \rightarrow pp$ reaction.

1.4 Extraction of A_y from the experiment

In the first step we can obtain the value of the polarization, P , from the $\bar{p}p \rightarrow pp$ reaction using the analysing power already measured by the EDDA experiment [10]. In the second step, we will calculate the geometrical averages, N_{\pm} , of the number of η meson produced in direction (θ, φ) during the spin down N_{-}^{\downarrow} and spin up N_{+}^{\uparrow} modes, defined as follows:

$$\begin{aligned} N_{-} &\equiv \sqrt{N_{-}^{\uparrow} N_{-}^{\downarrow}} = \sqrt{\frac{N_{R}^{\uparrow}}{\epsilon_{R} L^{\uparrow}} \cdot \frac{N_{L}^{\downarrow}}{\epsilon_{L} L^{\downarrow}}} \\ N_{+} &\equiv \sqrt{N_{+}^{\uparrow} N_{+}^{\downarrow}} = \sqrt{\frac{N_{L}^{\uparrow}}{\epsilon_{L} L^{\uparrow}} \cdot \frac{N_{R}^{\downarrow}}{\epsilon_{R} L^{\downarrow}}} \end{aligned} \quad (1.2)$$

N_{-}^{\downarrow} and N_{+}^{\uparrow} can be determined according to the Madison convention[11]. Knowing the angles θ and φ of the outgoing η meson we can calculate the analysing power for the three particle final state using the following formula:

$$A_y(\theta) = \frac{1}{P \cos \varphi} \cdot \frac{N_{+}(\theta, \varphi) - N_{-}(\theta, \varphi)}{N_{+}(\theta, \varphi) + N_{-}(\theta, \varphi)} \quad (1.3)$$

where the polarization P was calculated in the first step.

An A_y for the proton-proton elastic scattering at 2026 MeV and 2188 MeV beam momenta, based on the results of the EDDA experiment is shown in Fig. 1.2. We can conclude that values of A_y for $Q=15$ MeV and $Q=72$ MeV are within the range of [0.32-0.38].

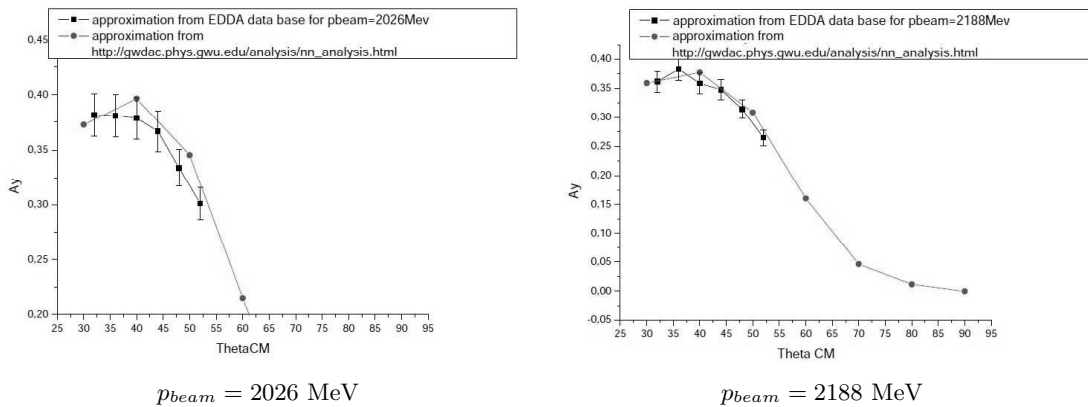


Figure 1.2: Distribution of A_y for $\bar{p}p \rightarrow pp$ reaction as a function of the protons scattering angle, θ , in the centre of mass system. Square points denotes data based on EDDA experiment [12] and superimposed line indicates results of Ref. [13].

Acknowledgements

This publication has been supported by COSY-FFE and by the European Commission under the 7th Framework Programme through the Research Infrastructures action of the Capacities Programme, Call: FP7-INFRASTRUCTURES-2008-1, Grant Agreement N. 227431 and by the Polish Ministry of Science and Higher Education under grants No. 2861/B/H03/2010/38 and 0320/B/H03/2011/40.

Bibliography

- [1] H. Calén et al., *Phys. Rev.* **C58** (1998) 2667.
- [2] R. Czyżykiewicz et al., *Phys. Rev. Lett.* **98** (2007) 122003.
- [3] P. Moskal et al., *Phys. Rev.* **C79** (2009) 015208.
- [4] F. Balestra et al., *Phys. Rev.* **C69** (2004) 064003.
- [5] P. Moskal et al., *Eur. Phys. J.* **A43** (2010) 131.
- [6] C. Hanhart, *Phys. Rept.* **397** (2004) 155.
- [7] P. Moskal et al., *Prog. Part. Nucl. Phys.* **49** (2002) 1.
- [8] H. H. Adam et al., nucl-ex/0411038, (2004).
- [9] P. Moskal, M. Hodana, *J. Phys. Conf. Ser* **295** (2011) 012080.
- [10] M. Altmeier et al., *Phys. Rev. Lett.* **85** (2000).
- [11] Madison convention, Polarisation Phenomena in Nuclear Reaction, University of Wisconsin Press, Madison, (1971), pp. XXV.
- [12] <http://hepdata.cedar.ac.uk/view/p5861>
- [13] http://gwdec.phys.gwu.edu/analysis/nn_analysis.html

DETERMINATION OF THE η MASS WITH THE CRYSTAL BALL AT MAMI-B

ALEXANDER NIKOLAEV*

for the Crystal Ball MAMI and A2 Collaborations

The viewgraph of this presentation can be found at:

http://www2.fz-juelich.de/ikp/primenet/2011_Workshop_Juelich/posters/nikolaev_primenet2011.pdf

*Helmholtz-Institut für Strahlen- und Kernphysik, Universität Bonn, nikolaev@hiskp.uni-bonn.de

HIGH PRECISION η MESON MASS DETERMINATION AT COSY-ANKE

PAUL GOSLAWSKI* for the ANKE-Collaboration

Recent measurements on the η meson mass performed at different experimental facilities (i.e. CERN-NA48, COSY-GEM, CESR-CLEO, DAΦNE-KLOE, MAMI-Crystal Ball) resulted in very precise data but differ by up to more than eight standard deviations, i.e. 0.5 MeV/c² [1]. In order to clarify this situation a high precision measurement using the ANKE spectrometer at the COoler SYnchrotron COSY has been realized.

Using the two-body reaction $dp \rightarrow {}^3\text{He}\eta$ at low excess energies the η mass can be determined only from pure kinematics by the determination of the production threshold. Therefore, twelve data points at fixed excess energies in the range of $Q = 1 - 12$ MeV were investigated. The final state momentum p_f of the ${}^3\text{He}$ -particles in the Center of Mass System (CMS)

$$p_f(s) = \frac{\sqrt{[s - (m_{{}^3\text{He}} + m_\eta)^2] \cdot [s - (m_{{}^3\text{He}} - m_\eta)^2]}}{2 \cdot \sqrt{s}}, \quad (1.1)$$

measured with the ANKE spectrometer, is very sensitive on the η mass and the total energy \sqrt{s} , where the latter one is completely defined in a fixed target experiment by the masses of the initial particles and the momentum of the deuteron beam p_d :

$$\sqrt{s} = \sqrt{2m_p \sqrt{m_d^2 + p_d^2} + m_d^2 + m_p^2}. \quad (1.2)$$

For a precise determination of the production threshold both quantities, the final state momenta of the ${}^3\text{He}$ -particles and the corresponding deuteron beam momenta have to be measured with highest accuracy. Fitting the dependency of the final state momentum p_f on the beam momentum p_d and the η mass, $p_f = p_f(p_d, m_\eta)$, for the twelve points the mass can be extracted as fitting parameter (see Fig. 1.3).

The beam momentum for each fixed excess energy was determined using a method developed at VEPP-2M at Novosibirsk at an electron-positron machine [2] using the spin dynamics of a polarized beam. Here the spin precession frequency of a relativistic particle is disturbed by an artificial spin resonance induced by a horizontal rf-magnetic field of a solenoid leading to a depolarization of the polarized accelerator beam. The depolarizing resonance frequency f_r depends on the kinematical γ -factor (i.e. the beam momentum $p = m\sqrt{\gamma^2 - 1}$) and the beam revolution frequency f_0 via the resonance condition:

$$f_r = (k + \gamma G) f_0, \quad (1.3)$$

where k is an integer and G the gyromagnetic anomaly of the beam particle. By measuring these two frequencies the beam momentum of a polarized beam can be determined with a precision below $\Delta p/p < 10^{-4}$. For the first time this method was used at COSY with a vector polarized deuteron beam and the momenta in the threshold range of 3.1 – 3.2 GeV/c were determined with an accuracy of $\Delta p/p < 6 \cdot 10^{-5}$, i.e. with 170 keV/c [3].

The correct final state momenta for the twelve different energies of the ${}^3\text{He}$ -nuclei of the reaction $dp \rightarrow {}^3\text{He}\eta$ can only be extracted fulfilling two conditions: a clear identification of the reaction of interest and a precise detector calibration. At ANKE the produced ${}^3\text{He}$ -nuclei can be identified by the energy loss and time of flight information. By this, the background consisting mainly of protons and deuterons of the dp elastic scattering and the deuteron break-up, can be suppressed effectively. For a two-body reaction at a fixed center of mass energy \sqrt{s} the final state momenta in the CMS are distributed on a momentum sphere with constant radius p_f , which can be visualized by plotting the transversal versus the longitudinal reconstructed momentum, as shown in Fig 1.1a.

*Institut für Kernphysik, Westfälische-Wilhelms Universität Münster, 48149 Münster, Germany, paul.goslowski@uni-muenster.de

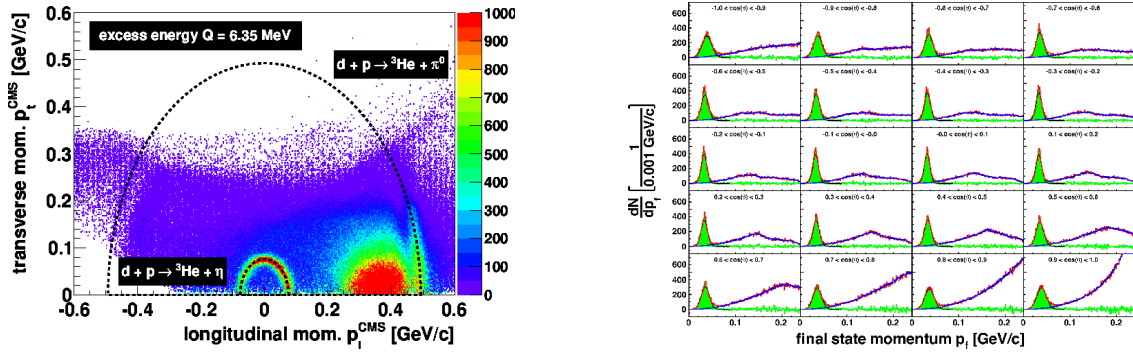


Figure 1.1: **a)** The momentum loci for the ${}^3\text{He}\eta$ and ${}^3\text{He}\pi$ channels. For the ${}^3\text{He}\eta$ channel ANKE covers near threshold the full solid angle, while for the ${}^3\text{He}\pi$ channel only forward scattered ${}^3\text{He}$ -nuclei are detected. **b)** Final state momentum $p_f = p_f(\cos\vartheta)$ (red) at an excess energy of $Q \approx 1$ MeV, the background description (blue) and the extracted ${}^3\text{He}\eta$ signal (green).

According to Eq. 1.1, one expects a centered momentum locus with a fixed radius $p_f = (p_x^2 + p_y^2 + p_z^2)^{1/2}$, indicated in Fig. 1.1a as dashed line. Using the feature that the ANKE facility has full geometrical acceptance for the reaction $dp \rightarrow {}^3\text{He}\eta$ near threshold up to 15 MeV the detector calibration can be verified and improved by studying the kinematics of this two-body reaction. The main idea to verify the calibration is that the momentum sphere has to be completely symmetric in p_x , p_y and p_z (or ϑ and ϕ) so that the final state momentum p_f should be constant in all directions. By a careful investigation of the momentum dependency on the cosine of the polar angle ϑ and the azimuthal angle ϕ

$$p_f = p_f(\cos\vartheta) \quad (1.4)$$

$$p_f = p_f(\phi) \quad (1.5)$$

the shape of the momentum sphere or locus can be studied in more detail. Deviations from this symmetric shape will indicate the need of an improvements of the calibration. Therefore the ${}^3\text{He}\eta$ signal has to be extracted background free. The background left after cutting on ${}^3\text{He}$ -nuclei (see Fig. 1.1a originating mainly from the multi pion production) can be subtracted by data taken below the η threshold at an excess energy of $Q \approx -5$ MeV, but analyzed as if they were taken above. In [4] the successful applicability of this approach on missing mass spectra is shown, but it is also applicable to final state momentum spectra as shown in Fig. 1.1b for different $\cos\vartheta$ bins for a data point close to threshold, i.e. $Q \approx 1$ MeV. Similarly the final state momentum dependency on ϕ can be studied. The background free ${}^3\text{He}\eta$ distribution allows to extract the mean final state momentum $p_f(\cos\vartheta)$ and $p_f(\phi)$ as shown in Fig. 1.2. In contrast to Monte-Carlo simulations on

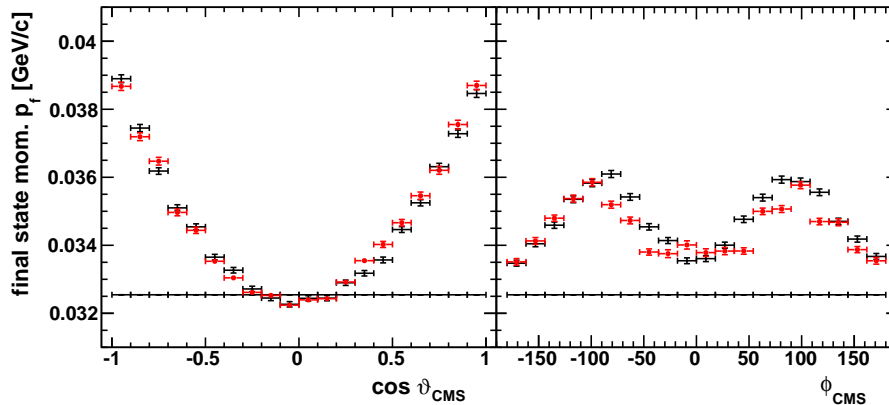


Figure 1.2: Final state momentum dependency: $p_f = p_f(\cos\vartheta)$ and $p_f(\phi)$ for data (red) simulations without momentum smearing (black line) and with momentum smearing (black).

$p_f(\cos\vartheta)$ and $p_f(\phi)$ without momentum smearing (black line) the obtained data points indicated

as red crosses show a dependency of the final state momentum in $\cos\vartheta$ and ϕ . The shape of the momentum sphere is stretched to values $\cos\vartheta \rightarrow \pm 1$ and shows an oscillation in ϕ . This behavior is caused by a kinematic effect due to different momentum resolutions of the ANKE detector for p_x , p_y and p_z . Assuming that the p_x , p_y and p_z distributions are gaussian distributed with different widths σ , it is possible to reproduce the final state momentum dependency on $\cos\vartheta$ and ϕ with Monte-Carlo simulations shown as black crosses.

For the final state momentum determination the plots shown in Fig. 1.2 are of high importance because of following three reasons

- i) Improvement of the calibration. Asymmetric shapes in $\cos\vartheta$ and ϕ can be corrected by minor changes of the ANKE calibration parameters. These changes are so small that typical calibration quantities like missing masses of different reactions show no variations, because they are not sensitive enough.
- ii) Extraction of the correct momentum resolution in (p_x, p_y, p_z) . Assuming gaussian distributions with different widths we found for ANKE $(\sigma_x, \sigma_y, \sigma_z) = (3.2, 7.8, 16.4)$ MeV/c.
- iii) Correction of the reconstructed final state momentum. Because of the finite momentum resolution the extracted momentum (red) are larger compared to the original one (black line). This has to be considered in the determination of the twelve final state momenta.

Currently the final state momentum analysis is still in progress but already now the twelve momenta in the range of 30–100 MeV/c can be determined with a precision below 400 keV/c. Fitting the $p_f = p_f(p_d, m_\eta)$ dependency, as shown in Fig. 1.3 the η mass is determined preliminary to

$$m_\eta = (547.869 \pm 0.007 \pm 0.040) \text{ MeV}/c^2. \quad (1.6)$$

The accuracy, which will be achieved at ANKE, will be comparable and competitive to the precision achieved at other recent experiments.

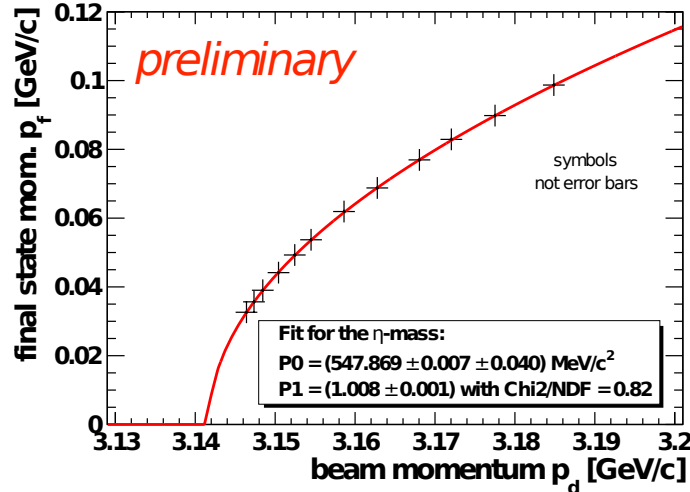


Figure 1.3: Determination of the η mass by fitting the dependency $p_f = p_f(p_d, m_\eta)$.

Bibliography

- [1] C. Amsler et al., Phys. Lett. B **667**, 1 (2008).
- [2] Ya. S. Derbenev et al., Part. Accel. **10**, 177 (1980).
- [3] P. Goslawski, Diploma thesis, Westfälische-Wilhelms Universität Münster (2008);
P. Goslawski et al., Phys. Rev. ST Accel. Beams **13** 022803 (2010).
- [4] T. Mersmann et al., Phys. Rev. Lett. **98**, (2007) 242301 .

This work is supported by FZ Jülich FFE.

MEASUREMENT OF THE η' MESON TOTAL WIDTH AT THE COSY-11 FACILITY

E. CZERWIŃSKI^{†‡§}, D. GRZONKA[†] and P. MOSKAL^{*†}
for the COSY-11 Collaboration*

1.1 COSY-11 detection setup

The reported experiment has been performed in the Research Centre Jülich at the cooler synchrotron COSY [1] by means of the COSY-11 detector system [2, 3] presented in Figure 1.1.

The collision of a proton from the COSY beam with a proton cluster target may cause an η' meson creation. In that case all outgoing nucleons have been registered by the COSY-11 detectors, whereas for the η' meson identification the missing mass technique was applied.

The cluster target width was reduced by a factor of 5 compared to the normal operation mode in order to decrease the systematic uncertainties during the determination of the total width of the η' meson. The dimensions of the target stream were determined using a wire probe installed for this purpose.

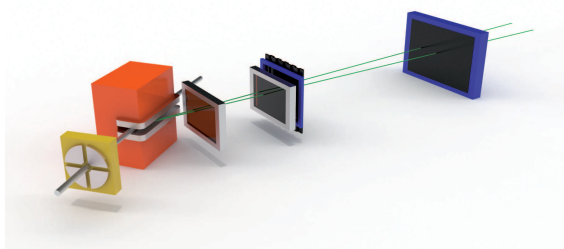


Figure 1.1: COSY-11 detector setup. From left to right: quadrupole (yellow) and dipole (orange) magnets of COSY, two drift chambers (silver) and two scintillator detectors (blue-black).

1.2 Total width of the η' meson

The mass of unregistered meson was determined via the missing mass technique, while the total width was directly derived from the mass distributions established at five different beam momenta [4, 5]. Based on the sample of more than 2300 reconstructed $pp \rightarrow pp\eta'$ events the determined total width of the η' meson amounts to $\Gamma_{\eta'} = 0.226 \pm 0.017(\text{stat.}) \pm 0.014(\text{syst.}) \text{ MeV}/c^2$, which is the most precise measurement until now [6, 7, 8]. On the plots in Figure 1.2 the experimental data are presented as black points, while the histograms correspond to the sum of the Monte Carlo generated signal for $\Gamma_{\eta'} = 0.226 \text{ MeV}/c^2$ and a normalised second order polynomial obtained as a fit to the signal-free background region for another energy [4, 5]. The plot in the bottom right corner presents the χ^2 distribution as a function of the $\Gamma_{\eta'}$ determined by the comparison of the missing mass spectra from the measurement with Monte Carlo simulations.

1.3 Acknowledgments

The work was partially supported by the European Commission under the 7th Framework Programme through the *Research Infrastructures* action of the *Capacities* Programme. Call: FP7-INFRASTRUCTURES-2008-1, Grant Agreement N. 227431, by the PrimeNet, by the Polish Ministry of Science and Higher Education through grants No. 1202/DFG/2007/03 and 1253/B/H03/2009/36, by the German Research Foundation (DFG) and by the FFE grants from the Research Center Jülich.

^{*}Institute of Physics, Jagiellonian University, PL-30-059 Cracow, Poland

[†]Institute for Nuclear Physics and Jülich Center for Hadron Physics, Research Center Jülich, D-52425 Jülich, Germany

[‡]INFN, Laboratori Nazionali di Frascati, IT-00044 Frascati, Italy

[§]eryk.czerwinski@uj.edu.pl

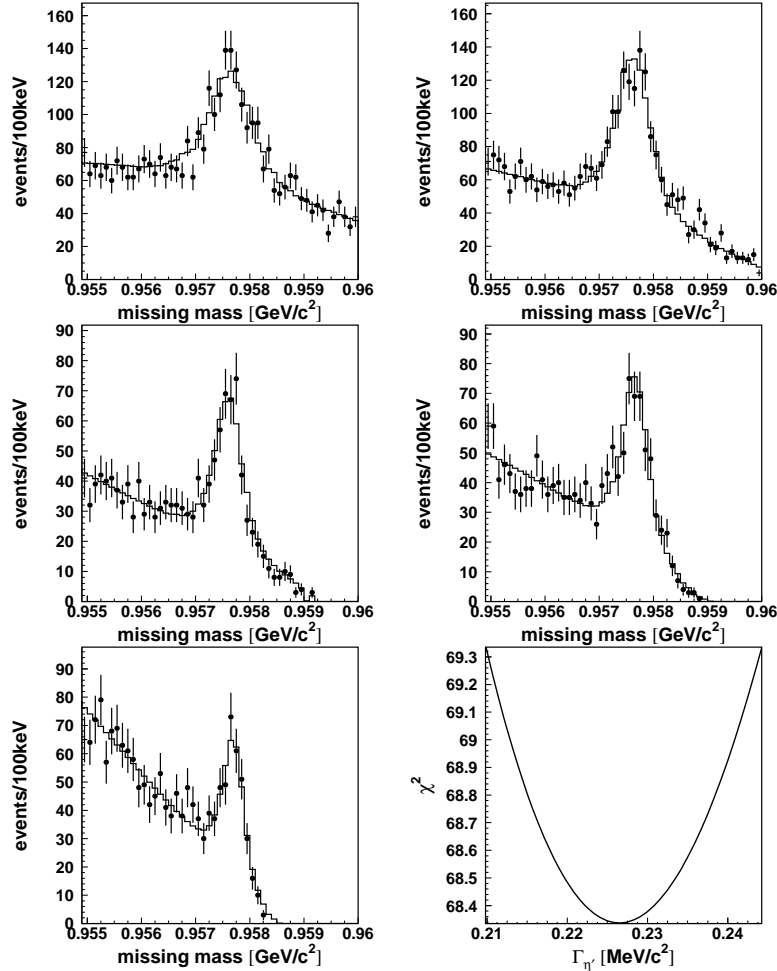


Figure 1.2: The missing mass spectra for the $pp \rightarrow ppX$ reaction for excess energies in the CM system equal to 4.8, 2.8, 1.7, 1.4, and 0.8 MeV (from left to right, top to bottom). The η' meson signal is clearly visible. The experimental data are presented as black points, while in each plot the histogram corresponds to the sum of the Monte Carlo generated signal for $\Gamma_{\eta'} = 0.226$ MeV and the shifted and normalised second order polynomial obtained as a fit to the signal-free background region for another energy. Bottom right: χ^2 as a function of $\Gamma_{\eta'}$ in the range up to $\chi^2 = \chi_{min}^2 + 1$. The minimum corresponds to the determined $\Gamma_{\eta'}$ value.

Bibliography

- [1] R. Maier *et al.*, *Nucl. Instrum. Methods Phys. Res., Sect. A*, **390**, 1, (1997).
- [2] S. Brauksiepe *et al.*, *Nucl. Instrum. Methods Phys. Res., Sect. A*, **376**, 397, (1996).
- [3] P. Moskal *et al.*, *Nucl. Instrum. Methods Phys. Res., Sect. A*, **466**, 448, (2001).
- [4] E. Czerwiński *et al.*, *Phys. Rev. Lett.*, **105**, 122001, (2010).
- [5] E. Czerwiński, PhD thesis, arXiv: 0909.2781, (2009).
- [6] K. Nakamura *et al.* (Particle Data Group), *J. Phys. G*, **37**, 075021, (2010) and 2011 partial update for the 2012 edition
- [7] R. Wurzinger *et al.*, *Phys. Lett. B*, **374**, 283, (1996).
- [8] D. M. Binnie *et al.*, *Phys. Lett. B*, **83**, 41, (1979).

TWO-PION PRODUCTION IN ISOSCALAR NN COLLISIONS: ABC EFFECT AND RESONANCE

*M. BASHKANOV**[†], *H. CLEMENT**, *E. DOROSHKEVICH**,
*E. PEREZ DEL RIO**, *A. PRICKING** and *T. SKORODKO**
for the WASA-AT-COSY Collaboration

1.1 Introduction

More than fifty years ago Abashian, Booth and Crowe [1] observed in the reaction $pd \rightarrow {}^3\text{HeX}$ that the missing mass of the detected ${}^3\text{He}$ ejectile corresponding kinematically to the production of a pion pair, *i.e.* $X = \pi\pi$, contains a peculiar enhancement starting right at threshold at low $\pi\pi$ -masses. In subsequent bubble-chamber [2, 3] and single-arm magnetic spectrometer measurements [4, 5, 6, 7, 8, 9, 10, 11] this enhancement was found in fusion reactions to d , ${}^3\text{He}$ and ${}^4\text{He}$, where an isoscalar pion pair was produced, however, not in the fusion reaction leading to tritium, where an isovector pion pair was produced. From these results it was concluded that this effect, which later-on was named ABC effect after the initials of the first authors, only appears in the double-pionic fusion in combination with the production of an isoscalar pion pair.

Since these experiments were undertaken at beam energies, which energetically allow the mutual excitation of two colliding nucleons into their first excited state, the $\Delta(1232)P_{33}$, theoretical attempts were undertaken to understand the ABC effect by the excitation of a $\Delta\Delta$ system via t -channel meson exchange or variations of it [12, 13, 14, 15, 16, 17]. These calculations, indeed, predicted a low-mass enhancement, however, also a high-mass enhancement. Surprisingly enough, the inclusive single-arm measurements seemed to support such a high-mass enhancement. And it was only recently that the first exclusive and kinematically complete measurements of solid statistics [18, 19, 20, 21, 22, 23] over practically the full phase space revealed that such a high-mass enhancement is not present.

1.2 Recent Experiments

In order to understand the two-pion production process in pp , pd and dd collisions in more detail, systematic experimental studies were initiated at CELSIUS and continued later-on at COSY. These exclusive and kinematically complete high-statistics measurements have been carried out at the detector installations PROMICE/WASA [24, 25, 26], CELSIUS/WASA [27, 28, 19, 29, 30, 31, 32], COSY-TOF [33, 34], WASA-at-COSY [35, 23, 36] and COSY-ANKE [37] covering the energy range from the two-pion production threshold up to $\sqrt{s} = 2.5$ GeV (corresponding to a nucleon beam energy of 1.4 GeV). The bulk of these experiments has been performed with the WASA detector setup, which has an angular coverage of nearly 4π and features windowless hydrogen and deuterium pellet target systems [27, 35] as well as a very reliable particle identification for γ , π , p , n , d , ${}^3\text{He}$ and ${}^4\text{He}$. Measurements at WASA generally are performed with detection of all ejectiles of an event (with the exception of spectator nucleons) leading thus to kinematic fits with overconstraints in the data analysis. For the investigation of the pn initiated reactions the quasifree pd process with a spectator proton resulting from the target deuteron is utilized. By exploiting the Fermi motion of the active nucleon in the deuteron target that way the energy dependence of pn and pp initiated reactions can be measured over a range of more than 100 MeV by use of a single beam energy.

*Physikalisches Institut der Universität Tübingen, Germany

[†]bashkano@pit.physik.uni-tuebingen.de

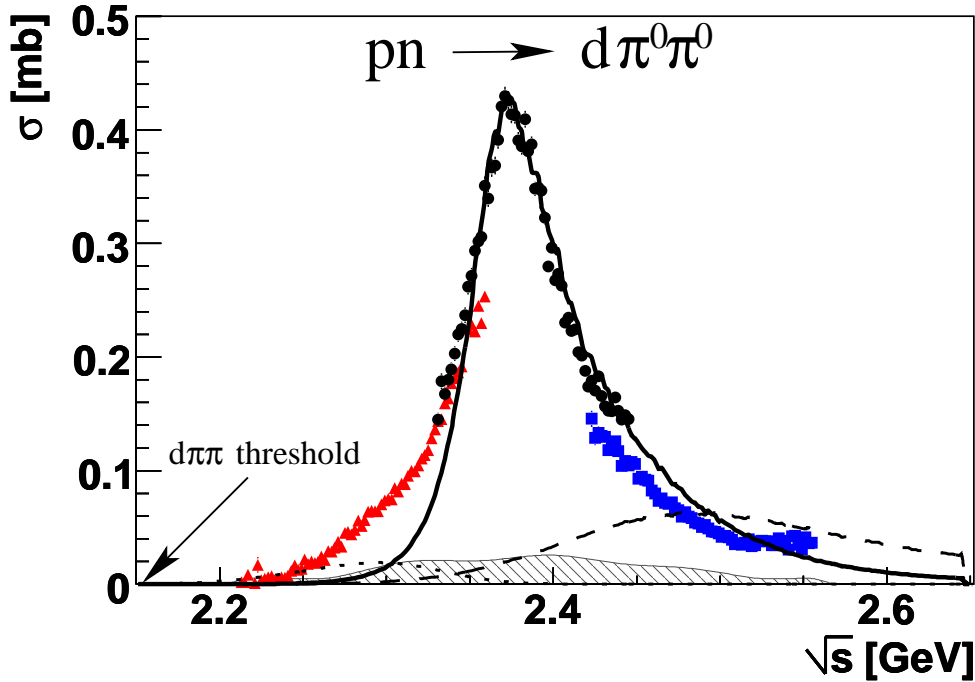


Figure 1.1: Total cross sections obtained from this experiment on $pd \rightarrow d\pi^0\pi^0 + p_{spectator}$ for the beam energies $T_p = 1.0$ GeV (triangles), 1.2 GeV (dots) and 1.4 GeV (squares) normalized independently. Shown are the total cross section data after acceptance, efficiency and Fermi motion corrections. The hatched area indicates systematic uncertainties. The drawn lines represent the expected cross sections for the Roper excitation process (dotted) and the t -channel $\Delta\Delta$ contribution (dashed) as well as a calculation for a s -channel resonance with $m = 2.37$ GeV and $\Gamma = 68$ MeV (solid). From Ref. [23]

1.3 Results

From the overwhelming amount of high-quality data for total (integral) and differential cross sections in the various two-pion production channels the following features emerge for the energy region from threshold up to $\sqrt{s} = 2.6$ GeV:

- The **isovector** two-pion production [38] initiated by pp collisions can be quantitatively understood by t -channel meson exchange with
 - excitation of one of the colliding nucleons into the Roper resonance, $N^*(1440)P_{11}$ and its subsequent decay into the $N\pi\pi$ system either directly ($N\sigma$ channel) or via the $\Delta\pi$ intermediate state,
 - mutual excitation of the two colliding nucleons into the Δ state each with subsequent decay into $N\pi$, or
 - excitation of a higher lying Δ state, favorably the $\Delta(1600)P_{33}$ state with subsequent decay into $N\pi\pi$ via $\Delta\pi$. Such an excitation, however, plays a dominant role only in the $nn\pi^+\pi^+$ channel possessing an isotensor pion pair.

Whereas the Roper process dominates at lower energies close to threshold, the $\Delta\Delta$ process dominates at higher energies close to $\sqrt{s} = 2m_\Delta = 2.46$ GeV. In particular the isovector double-pionic fusion reaction $pp \rightarrow d\pi^+\pi^0$ is well described in its energy dependence up to at least 3 GeV by the latter process [30].

- The **isoscalar** two-pion production reaction $pn \rightarrow d\pi^0\pi^0$ – measured as quasifree process in pd collisions [19, 23] – exhibits a pronounced low-mass enhancement in the $\pi\pi$ -invariant mass distribution as expected in view of the ABC history on double-pionic fusion reactions. However, what was not expected is a strict correlation of this ABC effect with the appearance

of a resonance-like structure in the total cross section – see Fig. 1 – with $m = 2.37$ GeV and $\Gamma = 70$ MeV, i.e. roughly 100 MeV below $2m_\Delta$ and three times narrower than expected from the t -channel $\Delta\Delta$ process. From the angular distributions the spin-parity of this structure is derived with the result that $I(J^P) = 0(3^+)$.

Note that this reaction constitutes the only purely isoscalar two-pion production channel in NN collisions. Hence exotic processes in the isoscalar channel are likely to be seen best in this particular reaction without being diluted by isovector contributions.

- The **isoscalar** double-pionic fusion reaction $dd \rightarrow {}^4\text{He}\pi\pi$ also exhibits the ABC effect in strict correlation with a resonance-like structure in the total cross section at the same energy above the two-pion threshold [21, 22]. The increased width of this structure can be explained by the Fermi motion of the active **isoscalar** pn pair in target, projectile and fused nucleus. The energy dependence of the reaction $pd \rightarrow {}^3\text{He}\pi\pi$ is under investigation. Preliminary results [39] indicate a similar trend as observed for the ${}^4\text{He}$. If true than this **isoscalar** pn resonance structure is obviously strong enough to survive even in helium nuclei.

1.4 Acknowledgments

We acknowledge valuable discussions with L. Alvarez-Ruso, C. Hanhart, E. Oset, A. Sibirtsev and C. Wilkin on this issue. This work has been supported by BMBF(06TU9193), Forschungszentrum Jülich (COSY-FFE) and DFG (Europ. Grad. School 683).

Bibliography

- [1] N. E. Booth, A. Abashian, K. M. Crowe, *Phys. Rev. Lett.* **7** (1961) 35; **6** (1960) 258; *Phys. Rev.* **C 132** (1963) 2296ff.
- [2] I. Bar-Nir *et al.*, *Nucl. Phys.* **B 54** (1973) 17.
- [3] A. Abdivaliev *et al.*, *Sov. J. Nucl. Phys.* **29** (1979) 796.
- [4] R. J. Homer *et al.*, *Phys. Rev. Lett.* **9** (1964) 72.
- [5] J. H. Hall *et al.*, *Nucl. Phys.* **B 12** (1969) 573.
- [6] J. Banaigs *et al.*, *Nucl. Phys.* **B 67** (1973) 1.
- [7] J. Banaigs *et al.*, *Nucl. Phys.* **B 105** (1976) 52.
- [8] F. Plouin *et al.*, *Nucl. Phys.* **A 302** (1978) 413.
- [9] F. Plouin, P. Fleury, C. Wilkin, *Phys. Rev. Lett.* **65** (1990) 690.
- [10] R. Wurzinger *et al.*, *Phys. Lett.* **B 445** (1999) 423.
- [11] for a review see A. Codino and F. Plouin, *LNS/Ph/94-06*.
- [12] T. Risser and M. D. Shuster, *Phys. Lett.* **43 B** (1973) 68.
- [13] I. Bar-Nir, T. Risser, M. D. Shuster, *Nucl. Phys.* **B 87** (1975) 109.
- [14] J. C. Anjos, D. Levy, A. Santoro, *Nucl. Phys.* **B 67** (1973) 73.
- [15] see, e.g., A. Gardestig, G. Fäldt, C. Wilkin, *Phys. Rev.* **C 59** (1999) 2608 and *Phys. Lett.* **B 421** (1998) 41.
- [16] C. A. Mosbacher, F. Osterfeld, *nucl-th/990364*
- [17] L. Alvarez-Ruso, *Phys. Lett.* **B 452**, 207(1999); PhD thesis, Univ. Valencia 1999.
- [18] M. Bashkanov *et al.*, *Phys. Lett.* **B 637**, (2006) 223.
- [19] M. Bashkanov *et al.*, *Phys. Rev. Lett.* **102**, (2009) 052301.
- [20] S. Keleta *et al.*, *Nucl. Phys.* **A 825**, (2009) 71.

- [21] A. Pricking, PhD thesis, Univ. Tübingen, 2011;
<http://tobias-lib.uni-tuebingen.de/volltexte/2011/5695/pdf/ThesisFinal.pdf>
- [22] JCHP COSY Annual Report, Forschungszentrum Jülich (2010) 5
- [23] P. Adlarson et al., *Phys. Rev. Lett.* **106**, (2011) 202302.
- [24] J. Johanson et al., *Nucl. Phys. A* **712**, (2002) 75.
- [25] W. Brodowski et al., *Phys. Rev. Lett.* **88**, (2002) 192301.
- [26] J. Pätzold et al., *Phys. Rev. C* **67**, (2003) 052202.
- [27] Ch. Bargholtz et al., *Nucl. Instrum. Methods A* **547**, (2005) 294.
- [28] T. Skorodko, et al., *Eur. Phys. J. A* **35**, (2008) 317.
- [29] T. Skorodko, et al., *Phys. Lett. B* **679**, (2009) 30.
- [30] F. Kren et al., *Phys. Lett. B* **684**, (2010) 110 and *Phys. Lett. B* **702** (2011) 312.
- [31] T. Skorodko et al., *Phys. Lett. B* **695**, (2011) 115.
- [32] T. Skorodko et al., *Eur. Phys. J. A* **47**, (2011) 108.
- [33] S. Abd El-Bary et al., *Eur. Phys. J. A* **37**, (2008) 267.
- [34] S. Abd El-Samad et al., *Eur. Phys. J. A* **42**, (2009) 159.
- [35] H. H. Adam et al., *arXiv:nucl-ex/0411038*, (2004).
- [36] P. Adlarson et al., submitted for publication; arXiv:1107.0879 [hep-ex]
- [37] S. Dymov et al., *Phys. Rev. Lett.* **102**, (2009) 192301.
- [38] T. Skorodko et al., contribution to this workshop
- [39] E. Perez del Rio et al., contribution to this workshop

ABC EFFECT IN DOUBLE-PIONIC FUSION TO ${}^3\text{He}$

*E. PEREZ DEL RIO**[†], *M. BASHKANOV**, *H. CLEMENT**,
*A. PRICKING** and *T. SKORODKO**
for the WASA-AT-COSY Collaboration

1.1 Introduction

The ABC effect named after Abashian, Booth and Crowe [1] denotes a low-mass enhancement in the $\pi\pi$ -invariant mass distribution resulting from two-pion production processes. More than fifty years ago Abashian, Booth and Crowe were the first to observe this enhancement in the reaction $pd \rightarrow {}^3\text{He}X$ by measuring the momentum spectrum of the detected ${}^3\text{He}$ ejectile. This spectrum translates into a ${}^3\text{He}$ -missing mass spectrum, which corresponds to the $\pi\pi$ -invariant mass spectrum for $X = \pi\pi$. In subsequent bubble-chamber [2, 3] and single-arm magnetic spectrometer measurements [4, 5, 6, 7, 8, 9, 10, 11] this enhancement was observed in double-pionic fusion reactions leading to d , ${}^3\text{He}$ and ${}^4\text{He}$, if an isoscalar pion pair was produced. However, such an enhancement was not seen in fusion reactions leading to deuteron and triton, if an isovector pion pair was produced. These results led to the conclusion that this effect only appears in the double-pionic fusion in combination with the production of an isoscalar pion pair.

Recent exclusive and kinematically complete measurements [12, 13, 14] of the $pn \rightarrow d\pi^0\pi^0$ reaction from threshold up to $\sqrt{s} = 2.5$ GeV revealed a strict correlation between the appearance of the low-mass enhancement in the $\pi\pi$ -invariant mass spectrum (ABC effect) and a narrow resonance-like structure in the total cross section of this reaction. This surprising structure peaks at $m = 2.37$ GeV, *i.e.* roughly 100 MeV below $2m_\Delta$, where the conventional excitation of a $\Delta\Delta$ system peaks. Early attempts to theoretically understand the ABC phenomenon favored exactly this conventional t -channel process for its understanding [15, 16, 17, 18, 19, 20]. The recent high-statistics data do not only show that the reaction peaks far below the conventional $\Delta\Delta$ process, but that also the narrow width $\Gamma = 70$ MeV of the observed resonance-like structure is three times less than expected from the conventional process.

In fact, all pp -induced, *i.e.* **isovector** two-pion production processes including the double-pionic fusion reaction $pp \rightarrow d\pi^+\pi^0$ [21] show neither a pronounced ABC effect nor a narrow resonance-like structure in their total cross sections [22]. They rather are well understood by conventional t -channel nucleon excitations. From this follows that any unconventional process in connection with the ABC effect has to be associated not only with the **isoscalar** $\pi\pi$ system but also with the **isoscalar** NN system. This hypothesis is supported by the finding that also in the double-pionic fusion to ${}^4\text{He}$ the appearance of the ABC effect is strictly connected with a resonance-like structure in the total cross section [23, 24].

1.2 New Experiments and Results

Since the only other double-pionic fusion reaction exhibiting an ABC effect is the one leading to ${}^3\text{He}$, this reaction is ideally suited to test this hypothesis. Hence corresponding exclusive and kinematically complete measurements have been performed at the WASA-at-COSY facility [25]. These measurements covering the energy range from threshold up to the $\Delta\Delta$ region have been carried via the reactions $pd \rightarrow {}^3\text{He}\pi^0\pi^0$ at $T_p = 1.0$ GeV and via the quasifree process $dd \rightarrow {}^3\text{He}\pi^0\pi^0 + n_{\text{spectator}}$, which covers a wide range of energies due to the nucleons' Fermi motion in the target. The experiments are complemented by the recent CELSIUS/WASA measurement at $T_p = 0.875$ GeV [26]. The data analysis is still in progress. As a preliminary result we show the energy dependence of the total cross section in Fig.1, where also the results from previous experiments at CELSIUS [26, 27] and COSY [28] are plotted. Again we find a resonance-like behavior of the total cross section connected with the appearance of the ABC effect in the $\pi\pi$ -invariant mass spectrum.

*Physikalisches Institut der Universität Tübingen, Germany

[†]perez@pit.physik.uni-tuebingen.de

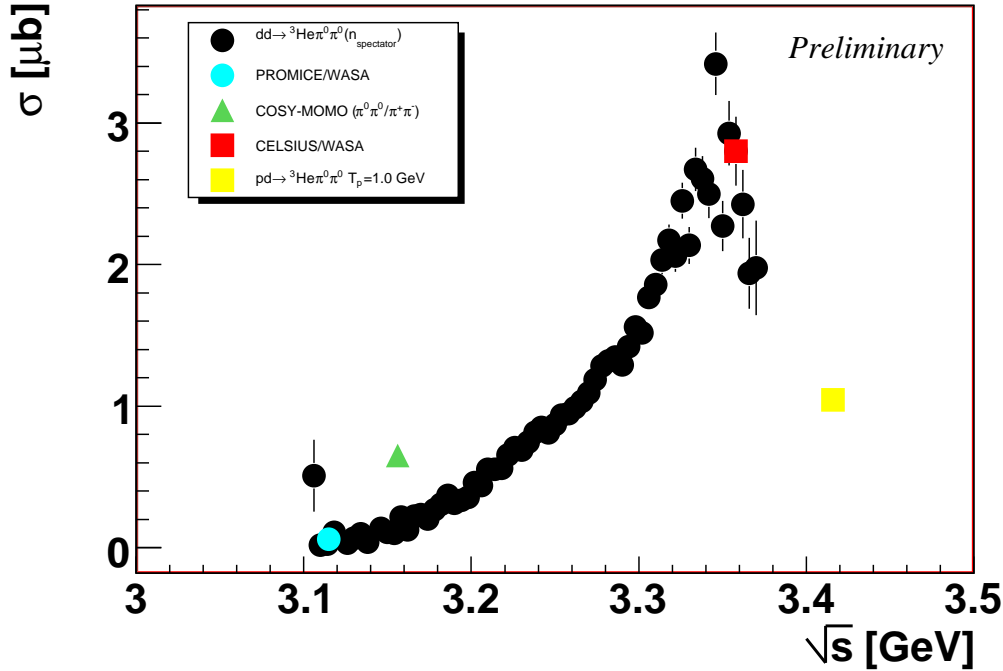


Figure 1.1: Preliminary results for the total cross section for the double-pionic fusion to ${}^3\text{He}$ obtained from this experiment on $pd \rightarrow {}^3\text{He}\pi^0\pi^0$ at $T_p = 1.0$ GeV (yellow square) and $dd \rightarrow {}^3\text{He}\pi^0\pi^0 + n_{\text{spectator}}$ for the beam energy $T_d = 1.4$ GeV (black dots) in comparison with previous results from PROMICE/WASA [27], CELSIUS/WASA [26] and COSY-MOMO [28].

1.3 Acknowledgments

We acknowledge valuable discussions with L. Alvarez-Ruso, C. Hanhart, E. Oset, A. Sibirtsev and C. Wilkin on this issue. This work has been supported by BMBF(06TU9193), Forschungszentrum Jülich (COSY-FFE) and DFG (Europ. Grad. School 683)

Bibliography

- [1] N. E. Booth, A. Abashian, K. M. Crowe, *Phys. Rev. Lett.* **7** (1961) 35; **6** (1960) 258; *Phys. Rev.* **C 132** (1963) 2296ff.
- [2] I. Bar-Nir *et al.*, *Nucl. Phys.* **B 54** (1973) 17.
- [3] A. Abdivaliev *et al.*, *Sov. J. Nucl. Phys.* **29** (1979) 796.
- [4] R. J. Homer *et al.*, *Phys. Rev. Lett.* **9** (1964) 72.
- [5] J. H. Hall *et al.*, *Nucl. Phys.* **B 12** (1969) 573.
- [6] J. Banaigs *et al.*, *Nucl. Phys.* **B 67** (1973) 1.
- [7] J. Banaigs *et al.*, *Nucl. Phys.* **B 105** (1976) 52.
- [8] F. Plouin *et al.*, *Nucl. Phys.* **A 302** (1978) 413.
- [9] F. Plouin, P. Fleury, C. Wilkin, *Phys. Rev. Lett.* **65** (1990) 690.
- [10] R. Wurzinger *et al.*, *Phys. Lett.* **B 445** (1999) 423 .
- [11] for a review see A. Codino and F. Plouin, *LNS/Ph/94-06*.
- [12] M. Bashakanov *et al.*, contribution to this workshop.

- [13] M. Bashkanov et al., *Phys. Rev. Lett.* **102** (2009) 052301.
- [14] P. Adlarson et al., *Phys. Rev. Lett.* **106** (2011) 202302.
- [15] T. Risser and M. D. Shuster, *Phys. Lett.* **43 B** (1973) 68.
- [16] I. Bar-Nir, T. Risser, M. D. Shuster, *Nucl. Phys.* **B 87** (1975) 109.
- [17] J. C. Anjos, D. Levy, A. Santoro, *Nucl. Phys.* **B 67** (1973) 73.
- [18] see, e.g., A. Gardestig, G. Fäldt, C. Wilkin, *Phys. Rev.* **C 59** (1999) 2608 and *Phys. Lett.* **B 421** (1998) 41.
- [19] C. A. Mosbacher, F. Osterfeld, *nucl-th/990364*.
- [20] L. Alvarez-Ruso, *Phys. Lett.* **B 452** (1999) 207; PhD thesis, Univ. Valencia 1999.
- [21] F. Kren et al., *Phys. Lett.* **B 684** (2010) 110 and *Phys. Lett.* **B 702** (2011) 312.
- [22] T. Skorodko et al., contribution to this workshop.
- [23] A. Pricking, PhD thesis, Univ. Tübingen 2011;
<http://tobias-lib.uni-tuebingen.de/volltexte/2011/5695/pdf/ThesisFinal.pdf>
- [24] JCHP COSY Annual Report, Forschungszentrum Jülich (2010) 5.
- [25] H. H. Adam et al., *arXiv:nucl-ex/0411038*.
- [26] M. Bashkanov et al., *Phys. Lett.* **B 637** (2006) 223.
- [27] M. Andersson et al., *Phys. Lett.* **B 485** (2000) 327.
- [28] F. Bellemann et al., *Phys. Rev.* **C 60** (1999) 061002.

TWO-PION PRODUCTION IN PROTON-PROTON COLLISIONS

*T. SKORODKO**[†], *M. BASHKANOV**, *H. CLEMENT**
*and E. DOROSHKEVICH**
for the CELSIUS-WASA Collaboration

1.1 Introduction

Two-pion production in NN collisions gives access to the investigation of nucleon excitations in course of the production process. In particular, it provides the unique possibility to study the mutual excitation of the two colliding nucleons into one of their excited states. The simplest such process is the excitation of a $\Delta\Delta$ system by t -channel meson exchange in the collision process.

In case that the two-pion production process leads to a fused nucleus in the final state the so-called ABC effect – a peculiar low-mass enhancement in the $\pi\pi$ -invariant mass spectrum – shows up, if the pion pair is of isoscalar nature [1, 2, 3, 4, 5, 6, 7, 8, 9, 10, 11, 12, 13, 14, 15, 16]. Recently it has been demonstrated [17, 18] that the ABC effect in the $pn \rightarrow d\pi^0\pi^0$ reaction is strictly correlated with the appearance of a pronounced resonance-like structure in the total cross section. This structure with maximum at $\sqrt{s} = 2.37$ GeV peaks roughly 100 MeV below the maximum of the conventional t -channel $\Delta\Delta$ process. Moreover it has a width of only 70 MeV, *i.e.* about three times less than the conventional process in its energy dependence.

In a recent work it has been claimed that a kind of ABC effect is also present in the $pp \rightarrow pp\pi^0\pi^0$ reaction, when the two emitted protons have very small relative momenta representing a kind of quasi-bound ${}^2\text{He}$ system [19].

In order to clarify the situation and to contribute to a detailed understanding of the two-pion production process, we have studied all different two-pion production channels in pp collisions constituting the *isovector* part of the NN and $NN\pi\pi$ systems.

1.2 Experiments and Results

In order to complement other data sets [19, 20, 21, 22, 23, 24, 25] exclusive and kinematically complete measurements of the reactions $pp \rightarrow pp\pi^0\pi^0$ [26, 27, 29], $pp \rightarrow pp\pi^+\pi^-$, $pp \rightarrow pn\pi^+\pi^0$ [27], $pp \rightarrow nn\pi^+\pi^+$ [30] and $pp \rightarrow d\pi^+\pi^0$ [28] were carried out at the CELSIUS storage ring using the 4π WASA detector setup including the pellet target system [31]. The $pp \rightarrow pp\pi^0\pi^0$ and $pp \rightarrow pp\pi^+\pi^-$ reactions were evaluated from close to threshold up to $T_p = 1.36$ GeV, the other channels only at $T_p = 1.1$ GeV.

Forward going charged pions, protons, neutrons and deuterons were detected in the forward detector and identified by the ΔE -E technique. Charged pions as well as gammas from π^0 decay have been detected in the central part of WASA detector, which contains a mini drift chamber surrounded by thin superconducting magnet and the electromagnetic calorimeter. With the exception of neutrons the four-momenta of all emitted particles have been measured giving rise to 1-6 overconstraints for the subsequent kinematical fit.

1.2.1 $(\pi\pi)_{I=0} : pp \rightarrow pp\pi^0\pi^0$

In Fig. 1, left, the total reaction cross section is shown. It keeps rising from threshold up to $T_p \approx 1$ GeV, where the total cross section levels off and proceeds only slowly rising until 1.2 GeV. Thereafter it continues steeply rising. Whereas the low-energy region is due to the Roper resonance [26], the renewed rise at higher energies can be associated with the dominance of the $\Delta\Delta$ excitation. In Fig. 1, right, the $\pi^0\pi^0$ -invariant mass spectrum is shown for $T_p = 1.2$ GeV, the energy which is close to the maximum cross section in the $pn \rightarrow d\pi^0\pi^0$ reaction. In fact we also observe a slight low-mass enhancement, however, in our case it is well accounted for by

*Physikalisches Institut der Universität Tübingen, Germany

[†]skorodko@pit.physik.uni-tuebingen.de

the conventional calculations. The solid lines in Fig.1 show calculations based on the Valencia model [32], where Roper and $\Delta\Delta$ processes have been modified [29].

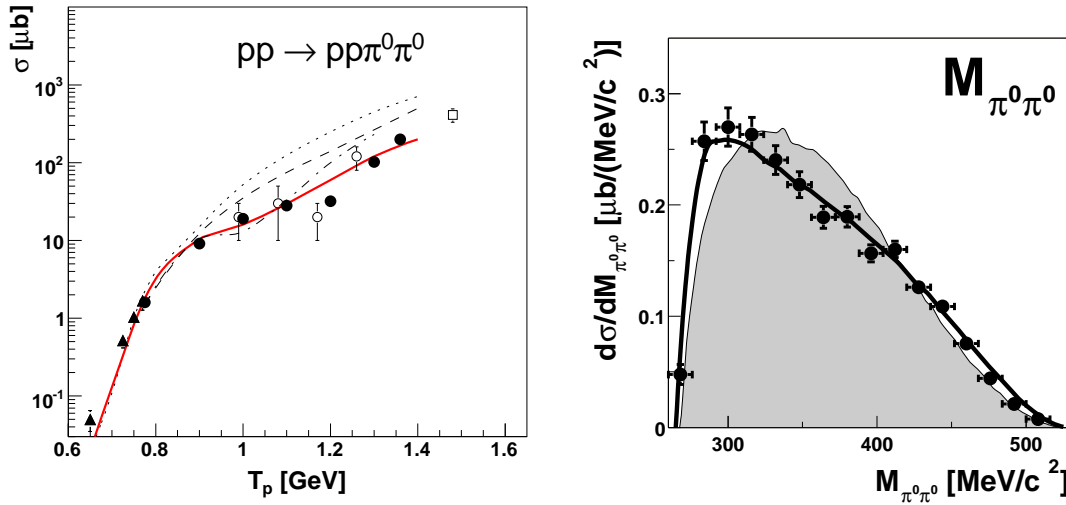


Figure 1.1: Energy dependence of the total cross section (left) and $\pi^0\pi^0$ -invariant mass spectrum at $T_p = 1.2$ GeV (right) of the $\pi^0\pi^0$ reaction. Solid lines show calculations with the modified Valencia model, see Ref. [29]

1.2.2 $(\pi\pi)_{I=1} : pp \rightarrow d\pi^+\pi^0$

In the $\pi^+\pi^0$ -invariant mass spectrum of this fusion reaction no ABC effect is observed [28]. Due to Bose symmetry the isovector $\pi^+\pi^0$ system must be in relative p-wave. Both differential distributions and the energy dependence of the total cross section are well described by the conventional $\Delta\Delta$ process. Note that the Roper process is strongly suppressed in this isovector $\pi\pi$ channel even at energies close to threshold.

1.2.3 $(\pi\pi)_{I=2} : pp \rightarrow nn\pi^+\pi^+$

This isotensor $\pi\pi$ channel is special, since single baryon excitations can only contribute, if they originate from the excitation of a higher-lying Δ state. Hence it was expected that the $\Delta\Delta$ process provides the main contributions to this channel. However, as demonstrated in Ref. [30], a large contribution has to come also from the excitation of a higher-lying Δ state, favorably the $\Delta(1600)$.

1.3 Conclusions

Summarizing we find all data for the two-pion production initiated by **isovector** pp collisions to be well accounted for by conventional t -channel processes involving single or double nucleon excitations. This includes also double-pionic fusion processes to d and quasi-bound ${}^2\text{He}$. This situation is fundamentally different from that in the two-pion production initiated by **isoscalar** NN collisions, where the ABC effect has been shown to be correlated with a narrow resonance-like structure in the total cross section.

1.4 Acknowledgments

We acknowledge valuable discussions with L. Alvarez-Ruso, C. Hanhart, E. Oset, A. Sibirtsev and C. Wilkin on this issue. This work has been supported by BMBF(06TU9193), Forschungszentrum Jülich (COSY-FFE) and DFG (Europ. Grad. School 683).

Bibliography

- [1] N. E. Booth, A. Abashian, K. M. Crowe, *Phys. Rev. Lett.* **7** (1961) 35; **6** (1960) 258; *Phys. Rev. C* **132** (1963) 2296ff.
- [2] I. Bar-Nir *et al.*, *Nucl. Phys.* **B 54** (1973) 17.
- [3] A. Abdivaliev *et al.*, *Sov. J. Nucl. Phys.* **29** (1979) 796.
- [4] R. J. Homer *et al.*, *Phys. Rev. Lett.* **9** (1964) 72.
- [5] J. H. Hall *et al.*, *Nucl. Phys.* **B 12** (1969) 573.
- [6] J. Banaigs *et al.*, *Nucl. Phys.* **B 67** (1973) 1.
- [7] J. Banaigs *et al.*, *Nucl. Phys.* **B 105** (1976) 52.
- [8] F. Plouin *et al.*, *Nucl. Phys.* **A 302** (1978) 413.
- [9] F. Plouin, P. Fleury, C. Wilkin, *Phys. Rev. Lett.* **65** (1990) 690.
- [10] R. Wurzinger *et al.*, *Phys. Lett.* **B 445** (1999) 423.
- [11] for a review see A. Codino and F. Plouin, *LNS/Ph/94-06*.
- [12] M. Bashkanov *et al.*, *Phys. Lett.* **B 637**, (2006) 223.
- [13] M. Bashkanov *et al.*, *Phys. Rev. Lett.* **102**, (2009) 052301.
- [14] S. Keleta *et al.*, *Nucl. Phys.* **A 825**, (2009) 71.
- [15] A. Pricking, PhD thesis, Univ. Tübingen 2011;
<http://tobias-lib.uni-tuebingen.de/volltexte/2011/5695/pdf/ThesisFinal.pdf>
- [16] E. Perez *et al.*, contribution to this workshop.
- [17] P. Adlarson *et al.*, *Phys. Rev. Lett.* **106**, (2011) 202302.
- [18] M. Bashkanov *et al.*, contribution to this workshop.
- [19] S. Dymov *et al.*, *Phys. Rev. Lett.* **102**, (2009) 192301.
- [20] J. Johanson *et al.*, *Nucl. Phys.* **A 712**, (2002) 75.
- [21] W. Brodowski *et al.*, *Phys. Rev. Lett.* **88**, (2002) 192301.
- [22] J. Pätzold *et al.*, *Phys. Rev. C* **67**, (2003) 052202.
- [23] S. Abd El-Bary *et al.*, *Eur. Phys. J.* **A 37**, (2008) 267.
- [24] S. Abd El-Samad *et al.*, *Eur. Phys. J.* **A 42**, (2009) 159.
- [25] P. Adlarson *et al.*, submitted for publication; arXiv:1107.0879
- [26] T. Skorodko, *et al.*, *Eur. Phys. J.* **A 35**, (2008) 317.
- [27] T. Skorodko, *et al.*, *Phys. Lett.* **B 679**, (2009) 30.
- [28] F. Kren *et al.*, *Phys. Lett.* **B 684**, (2010) 110 and *Phys. Lett.* **B 702** (2011) 312.
- [29] T. Skorodko *et al.*, *Phys. Lett.* **B 695**, (2011) 115.
- [30] T. Skorodko *et al.*, *Eur. Phys. J.* **A 47**, (2011) 108.
- [31] Ch. Bargholtz *et al.*, *Nucl. Instrum. Methods* **A 547**, (2005) 294.
- [32] L. Alvarez-Ruso, E. Oset, E. Hernandez, *Nucl. Phys.*, **A 633** (1998) 519.

OVERVIEW ON ONE AND DOUBLE PION PRODUCTION IN PP COLLISIONS IN HADES

*MALGORZATA GUMBERIDZE**
for the HADES Collaboration

1.1 Introduction

The High Acceptance Di-Electron Spectrometer (HADES) installed at GSI Helmholtzzentrum für Schwerionenforschung in Darmstadt was designed to investigate dielectron production in heavy-ion collisions in the 1-2 AGeV beam kinetic energy range. The main goal of the HADES experiment is to study the properties of hadrons inside the hot and dense nuclear medium via their dielectron decays [1, 2, 3].

One specific issue of heavy-ion reactions in that regime is the important role played by the baryonic resonances, which propagate and regenerate due to the long life-time of the dense hadronic matter phase. The $\Delta(1232)$ resonance is the most copiously produced but with increasing incident energy, higher lying resonances also contribute to pion production. A detailed description of the resonance excitation and coupling to the pseudoscalar and vector mesons is important for the interpretation of the dilepton spectra measured by HADES. Baryonic resonances are indeed important sources of dileptons through two mechanisms: their Dalitz decays (e.g. $\Delta/N^* \rightarrow Ne^+e^-$) and the mesonic decay with subsequent dielectron production.

Simultaneous measurement of one and two-pion production channels can bring information on the baryonic resonances excitation. Two-pion production, in particular, is an important subject since it connects $\pi\pi$ dynamics with baryon and baryon-baryon degrees of freedom. In our energy regime, $\Delta\Delta$ excitation is the leading process [8, 9]. We report on one- and two-pion production in pp and np reactions investigated with HADES in exclusive measurements for the beam kinetic energies 1.25 and 2.2 GeV.

1.2 HADES experiment

The HADES detector [4], as shown in Fig. 1.1, consists of 6 identical sectors covering the full azimuthal range and polar angles from 15° to 85° with respect to the beam direction. Each sector contains: A Ring Imaging CHerenkov (RICH) detector used for electron identification; two sets of Mini-Drift Chambers (MDC) with 4 modules per sector placed in front and behind the magnetic field to determine momenta of charged particles; the Time Of Flight detectors (TOF/TOFINO) and the Pre-Shower detector improving the electron identification. For reaction time measurement in heavy-ion reactions, a diamond START detector is located in front of the target. An (e^+, e^-) invariant mass resolution at the ω peak of $\simeq 2.7\%$ and a momentum resolution for protons of $\simeq 3\%$ can be achieved. The first level trigger is obtained by a fast multiplicity signal coming from the TOF/TOFINO wall, combined with a signal from the START detector, while the second level trigger is made by using the informations from the RICH and Pre-Shower to select the lepton candidates.

In the pp experiment at 1.25 and 2.2 GeV kinetic energy, the intensity was about 10^7 particles/second, and a target filled with liquid hydrogen was used. The START detector was not used in this run because of the too high rate of secondaries produced by the START detector itself. Thus a specific algorithm has been developed to calculate the time of flight and then to identify the charged particles.

*IPN Orsay, sudol@ipno.in2p3.fr

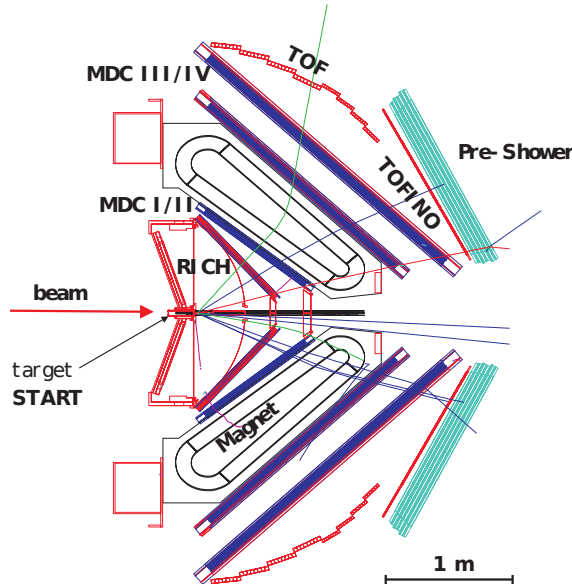


Figure 1.1: (Color online) Schematic view of the HADES detector as implemented in the simulation. Simulated particle tracks are shown as well.

1.3 Results

As mentioned in the introduction, it is important to constrain the models predicting the cross section and the production mechanisms of the Δ resonance. In order to do that the hadronic channels ($pp \rightarrow np\pi^+$ and $pp \rightarrow pp\pi^0$) have been measured and studied in parallel to the leptonic channels.

The $pp \rightarrow np\pi^+$ channel is studied using the reconstruction of the undetected neutron. The reaction was selected first by the charged particle identification based on momentum and reconstructed time of flight, then a (p, π^+) missing mass cut was imposed around the neutron mass. This cut efficiently suppresses the background coming from misidentified protons and two- π contributions.

The $pp\pi^0$ reaction was extracted from the (p, p) missing mass spectrum by subtracting the background under the π^0 peak after suppression of the pp elastic and two-pion contribution.

The absolute normalization of the data has been achieved by a simultaneous measurement of elastic scattering for which the cross section is known. Error bars include statistical and systematic errors.

Experimental data have been compared with the original and modified version of the resonant model [5] using model A and model B (for details see Table 1.1). A comparison to different spectra has been made. In particular the neutron angular distribution in the center of mass system measured in the $pp \rightarrow pn\pi^+$ channel, has been investigated, since it is sensitive to the angular distribution of Δ resonance production (dominant process is $pp \rightarrow n\Delta^{++}$). The acceptance corrected experimental spectra are presented in Fig. 1.2 (black points) together with slightly modify resonance model "model A" (for details of the modification, see Tab. 1.1). The distribution shows strong forward/backward peaking, as expected due to the peripheral character of the Δ resonance. The original Teis model (black solid line) shows underestimation at $\cos\theta_n \approx 0$, which is improved by changing cut-off parameter (Λ_π) (black dashed line). In addition in Fig. 1.2 comparison between HADES and WASA measurement is presented. WASA data were taken from [7] and normalized to the cross-section obtained by HADES. One can see reasonable quantitative agreement, keeping in mind, that the WASA data are presented without systematic errors.

Fig. 1.3 exhibits the projection on the (p, π^0) (Left), (p, π^+) (Middle) and (n, π^+) (Right) invariant masses for $T_p = 1.25$ and 2.2 GeV. The data are corrected for reconstruction efficiencies.

The prominent peak of $M_{inv}(p, \pi^+)$ and $M_{inv}(p, \pi^0)$ around 1.23 GeV/ c^2 confirms that most of the pions are produced via Δ decay, which is consistent with the resonance model. However, the data present some deviations with respect to the model A, which is close to the original Teis's model ([5]). This, together with the above mentioned failure in the description of the angular distribution motivates some changes in the model. A better description of the yield and shape

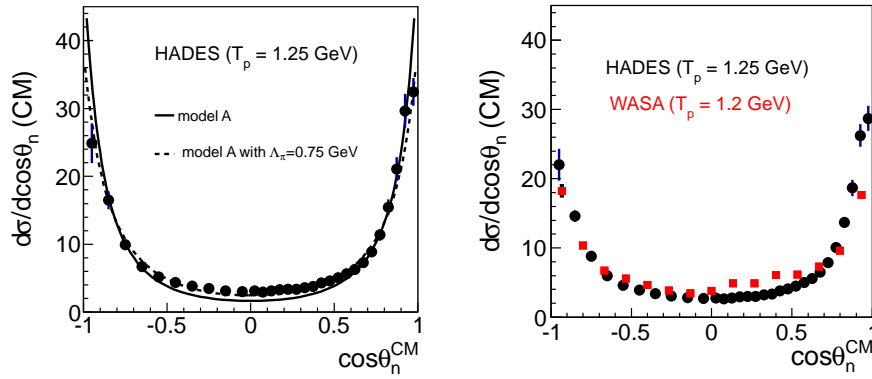


Figure 1.2: Angular distribution of neutron in centre of mass system after acceptance correction for the $pp \rightarrow pn\pi^+$ reaction. (Left) Comparison of the HADES data to simulation based on [5] and model A. Both simulation curves are normalized to reproduce the integrated experimental yield. (Right) Comparison of HADES and WASA data [7].

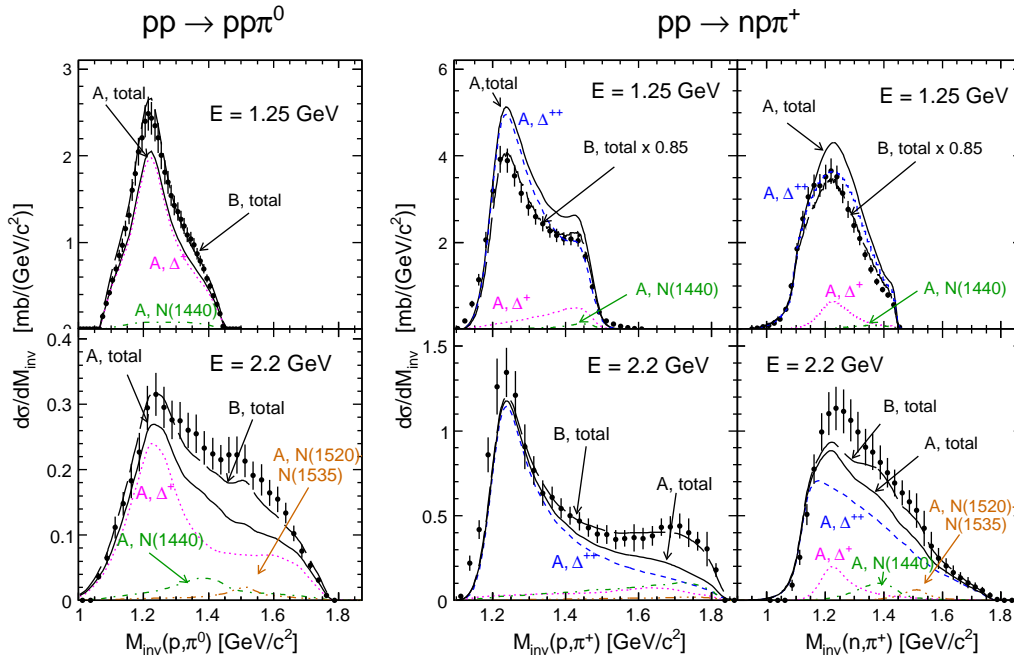


Figure 1.3: (Color online) Invariant mass distributions measured of (p, π^0) (Left), (p, π^+) (Middle) and (n, π^+) (Right) measured in $pp \rightarrow pp\pi^0$ and $pp \rightarrow np\pi^+$ at 1.25 GeV (top row) and 2.2 GeV (bottom row). HADES data (full dots) are compared within the experimental acceptance to the predictions of the modified resonance model (see text).

of the missing mass spectra is indeed obtained after some modifications which are included in the model B (see Tab. 1.1 for details). Due to the dominance of the Delta(1232) resonance, the two channels are correlated by isospin symmetry: $\sigma(pp \rightarrow n\Delta^{++}) \sim 3(pp \rightarrow p\Delta^+)$, leading to $\sigma(pp \rightarrow np\pi^+) \sim 5(pp \rightarrow pp\pi^0)$. N^* contribution seems also reasonable and the invariant mass distributions are rather well reproduced by the $pp \rightarrow n\Delta^{++}$ and $pp \rightarrow p\Delta^+$ simulations. At 2.2 GeV, the contribution of higher lying resonances is clearly visible at high invariant masses.

Furthermore, as another important platform for studying resonances properties, double-pion production in nucleon-nucleon collisions is also of interest. Preliminary results obtained for the analysis of 2 channels: (1) $pp \rightarrow pp\pi^+\pi^-$ and (2) $pn \rightarrow pn\pi^+\pi^-$ have been presented in comparison to model predictions [5, 6] including double- Δ and $N(1440)$ excitation. Both channels were selected by identifying all charged hadrons involved in the reaction and applying a missing mass cut

T_p /Model	Model A	Model B
1.25 [GeV]	[5], (1)	Model A, (2)
2.2 [GeV]	[5], (1)	Model A, (3)

Table 1.1: Summary of the modifications introduced to the resonance model [5] in order to better fit the data: (1) pp and pn final state interactions have been implemented using the Jost function and adjustment of the cut-off parameter (Λ_π) entering the $\pi N\Delta$ and πNN vertex form factor has been changed from 0.63 to 0.75 GeV, (2) the Δ production angular distribution has been further adjusted to reproduce the measured neutron angular distribution, (3) the cross section of the higher lying resonances has been increased and a non-resonant contribution has been added.

($M_{pp\pi^+\pi^-}$ in case (1) and $M_{p\pi^+\pi^-}$ in case of (2)). It turns out that the invariant mass ($M_{\pi^+\pi^-}$) and the opening angle in CM ($\cos\delta_{\pi^+\pi^-}$) of the pion pair are the most sensitive distributions to the different model contributions. Fig. 1.4 exhibits an experimental distributions of the invariant mass and opening angle of $\pi^+\pi^-$ in comparison to the pure phase space (PHPS) calculations. The PHPS calculations has been normalized to the experimental yield. It is seen, that both experimental distributions deviate from PHPS calculations. Some enhancement can be observed at low $\pi^+\pi^-$ invariant masses, which is not present in the simulation with the PHPS only. This peak at small invariant masses appears in the models [8, 9] as being due to the $\Delta\Delta$ excitation and to the decay channel of the Roper resonance $N(1440)$ into $N\Delta$ ($N^* \rightarrow N\Delta$).

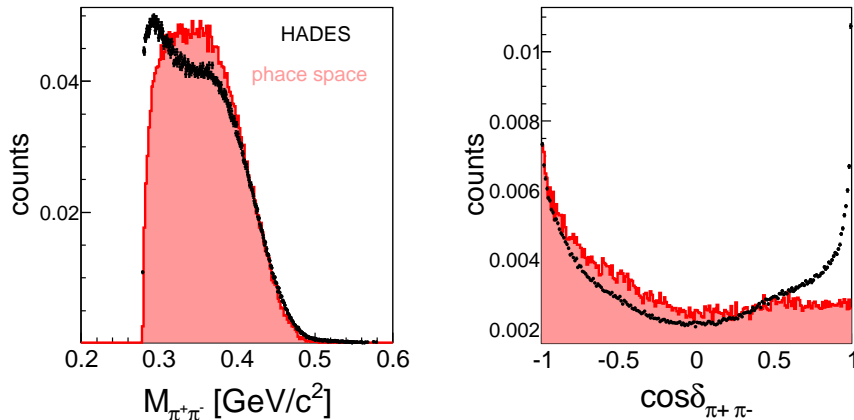


Figure 1.4: Distribution of the $\pi^+\pi^-$ invariant mass $M_{\pi^+\pi^-}$ (left) and the $\pi^+\pi^-$ opening angle in centre of mass $\delta_{\pi^+\pi^-}$ (right) for $pp \rightarrow pp\pi^+\pi^-$ reaction at beam energy $T_{kin} = 1.25$ GeV are shown in comparison to the phase space calculation. Both spectra are inside HADES acceptance and efficiency. The simulation is normalized to reproduce the measured experimental yield. Only statistical errors are shown.

1.3.1 Conclusion

The aim of measuring one and two-pion production in elementary reactions with HADES are three fold: (1) to study the detector response, and cross-check the analysis of dilepton channels, (2) test the ingredients of the transport models used for the dielectron production, which are based on resonance models and (3) to obtain a parametrization of meson and baryon resonance production for dielectron channels analysis.

HADES provides high statistics data in one and two-pion production channels, which complements measurements of previous experiments. For the one pion channel, which is dominated by Δ resonance, the data have been compared to the resonance model usually used in transport models, and modifications have been proposed to better reproduce the data. The ongoing analysis of the two-pion production and comparison to the models will bring constrain on double- Δ production as well as $N(1440)$ production and decay mechanism.

Bibliography

- [1] G. Agakishiev et al, *Phys. Rev. Lett.*, **98**, 052302, (2007).
- [2] G. Agakishiev et al, *Phys. Lett. B* , **663**, 43, (2008).
- [3] G. Agakishiev et al, *Phys. Rev. B*, **690**, 118-122, (2010).
- [4] G. Agakishiev et al, *Eur. Phys. J. A.* **41**, 243, (2009).
- [5] S. Teis et al, *Z. Phys. A.* **356**, 421, (1997).
- [6] V. Dmitriev et al, *Nucl. Phys. A.* **459**, 503, (1986).
- [7] T. Skorodko PhD thesis, "Production of $\pi^0\pi^0$ and $\pi^+\pi^-$ Pairs in Proton-Proton Collisions", Eberhard-Karls-Universität Tübingen, Germany
- [8] L. Alvarez-Ruso, E. Oset, E. Hernandez *Phys. Rev. B*, **633**, 519, (1998).
- [9] Xu Cao et al, *Eur. Phys. J.*, **A. 41**, 243, (2010).
- [10] A. I. Titov et al, *Eur. Phys. J.*, **A. 7**, 543, (2000).

EXCLUSIVE CHANNELS IN PP @ 3.5 GeV

ADRIAN DYBCZAK*
for the HADES Collaboration

1.1 Introduction

The High Acceptance Di-Electron Spectrometer (HADES) [1] operates at the GSI Helmholtzzentrum für Schwerionenforschung in Darmstadt, Germany. One of the main physics goals of HADES is to investigate spectral modifications of light vector mesons in strongly interacting matter via dilepton (e^+e^-) decay channel. The HADES collaboration has set up an experimental program to measure dilepton spectra in p+p and p+n collisions [2]. In year 2007 electron-positron pair production has been measured in elementary collisions of two protons with 3.5 GeV projectile kinetic energy. One of basic observables in this measurement is inclusive e^+e^- mass distribution, shown in Fig. 1a after Combinatorial Background (CB) subtraction. The expected e^+e^- production channels are given by Dalitz decays of π^0 , η , ω mesons and $\Delta(1232)$ resonance. In the high mass region 2-body decays of ρ/ω play a role. Indeed, the experimental data can be described by PLUTO [3] simulation (see Fig. 1a) assuming aforementioned components, but not in the mass region below vector meson pole ($M_{inv}^{e^+e^-} \in (0.5 - 0.7)$). However, only Dalitz decay channel for baryonic resonances is included for $\Delta(1232)$ here.

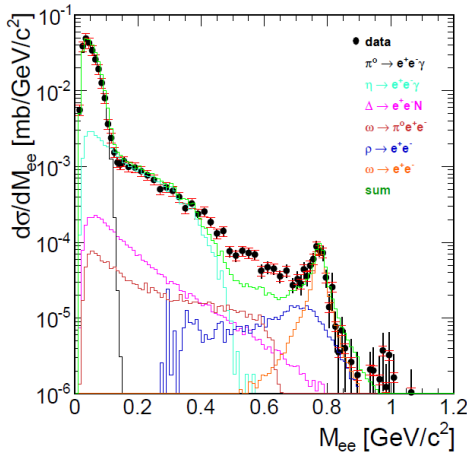


Fig. 1a) Efficiency corrected inclusive invariant mass distribution of dielectrons inside the geometrical acceptance of HADES. e^+e^- - signal pairs (black dots), after combinatorial background subtraction for p(3.5GeV)+p collisions with corresponding simulation cocktail components. The data are normalized to the measured p+p elastic events.

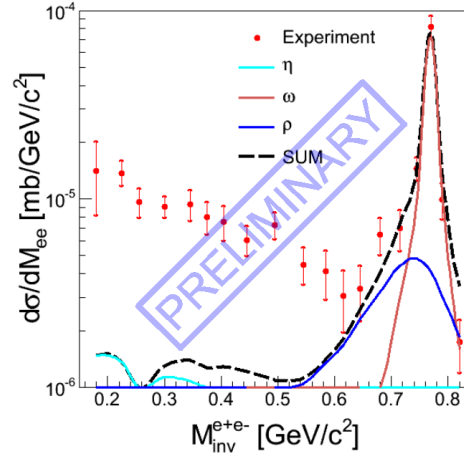


Fig. 1b) Efficiency corrected invariant mass distribution of dielectrons for exclusive ppe^+e^- channel inside the geometrical acceptance of HADES after combinatorial background subtraction. The data are normalized to p+p elastic events and compared to simulation cocktail assuming sources given in the legend.

In order to study contribution of higher lying baryonic resonances ppe^+e^- , $pp\pi^0$, $pn\pi^+$, $pp\omega(\eta) \rightarrow \pi^+\pi^-\pi^0$ exclusive channels have been analysed. The $ppe + e^-$ channel has been selected by condition on pe^+e^- missing mass ~ 0.938 [MeV/c^2] and the respective e^+e^- invariant mass spectrum is shown in Fig. 1b. The mass region below vector meson pole is not described by channels including ω , η decays which are constrained by hadronic channels mentioned above (see [7]). This means that Dalitz decays of baryon resonances must contribute in this area. In order to estimate production cross sections of the resonances which decay in the $pn\pi^+$ and $pp\pi^0$ final states, the results have been compared to Monte-Carlo calculations based on the resonance model [4] assuming incoherent sum of various resonances.

*Jagiellonian University, Cracow; adybczak@gmail.com

To convert resonances cross sections into e^+e^- yield one should remember that the respective partial decay widths are mass dependent. Two models of $\Gamma_{R \rightarrow pe^+e^-}(M)$ of ([5], [6]) are applied in the simulation.

1.2 Analysis of $pn\pi^+$, $pp\pi^0$ final states

In both final states only events with two positive tracks were selected. Protons and positive pions were distinguished using measured momentum and particle velocity of reconstructed tracks. Channels were selected via condition on missing mass of neutral particles (n and π^0 , respectively). Signal was obtained as a number of counts above fitted continuous background. In the case of $pp\pi^0$ discrimination on elastic scattering and multipion production was required additionally to enhance purity of the signal. Resonances cross section were estimated by simultaneous fit of invariant masses ($M_{inv}^{p\pi^+}$, $M_{inv}^{n\pi^+}$, $M_{inv}^{p\pi^0}$) and angular distributions ($\cos\theta_{CM}^{p\pi^+}$, $\cos\theta_{CM}^{n\pi^+}$, $\cos\theta_{CM}^{p\pi^0}$) in several bins of the $N - \pi$ invariant mass. Iterative procedure was applied: In the first step a flat angular distribution has been assumed for resonances production. Since experimental distributions show a clear forward-backward peaking, in the next step a modified distribution of the form $d\sigma/dt \sim A/t^\alpha$ has been used. The t , A , α are t-Mandelstam variable and fit parameters depending on resonance mass, respectively. Furthermore, the isospin relations between cross sections of various resonance have been preserved.

1.2.1 Acceptance corrected $pn\pi^+$, $pp(\pi^0)$ results

In Fig. 2a, the results obtained after acceptance/efficiency corrections assuming aforementioned model are presented. The $pn\pi^+$ channel allows to distinguish doubly and singly charged resonances.

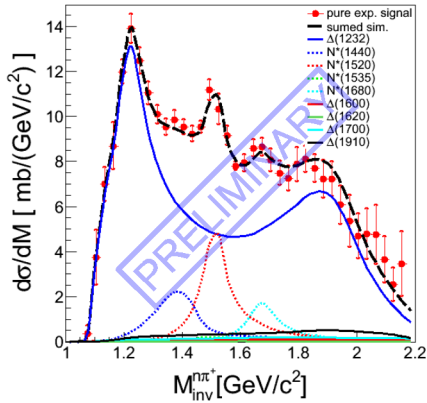


Fig. 2a) Acceptance and efficiency corrected spectra of $p\pi^+$, $n\pi^+$ invariant mass with corresponding simulation components.

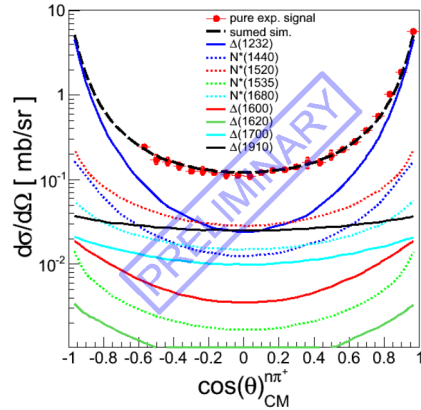


Fig. 2b) Acceptance and efficiency corrected spectra of $p\pi^+$, $n\pi^+$ angular distribution in the center of mass of with corresponding components obtained from fitting procedure described in the text.

1.3 Conclusions and outlook

The applied resonance model of baryon resonance production can fully describe production of pions in the two $pp\pi^0$ and $pn\pi^+$ channels. Obtained cross sections for the various resonances fulfill all isospin relations. The derived cross section for the $\Delta(1232)$ production is in a good agreement with observations of other experiments. Estimated cross sections for the total π^0 and π^+ yields are also in a good agreement with previous measurements. The obtained cross sections for resonance production will be further used to calculate dielectron production in the ppe^+e^- channel.

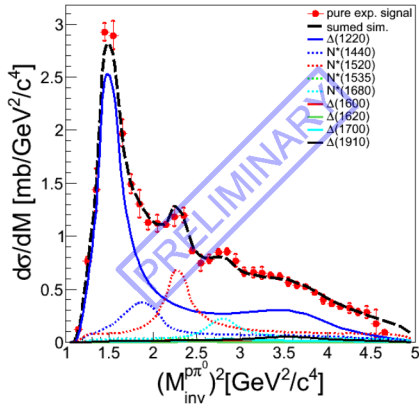


Fig. 3a) Acceptance and efficiency corrected spectra of $p\pi^0$ invariant mass with corresponding simulation components.

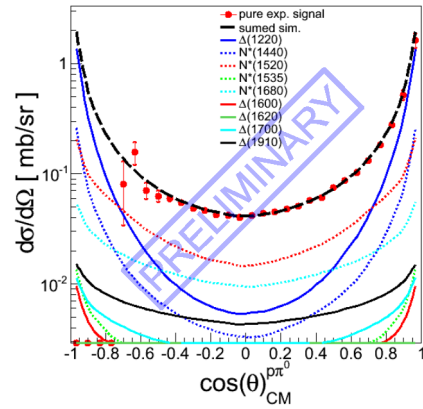


Fig. 3b) Acceptance and efficiency corrected spectra of $p\pi^0$ angular distribution in the centrum of mass of resonance with corresponding simulation components.

Bibliography

- [1] G. Agakichiev et al. , *Eur. Phys. J. A*, **41**, 243, (2009).
- [2] P. Salabura, contribution to this conference.
- [3] I. Froehlich, contribution to this conference.
- [4] S. Teis et al. , *Z. Phys. A*, **356**, 421-435, (1997).
- [5] M. Zetenyi and G. Wolf, *Heavy Ion Phys.*, **17**, 27-39, (2003).
- [6] M.I. Krivoruchenko and B.V. Martemyanov., *Annals Phys.*, **296**, 299-346, (2002).
- [7] K. Theilab, *nt.J.Mod.Phys.*, **A26**, 694-696, (2011).

OVERVIEW OF e^+e^- PRODUCTION IN $p + p$ AND $p + n$ COLLISIONS

PIOTR SALABURA*
for the HADES Collaboration

1.1 Introduction

The High Acceptance Dielectron Spectrometer (HADES) is a second-generation experimental setup located at the heavy-ion synchrotron SIS18/GSI Darmstadt. Its powerful particle identification capabilities and excellent momentum resolution allows for simultaneous measurements of hadronic (p , π^\pm , K^\pm) and electromagnetic (e^+e^-) final states over a wide angular range ($18^\circ < \theta < 85^\circ$) in proton, deuteron and HI induced reactions [1]. One of the main goals of the HADES experiments is to achieve a detailed understanding of dielectron emission from hadronic systems at moderate (1 – 4 AGeV) bombarding energies. A particular feature of this energy domain is the important role of baryonic sources as $N + N$ bremsstrahlung and resonance Dalitz decays (i.e $\Delta(N^*) \rightarrow Ne^+e^-$) which are poorly known. The results obtained on electron pair production in elementary $N + N$ collisions represent a doorway for the understanding of pair production in HI collisions where additional in-medium effects, as for example hadron mass modifications, are expected to occur [2, 3, 4]. In order to shed more light on the aforementioned processes, HADES performs a combined study of pion and dielectron production in $p + p$ and $d + p$ reactions. The results from pion production are given in the contributions of M. Gumberidze [5] and A. Dybczak [6]. In this report, a survey on important results on e^+e^- pair production is given.

1.2 e^+e^- results from $p + p$ and quasi-free $p + n$ collisions

Results from the pioneering DLS experiment at Bevelac on inclusive e^+e^- production in $p + p$ and $p + d$ reactions indicate a strong isospin dependence of the pair production in the 1 – 4 AGeV region [7]. The cross section ratio of pair production is significantly larger than 2 which was observed at $E_{kin} \geq 2$ GeV and could only be qualitatively described by model calculations.

Fig. 1 shows inclusive e^+e^- invariant mass distributions measured in $p + p$ (left-top) and quasi-free $p + n$ (left-bottom) collisions at 1.25 GeV [8] inside the HADES acceptance. Quasi-free $n + p$ reactions were selected from $d + p \rightarrow e^+e^- + X$ reaction on trigger level by the detection of a fast spectator protons from the deuterium break-up in a dedicated forward hodoscope wall at small angles w.r.t. beam direction. As one can see, a large (at least one order of magnitude) excess of the pair yield is visible for the $p + n$ reaction channel at higher invariant masses. The data are compared to simulated pair distributions calculated with the Pluto event generator [9] assuming a dominant role of the $\pi^0 \rightarrow e^+e^- + \gamma$ and $\Delta(1232) \rightarrow e^+e^- + N$ Dalitz decays. For both reaction channels the measured yield in the π^0 Dalitz decay region is very well reproduced taking into account the inclusive π^0 production cross section from the resonance model assuming $\Delta(1232)$ dominance [8]. This assumption is also corroborated directly by the HADES measurements of the dominant exclusive channels $pp \rightarrow pp\pi^0$ and $pp \rightarrow pn\pi^+$ (see [5]). To model $\Delta(1232)^{+(0)} \rightarrow p(n)e^+e^-$ the differential partial decay width $d\Gamma_{Ne+e-}(M_\Delta)/dM_{e+e}$ from [10] has been utilized, assuming a constant magnetic transition form factor $G_M = 3.02 \pm 0.03$ fixed by photo-production experiments (the other two form factors, electric and Coulomb, are assumed to be zero) [8]. A possible modification of the magnetic transition form factor due to intermediate vector mesons was simulated assuming the two-component quark model [11] and is visualized by the shaded area. As expected, it leads to a slightly enhanced yield for high pair masses. Whereas the $p + p$ spectrum is very well described by both contributions, the description of the $p + n$ channel is not satisfactory even if the $\eta \rightarrow e^+e^- + \gamma$ decay is included. The latter one is fixed by precise data from WASA at CELSIUS on near threshold production in $pn \rightarrow d\eta$ and $pn \rightarrow pn\eta$ [12].

*M. Smoluchowski Institute of Physics

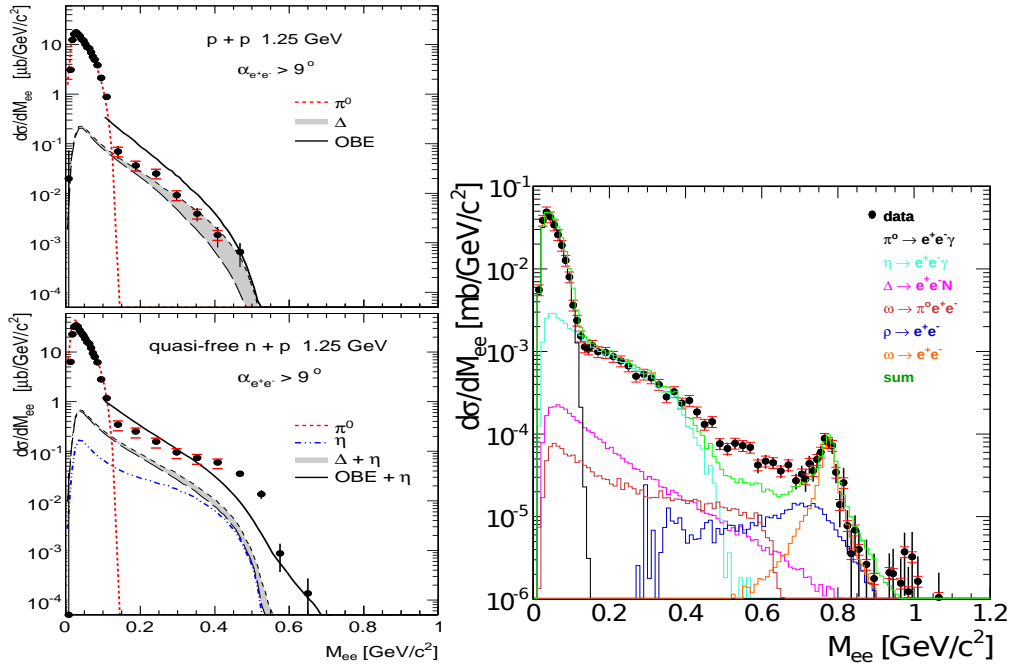


Figure 1.1: Differential cross sections for dielectron production as a function of the invariant mass as measured in $p + p$, quasi-free $p + n$ reactions at 1.25 GeV (left) and $p + p$ at 3.5 GeV (right). The distributions are compared to model calculations assuming various hadronic sources (for more details see the text).

Next, the obtained results are compared to predictions of the OBE model [13], where resonant (Δ) and non-resonant ("quasi-free" $N + N$ bremsstrahlung) contributions are added coherently. The result of the simulation is shown in Fig. 1 as solid black line. The yield calculated in this approach overestimates (underestimates) measured distribution in the $p + p$ ($p + n$) reactions. One should add here that more recent calculations of [14] based on similar effective Lagrangian are successful in description of the $p + p$ reaction channel and also come closer to the data measure in the $p + n$ reaction channel. For the latter case, the implementation of the pion electromagnetic form factor in graphs including exchange of charged pions turns out to be decisively to produce e^+e^- yield enhancement visible in the $p + n$ reaction channel at higher masses.

The right part of Fig. 1 shows the e^+e^- invariant mass distributions measured in $p + p$ collisions at 3.5 GeV [15]. In contrast to lower energy, the spectrum extends to much higher masses due to the rapidly changing excitation function of dielectron production. A clear ω peak with mass resolution $\Delta M/M \sim 2\%$ can be seen in e^+e^- channel, for the first time at such low energy. Below the vector meson mass region dielectron production is dominated by the η and π^0 Dalitz decays. The comparison of the experimentally measured invariant mass distribution to an incoherent sum of known hadronic sources is also shown in this figure. Calculations have been performed with PYTHIA + PLUTO codes [16, 15]. The simulated cocktail describes the data reasonably well except for the mass range around 0.55 GeV/ c^2 where the yield is underestimated. The latter deviation is not too surprising since in this energy region contribution from the resonances (in our calculations only from $\Delta(1232)$) can be expected. Furthermore, the virtuality of the photon reaches quite high values and one can expect shape modifications due to unknown mass dependency of the $\Delta(1232)$ transition form factor. Moreover, contributions of higher lying (Δ, N^*) resonances has not been included, yet. The respective contributions can be better constrained by means of the exclusive dielectron and hadronic channels: $pp e^+e^-$, $pp\pi^0$, $pn\pi^+$, $pp\eta$ and $pp\omega$ inside the HADES acceptance. The strategy is to fix the cross sections for resonance ($\Delta, N^{*(+,0)}$) production from the hadronic final states and convert it to $pp e^+e^-$ yields by means of $d\Gamma_{N e^+e^-}(M_{res})/dM_{e^+e^-}$ given by available calculations [17, 18]. Many of these hadronic channels have already been analyzed. The channels with pion production is discussed in the contribution of A. Dybczak [6].

1.3 Summary and outlook

HADES measured dielectron production in proton, deuteron and HI induced reactions in the 1 – 4 AGeV energy region. Dielectron production in $N + N$ collisions is a mandatory prerequisite for the understanding of pair production in HI collisions and already observed in-medium effects. The interesting feature of the pair production in low-energy domain is the important role of baryonic e^+e^- sources, i.e. resonance Dalitz decays and $N + N$ bremsstrahlung. The description of the respective pair production process is directly linked to the questions of how the virtual massive photon couples to baryons and how do the respective transition form factors look like. The results already obtained by HADES in $p+p$ (1.25, 2.2, 3.5 GeV) and $p+n$ (1.25 GeV) indicate a sensitivity to such effects. Further measurements are however mandatory to pin down respective effects. In this context, future experiments with pion beams planned with HADES at GSI can be extremely helpful. In contrast to proton induced reactions, resonances can be directly excited in the s channel and separated by means of excitation function and angular measurements [19].

Bibliography

- [1] G. Agakichiev et al. (HADES Collab.), Eur. Phys. J. A 41, 243 (2009).
- [2] G. Agakichiev et al. (HADES Collab.), Phys. Rev. Lett. 98, 052302 (2007).
- [3] G. Agakichiev et al. (HADES Collab.), Phys. Lett. B 663, 43 (2008).
- [4] G. Agakichiev et al. (HADES Collab.), Phys.Rev. C84, 014902 (2011).
- [5] M.Gumberidze, contribution to this conference
- [6] A.Dyczak, contribution to this conference
- [7] W.K. Wilson et al. (DLS Collab.), Phys. Rev. C 57 1865 (1998).
- [8] G. Agakichiev et al. (HADES Collab.), Phys. Lett. B 690, 118 (2010).
- [9] I. Froehlich et al., Eur. Phys. J. A 45, 401 (2010).
- [10] M.I. Krivoruchenko and A. Faessler, Phys. Rev. D 65, 017502 (2001).
- [11] Q. Wan and F. Iachello, Int. J. Mod. Phys. A 20, 1846 (2005).
- [12] H. Calen et al., Phys. Rev. C 58, 2667 (1998)
- [13] L. P. Kaptari and B. Kampfer, Nucl. Phys. A 764, 338 (2006);
L. P. Kaptari and B. Kampfer, Phys. Rev. C 80, 064003 (2009).
- [14] R. Shyam, U. Mosel, Phys. Rev. C 82, 062201 (2010)
- [15] A. Rustamov et al. (HADES Collab.), AIP Conf. Proc. 1257, 736 (2010)
- [16] J. Weil et al., XLIX Int. Winter Meeting on Nucl. Phys., BORMIO, Italy, 380 (2011).
- [17] M. Zetenyi and Gy. Wolf, Phys. Rev. C 67, 044002 (2003)
- [18] M. I. Krivoruchenko et al., Ann. Phys. 296, 299 (2002).
- [19] H. Kuc, contribution to this conference

HADES SPECTROMETER AND FUTURE EXPERIMENTS WITH PION BEAMS

HUBERT KUC†*
for the HADES Collaboration

1.1 Introduction

The HADES [1] (Acceptance Dielectron Spectrometer) collaboration demonstrated, using pp and quasifree pn reactions [3] that baryonic resonances play an important role in dielectron emission at SIS accelerator energies (1-2 AGeV). This is first due to their mesonic decays and the subsequent direct dilepton (e.g. $\rho/\omega \rightarrow e^+e^-$) or Dalitz (also called conversion) decay ($\pi^0/\eta \rightarrow \gamma e^+e^-$ or $\omega \rightarrow \pi^0 e^+e^-$) modes of these mesons. Baryonic resonances are also expected to contribute directly to dilepton emission via their Dalitz decay modes ($N^*/\Delta \rightarrow Ne^+e^-$). (see Piotr Salabura's talk for more details)

The Dalitz decay of baryonic resonances can be studied in a more precise way using the GSI pion beam. In $\pi^- + p$ reactions, the production mechanisms are better controlled and all resonances are produced at fixed mass, in the s channel. In addition to electromagnetic channels, meson production channels ($\pi N \rightarrow \pi\pi N$, $\pi N \rightarrow \eta N$, $\pi N \rightarrow \rho/\omega N$, $\pi N \rightarrow K\Lambda$...) can also bring useful information to study resonance properties, via partial wave analysis (PWA). There is indeed a big interest from theoreticians, for new precise differential cross section data for various reaction channels and at various incident momenta.

These experiments present some technical challenges. This secondary pion beam is produced on a beryllium targets in C+Be or p+Be reactions. To achieve pion beam intensities of the order of $10^6/s$, primary carbon or proton beams need to reach an intensity close to space charge limit of the accelerator. To produce pions with momentum from 0.7 to 1.5 GeV/c, the reaction C+Be@2.0GeV should be chosen but to produce pions with momenta from 1.5 to 2.2 GeV/c with sufficient intensity, p+Be@3.5GeV has to be used. The acceptance of the beam line is $\Delta p/p \approx \pm 4\%$. For exclusive studies momentum reconstruction is needed. Furthermore, the background due to secondary particles produced by the beam halo has to be suppressed. Therefore, an additional event by event pion in-beam tracking is required. This task is handled by two in-beam silicon detectors X1,X2. Trackers are two double sided, 2x128 strip, 300 μ m thick silicon detectors manufactured in high radiation hard technology. This system provides a momentum resolution of $\Delta p/p \sim 0.1\%$ which is sufficient for exclusive analysis studies. A diamond detector placed in front of the target complements the beam tracking and will be used as start detector.

1.2 Results

The poster shows simulations and feasibility studies for future experiments with the pion beams. First the total cross section to produce baryon resonances up to $\Delta^0(1950)$ [4] were calculated. Next step consisted in Dalitz decay simulations of the baryonic resonances, where two electromagnetic decay models of baryons were compared. The first one where they are treated as point like [5] and the other one using the eVMD (extended Vector Meson Dominance) model for the electromagnetic form factors [6]. In addition, the production and decay of ρ, ω and η mesons is included in the simulations. Finally, the HADES spectrometer acceptance for dilepton pairs was determined. This allowed to produce inclusive invariant mass spectra inside HADES acceptance and estimate count rate per one week of experiment at two different energies (fig. 1 right).

A second type of simulations was devoted to two pion production in $\pi^- + p$ reactions. Like in the case of dilepton analysis, cross sections and branching ratios were determined for bench mark

*Jagiellonian University Cracow, Poland

†IPN Orsay, France; hubertkuc@gmail.com

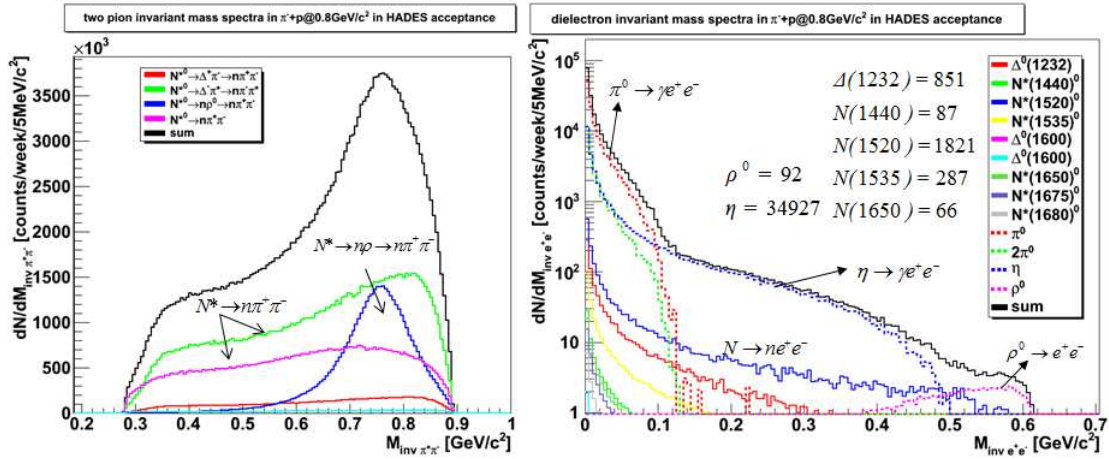


Figure 1.1: **Left:** Invariant mass spectra of $\pi^+\pi^-$ pairs from simulations of $\pi^- + p \rightarrow n\pi^+\pi^-$ reactions at 0.8 GeV/c and estimated count rates per 1 week of experiment. **Right:** Inclusive invariant mass spectra of e^+e^- pairs from simulations of $\pi^- + p$ reactions at 0.8 GeV/c and estimated count rates per 1 week of experiment.

channels. Next the HADES acceptance for $\pi^+\pi^-$ pairs and the inclusive $\pi^+\pi^-$ invariant mass spectra with estimated count rate per one week of experiment have been presented.

1.3 Perspectives

Pion beams at GSI are available for many years and used by other groups (e.g. FOPI coll.). After the heavy ion campaign scheduled for nearest future, the HADES collaboration is preparing a physics program for experiments with pion beams. The simulations will be further developed by including Dalitz decay of higher lying resonances and by studying exclusive channel analysis like $\pi^-p \rightarrow ne^+e^-$, $\pi^-p \rightarrow n\pi^+\pi^-$, $\pi^-p \rightarrow n\eta$. The aim is to define in detail the physics case and beam momenta for these future experiments.

Bibliography

- [1] G. Agakichiev et al.(HADES Collaboration), *Eur. Phys. J.*, **A41**, 243, (2009).
- [2] S. Leupold et al, *Int. J. Mod. Phys.*, **E19**, 147, (2010).
- [3] G. Agakichiev et al.(HADES Collaboration), *Phys.Lett*, **B690**, 118-122, (2010).
- [4] S. Teis et al., *Z. Phys. A*, **356**, 421435, (1997).
- [5] M. Zetenyi et at., *arXiv:nucl-th/0202047v1*, (2002).
- [6] M. I. Krivoruchenko et al., *Annals of Physics*, **296**, 299346, (2002).

TWO-PHOTON PHYSICS AT KLOE/KLOE-2

IVAN PRADO LONGHI*
for the KLOE/KLOE-2 Collaboration

1.1 Introduction

A data sample of integrated luminosity $\mathcal{L} = 242.5 \text{ pb}^{-1}$ collected at $\sqrt{s} = 1 \text{ GeV}$ with the KLOE detector at the DAΦNE ϕ -factory has been analyzed in order to study the $e^+e^- \rightarrow e^+e^-X$ reactions, X being the η meson or the $\pi^0\pi^0$ state produced in the scattering of two quasi-real photons. The measurement is done with final state e^\pm going along the beam pipe and escaping detection. In this case the virtual photons are quasi-real and the overall cross section can be factorized as the $\gamma\gamma$ subprocess cross section times a $\gamma\gamma$ luminosity function, $\sigma_{e^+e^- \rightarrow e^+e^-X} = \int \sigma_{\gamma\gamma \rightarrow X}(w) \frac{dL_{\gamma\gamma}}{dw} dw$ [1].

1.2 $\gamma\gamma \rightarrow \eta$

Two independent analyses have been performed looking for $\gamma\gamma \rightarrow \eta$ production with $\eta \rightarrow \pi^+\pi^-\pi^0$ and $\eta \rightarrow \pi^0\pi^0\pi^0$. In both analyses the signal has been simulated with a Monte Carlo generator based on the complete matrix element calculation which allows the full phase space generation [2].

$\gamma\gamma \rightarrow \eta \rightarrow \pi^+\pi^-\pi^0$. Events are selected asking for two photons from a π^0 decay and two tracks with opposite curvature coming from the interaction point, the π^\pm mass being assigned to each track. A kinematic fit is performed using the $\eta \rightarrow \pi^+\pi^-\pi^0$ decay hypothesis; the fit returns a χ^2 value and events with $\chi^2 > 20$ are rejected. Further cuts are applied to suppress processes with photons and e^+e^- in the final state. The number of signal events is extracted from the fit to the squared missing mass distribution M_{miss}^2 using Monte Carlo distribution for both signal and backgrounds (Fig. 1.1). From the number of signal events given by the fit one obtains the cross section $\sigma(e^+e^- \rightarrow e^+e^-\eta, \sqrt{s} = 1 \text{ GeV}) = (41.7 \pm 4.0_{\text{stat}}) \text{ pb}$, the systematic error being under evaluation. Work is in progress to extract the partial width $\Gamma_{\eta \rightarrow \gamma\gamma}$.

The main irreducible background is due to $e^+e^- \rightarrow \eta\gamma \rightarrow \pi^+\pi^-\pi^0\gamma$ events with the monochromatic photon ($E_\gamma = 350 \text{ MeV}$) lost in the beam pipe. In order to normalize this process properly a dedicated analysis has been done using the same $\mathcal{L} = 242.5 \text{ pb}^{-1}$ data sample, selecting events with three photons in the final state and performing a kinematic fit asking for energy and momentum conservation; improved variables have been used to fit to data distribution of the energy of the monochromatic photon. The preliminary result for the cross section is $\sigma(e^+e^- \rightarrow \eta\gamma, \sqrt{s} = 1 \text{ GeV}) = (0.866 \pm 0.009_{\text{stat}} \pm 0.093_{\text{syst}}) \text{ nb}$ [3].

$\gamma\gamma \rightarrow \eta \rightarrow \pi^0\pi^0\pi^0$. Events are selected with six photons from the interaction point (prompt photons); the photons are paired choosing the combination which minimizes the χ^2 variable

$$\chi_{\gamma\gamma}^2 = \frac{(m_\pi - m_{ij})^2}{\sigma_{ij}^2} + \frac{(m_\pi - m_{kl})^2}{\sigma_{kl}^2} + \frac{(m_\pi - m_{st})^2}{\sigma_{st}^2}, \quad (1.1)$$

with m_{ij} the two-photon invariant masses and σ_{ij} their resolutions. A kinematic fit is performed constraining the six-photon invariant mass to the η meson mass and asking for the space-time relation $t - |\vec{r}|/c = 0$ to be satisfied for each photon; a cut is then applied on the value of the kinematic fit χ^2 . Events with tracks in the drift chamber are rejected; a cut is applied on the energy of the most energetic photon, to reject $\eta\gamma$ events. The squared missing mass distribution shows an excess of events well reproduced by the $e^+e^- \rightarrow e^+e^-\eta \rightarrow e^+e^-\pi^0\pi^0\pi^0$ Monte Carlo. The fit gives normalization for the Monte Carlo signal and the backgrounds distributions (Fig. 1.2 left). The preliminary result for $e^+e^- \rightarrow e^+e^-\eta$ production cross section at $\sqrt{s} = 1 \text{ GeV}$ is $\sigma(e^+e^- \rightarrow e^+e^-\eta, 1 \text{ GeV}) = (37.0 \pm 1.4_{\text{stat}} \pm 2.2_{\text{syst}}) \text{ pb}$, to be compared with the result obtained studying the $\eta \rightarrow \pi^+\pi^-\pi^0$ decay channel. From $\eta\gamma$ normalization a preliminary value

*Università degli Studi Roma Tre and INFN, Sezione Roma Tre; plonghi@roma3.infn.it

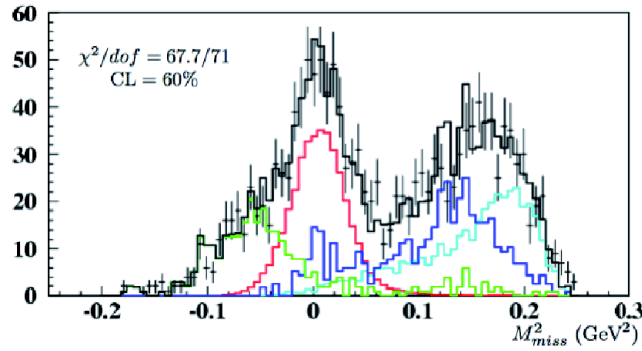


Figure 1.1: $\gamma\gamma \rightarrow \eta \rightarrow \pi^+\pi^-\pi^0$ analysis: squared missing mass distributions for data (points) and Monte Carlo normalized according to fit result (solid lines). Colour code: red = $\eta\gamma$, light blue = signal, blue = $\omega\pi^0$, green = $e^+e^-\gamma$ (preliminary plot).

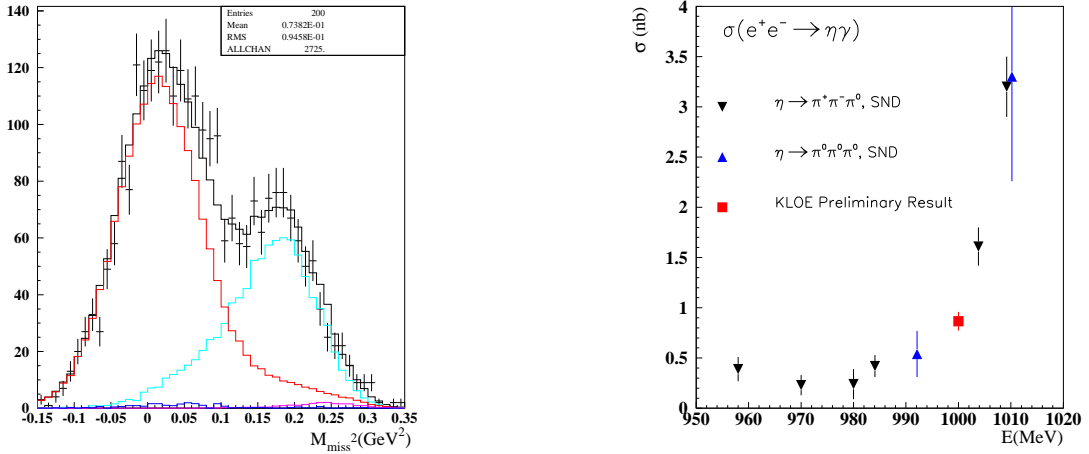


Figure 1.2: $\gamma\gamma \rightarrow \eta \rightarrow \pi^0\pi^0\pi^0$ analysis. Left: squared missing mass distributions for data (points) and Monte Carlo normalized according to fit result (solid lines). Colour code: red = $\eta\gamma$, light blue = signal, blue = $\omega\pi^0$ (preliminary plot). Right: preliminary KLOE result for $\sigma(e^+e^- \rightarrow \eta\gamma)$ at $\sqrt{s} = 1$ GeV, (red point, with statistical uncertainty only) and SND results [4] at several values of \sqrt{s} .

for the cross section $\sigma(e^+e^- \rightarrow \eta\gamma, \sqrt{s} = 1 \text{ GeV}) = (0.875 \pm 0.018_{\text{Stat}} \pm 0.035_{\text{Syst}}) \text{ nb}$ is evaluated, in agreement with the measurement done in the $\eta \rightarrow \pi^+\pi^-\pi^0$ decay channel. This value is shown in Fig. 1.2 (right) together with the SND experimental results [4] as a function of \sqrt{s} .

1.3 $\gamma\gamma \rightarrow \pi^0\pi^0$

The main goal of this analysis is to investigate the low $\pi^0\pi^0$ invariant mass region, just above the production threshold, where a contribution from the $\sigma(600)$ scalar meson as a resonant intermediate state is expected. The main background processes are annihilation reactions to states with four or more prompt photons: $e^+e^- \rightarrow K_S K_L, \eta\gamma, \omega\pi^0, f_0\gamma, a_0\gamma$. In addition, the $e^+e^- \rightarrow \gamma\gamma$ process is also considered as a source of background due to possible splitting of the photons energy deposits in the calorimeter. Events with 4 prompt photons are selected. The photons are paired as in the $\gamma\gamma \rightarrow \eta \rightarrow \pi^0\pi^0\pi^0$ analysis, and events with $\chi^2_{\gamma\gamma} > 4$ are rejected: the effect of this selection is shown in Fig. 1.3 (left). Events with no tracks in the drift chamber are selected; cuts on photons energies and on the transverse momentum of the four-photon system are applied; a cut is applied on the ratio of the sum of the energies of four photons to the total energy deposit in the calorimeter, to reject $K_S K_L$ events with large amount of non-prompt energy released in

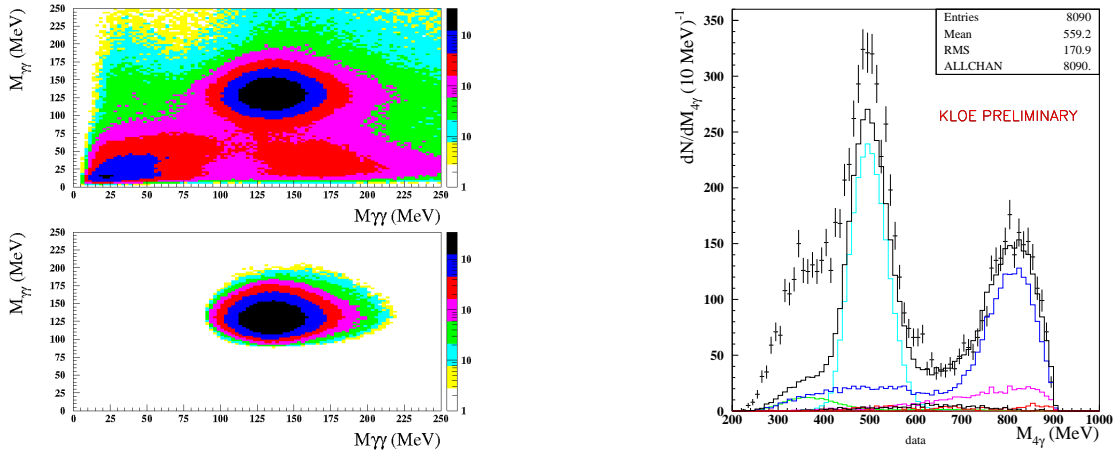


Figure 1.3: $\gamma\gamma \rightarrow \pi^0\pi^0$ analysis. Left: two-photon pairs invariant masses before (top) and after (bottom) $\chi^2_{\gamma\gamma}$ rejection; selected events have both photons pairs invariant masses centered around π^0 mass value. Right: four-photon invariant mass spectrum for data (points with error bars) and backgrounds Monte Carlo. Colour code: light blue = $K_S K_L$, blue = $\omega\pi^0$, violet = $f_0\gamma$, green = $\eta\gamma$, red = $\gamma\gamma$ (preliminary plot).

the detector. The four-photon invariant mass spectrum for the selected data sample is shown in Fig. 1.3 (right) together with the normalized Monte Carlo background. An excess of events in the low invariant mass region signals $\pi^0\pi^0$ production processes.

1.4 Conclusions

The reported analyses show excess of events with respect to the annihilation processes in the region where the signal from η or $\pi^0\pi^0$ production via $\gamma\gamma$ interaction is expected. For the $e^+e^- \rightarrow e^+e^-\eta$ cross section at $\sqrt{s} = 1$ GeV two compatible measurements are obtained studying the $\eta \rightarrow \pi^+\pi^-\pi^0$ and the $\eta \rightarrow \pi^0\pi^0\pi^0$ decay channels. For the $\gamma\gamma \rightarrow \pi^0\pi^0$ process work is in progress to determine the signal efficiency and the $\gamma\gamma$ luminosity function in order to extract the cross section and compare it with the only available measurement in literature [5].

The forthcoming data taking with KLOE-2 detector, equipped with dedicated small angles taggers for e^\pm in the final state, will give precious additional information on $\gamma\gamma$ hadron production at low energy [6].

Bibliography

- [1] S.J. Brodsky, T. Kinoshita and H. Terazawa, *Phys. Rev. D*, **4**, 1532 (1971).
- [2] F. Nguyen, F. Piccinini and A. D. Polosa, *Eur. Phys. J. C*, **47**, 65, (2006).
- [3] KLOE-2 Collaboration, *ArXiv:1107.3782*.
- [4] M. N. Achasov *et al.*, *Phys. Rev. D*, **76**, 077101, (2007).
- [5] H. Marsiske *et al.*, *Phys. Rev. D*, **41**, 3324, (1990).
- [6] G. A. Amelino Camelia *et al.*, *Eur. Phys. J. C*, **68**, 619 (2010).

ROY–STEINER EQUATIONS FOR $\gamma\gamma \rightarrow \pi\pi$

MARTIN HOFERICHTER^{*†}, DANIEL R. PHILLIPS[†] AND CARLOS SCHAT[‡]

1.1 Introduction

Presently, there are several experiments dedicated to the study of low-energy pion–photon interactions. At COMPASS, pion Compton scattering is being investigated by means of the Primakoff effect in $\pi^- Z \rightarrow \pi^- Z \gamma$ with the aim to extract pion polarizabilities [1], while at KLOE the reaction $\gamma\gamma \rightarrow \pi^0\pi^0$ is being measured in $e^+e^- \rightarrow e^+e^-\pi^0\pi^0$ [2]. Measurements of the cross section for $\gamma\gamma \rightarrow \pi^0\pi^0$ at low energies are particularly valuable, since they provide an alternative way to access the pion polarizabilities and the absence of Born-term contributions in this channel renders the cross section sensitive to the influence of the σ resonance. However, in both cases one needs theory input to reliably extract the information of interest, as the polarizabilities are defined at the threshold for pion Compton scattering, and studying the σ even requires analytic continuation far into the complex plane. The necessary extrapolations should be performed respecting all available constraints, i.e. analyticity, unitarity, crossing symmetry, and gauge invariance. Roy–Steiner equations for $\gamma\gamma \rightarrow \pi\pi$ provide a framework that meets all these requirements [3].¹

The Roy equations for $\pi\pi$ scattering [5] are a coupled system of partial wave dispersion relations that respects analyticity, unitarity, and crossing symmetry of the scattering amplitude. In recent years, partial wave dispersion relations in combination with unitarity (and chiral symmetry) have been used for high-precision studies of low-energy processes, both in $\pi\pi$ [6, 7] and πK [8] scattering. An important application of $\pi\pi$ Roy equations in combination with Chiral Perturbation Theory (ChPT) was the precise prediction of the pole parameters of the σ resonance [9]

$$M_\sigma = 441_{-8}^{+16} \text{ MeV}, \quad \Gamma_\sigma = 544_{-25}^{+18} \text{ MeV}. \quad (1.1)$$

The reaction $\gamma\gamma \rightarrow \pi\pi$ provides an alternative to $\pi\pi$ scattering for the excitation of the σ . In particular, Roy-equation techniques in $\gamma\gamma \rightarrow \pi\pi$ allow us to constrain the σ 's two-photon width $\Gamma_{\sigma\gamma\gamma}$ at a similar level of rigor as M_σ and Γ_σ based on $\pi\pi$ Roy equations [3].

1.2 Roy equations for $\pi\pi$ scattering

Roy equations for $\pi\pi$ scattering are obtained by starting from a twice-subtracted dispersion relation at fixed Mandelstam t , determining the t -dependent subtraction constants by means of crossing symmetry, and finally performing a partial wave expansion. This leads to a coupled system of integral equations for the $\pi\pi$ partial waves $t_J^I(s)$ with isospin I and angular momentum J

$$t_J^I(s) = k_J^I(s) + \sum_{I'=0}^2 \sum_{J'=0}^{\infty} \int_{4M_\pi^2}^{\infty} ds' K_{JJ'}^{II'}(s, s') \text{Im} t_{J'}^{I'}(s'), \quad (1.2)$$

where $K_{JJ'}^{II'}$ are known kinematical kernel functions and the $\pi\pi$ scattering lengths—the only free parameters—appear in the subtraction term k_J^I . Assuming elastic unitarity

$$\text{Im} t_J^I(s) = \sigma(s) |t_J^I(s)|^2, \quad t_J^I(s) = \frac{e^{2i\delta_J^I(s)} - 1}{2i\sigma(s)}, \quad \sigma(s) = \sqrt{1 - \frac{4M_\pi^2}{s}}, \quad (1.3)$$

(1.2) translates into a coupled integral equation for the phase shifts δ_J^I themselves.

^{*}Helmholtz-Institut für Strahlen- und Kernphysik (Theorie) and Bethe Center for Theoretical Physics, Universität Bonn, hoferichter@hiskp.uni-bonn.de

[†]Institute of Nuclear and Particle Physics and Department of Physics and Astronomy, Ohio University

[‡]CONICET - Departamento de Física, FCEyN, Universidad de Buenos Aires

¹The following presentation involves significant textual overlap with [4].

1.3 Roy–Steiner equations for $\gamma\gamma \rightarrow \pi\pi$

Crossing symmetry in this case is less restrictive than for $\pi\pi$ scattering, as it couples $\gamma\gamma \rightarrow \pi\pi$ to pion Compton scattering $\gamma\pi \rightarrow \gamma\pi$, which we will consider as the s -channel process. Roy–Steiner equations are then most conveniently constructed based on hyperbolic dispersion relations [10]. The resulting system of integral equations couples the $\gamma\gamma \rightarrow \pi\pi$ partial waves $h_{J,\pm}^I(t)$ to the $\gamma\pi \rightarrow \gamma\pi$ partial waves $f_{J,\pm}^I(s)$ (with photon helicities \pm), e.g.

$$h_{J,-}^I(t) = \tilde{N}_J^-(t) + \frac{1}{\pi} \int_{M_\pi^2}^{\infty} ds' \sum_{J'=1}^{\infty} \tilde{G}_{JJ'}^-(t, s') \text{Im} f_{J',+}^I(s') + \frac{1}{\pi} \int_{4M_\pi^2}^{\infty} dt' \sum_{J'} \tilde{K}_{JJ'}^-(t, t') \text{Im} h_{J',-}^I(t'), \quad (1.4)$$

where $\tilde{N}_J^-(t)$ includes the QED Born terms. Subtracting at $t = 0$, $s = M_\pi^2$, the subtraction constants directly correspond to pion polarizabilities. In the once-subtracted case, one needs the dipole polarizabilities $\alpha_1 \pm \beta_1$, while a second subtraction requires in addition knowledge of the quadrupole polarizabilities $\alpha_2 \pm \beta_2$.

Elastic unitarity is also less restrictive than for $\pi\pi$ scattering, since the unitarity relation is linear in $h_{J,\pm}^I$

$$\text{Im} h_{J,\pm}^I(t) = \sigma(t) h_{J,\pm}^I(t) t_J^I(t)^*. \quad (1.5)$$

Below inelastic thresholds the phase of $h_{J,\pm}^I$ coincides with δ_J^I (“Watson’s theorem”). Assuming this phase to be known, the equations thus reduce to a Muskhelishvili–Omnès problem for $h_{J,\pm}^I$ [11].

1.4 Muskhelishvili–Omnès solution and results for $\Gamma_{\sigma\gamma\gamma}$

To solve the equations for $h_{J,\pm}^I$, we truncate the system at $J = 2$. Furthermore, we assume the amplitudes to be known above the matching point $t_m = (0.98 \text{ GeV})^2$. The solution can then be written down in terms of Omnès functions

$$\Omega_J^I(t) = \exp \left\{ \frac{t}{\pi} \int_{4M_\pi^2}^{t_m} dt' \frac{\delta_J^I(t')}{t'(t' - t)} \right\}. \quad (1.6)$$

We find that the solutions for different partial waves in general do not decouple, e.g. the equation for the S -wave involves spectral integrals over the D -waves as well [3]. This is a new result of our dispersive treatment of $\gamma\gamma \rightarrow \pi\pi$ based on Roy–Steiner equations.

We approximate $\text{Im} f_{J,\pm}^I(s)$, which at low energies is dominated by multi-pion states, by a sum of resonances [12]. Above the matching point we use a Breit–Wigner description of the $f_2(1270)$, which dominates the cross section at higher energies. Within our formalism [3] we derive a sum rule for the $I = 2$ polarizabilities, which—in combination with ChPT results for dipole and neutral-pion quadrupole polarizabilities [13]—produces an improved prediction

$$(\alpha_2 - \beta_2)^{\pi^\pm} = (15.3 \pm 3.7) \cdot 10^{-4} \text{ fm}^5 \quad (1.7)$$

for the charged-pion quadrupole polarizability. This sum-rule result together with the ChPT values for the other polarizabilities [13] leads to the “ChPT” prediction for the total cross section of $\gamma\gamma \rightarrow \pi^0\pi^0$ depicted in the left panel of Fig. 1.1. The result labeled “GMM” is found when we adopt the polarizability values of a recent fit of a two-channel Muskhelishvili–Omnès representation to $\gamma\gamma \rightarrow \pi\pi$ cross section data [12]. The uncertainty due to the $\pi\pi$ phases represented by the grey band is estimated by varying between two recent state-of-the-art analyses based on Roy and Roy-like equations [7, 14]. We see that especially for the twice-subtracted version the agreement with experiment in the low-energy region is very good. Given sufficiently accurate data on $\gamma\gamma \rightarrow \pi^0\pi^0$ such an analysis could be used to extract pion polarizabilities.

Since we have shown that the σ lies within the domain of validity of our Roy–Steiner equations [3], this formalism allows for a reliable analytic continuation to the σ pole. The main result of our analysis is shown in the right panel of Fig. 1.1: there is a correlation between $\Gamma_{\sigma\gamma\gamma}$ and the $I = 0$ pion polarizabilities that follows from Roy–Steiner equations and input for the $\pi\pi$ phases alone. In combination with the ChPT-plus-sum-rule input for the polarizabilities, we obtain

$$\Gamma_{\sigma\gamma\gamma} = (1.7 \pm 0.4) \text{ keV}. \quad (1.8)$$

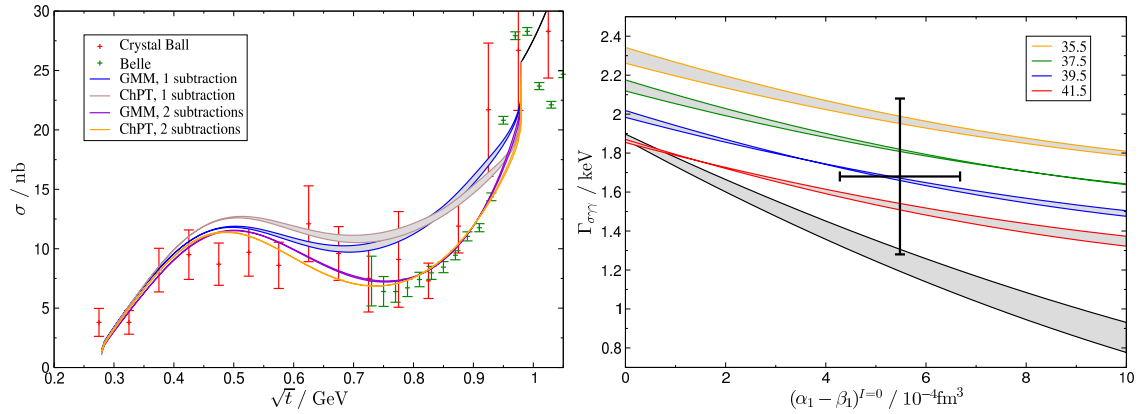


Figure 1.1: Total cross section for $\gamma\gamma \rightarrow \pi^0\pi^0$ for $|\cos\theta| \leq 0.8$ (left) and $\Gamma_{\sigma\gamma\gamma}$ as a function of the $I = 0$ pion polarizabilities (right). The black line refers to the unsubtracted case and the colored lines to the twice-subtracted version with $(\alpha_2 - \beta_2)^{I=0}$ as indicated (in units of 10^{-4}fm^5). The grey bands represent the uncertainty due to the $\pi\pi$ input. The cross corresponds to the twice-subtracted case plus ChPT input.

1.5 Outlook

The framework presented here should prove valuable for the interpretation of upcoming KLOE data for $\gamma\gamma \rightarrow \pi^0\pi^0$. Especially in combination with the ongoing efforts at COMPASS concerning $\gamma\pi^- \rightarrow \gamma\pi^-$, this will further improve knowledge of the pion polarizabilities and thus of $\Gamma_{\sigma\gamma\gamma}$.

Acknowledgements

This research was supported by the DFG (SFB/TR 16), the program “Kurzstipendien für DoktorandInnen” of the DAAD, the Bonn-Cologne Graduate School of Physics and Astronomy, the US Department of Energy (Office of Nuclear Physics), and CONICET.

Bibliography

- [1] A. V. Guskov, Phys. Part. Nucl. Lett. **7** (2010) 192; Nucl. Phys. Proc. Suppl. **198** (2010) 112.
- [2] The KLOE2 Collaboration, arXiv:1107.3782 [hep-ex]; I. Prado Longhi, *these proceedings*.
- [3] M. Hoferichter, D. R. Phillips and C. Schat, Eur. Phys. J. C **71** (2011) 1743.
- [4] M. Hoferichter, D. R. Phillips and C. Schat, arXiv:1108.4776 [hep-ph].
- [5] S. M. Roy, Phys. Lett. B **36** (1971) 353.
- [6] B. Ananthanarayan, G. Colangelo, J. Gasser and H. Leutwyler, Phys. Rept. **353** (2001) 207.
- [7] R. García-Martín, R. Kamiński, J. R. Peláez, J. Ruiz de Elvira and F. J. Ynduráin, Phys. Rev. D **83** (2011) 074004.
- [8] P. Büttiker, S. Descotes-Genon and B. Moussallam, Eur. Phys. J. C **33** (2004) 409.
- [9] I. Caprini, G. Colangelo and H. Leutwyler, Phys. Rev. Lett. **96** (2006) 132001.
- [10] G. E. Hite and F. Steiner, Nuovo Cim. A **18** (1973) 237.
- [11] N. Muskhelishvili, *Singular Integral Equations*, P. Noordhof, Groningen, 1953; R. Omnès, Nuovo Cim. **8** (1958) 316.
- [12] R. García-Martín and B. Moussallam, Eur. Phys. J. C **70** (2010) 155.
- [13] J. Gasser, M. A. Ivanov and M. E. Sainio, Nucl. Phys. B **728** (2005) 31; **745** (2006) 84.
- [14] I. Caprini, G. Colangelo, H. Leutwyler, in preparation.

MEASUREMENT OF THE DOUBLE POLARIZATION OBSERVABLE G IN π^0 AND η PHOTOPRODUCTION

ANNIKA THIEL* *for the CBELSA/TAPS-Collaboration*

1.1 Introduction

The excitation spectrum of the nucleon consists of several strongly overlapping resonances with different strengths. To disentangle these resonances and to determine their contributions in the different final states, a partial wave analysis has to be performed. The model-independent determination of all amplitudes can be achieved by a “complete experiment”, for which a set of 8 well chosen polarization observables is needed in each final state for single pseudoscalar meson production[1]. This set consists of at least 4 double polarization observables like the observable G, which has been measured with the CBELSA/TAPS experiment in Bonn. In the experiment linearly or circularly polarized photons and a longitudinally or transversally polarized target are provided, therefore several polarization observables are accessible.

The first results for the double polarization observable G, which utilizes linearly polarized photons on a longitudinally polarized target, are shown here for π^0 and η photoproduction off the proton.

1.2 Experimental Setup

The Crystal Barrel experiment is located in Bonn at the electron accelerator ELSA, which provides polarized or unpolarized electrons up to 3.5 GeV. Via bremsstrahlung an unpolarized, linearly polarized or circularly polarized photon beam can be produced, whose energies are determined in a tagging system. The polarized target is surrounded by the main calorimeter, the Crystal Barrel detector, while the forward direction is covered by the Mini-TAPS detector up to small angles. Each calorimeter is equipped with detectors for charge identification.

This setup allows an angular coverage of nearly 4π with a high detection efficiency for photons and is therefore well suited for the measurement of reactions with neutral mesons like π^0 and η in the final state.

1.3 Selection of the Reactions

Two different polarization settings were used for this analysis with coherent edge at 950 MeV and at 1150 MeV. With these two settings, which are shown in figure 1.1, left, the photon energy range of $E_\gamma = 700 \text{ MeV} - 1100 \text{ MeV}$ can be covered with a high degree of photon polarization.

For the selection of the two photon decay of the η and π^0 , first, the reactions were checked for two neutral particles and one charged for the recoiling proton. The time information of all particles of the reaction were used, to confirm that the observed particles originated from the same reaction. Also, the data was corrected for random time background. To ensure that the meson and the recoiling proton were detected in opposite directions in the center of mass system, the ϕ and θ angle difference were analyzed. By treating the proton as a missing particle and plotting the missing mass of the system, a peak at the mass of the proton could be observed. In the invariant mass of the two photons, which is shown in figure 1.1, center, a clear signal for the π^0 and η can be seen above nearly no background. To choose the desired reaction, a cut on either meson was done.

1.4 Determination of the Polarization Observables

In the frozen spin target, butanol is used as target material, which is composed of hydrogen, carbon and oxygen. Because of that, reactions on free and on bound protons are contributing.

*Helmholtz-Institut für Strahlen- und Kernphysik, Universität Bonn, thiel@hiskp.uni-bonn.de

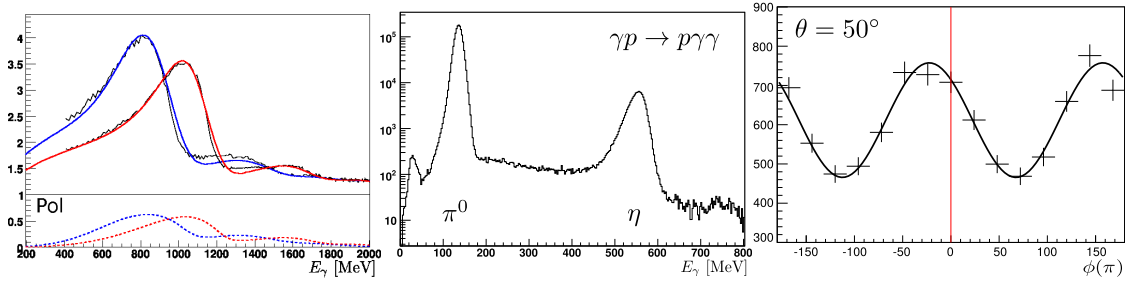


Figure 1.1: The two different settings of the coherent peaks for linearly polarized photons (left). Invariant mass of the two photons in logarithmic scale (center) with the peaks for the π^0 and the η meson. Example fit to the $\phi(\pi^0)$ distribution of the data (right) to extract the observables.

The count rate for the reactions on the butanol target can be written as

$$N(\theta, \phi) = (N_b + N_f) \cdot \left[1 - \frac{N_b \Sigma_b + N_f \Sigma_f}{N_b + N_f} \cdot p_\gamma^{lin} \cos(2\phi) + \frac{N_f}{N_b + N_f} p_z \cdot p_\gamma^{lin} G \sin(2\phi) \right] \quad (1.1)$$

with $N_f(\theta)$ ($N_b(\theta)$) being the count rate on the free (bound) protons. The observables, which can be measured are the beam asymmetries Σ_b and Σ_f and the double polarization observable G , which can only be observed on the polarizable hydrogen protons. To successfully determine the double polarization observable G and the beam asymmetry Σ on the butanol the following equation was used to fit the data:

$$N(\theta, \phi) = A \cdot [1 - B \cdot \cos(2\phi) + C \cdot \sin(2\phi)] \quad (1.2)$$

An example fit is shown in figure 1.1, right.

1.4.1 The Beam Asymmetry Σ

The fit parameter B allows the extraction of the beam asymmetry on the free (Σ_f) and on the bound protons (Σ_b). By reducing the fraction of bound protons in the data set, the measured beam asymmetry converges to the beam asymmetry on the free proton and can be compared to previous measurements. In figure 1.2 the beam asymmetry for π^0 and η photoproduction is shown, compared to previous measurements and results of the different partial wave analyses. The data agrees well with the measurements on the free proton, which indicates that the influence of the bound protons could successfully be reduced.

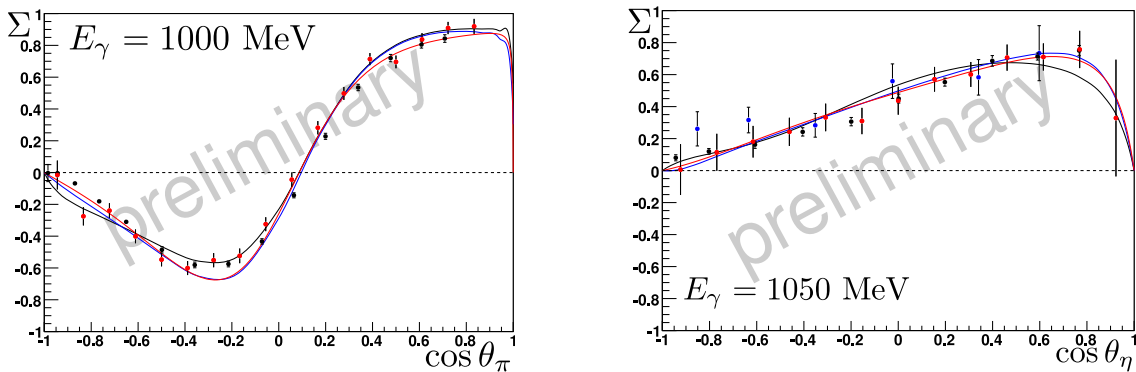


Figure 1.2: The beam asymmetry Σ (red) for π^0 - (left) and η -production (right). The values are compared with the measurements of the GRAAL collaboration[5] (black) and for the η with previous CBELSA/TAPS measurements[6] (blue). The lines give the solutions of the partial wave analyses: MAID[2] (black), SAID[3] (blue) and BnGa[4] (red).

1.4.2 The Double Polarization Observable G

From the fit parameter C the double polarization observable G can be extracted, modified by the dilution factor $D = \frac{N_f}{N_b + N_f}$. To determine this factor, data sets with hydrogen and carbon targets

were compared. The comparison of the missing mass for the different materials in fig. 1.3, left, shows that the sum of the hydrogen and carbon measurements describes the butanol data. The

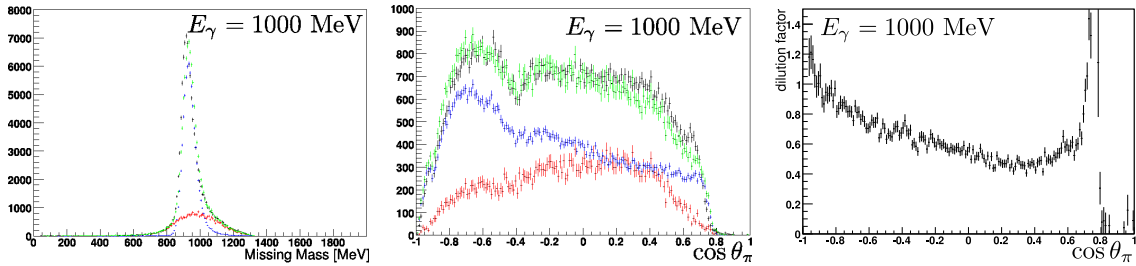


Figure 1.3: Missing mass distribution (left) and meson $\cos\theta$ (center) for π^0 production on the different target materials: butanol (black), hydrogen (blue), carbon (red) and the sum of hydrogen and carbon (green). The dilution factor (right) was determined using these distributions.

same applies to the $\cos\theta$ of the meson (fig. 1.3, center). With these distributions, it is possible to determine the dilution factor (fig. 1.3, right). This factor was determined for both mesons and all energies and is used to correct the values of the observable G . The double polarization observable, which is shown in fig. 1.4, was successfully extracted in the energy range for both mesons.

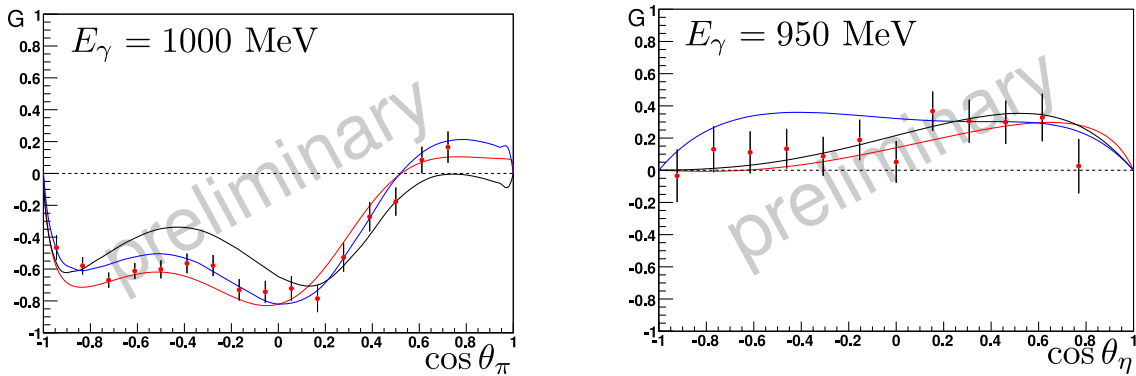


Figure 1.4: The double polarization observable G for the π^0 (left) and the η (right). Colors of the predictions of the partial wave analyses as in figure 1.2.

1.5 Summary

The determination of polarization observables is crucial for the understanding of the excitation spectrum of the nucleon. For the beam asymmetry Σ and the double polarization observable G data has been taken by the CBELSA/TAPS experiment in Bonn. These data will provide new information for the partial wave analysis, which will help to identify the contributing resonances to the different final states.

Supported by the DFG (SFB/TR16).

Bibliography

- [1] Chiang W., Tabakin F., Phys. Rev. C **55**, 2054 (1997).
- [2] Drechsel D., Kamalov S.S. and Tiator L., Eur. Phys. J A **34**, 69 (2007), Chiang W.-T., Yang S.N., Tiator L., Vanderhaeghen M., Drechsel D., Phys. Rev. C **68**, 045202 (2003).
- [3] Arndt R.A. et al., Phys. Rev C **53**, 430 (1996).
- [4] Anisovich A.V. et al., Eur. Phys. J. A **44**, 203 (2010)
- [5] Bartalini O. et al., Eur. Phys. J A **26**, 399 (2005), Ajaka J. et al., Phys. Rev. Lett. **81**, 1797 (1998).
- [6] Elsner D. et al., Eur. Phys. J A **33**, 147 (2007).

THE $N^*(1535)$ EXCITATION – THE ELECTROMAGNETIC TRANSITION FORM FACTORS

*G. RAMALHO**, *M.T. PEÑA*†* and *K. TSUSHIMA‡*

The $N^*(1535)$ resonance, an S_{11} state with $J^P = \frac{1}{2}^-$, is a very important nucleon excitation. It has a strong decay channel for ηN ($\approx 50\%$), and has been studied by several models and frameworks [1, 2, 3, 4, 5, 6, 7, 8]. A notable propriety of the $N^*(1535)$ resonance is the relation between the two independent helicity amplitudes for the transverse $A_{1/2}$ and the longitudinal $S_{1/2}$. Although it has been assumed till recently that the amplitude $S_{1/2}$ was negligible compared to $A_{1/2}$, recent data [9] revealed that these two amplitudes are correlated for the region $Q^2 > 2$ GeV², where Q^2 is the negative of the momentum transfer squared. The ratio between the two amplitudes for $Q^2 > 2$ GeV² can be expressed as [2]

$$S_{1/2}(Q^2) = -\frac{\sqrt{1+\tau}}{\sqrt{2}} \frac{M_S^2 - M^2}{2M_S Q} A_{1/2}(Q^2), \quad (1.1)$$

where $Q = \sqrt{Q^2}$, M_S is the $N^*(1535)$ mass, M the nucleon mass and $\tau = \frac{Q^2}{(M_S+M)^2}$. The test of the relation (1.1) using the $A_{1/2}$ data [9, 10] and the model from Ref. [1], is presented in Figure 1.1.

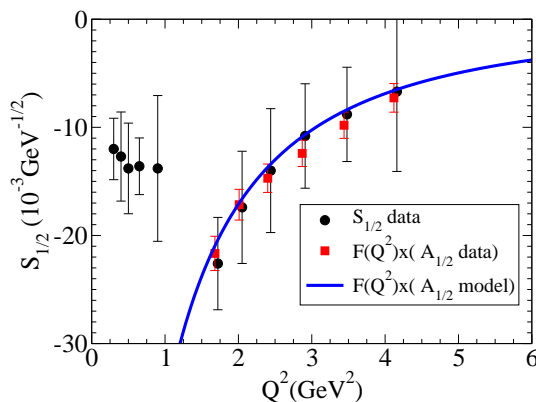


Figure 1.1: $S_{1/2}$ helicity amplitude for the $\gamma N \rightarrow N^*(1535)$ reaction. The function $F(Q^2)$ in the figure is $F(Q^2) = -\frac{\sqrt{1+\tau}}{\sqrt{2}} \frac{M_S^2 - M^2}{2M_S Q}$, as defined by Eq. (1.1). Model for $A_{1/2}$ is from Ref. [1]. Data are from Refs. [9, 10].

Although small, the magnitude of $S_{1/2}$ is about 10% of $A_{1/2}$ for very high Q^2 [2]. The results for $S_{1/2}$ can be interpreted as a correlation between the valence quark degrees of freedom and the quark-antiquark excitations (or meson cloud excitations), in the framework of the spectator quark model [1, 2, 11, 12].

In general at high Q^2 the valence quark degrees of freedom are dominant, since meson cloud effects are expected to be suppressed in QCD according to the dimensional counting rules [8]. At low Q^2 , meson cloud effects can be very important particularly for the lightest meson, the pion, due to chiral perturbation theory [13]. An example of the insufficiency of the valence quark degrees of freedom alone to explain the experimental data at low Q^2 , is the $\gamma N \rightarrow \Delta$ reaction. Including only the valence quark effects it is impossible to describe the data and misses at least

*CFTP, Instituto Superior Técnico, Av. Rovisco Pais 1049-001, Lisboa, Portugal

†Physics Department, Instituto Superior Técnico, Av. Rovisco Pais 1049-001, Lisboa, Portugal

‡CSSM, School of Chemistry and Physics, University of Adelaide, Adelaide SA 5005, Australia

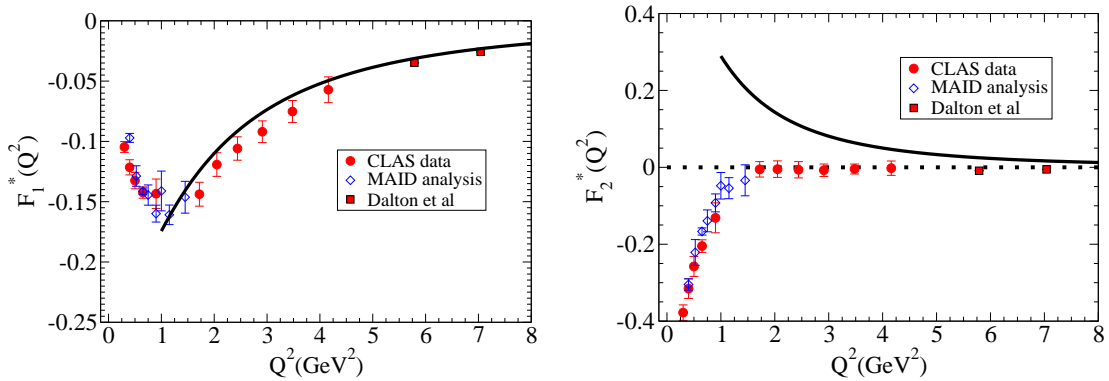


Figure 1.2: $\gamma N \rightarrow N^*(1535)$ transition form factors in the spectator quark model. Data are from Refs. [9, 10].

30% of the magnetic transition form factor strength for the $\gamma N \rightarrow \Delta$ reaction, in a non-relativistic framework near $Q^2 = 0$ [8, 14, 15]. This is interpreted as a manifestation for the necessity of including the explicit meson cloud effects [8, 14, 15, 16, 17, 18, 19].

A definite decomposition into the valence quark and meson cloud effects is however impossible [13, 20]. The decomposition can be done only for a particular model.

The application of a valence quark model to describe an electromagnetic transition between two baryon states has the advantage of accounting the quark structure (baryon wave functions and quark electromagnetic current), and can provide an upper limit for the magnitude of the quark core contribution for the electromagnetic form factors. [Recall the case for the $\gamma N \rightarrow \Delta$ reaction]. Recent models developed for the treatment of meson-baryon reactions using the meson and baryon effective degrees of freedom, take the quark core contributions in consideration [15, 21]. In addition the quark model estimates can be tested in the high Q^2 regime, where meson cloud effects fall down. Another regime where meson cloud effects can be suppressed and test the quark model estimates are the lattice QCD simulations with large pion masses, if some quark models can be extended to that regime.

To study the $N^*(1535)$ system we use the covariant spectator quark model [1, 11, 12, 22]. In the model a baryon is described as a 3 constituent-quark system that can be re-arranged in a quark-diquark structure, where the quark can couple with photon in terms of a vector meson dominance (VMD) process and the diquark is treated as an on-shell (spectator) particle [11, 12]. The model has been developed, and calibrated by the nucleon [11] and Δ [16, 17, 18] systems, and later extended to study the other resonances such as the Roper and $\Delta(1600)$ [23, 24]. Using the VMD parametrization for the quark current, the model was also extended successfully to the lattice QCD regime for $m_\pi > 400$ MeV, particularly for the elastic reaction [19] and for the transitions from the nucleon to the $\Delta(1232)$ and $N^*(1440)$ systems [18, 19, 23]. The results show that the covariant spectator quark model has a good control of the valence quark model degrees of freedom.

In the covariant spectator quark formalism the $N^*(1535)$ is described as a quark-diquark system with negative parity, a relative orbital angular momentum 1 and a quark core with spin 1/2 [1]. In addition we assume that the diquark has no internal P-state structure and can be treated as pointlike [1]. Furthermore, we note that the $N^*(1535)$ wave function can only be reliably applied for $Q^2 \gg |\mathbf{q}|_0^2 = 0.23 \text{ GeV}^2$, where $|\mathbf{q}|_0 = \frac{M_S^2 - M^2}{2M_S}$ is the photon three-momentum in the $N^*(1535)$ rest frame. The results for the transition form factors F_1^* and F_2^* are presented in Figure 1.2 for $Q^2 \geq 1 \text{ GeV}^2$. From the figure, one can conclude that the model is reasonable to explain the results for F_1^* for $Q^2 \geq 1 \text{ GeV}^2$. As for F_2^* one can notice that the model results differ in sign from the data, and also that it overestimates in absolute values of the data, where the data show $F_2^* \approx 0$ for $Q^2 > 1.5 \text{ GeV}^2$. The result $F_2^* = 0$ is equivalent to the relation given by Eq. (1.1). In the spectator quark model the deviation from the data can be interpreted as the missing of the meson cloud effects in the calculation [2]. If this interpretation is correct we can expect a negative contribution from the meson cloud for F_2^* around $Q^2 = 2 \text{ GeV}^2$ with the magnitude similar to the present model.

Although one cannot compare directly the valence quark effects and/or meson cloud effects, from different formalisms, it is encouraging to note that our results for F_2^* are close to the estimate

of the EBAC/Jlab group [6] for the quark core contributions, using a framework based in effective baryon-meson interactions. It is also worth to note that a calculation of the form factors with the assumption that the $N^*(1535)$ is a dynamically generated resonance, and therefore takes into account only the meson cloud effects, gives only negative contributions for F_2^* [4].

Based on the results from different works, one can conclude that valence quark effects are very important [4], or are the dominant contribution [1, 5, 6, 7, 8, 25] for the $N^*(1535)$ transition form factors, although meson cloud is certainly necessary to describe the data accurately.

Bibliography

- [1] G. Ramalho and M. T. Peña, Phys. Rev. D **84**, 033007 (2011).
- [2] G. Ramalho and K. Tsushima, Phys. Rev. D **84**(R), 051301 (2011).
- [3] S. Capstick and B. D. Keister, Phys. Rev. D **51**, 3598 (1995).
- [4] D. Jido, M. Döring and E. Oset, Phys. Rev. C **77**, 065207 (2008).
- [5] V. M. Braun *et al.*, Phys. Rev. Lett. **103**, 072001 (2009).
- [6] B. Julia-Diaz, H. Kamano, T. S. Lee, A. Matsuyama, T. Sato and N. Suzuki, Phys. Rev. C **80**, 025207 (2009).
- [7] B. Golli and S. Sirca, Eur. Phys. J. A **47**, 61 (2011).
- [8] I. G. Aznauryan and V. D. Burkert, arXiv:1109.1720 [hep-ph].
- [9] I. G. Aznauryan *et al.* [CLAS Collaboration], Phys. Rev. C **80**, 055203 (2009).
- [10] D. Drechsel, O. Hanstein, S. S. Kamalov and L. Tiator, Nucl. Phys. A **645**, 145 (1999).
- [11] F. Gross, G. Ramalho and M. T. Peña, Phys. Rev. C **77**, 015202 (2008).
- [12] G. Ramalho, F. Gross, M. T. Peña and K. Tsushima, Proceedings of Exclusive Reactions at High Momentum Transfer IV, 287 (2011).
- [13] H. W. Hammer, D. Drechsel and U. G. Meissner, Phys. Lett. B **586**, 291 (2004); U. G. Meissner, AIP Conf. Proc. **904**, 142 (2007).
- [14] V. Pascalutsa, M. Vanderhaeghen and S. N. Yang, Phys. Rept. **437**, 125 (2007).
- [15] B. Julia-Diaz, T. S. Lee, T. Sato and L. C. Smith, Phys. Rev. C **75**, 015205 (2007).
- [16] G. Ramalho, M. T. Peña and F. Gross, Eur. Phys. J. A **36**, 329 (2008).
- [17] G. Ramalho, M. T. Peña and F. Gross, Phys. Rev. D **78**, 114017 (2008).
- [18] G. Ramalho and M. T. Peña, Phys. Rev. D **80**, 013008 (2009).
- [19] G. Ramalho and M. T. Peña, J. Phys. G **36**, 115011 (2009).
- [20] S. Capstick *et al.*, Eur. Phys. J. A **35**, 253 (2008).
- [21] S. S. Kamalov and S. N. Yang, Phys. Rev. Lett. **83**, 4494 (1999).
- [22] F. Gross, Phys. Rev. **186**, 1448 (1969).
- [23] G. Ramalho and K. Tsushima, Phys. Rev. D **81**, 074020 (2010).
- [24] G. Ramalho and K. Tsushima, Phys. Rev. D **82**, 073007 (2010).
- [25] I. G. Aznauryan, V. D. Burkert, Proceedings of the 8th International Workshop on the Physics of Excited Nucleons (2011).

THE STRUCTURE AROUND $W=1680$ MeV IN η -PHOTOPRODUCTION OFF THE NEUTRON

DOMINIK WERTHMÜLLER*[†] and LILIAN WITTHAUER*
for the A2, Crystal Ball and TAPS collaborations

1.1 Motivation

Previous experiments of the GRAAL [1, 2], LNS-Sendai [3] and CBELSA/TAPS [4, 5] collaborations have reported a narrow structure at $W \approx 1680$ MeV in the total cross section of quasi-free η -photoproduction off the neutron. This structure is not seen on the proton and its nature is up to now still unknown. As the width of the structure is close to the experimental resolution of the different experiments the true width should be unusually small compared to known resonances in this energy region. Therefore the structure can hardly be described using a single well-know broad nucleon resonance. Theoretical explanations thus include interferences of resonances [6] or contributions from intermediate meson loops [7]. Another solution is provided by the chiral quark soliton model [8] which predicts an anti-decuplet nucleon resonance that couples strongly to the formation channel γn as well as to the final state ηN .

We report preliminary results from two different experiments performed at the tagged-photon beam facility at MAMI. In one experiment a liquid deuterium target was used as a neutron target whereas in the other one a liquid ^3He target was installed.

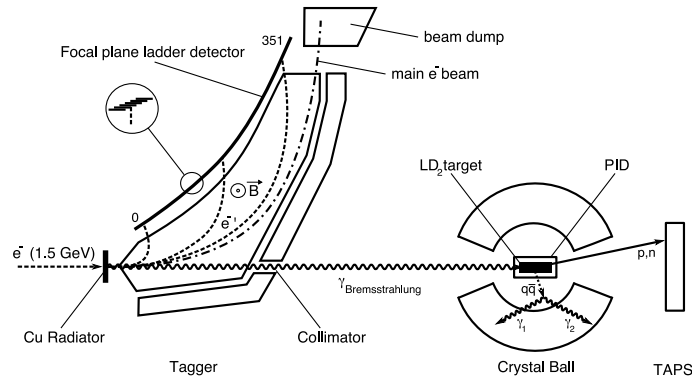


Figure 1.1: Scheme of the experimental setup.

1.2 Experimental setup

The measurements were performed at the electron accelerator facility MAMI [9, 10] in Mainz. A schematic view of the experimental setup is shown in figure 1.1. A photon beam was produced from an electron beam of 1.5 GeV energy via bremsstrahlung using a copper radiator. The energy of the photons was determined by a momentum analysis of the scattered electron in a magnetic spectrometer (Glasgow photon tagger [11, 12, 13]). After collimation the beam impinged on the target (liquid deuterium or ^3He , respectively). The target was surrounded by a cylindrical plastic scintillator strip detector [14], which was used for charged particle identification, and the spherical electromagnetic calorimeter Crystal Ball [15]. This detector consists of 672 NaI crystals and covers 94% of 4π steradians. The hole in forward direction of Crystal Ball is closed by the TAPS detector [16, 17] which is made of 384 BaF₂ crystals (378 BaF₂ + 24 PbWO₄ crystals in the ^3He experiment). In front of every crystal a thin plastic scintillator element is installed as a charged

*Department of Physics, University of Basel, CH-4056 Basel, Switzerland

[†]dominik.werthmueller@unibas.ch

particle veto detector. As trigger condition a deposited energy sum of 300 MeV in the Crystal Ball and a total multiplicity of two or more hits in both calorimeters was requested.

1.3 Data analysis

Using the $\eta \rightarrow \gamma\gamma$ decay of the η -meson the final state products of the quasi-free reactions $\gamma p \rightarrow \eta p$ and $\gamma n \rightarrow \eta n$ were selected by requesting 2 neutral clusters + 1 charged cluster or 3 neutral clusters, respectively, in the detector system. The η -meson was identified in the invariant mass of the two photons by applying a cut around the η mass. Background coming from e.g. $\eta\pi$ -photoproduction was suppressed by cutting on the ηN -coplanarity and the missing mass.

Excitation functions were calculated as functions of

1. the incoming photon beam energy E_γ (converted for better comparison to the center-of-mass energy $W_{beam} = \sqrt{2E_\gamma m_N + m_N^2}$ of the photon-nucleon system)
2. the invariant mass of the final state η -nucleon system $W_{rec} = M(\eta N)$ by reconstructing the energy of the recoil nucleon by kinematics

In case of 1) structures are smeared by the Fermi motion of the initial state nucleon inside the target nucleus (deuteron or ^3He). In contrast structures appearing in 2) are not affected by Fermi smearing and the resolution only depends on the energy and angular resolution of the detector system.

The multiple hits in the photon tagger were treated as single events and weighted accordingly to the tagger-detector timing to achieve a statistical subtraction of the accidental coincident background.

Finally, cross sections were extracted by normalizing the excitation functions with the target density, the photon flux and the detector acceptance obtained by a Geant4 based simulation of the detector setup.

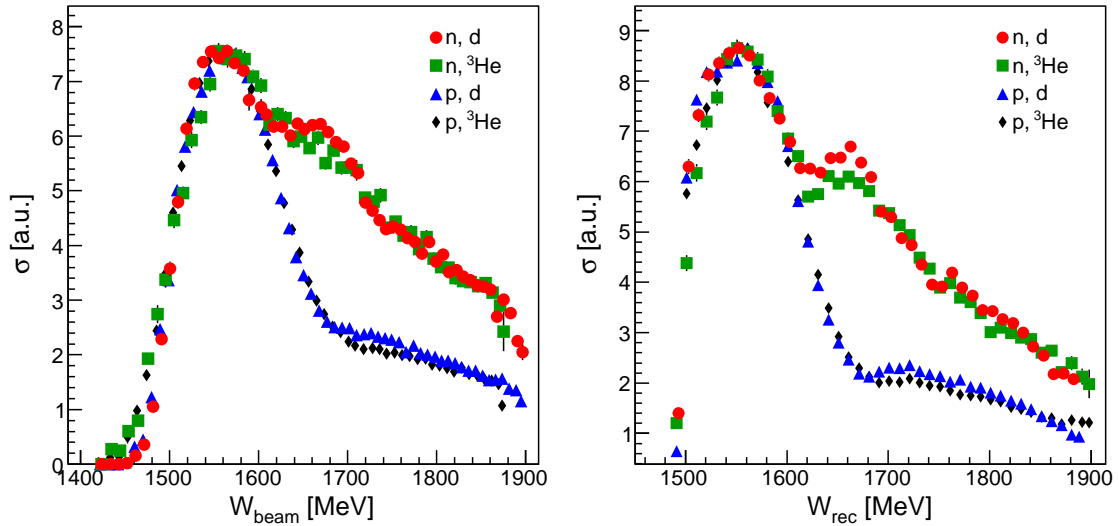


Figure 1.2: Very preliminary excitation functions for the quasi-free $\gamma p \rightarrow \eta p$ and $\gamma n \rightarrow \eta n$ reactions obtained by the LD₂ and the ^3He experiments.

1.4 Preliminary results

Preliminary results of the analysis are shown in figure 1.2. Since the absolute normalization of the data is not final all results were scaled to σ_n in the $S_{11}(1535)$ -maximum of the deuterium analysis and are given in arbitrary units.

The previous results are confirmed by both experiments: An excess in the neutron cross section is observed which is not seen on the proton. The width of the structure in $\sigma(W_{rec})$, that is not affected by Fermi motion, is around 50 MeV and is mainly resolution dominated.

Furthermore the results of the LD₂ and the ³He measurement are in good agreement. The differences in $\sigma(W_{beam})$ seem to be only related to the larger Fermi motion inside the ³He nucleus (smearing at threshold and at the shoulder of the S₁₁(1535)). The deviation in $\sigma(W_{rec})$ is due to the fact that the kinematic reconstruction within the participant-spectator model is only an approximation in case of ³He. Obtaining consistent results by using nuclei with different Fermi motion and n/p-ratio makes it very unlikely that the observed effect is caused by rescattering of mesons or FSI.

The final results of the LD₂ measurement will include the analysis of the $\eta \rightarrow 3\pi^0$ decay channel and will provide angular distributions with high statistics.

Bibliography

- [1] V. Kuznetsov et al., *arXiv:hep-ex/0409032*
- [2] V. Kuznetsov et al., *Phys. Lett. B*, **647**, 23, (2007).
- [3] F. Miyahara et al., *Prog. Theor. Phys. Suppl.*, **168**, 90, (2007).
- [4] I. Jaeglé et al., *Phys. Rev. Lett.*, **100**, 252002, (2008).
- [5] I. Jaeglé et al., *Eur. Phys. J. A*, **47**, 89, (2011).
- [6] A. Anisovich et al., *Eur. Phys. J. A* **41**, 13, (2009).
- [7] M. Döring, K. Nakayama, *Phys. Lett. B*, **683**, 145, (2010).
- [8] D. Diakonov, V. Petrov and M. V. Polyakov, *Z. Phys. A*, **359**, 305, (1997).
- [9] H. Herminghaus et al., *IEEE Trans. Nucl. Sci.*, **30**, 3274, (1983).
- [10] K.-H. Kaiser et al., *Nucl. Instrum. Methods A*, **593**, 159, (2008).
- [11] I. Anthony et al., *Nucl. Instrum. Methods A*, **301**, 230, (1991).
- [12] S. J. Hall et al., *Nucl. Instrum. Methods A*, **368**, 698, (1996).
- [13] J. C. McGeorge et al., *Eur. Phys. J. A*, **37**, 129, (2008).
- [14] D. Watts., *Proc. of the 11th International Conference on Calorimetry in Particle Physics, Perugia, Italy, 2004, World Scientific, Singapore, 2005*, (2005).
- [15] A. Starostin et al., *Phys. Rev. C*, **64**, 055205, (2001).
- [16] R. Novotny., *IEEE Trans. Nucl. Sci.*, **38**, 379, (1991).
- [17] A. R. Gabler et al., *Nucl. Instrum. Methods A*, **346**, 168, (1994).

Interaction of η and η'
with Nucleons and Nuclei

A THEORETICAL APPROACH TO $\eta'N$ SCATTERING

A. RAMOS* and E. OSET†

1.1 Introduction

The η' meson has interesting properties associated to the underlying QCD dynamics of hadrons, in particular to the $U(1)_A$ axial vector anomaly [1]. Being close to a singlet of $SU(3)$, its interaction with nucleons is supposed to be weak compared for instance with the case of its partner, the η meson. Experimentally, there are only poor estimations of the $\eta'N$ scattering length from analyses of the $pp \rightarrow pp\eta'$ cross section near threshold at COSY [2], establishing a value around $|a_{\eta'N}| \sim 0.1$ fm. The $\eta'N$ interaction has also an influence on photoproduction $\gamma p \rightarrow \eta'p$ reactions measured at ELSA and Jlab [3], which have been analyzed so far in the framework of resonant models [4]. Finally, some information on the $\eta'N$ interaction can be extracted from the transparency ratio in (γ, η') reactions on nuclei [5].

We present a theoretical study of the $\eta'N$ interaction within a unitary approach in coupled channels [6]. Our study also includes the explicit effect of resonances lying very close to the $\eta'N$ threshold, which are generated dynamically from the vector meson-baryon (VB) interaction in s-wave [7]. Finally, we also consider a term in the Lagrangian coupling the baryons to the singlet component of the pseudoscalar meson, which is allowed by the symmetries of QCD [8]. We find that the elastic $\eta'N$ cross section is very sensitive to the unknown singlet strength, while the inelastic cross sections are rather stable and constitute a genuine prediction of our model.

1.2 Model

The meson-baryon scattering dynamics is taken from the lowest order chiral Lagrangian reduced to the two meson fields needed in the process,

$$\mathcal{L}_{\Phi B} = \langle \bar{B} i \gamma^\mu \frac{1}{4f^2} [(\Phi \partial_\mu \Phi - \partial_\mu \Phi \Phi)B - B(\Phi \partial_\mu \Phi - \partial_\mu \Phi \Phi)] \rangle \quad (1.1)$$

where f is the pion decay constant, B represents the baryon octet matrix and Φ contains the pseudoscalar meson octet as well as the singlet field $\eta_1/\sqrt{3}$ added to its diagonal elements. The physical η, η' mesons are given by $\eta = \cos \theta_P \eta_8 - \sin \theta_P \eta_1$ and $\eta' = \sin \theta_P \eta_8 + \cos \theta_P \eta_1$, where θ_P is the $\eta_1 - \eta_8$ mixing angle, for which we take the value $\theta_P = -14.34^\circ$ reported in [9]. Our basis of pseudoscalar meson-baryon states (PB) is $\pi N, \eta N, \eta' N, K\Lambda$ and $K\Sigma$.

We have also implemented in our model the effect of a resonance appearing around 1970 MeV, close to the $\eta'N$ threshold at $\sqrt{s} = 1896$ MeV, which is generated dynamically from the vector meson-baryon (VB) interaction in s-wave [7] and couples mostly to the $K^*\Lambda$ and $K^*\Sigma$ channels. As described in Ref. [6], this is achieved by still working within a basis of coupled PB states but including explicitly, as part of a $PB - PB$ potential, the transition of the PB to the VB channels, the later ones interacting among themselves to produce the resonance. The $PB - VB$ transition vertex contains the standard PPV couplings as well as the anomalous PVV terms since the standard ones are suppressed by $\sin \theta_P$ for transitions involving $\eta'N$ states.

Finally, we also include a Lagrangian that couples the singlet component of the meson field to the baryons [8] and gives rise to new contributions to the transition potentials between ηN and $\eta' N$ states, $V_{\eta N, \eta N}^{(1)} = C \sin^2 \theta_P$, $V_{\eta N, \eta' N}^{(1)} = -C \sin \theta_P \cos \theta_P$ and $V_{\eta' N, \eta' N}^{(1)} = C \cos^2 \theta_P$, where the unknown singlet strength C is written in terms of a parameter α obtained from $C = \alpha 2m_{\eta'} (E_B + E_{B'})/4f_\pi^2/2M_N$.

*Departament d'Estructura i Constituents de la Matèria and Institut de Ciències del Cosmos. Universitat de Barcelona, Avda. Diagonal 645, 08028 Barcelona, Spain; ramos@ecm.ub.edu

†Departamento de Física Teórica and IFIC, Centro Mixto Universidad de Valencia-CSIC, Institutos de Investigación de Paterna, Aptdo. 22085, 46071 Valencia, Spain

With the obtained meson-baryon transition potential V we derive the scattering amplitude T by solving the Bethe-Salpeter equations in their on-shell factorization form, $T = [1 - VG]^{-1}V$, where G is the loop function for the intermediate meson-baryon states which we evaluate using dimensional regularization.

1.3 Results

Our results for the $\eta'p$ scattering length are shown in Table 1.1, while the elastic and inelastic $\eta'p$ cross sections, together with the cross section of the reaction $\pi^-p \rightarrow \eta'n$, are displayed in Fig. 1.1.

α	model	$a_{\eta p}$ [fm]	$ a_{\eta'p} $ [fm]
0	PB	0.0017+i0.0139	0.014
	$PB + VB$	0.0210+i0.0192	0.029
-0.126	$PB + VB$	0.073 + i0.019	0.075
0.204	$PB + VB$	-0.072 + i0.020	
-0.193	$PB + VB$	0.098 + i0.020	0.1
0.256	$PB + VB$	-0.098 + i0.020	
-0.333	$PB + VB$	0.149 + i0.020	0.15
0.352	$PB + VB$	-0.149 + i0.021	

Table 1.1: The $\eta'p$ scattering lengths for various models discussed in the text.

The $\eta'p$ scattering length is very small when only the Weinberg-Tomozawa terms are included ($\alpha = 0, PB$), since the particular structure of the Lagrangian of Eq. (1.1), $\Phi\partial_\mu\Phi - \partial_\mu\Phi\Phi$, makes the contribution of the singlet vanish. Including the VB states ($\alpha = 0, PB + VB$) increases the real part by an order of magnitude and enhances the imaginary part considerably due to the decay channels $K^*\Lambda \rightarrow \pi K\Lambda$ and $K^*\Sigma \rightarrow \pi K\Sigma$. The effect of the VB channels is more visible by comparing the thin and solid lines in Fig. 1.1. In all cases, one sees a pronounced structure around $p_{\eta'} = 500$ MeV/c ($p_\pi = 1600$ MeV/c) which corresponds to the energy 1970 MeV of the resonance. The strongest relative enhancements are seen for the elastic channel and for the $\pi^-p \rightarrow \eta'n$ reaction, but the results do not reproduce the available experimental information. The scattering length only amounts to $|a_{\eta'p}| = 0.029$ fm, while the $\pi^-p \rightarrow \eta'n$ cross section is six times smaller than the measured value of around 0.1 mb at a pion lab momentum of 1600 MeV/c [10].

Important changes are obtained when the singlet Lagrangian is considered with its strength α tuned to values of $|a_{\eta'p}|$ around 0.1 fm. Each assumed value of $|a_{\eta'p}|$ admits two types of solutions for α , one positive (repulsive) and one negative (attractive). For a given sign, the changes in α modify the real part of $a_{\eta'p}$ in a nearly proportional way. The imaginary part remains practically constant because the singlet Lagrangian induces the largest effect on the $\eta'N \rightarrow \eta'N$ amplitude as it behaves like $\cos^2\theta_P$. This also means that our model, in spite of using the $\eta'N$ scattering length as a free parameter, provides a robust prediction for the inelastic channels, as corroborated by the moderate changes seen in the inelastic cross sections displayed in Fig. 1.1.

The optical theorem allows us to obtain the total $\eta'p$ cross section from the elastic scattering amplitude and, by subtraction, we can derive the inelastic one, $\sigma^{\text{ine}} = \sigma^{\text{tot}} - \sigma^{\text{el}}$, which amounts to 5 mb at a value of 200 MeV/c for the η' momentum. The preliminar analysis of the transparency ratio of η' photoproduction in nuclei [5] estimate the inelastic cross section to be around 10 mb for a η' momentum of 1 GeV/c. This is an upper bound for the one-body absorption inelasticities, since the transparency ratio can also be contaminated by multinucleon absorption processes, although they are expected to be small [11]. In any case, the η' energies of the transparency ratio experiment are too high for our model, the validity of which we trust for momenta smaller than $p_{\eta'} = 600$ MeV/c, implying η' kinetic energies smaller than 200 MeV. Data analyses with momentum cuts will be available in the future and, although the statistics will be lowered, we expect them to help in constraining the properties of the $\eta'N$ interaction.

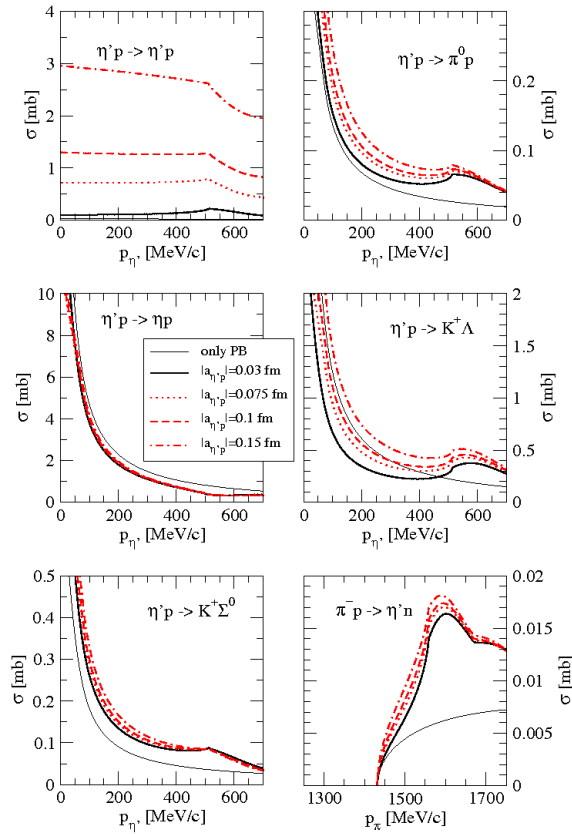


Figure 1.1: Elastic and inelastic η'/p cross sections, together with the cross section of the reaction $\pi^- p \rightarrow \eta' n$, for various models discussed in the text.

Bibliography

- [1] J. B. Kogut and L. Susskind, Phys. Rev. D **10**, 3468 (1974); S. Weinberg, Phys. Rev. D **11**, 3583 (1975); G. 't Hooft, Phys. Rev. Lett. **37**, 8 (1976); E. Witten, Nucl. Phys. B **149**, 285 (1979).
- [2] P. Moskal *et al.*, Phys. Lett. B **474**, 416 (2000); Phys. Lett. B **482**, 356 (2000).
- [3] R. Plotzke *et al.* [SAPHIR Collaboration], Phys. Lett. B **444** (1998) 555; J. Barth *et al.*, Nucl. Phys. A **691** (2001) 374; M. Dugger *et al.*, Phys. Rev. Lett. **96** (2006) 062001 [Erratum-ibid. **96** (2006) 169905]; V. Crede *et al.* [CBELSA/TAPS Collaboration], Phys. Rev. **C80**, 055202 (2009); I. Jaegle *et al.* [CBELSA/TAPS Collaboration], Eur. Phys. J. **A47**, 11 (2011).
- [4] W. T. Chiang, S. N. Yang, L. Tiator, M. Vanderhaeghen and D. Drechsel, Phys. Rev. C **68**, 045202 (2003); K. Nakayama and H. Haberzettl, Phys. Rev. C **69** (2004) 065212; K. Nakayama and H. Haberzettl, Phys. Rev. C **73** (2006) 045211;
- [5] M. Nanova *et al.*, to appear in Proceedings of the XIV International Conference on Hadron Spectroscopy, HADRON2011, June 13-17, 2011, München (Germany).
- [6] E. Oset, A. Ramos, Phys. Lett. **B704**, 334-342 (2011).
- [7] E. Oset and A. Ramos, Eur. Phys. J. A **44**, 445 (2010).
- [8] B. Borasoy, Phys. Rev. **D61**, 014011 (2000).
- [9] F. Ambrosino, A. Antonelli, M. Antonelli, F. Archilli, P. Beltrame, G. Bencivenni, S. Bertolucci, C. Bini *et al.*, JHEP **0907**, 105 (2009).
- [10] R. K. Rader, M. A. Abolins, O. I. Dahl, J. S. Danburg, D. W. Davies, P. L. Hoch, J. Kirz, D. H. Miller, Phys. Rev. **D6**, 3059-3068 (1972).
- [11] H. Nagahiro, S. Hirenzaki, E. Oset and A. Ramos, in preparation.

SEARCH FOR η -MESIC ${}^4\text{He}$ WITH WASA-at-COSY

WOJCIECH KRZEMIEN^{*†}, PAWEŁ MOSKAL^{†‡} and JERZY SMYRSKI[†]
for the WASA-at-COSY Collaboration

1.1 Introduction

The investigation of the exotic objects in the nuclear physics is a proven method for revealing many interesting properties of nuclear systems and for accessing to an unexplored areas of physics. The recent progress in the spectroscopy of pionic and kaonic atoms, as well as pionic and kaonic nuclei has permitted to obtain deeper insights into the meson-nucleus interaction and the in-medium behaviour of spontaneous chiral symmetry breaking [1].

Analogically to the other exotic nuclear systems, the investigation of the η -mesic nuclei would provide many interesting informations about the η -N interaction, N^* in-medium properties [2] and would deepen our knowledge of the fundamental structure of the η meson [3]. The η meson is electrically neutral, therefore such a system can be formed only via the strong interaction which distinguishes it qualitatively from pionic atoms where the binding is the effect of the sum of the attractive electromagnetic force and the repulsive strong interaction.

The search of the η - mesic nucleus was performed in many experiments in the past [4, 5, 6, 7, 8, 9] and is being continued at COSY [12, 10, 11], JINR [6], J-PARC [13] and MAMI [9]. Many promising indications were reported, however, so far there is no direct experimental confirmation of the existence of mesic nucleus. In the region of the light nuclei systems such as η -He or η -T, the observation of the strong enhancement in the total cross-section and the phase variation in the close-to-threshold region provided strong evidence to the hypothesis of the existence of a pole in the scattering matrix which can correspond to the bound state [14]. However, as it was stated in [15, 16], the theoretical predictions of width and binding energy of the η -mesic nuclei is strongly dependent on the not well known subthreshold η -nucleon interaction. Therefore, the direct measurements which could confirm the existence of the bound state, are mandatory.

1.2 Experiment

In June 2008 we performed a search for the ${}^4\text{He} - \eta$ bound state by measuring the excitation function of the $dd \rightarrow {}^3\text{He}p\pi^-$ reaction near the η meson production threshold using the WASA-at-COSY detector[17]. During the experimental run the momentum of the deuteron beam was varied continuously within each acceleration cycle from 2.185 GeV/c to 2.400 GeV/c, crossing the kinematic threshold for the η production in the $dd \rightarrow {}^4\text{He}\eta$ reaction at 2.336 GeV/c. This range of beam momenta corresponds to the variation of ${}^4\text{He} - \eta$ excess energy from -51.4 MeV to 22 MeV. The experimental method is based on measuring the excitation function for $dd \rightarrow {}^3\text{He}p\pi^-$ and a search for a resonance-like structure below the ${}^4\text{He} - \eta$ threshold. The relative angle between the outgoing $p - \pi^-$ pair which originates from the decay of the $N^*(1535)$ resonance created via absorption of the η meson on a nucleon in the ${}^4\text{He}$ nucleus, is 180° in the N^* reference frame and is smeared by about 30° in the reaction center-of-mass frame (CM) due to the Fermi motion of nucleons inside the ${}^4\text{He} - \eta$ nucleus. The ${}^3\text{He}$ plays the role of a spectator and therefore its momentum in the CM frame is relatively low and determined only by the Fermi momentum distribution in the ${}^4\text{He} - \eta$. This signature distinguishes production of mesic helium from other reactions, in which the distribution of the ${}^3\text{He}$ momentum reaches much higher values.

Figure 1.1 presents the not normalized excitation functions for a "signal-rich" region: $p_{\text{He}}^{CM} < 0.3$ GeV/c (top) and a "signal-poor" region: $p_{\text{He}}^{CM} > 0.3$ GeV/c in 20 intervals in beam momentum (middle). Also, the difference between two regions is shown in the same Figure (bottom).

*wojciech.krziemien@if.uj.edu.pl

†Institute of Physics, Jagiellonian University, Cracow, Poland.

‡Institut für Kernphysik (IKP) and Jülich Center for Hadron Physics (JCHP), Forschungszentrum Jülich, Germany.

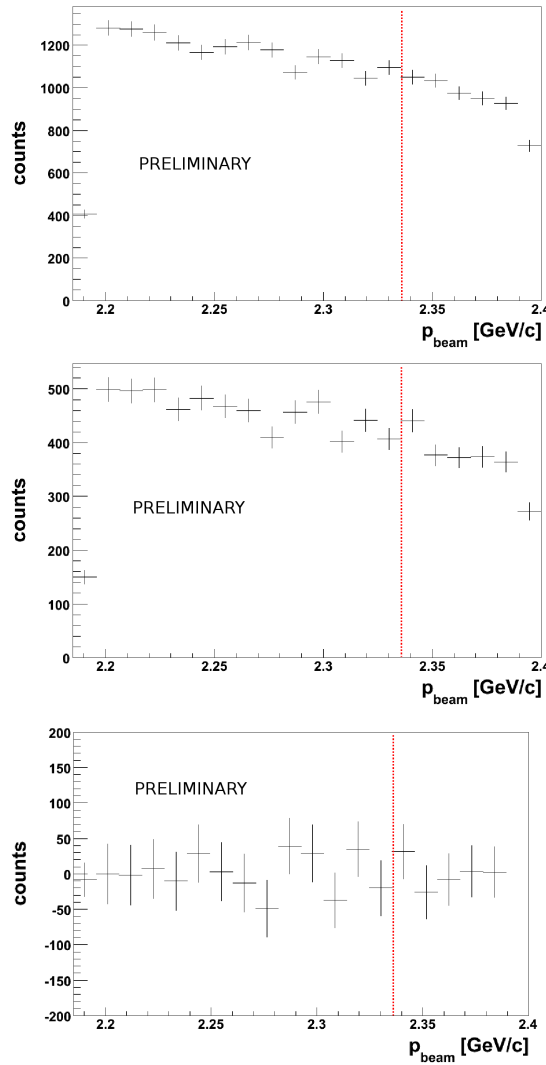


Figure 1.1: Excitation function for the $dd \rightarrow {}^3\text{He}p\pi^-$ reaction for the "signal-poor" region ${}^3\text{He}$ momentum above 0.3 GeV/c (top plot) and the "signal-rich" region, low ${}^3\text{He}$ momentum below 0.3 GeV/c (middle plot). The excitation functions are not normalized. The beam momentum corresponding to the ${}^4\text{He} - \eta$ kinematical threshold is marked as a red dashed line. The difference between the "signal-rich" and the "signal-poor" regions is shown at the bottom plot.

The figure indicates no structure below the kinematical threshold where the signal is expected. In order to estimate the maximum upper limit for the cross-section for the production of the bound state via $dd \rightarrow {}^4\text{He} - \eta_{\text{bound}} \rightarrow {}^3\text{He}p\pi^-$ reaction, the Breit-Wigner function along with the linear background was fitted to the normalized "signal-rich" region. The absolute normalization was obtained based on the $dd \rightarrow {}^3\text{He}n$ reaction, whereas the luminosity dependence of the beam momentum was determined using the quasi-elastic $dd \rightarrow pp(n_{sp}n_{sp})$ reaction. The integrated luminosity equals $L = 117.9 \pm 13.6 \text{ nb}^{-1}$.

1.3 Outlook

In November 2010 a new two-week measurement was performed with WASA-at-COSY. We collected the data with approximately 20 times higher statistics. In addition to the $dd \rightarrow {}^3\text{He}p\pi^-$ channel we registered also the $dd \rightarrow {}^3\text{He}n\pi^0$ reaction. The data analysis is undergoing. After two weeks of measurement with an estimated luminosity of $4 \cdot 10^{30} \text{ cm}^{-2} \text{ s}^{-1}$, we expect a statistical sensitivity of a few nb (σ). A non-observation of this signal will significantly lower the upper limit for the existence of the bound state.

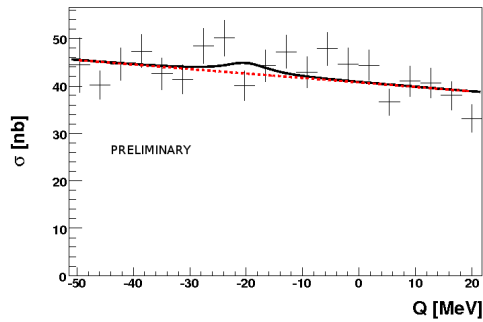


Figure 1.2: Normalized excitation function for the $dd \rightarrow {}^3\text{He}p\pi^-$ reaction for the "signal-rich" region. The Breit-Wigner function $f(Q) = \frac{A \cdot (\frac{\Gamma}{2})^2}{(Q - E_{BE})^2 + (\frac{\Gamma}{2})^2}$ along with the linear function was fitted. The parameters Γ and E_{BE} were fixed to the value of -20 MeV and 10 MeV respectively. The free parameter A is consistent with zero within the obtained accuracy. The dotted red line represents the linear background.

1.4 Support

This work has been supported by FFE funds of Forschungszentrum Jülich, grant No 41831803 (COSY-107), by the European Commission under the 7th Framework Programme through the 'Research Infrastructures' action of the 'Capacities' Programme. Call: FP7-INFRASTRUCTURES-2008-1, Grant Agreement N. 227431 and by the Polish Ministry of Science and Higher Education under grants No. 2367/B/H03/2009/37 and 0320/B/H03/2011/40.

Bibliography

- [1] S. Hirenzaki, *Prog. Theor. Phys. Suppl.* **168** (2007) 458-465.
- [2] D. Jido, H. Nagahiro, S. Hirenzaki, *Phys. Rev.* **C66** (2002) 045202.
- [3] S. D. Bass, A. W. Thomas, *Acta. Phys. Pol. B* **41** (2010) 2239.
- [4] B. J. Lieb *et al.*, *Proc. Int. Nucl. Phys. Conf., Sao Paulo, Brazil* (1989).
- [5] G. A. Sokol *et al.*, *arXiv:nucl-ex/9905006* (1999)
- [6] M. Kh. Anikina *et al.*, *arXiv:nucl-ex/0412036* (2004).
- [7] A. Gillitzer, *Acta Phys. Slovaca* **56** (2006) 269.
- [8] A. Budzanowski *et al.*, *Phys. Rev.* **C79** (2009) 061001(R).
- [9] B. Krusche, F. Pheron, Y. Magrbhi *Acta. Phys. Pol. B* **41** (2010) 2249.
- [10] J. Smyrski *et al.*, *Phys. Lett.* **B 649**, 258 (2007).
- [11] T. Mersmann *et al.*, *Phys. Rev. Lett.* **98**, 242301 (2007).
- [12] P. Moskal, J. Smyrski, *Acta. Phys. Pol. B* **41** (2010) 2281.
- [13] H. Fujioka, K. Itahashi, *Acta. Phys. Pol. B* **41** (2010) 2261.
- [14] C. Wilkin *Acta. Phys. Pol. B* **41** (2010) 2191.
- [15] Q. Haider, L.C. Liu, *Phys. Rev.* **C66** (2002) 045208.
- [16] Q. Haider, L.C. Liu, *Acta Phys. Polon. B* **41** (2010).
- [17] W. Krzemiński *et al.*, *Acta Phys. Polon. Supp.* **2** (2009) 141-148.

List of Participants

Name	Affiliation	Contribution
Adlarson, Patrick	Uppsala University	Page 21
Amaryan, Moskov	Old Dominion University	Page 80
Bashkanov, Mikhail	Tübingen University	Page 96
Beck, Reinhard	HISKP, Bonn University	
Bergmann, Florian	Westfälische Wilhelms Universität Münster	Page 11
Berłowski, Marcin	Soltan Institute Nuclear Studies	Page 9
Bijnens, Johan	Lund University	Page 68
Caldeira Balkeståhl, Li	Uppsala University	Page 18
Coderre, Daniel	Forschungszentrum Jülich	Page 77
Czerwinski, Eryk	Jagiellonian University Cracow	Page 94
Di Donato, Camilla	I.N.F.N. Naples	Page 35
Ditsche, Christoph	HISKP, Bonn University	
Dybczak, Adrian	Jagiellonian University Cracow	Page 111
Fariborz, Amir	State University of New York, Institute of Technology	Page 74
Fröhlich, Ingo	Goethe University Frankfurt	Page 16
Gauzzi, Paolo	Sapienza Università di Roma / INFN	
Giovannella, Simona	I.N.F.N. Frascati	
Goldenbaum, Frank	Forschungszentrum Jülich	
Goslawski, Paul	Westfälische Wilhelms Universität Münster	Page 91
Grzonka, Dieter	Forschungszentrum Jülich	
Gullström, Carl-Oskar	Uppsala University	Page 43
Gumberidze, Malgorzata	Institut de Physique Nucleaire d Orsay	Page 106
Hanhart, Christoph	Forschungszentrum Jülich	
Heijkenskjöld, Lena	Uppsala University	Page 61
Hejny, Volker	Forschungszentrum Jülich	
Hodana, Malgorzata	Jagiellonian University Cracow	Page 45
Hoferichter, Martin	HISKP, Bonn University	Page 122
Höistad, Bo	Uppsala University	
Johansson, Tord	Uppsala University	
Kampf, Karol	Lund University	
Khan, Farha Anjum	Forschungszentrum Jülich	Page 52
Khoukaz, Alfons	Westfälische Wilhelms Universität Münster	
Klaja, Joanna	Forschungszentrum Jülich	
Kolesár, Marian	Charles University Prague	Page 30
Krzemien, Wojciech	Jagiellonian University Cracow	Page 140
Kubis, Bastian	HISKP, Bonn University	Page 13
Kuc, Hubert	Jagiellonian University Cracow	Page 117
Kupsc, Andrzej	Uppsala University	
Lanz, Stefan	Bern University	Page 24
Lersch, Daniel	Forschungszentrum Jülich	Page 38
Leupold, Stefan	Uppsala University	
Machner, Hartmut	Universität Duisburg-Essen	
Masjuan, Pere	Universidad de Granada	Page 71
Messchendorp, Johan	KVI / RU Gronigen	Page 83
Metag, Volker	Universität Giessen	Page 51
Moskal, Pawel	Jagiellonian University Cracow	
Niecknig, Franz	HISKP, Bonn University	Page 63
Nikolaev, Alexander	HISKP, Bonn University	Page 90
Nuhn, Patrick	HISKP, Bonn University	
Ozerianska, Iryna	Jagiellonian University Cracow	Page 87
Perez del Rio, Elena	Tübingen University	Page 100
Prado Longhi, Ivan	Università degli Studi "Roma Tre" and I.N.F.N.	Page 119
Pricking, Annette	Tübingen University	
Pszczel, Damian	Andrzej Soltan Institute for Nuclear Studies Warsaw	

Continued on next page

List of Participants – continued from previous page

Name	Affiliation	Contribution
Ramos Gómez, Àngels	Universitat de Barcelona	Page 137
Ramalho, Gilberto	Instituto Superior Técnico Lisbon	Page 128
Ramstein, Beatrice	Institut de Physique Nucleaire d Orsay	
Redmer, Christoph Florian	Uppsala University	Page 68
Ritman, James	Ruhr-Universität Bochum and Forschungszentrum Jülich	
Salabura, Piotr	Jagiellonian University Cracow	Page 114
Sawant, Siddesh	Indian Institute of Technology Bombay	Page 61
Schadmand, Susan	Forschungszentrum Jülich	
Schneider, Sebastian	HISKP, Bonn University	Page 63
Sibirtsev, Alexander	Forschungszentrum Jülich	
Skorodko, Tatiana	Tübingen University	Page 103
Stollenwerk, Felix	Forschungszentrum Jülich	Page 33
Teilab, Khaled	Goethe University Frankfurt	
Terschlüsen, Carla	Uppsala University	Page 58, Page 40
Thiel, Annika	HISKP, Bonn University	Page 125
van Pee, Harald	HISKP, Bonn University	
Werthmüller, Dominik	University of Basel	Page 131
Wilkin, Colin	University College London	
Wirzba, Andreas	Forschungszentrum Jülich	Page 5
Witthauer, Lilian	University of Basel	
Wurm, Patrick	Forschungszentrum Jülich	Page 48
Zdebik, Jaroslaw	Jagiellonian University Cracow	Page 54
Zdráhal, Martin	IPNP, MFF, Charles University Prague	Page 27